STUDIES ON CELLULAR ROLES OF CALCIUM SIGNALING GENES IN *NEUROSPORA CRASSA*

A Thesis

submitted in partial fulfillment of the requirements

for the degree of

DOCTOR OF PHILOSOPHY

by

REKHA DEKA

Department of Biotechnology

Indian Institute of Technology

Guwahati, Assam, India

Pin-781039

November 2013

भारतीय प्रौद्योगिकी संस्थान गुवाहाटी
Indian Institute of Technology Guwahati
Department of Biotechnology
Guwahati - 781 039

DECLARATION

I do hereby declare that the content embodied in this thesis entitled **"Studies on cellular roles of calcium signaling genes in *Neurospora crassa*"** is the result of investigations carried out by me in the Department of Biotechnology, Indian Institute of Technology Guwahati, for the award of degree of Doctor of Philosophy, under the supervision of **Dr. Ranjan Tamuli**. The research work presented in this thesis is original and has not been submitted in part or full for any degree or diploma to any other institute or university to the best of my knowledge and belief.

Rekha Deka 18/11/2013

November 2013

REKHA DEKA

Roll No. 09610609

TH-1227_09610609

भारतीय प्रौद्योगिकी संस्थान गुवाहाटी
Indian Institute of Technology Guwahati
Department of Biotechnology
Guwahati - 781 039

CERTIFICATE

It is to certify that the research work in this thesis entitled **"Studies on cellular roles of calcium signaling genes in *Neurospora crassa*"** has been carried out at the Indian Institute of Technology Guwahati, by **Ms Rekha Deka** (Roll No. 09610609), for the award of degree of Doctor of Philosophy in Biotechnology, under my supervision. The outcome of the research work presented in this thesis is original and has not been submitted in part or full for any degree or diploma to any other university or institute.

Ranjan Tamuli
18.11.2013

November 2013

Thesis Supervisor: Dr Ranjan Tamuli

Assistant Professor
Department of Biotechnology
IIT Guwahati

TH-1227_09610609

Dedicated

to

My Family

TH-1227_09610609

	Pages
Table of contents	**i-v**
List of Figures	**vi-viii**
List of Tables	**ix-xi**
List of abbreviations	**xii-xiii**
Acknowledgements	**xiv-xv**
Synopsis	**xvi-xxii**
Chapter 1: An introduction to *Neurospora crassa* and calcium signaling	1-19
1.1 Introduction to the model organism *Neurospora crassa*	1-2
1.1.1 Calcium is a versatile and a ubiquitous signaling molecule	5-7
1.1.2 Overview of calcium signaling in fungi	8-9
1.1.3 Calcium signaling machinery in *N. crassa*	10-19
1.2 Objectives of this study	19
Chapter 2: Materials and methods	20-38
2.1 Materials	20-29
2.1.1 Chemicals and other materials	20
2.1.2 *Neurospora crassa* strains	20-21
2.1.3 Bacterial strains	21
2.1.4 Plasmid vectors	21-23
2.1.5 Bacterial media, antibiotics and commonly used solutions	23-26
2.1.6 Solutions for growth, maintenance and crossing of *Neurospora* strains	27-29
2.2 Methods	29-38
2.2.1 Growth conditions	29
2.2.2 Crossing and ascospore collection	29
2.2.3 Transformation of the *N. crassa* strain by electroporation	29-30
2.2.4 Scoring for Antibiotic resistance	30
2.2.5 Isolation of sterols from *N. crassa* strains and analysis by UV spectrophotometry	30-31

TH-1227_09610609

2.2.6 Preparation of ultra-competent cells 31
2.2.7 Transformation of ultracompetent *E. coli* cells by heat shock 31
2.2.8 Isolation of nucleic acids 31-34
(i) Small-scale isolation of plasmid DNA from bacterial culture 31-32
(ii) Large scale isolation of plasmid DNA from bacterial culture 32
(iii) *Neurospora* genomic DNA isolation 32-33
(iv) *Neurospora* RNA isolation 33-34
2.2.9 Quantitation of nucleic acids 34
2.2.10 Polymerase Chain Reaction 34
2.2.11 Reverse-transcriptase PCR and Real time PCR 35
2.2.12 Digestion of DNA with restriction endonuclease 35-36
2.2.13 Ligation reactions 36
2.2.14 Agarose gel electrophoresis 36
2.2.15 Purification of DNA fragments from agarose gels 36
2.2.16 Preparation of radiolabeled DNA probes by random primer labeling 36-37
2.2.17 Sephadex G-50 column chromatography for purification of radiolabeled probe 37
2.2.18 Southern hybridization 37
2.3 Databases and Computer software used 38

Chapter 3: Screening of knockout mutants of *Neurospora crassa* Ca^{2+} signaling genes and identification of cellular roles of the NCU04379 gene 39-63
3.1 Introduction 39
3.2 Results 39-63
3.2.1 Growth study of the *N. crassa* knockout mutants of calcium signaling genes 39
3.2.2 The ΔNCU04379.2 mutant displayed a slow growth rate 43
3.2.2.1 The slow growth phenotype of the ΔNCU04379.2 mutant was not due to a defect in ergosterol biosynthesis 43
3.2.3 Calcium sensitivity analysis 46

TH-1227_09610609

3.2.3.1 The ΔNCU04379.2 mutant was hypersensitive to $CaCl_2$ stress 46

3.2.3.2 The $CaCl_2$ hypersensitivity of the ΔNCU04379.2 mutant was not due to a mere osmotic effect 46

3.2.3.3 Effect of Ca^{2+} deprivation on growth 46

3.2.4 UV survival assay 51

3.2.4.1 The ΔNCU04379.2 mutant showed an increased sensitivity to UV-irradiation 51

3.2.5 Cloning of the NCU04379 fragment from the wild-type for complementation analysis 53

3.2.6 Transformation of the pRD-1 construct into the ΔNCU04379.2 mutant 53-54

3.2.7 Complementation of the ΔNCU04379.2 mutant 54

3.3 Discussion 63

Chapter 4: Identification of NCU04379 as the *Neurospora crassa* homologue of Neuronal Calcium Sensor-1 and its site-directed mutational analysis 64-101

4.1 Introduction 64

4.2 Results 64-99

4.2.1 NCU04379 gene encodes a homologue of Neuronal Calcium Sensor-1 64-65

4.2.2 Cloning of *N. crassa* homologue of *ncs-1* gene from the wild-type for site-directed mutational analysis 68

4.2.2.1 Double-joint polymerase chain reaction 68-71

4.2.2.2 Cloning of the final double joint PCR product carrying *ncs-1* gene in the pRS426 vector 72

4.2.3 Transformation of pRD-2-B-*ncs-1* construct into the Δ*ncs-1*Δ*mus-53 a (15)* strain 72

4.2.4 Site-directed mutational analysis of *N. crassa* homologue of NCS-1 74-76

4.2.5 Transformation of pRD-2-B-*ncs-1*^{G2A}, pRD-2-B- *ncs-1*^{R175A} and pRD-2-B-*ncs-1*^{E120Q} constructs into the Δ*ncs-1*Δ*mus53 a (15)* strain 83

4.2.6 The *ncs-1*^{G2A} mutant displayed growth phenotype like the wild-type 87

TH-1227_09610609

4.2.7 The *ncs-1*^{G2A} mutant displayed a faster growth in absence of extracellular Ca^{2+} and tolerates to high Ca^{2+} stress like the wild-type 89

4.2.8 The *ncs-1*^{G2A} mutant showed an increased sensitivity to UV irradiation like the Δ*ncs-1* mutant 89

4.2.9 The *ncs-1*^{R175A} mutant showed growth and Ca^{2+} stress tolerance like the wild-type 92

4.2.10 The *ncs-1*^{R175A} mutant showed an increased sensitivity to UV irradiation than the Δ*ncs-1* mutant 92

4.2.11 The *ncs-1*^{E120Q} mutant showed slow growth, sensitivity to Ca^{2+} and UV stress like the Δ*ncs-1* mutant 96

4.3 Discussion 99-101

Chapter 5: Genetic Interaction of *Neurospora crassa* homologue of Neuronal Calcium Sensor-1 102-118

5.1 Introduction 102

5.2 Results 102-116

5.2.1 Genetic location of the *ncs-1, mid-1*, and *nca-2* genes 102

5.2.2 Generation of the Δ*ncs-1*Δ*nca-2*, Δ*ncs-1*Δ*mid-1*, and Δ*mid-1*Δ*nca-2* double mutants 103-104

5.2.3 The Δ*ncs-1*Δ*nca-2* double mutant showed novel colony morphology 105

5.2.4 The Δ*ncs-1*Δ*nca-2*, Δ*ncs-1*Δ*mid-1*, and Δ*mid-1*Δ*nca-2* double mutant showed slow growth phenotype 107

5.2.5 Carotenoid accumulation was affected in the Δ*ncs-1*Δ*nca-2*, Δ*ncs-1*Δ*mid-1* and Δ*mid-1*Δ*nca-2* double mutants 109

5.2.6 The Δ*ncs-1*Δ*nca-2* double mutant was hypersensitive to Ca^{2+} and UV stress 111

5.2.7 The*Δncs-1Δnca-2, Δncs-1Δmid-1,* and *Δmid-1Δnca-2* double mutant showed a decreased sensitivity to the respiratory by-product CO_2 and produced conidial bands 114

5.3 Discussion 116-118

TH-1227_09610609

Additional work 119-122

A.1 Expression analysis of *ncs-1*, *nca-2*, *mid-1*, *crz1*, and *NCU06366* in *N. crassa* in response to Ca^{2+} stress

Conclusion and future perspectives 123-124

References 125-143

Publications 144-145

Reprints of Publications 145A

TH-1227_09610609

List of Figures

Figure 1.1	Morphology of *Neurospora crassa* .	3
Figure 1.2	The life cycle of a heterothallic fungus *N. crassa*.	4
Figure 1.3	The coordination polyhedron of the Ca^{2+} ion.	6
Figure 1.4	The coordination sphere of the EF hand loop.	7
Figure 1.5	Overview of calcium signaling system in *N. crassa*.	11
Figure 1.6	Mechanisms of Ca^{2+} release depicting the major pathways for mobilizing Ca^{2+} from internal stores.	12
Figure 2.1	Schematic of the pBARGEM7-1 vector.	22
Figure 2.2	Schematic of the pRS426 vector.	23
Figure 3.1	Strategy for generating deletion constructs.	40
Figure 3.2	Growth phenotype of the wild-type and the ΔNCU04379.2 mutant.	44
Figure 3.3	Ergosterol profiles in the wild-type, ΔNCU04379.2 and *erg-3* null mutant.	45
Figure 3.4	Effect of $CaCl_2$ stress on the growth of the wild-type and ΔNCU04379.2 mutant.	47
Figure 3.5	Effect of NaCl on the growth of the wild-type and ΔNCU04379.2 mutant.	48
Figure 3.6	Effect of sucrose on the growth of the wild-type and ΔNCU04379.2. mutant	49
Figure 3.7	Effect of EGTA on the growth of the wild-type and ΔNCU04379.2 mutant.	50
Figure 3.8	Effect of UV irradiation on the survival of the wild-type and ΔNCU04379.2 mutant.	52
Figure 3.9	Cloning of NCU04379 fragment from the wild-type for complementation analysis.	55
Figure 3.10	Confirmation of the ΔNCU04379.2 mutant and the pRD-1 transformants by Southern hybridization.	56
Figure 3.11	Verification of the ΔNCU04379.2 mutant allele in the strains transformed with pRD-1 construct.	57
Figure 3.12	Verification of the expression of NCU04379 gene in the pRD-1.	58

TH-1227_09610609

	homokaryotic transformant.	
Figure 3.13	Complementation of the slow growth phenotype of ΔNCU04379.2 mutant.	59
Figure 3.14	Complementation of the calcium sensitivity phenotype of the ΔNCU04379.2 mutant.	60
Figure 3.15	Complementation of the effect of EGTA on the ΔNCU04379.2 mutant.	61
Figure 3.16	Complementation of the UV sensitivity phenotype of the ΔNCU04379.2 mutant.	62
Figure 4.1	Sequence alignment of NCS-1 homologues.	66
Figure 4.2	Domain organization of *N. crassa* homologue of NCS-1.	67
Figure 4.3	Phylogenetic analysis of NCS-1 homologues from fungi to mammals.	67
Figure 4.4	Schematic of the pRD-2 construct.	68
Figure 4.5	Cloning of the *N. crassa* homologue of *ncs-1* gene from the wild-type for site-directed mutational analysis.	71
Figure 4.6	Confirmation of clones constructed for site-directed mutational analysis.	73
Figure 4.7	Translated sequence of *N. crassa* homologue of NCS-1 including the nucleotide sequence.	77
Figure 4.8	Chromatogram profile of the *ncs-1*^{G2A} mutant allele generated by partial sequencing of the pRD-2-B-*ncs-1*^{G2A} construct.	78
Figure 4.9	Confirmation of the G2A mutation in the pRD-2-B-*ncs-1*^{G2A} construct.	79
Figure 4.10	Chromatogram profile of the *ncs-1*^{R175A} mutant allele generated by partial sequencing of the pRD-2-B-*ncs-1*^{R175A} construct.	80
Figure 4.11	Confirmation of the R175A mutation in the pRD-2-B-*ncs-1*^{R175A} construct.	81
Figure 4.12	Chromatogram profile of the *ncs-1*^{E120Q} mutant allele generated by partial sequencing of the pRD-2-B-*ncs-1*^{E120Q} construct.	82
Figure 4.13	Confirmation of the E120Q mutation in pRD-2-B-*ncs-1*^{E120Q} construct.	83
Figure 4.14	Verification of the pRD-2-B-*ncs-1*^{G2A} transformants by PCR.	84
Figure 4.15	Verification of the pRD-2-B-*ncs-1*^{R175A} transformants by PCR.	85
Figure 4.16	Verification of the pRD-2-B-*ncs-1*^{E120Q} transformants by PCR.	86
Figure 4.17	Growth phenotype of the *ncs-1*^{G2A} mutant.	88

TH-1227_09610609

Figure 4.18	Effect of calcium stress on the growth of *ncs-1*^{G2A} mutant.	90
Figure 4.19	Dose response curves showing the relative UV-sensitivity of the *ncs-1*^{G2A} mutant.	91
Figure 4.20	Growth phenotype of the *ncs-1*^{R175A} mutant.	93
Figure 4.21	Effect of calcium stress on the growth of *ncs-1*^{R175A} mutant.	94
Figure 4.22	Dose response curves showing relative UV-sensitivity of the *ncs-1*^{R175A} mutant.	95
Figure 4.23	Growth phenotype of the *ncs-1*^{E120Q} mutant.	96
Figure 4.24	Effect of calcium stress on the growth of *ncs-1*^{E120Q} mutant.	97
Figure 4.25	Dose response curves showing relative UV-sensitivity of the *ncs-1*^{E120Q} mutant.	98
Figure 5.1	Schematics of *ncs-1*, *mid-1*, and *nca-2* genes showing their chromosomal location.	103
Figure 5.2	Verification of double mutants using PCR.	104
Figure 5.3	Morphology of the wild-type, single and double mutant strains grown in 250 ml flasks for 5 days at 30ºC.	105
Figure 5.4	Aerial hyphae of the wild-type, single and double mutant strains.	106
Figure 5.5	Growth phenotypes of the wild-type, single and the double mutant strains.	107
Figure 5.6	Total carotenoid contents of the wild-type, single and double mutant strains.	110
Figure 5.7	Effect of Ca^{2+} stress on the growth of wild-type, single and double mutant strains.	112
Figure 5.8	Dose response curves showing relative UV-sensitivity of the wild-type, single and double mutant strains.	113
Figure 5.9	Circadian regulated conidiation.	115
Figure 5.10	Model showing the cellular roles of NCS-1, MID-1, and NCA-2	116
Figure A.1	Average fold change in expression of *ncs-1, mid-1, nca-2*, NCU06366-Ca^{2+}/H^{+} exchanger and the *N. crassa* homologue of *crz1* genes.	122

TH-1227_09610609

List of Tables

Table 1.1	Calcium signaling proteins in *Neurospora crassa*	13
Table 3.1	List of *N. crassa* knockout mutant strains of Ca^{2+}signaling genes used in this study	41
Table 3.2	Average growth rate of the *N. crassa* calcium signaling knockout mutants	42
Table 3.3	Apical growth of the *N. crassa* wild-type and ΔNCU04379.2 mutant in race tube	44
Table 3.4	Average colony growth rate of the wild-type and ΔNCU04379.2 mutant at various concentrations of $CaCl_2$	47
Table 3.5	Average colony growth rate of the wild-type and ΔNCU04379.2 mutant at various concentrations of NaCl	48
Table 3.6	Average colony growth rate of the wild-type and ΔNCU04379.2 mutant at various concentrations of sucrose	49
Table 3.7	Primers used for complementation studies of the ΔNCU04379.2 mutant	54
Table 3.8	Apical growth of the wild-type, ΔNCU04379.2 mutant and homokaryotic transformant in race tube	59
Table 3.9	Average colony growth rate of the wild-type, ΔNCU04379.2 mutant and homokaryotic transformant at various concentrations of $CaCl_2$	61
Table 4.1	Summary of BLAST analysis using NCU04379 protein as a query	65
Table 4.2	Primers used for site-directed mutational analysis	69
Table 4.3	Apical growth of the wild-type, Δ*ncs-1*mutant, *ncs-1::bar* homokaryotic transformant, and *ncs-1*^{G2A} mutant strains in the race tube	88
Table 4.4	Average colony growth rate of the wild-type, Δ*ncs-1* mutant, *ncs-1::bar* homokaryotic transformant, and the *ncs-1*^{G2A} mutant strains at various concentration of $CaCl_2$	90
Table 4.5	Relative UV- sensitivity of the of the wild-type, Δ*ncs-1* mutant, *ncs-1::bar* homokaryotic transformant, *ncs-1*^{G2A} mutant , and *upr-1* mutant strains	91

TH-1227_09610609

Table 4.6	Apical growth of the wild-type, Δ*ncs-1*mutant, *ncs-1::bar* homokaryotic transformant, and *ncs-1*^{R175A} mutant strains in the race tube	93
Table 4.7	Average colony growth rate of the wild-type, Δ*ncs-1*mutant, *ncs-1::bar* homokaryotic transformant, and *ncs-1*^{R175A} mutant strains at various concentration of $CaCl_2$	94
Table 4.8	Relative UV- sensitivity of the of the wild-type, Δ*ncs-1* mutant, *ncs-1::bar* homokaryotic transformant, *ncs-1*^{R175A} mutant, and *upr-1* mutant strains	95
Table 4.9	Apical growth of the wild-type, Δ*ncs-1*mutant, *ncs-1::bar* homokaryotic transformant, and *ncs-1*^{E120Q} mutant strains in the race tube	97
Table 4.10	Average colony growth rate of the wild-type, Δ*ncs-1*mutant, *ncs-1::bar* homokaryotic transformant, and *ncs-1*^{E120Q} mutant strains at various concentration of $CaCl_2$	98
Table 4.11	Relative UV- sensitivity of the wild-type, Δ*ncs-1* mutant, *ncs-1::bar* homokaryotic transformant, *ncs-1*^{E120Q} mutant, and *upr-1* mutant strains	99
Table 5.1	Average height of aerial hyphae of wild-type, single and double mutant strains cultured in test tubes	106
Table 5.2	Apical growth of the wild-type, single and double mutant strains in race tube	108
Table 5.3	Average growth rate (cm h^{-1}) of the wild-type, single and double mutant strains	108
Table 5.4	Quantification of carotenoid in wild-type, single and double mutant strains	110
Table 5.5	Average colony growth rate of the wild-type, single and double mutant strains at different concentrations of $CaCl_2$ (M)	112
Table 5.6	Relative UV-sensitivity of the wild-type, single and double mutant strains	113
Table 5.7	Apical growth and distance of consecutive conidial bands of the wild-	115

TH-1227_09610609

type, single and double mutant strains in race tubes in absence of NAC

Table A.1 Primers used in the real time PCR analysis 120

TH-1227_09610609

List of abbreviations

A	absorbance
bp	base pair
°C	degree Celsius
CoA	coenzyme A
cm	centimeter
DNA	deoxyribonucleic acid
g	gram
h	hour
J/m^2	joule per square meter
K	kelvin
kb	kilobase
KV	kilovolt
LG	linkage group
min	minute
ms	milliseconds
M	molar
mM	millimolar
mg	milligram
ml	milliliter
mm	millimeter
N	normal
NADPH	nicotinamide adenine dinucleotide phosphate
ng	nanogram
nm	nanometer
µg	microgram
µl	microlitre
µF	microfarad
Ω	ohms
OD	optical density

TH-1227_09610609

ORF	open reading frame
PCR	polymerase chain reaction
psi	Pounds per square inch
RT-PCR	Reverse transcriptase polymerase chain reaction
qPCR	Quantitative real time pcr
RIP	repeat-induced point mutation
RNAi	RNA interference
rpm	revolutions per minute
sec	second
UV	ultraviolet
v/v	volume/volume
V/cm	Volt per centimeter
VGM	Vogel's glucose medium
w/v	weight/volume

TH-1227_09610609

Acknowledgements

First and foremost, I would like to thank my supervisor, Dr. Ranjan Tamuli, who was the first person to introduce me to the wonderful world of molecular biology and in particular, to the fascinating organism that is Neurospora crassa. I thank him for his guidance and training throughout my Ph. D. I appreciate his expertise and valuable comments. I am grateful to him for patiently going through the various versions of my thesis.

I would like to express my sincere gratitude to all my doctoral committee members Dr. U. Bora, Dr. V. Trivedi, and Dr. A. Sharma for their valuable suggestions and constructive criticism during my progress report presentations that has led to the successful completion of my thesis.

I would take this opportunity to thank Director of IITG, and Head of the Biotechnology Department, IITG for providing all the necessary facilities and a conductive academic environment. I specially thank the Department of Biotechnology (DBT) and Department of Science and Technology (DST), Govt. of India for research grants to my supervisor. I sincerely acknowledge the financial support from Council of Scientific and Industrial Research (CSIR) for providing me fellowship.

I am very thankful to the director of CCMB, Prof. Lalji Singh, and Prof D.P. Kasbeker for providing me facilities to complete the southern experiment which was very essential for my publication.

TH-1227_09610609

I am grateful to the Fungal Genetics Stock Centre (FGSC), University of Missouri, Kansas City, USA, for readily providing Neurospora strains. Charges for Neurospora strains and race tubes obtained from FGSC were generously waived.

I thank my present RT lab members Ravi, Vijya, Ananya, Rimli, Mayurakhi, Dibaker, Vishakha, Sanamaya for their warmth, suggestions and help. I sincerely thank Ravi for his help and support as we were the first students to start our RT lab. I thank my previous lab members such as Dhruv, Gedela, Yutika, Upasana, and Jagadeesh for their help in my work.

I thank all my friends at IITG who made my stay very pleasant.

Above all, I would like to pay my high regards to my parents, my grandfather, my elder brother Kamal, and my younger brother Kishore for their sincere encouragement, and inspiration throughout my research work and lifting me uphill this phase of life.

November, 2013 *Rekha Deka*

TH-1227_09610609

Synopsis

The calcium (Ca^{2+}) signaling system in the filamentous fungus *Neurospora crassa* is unique and this system lacks receptors for second messengers such as inositol-1,4,5-trisphosphate ($InsP_3$), ryanodine and cyclic ADP ribose (cADPR) that are responsible for Ca^{2+} release from internal stores in other organisms (Berridge et al. 2000; Sanders et al. 2001; Bootman et al. 2001). $InsP_3$ is synthesized by phospholipase C-δ subtype (PLC- δ) proteins. These proteins are identified in Neurospora as well as in other filamentous fungi; however, signaling via $InsP_3$ receptor is still unclear since no recognizable $InsP_3$ receptors have been identified in Neurospora. In addition, ADP-ribosyl cyclase protein that synthesizes second messengers such as cADP ribose or NAADP and ryanodine receptor, which are the key components of Ca^{2+} release mechanisms in animal cells, are not known in Neurospora and other fungi. Furthermore, no homologues of either sphingosine kinase, which synthesizes the second-messenger sphingosine-1-phosphate, or the sarcoplasmic reticulum Ca^{2+} release channel, SCaMPER, which is a possible target of sphingolipids, could be identified in *N. crassa*. These notable differences suggest that filamentous fungi might possess novel intracellular Ca^{2+} release mechanism that remains to be identified that might provide novel antifungal targets for drug discovery. In filamentous fungi including *N. crassa* where growth pattern and development are more complex than lower fungi, there is evidence for the involvement of Ca^{2+} in numerous physiological processes including cell cycle, circadian rhythms, cytoskeletal organization, hyphal branching, hyphal orientation, hyphal tip growth, infection structure differentiation, sporulation and spore germination (Ohya et al. 1991; Gadd 1994; Benito et al. 2000; Shaw and Hoch 2001; Deka et al. 2011; Tamuli et al. 2011, 2013). However, detailed knowledge about the main proteins involved in Ca^{2+}-mediated signal response pathway is still lacking for *N. crassa* or, indeed, any other filamentous fungus.

In Chapter 1, I describe the importance of Ca^{2+} in the living system and the current knowledge about the Ca^{2+} signaling in eukaryotes including the filamentous fungus *N. crassa*. Ca^{2+} signaling regulates diverse cell functions and regarded as life and death signal (Berridge et al. 1998). Ca^{2+} is found in all fungal cells and either excess external Ca^{2+} or the presence of substances such as chelators and ionophores that can change the cytosolic free Ca^{2+} concentration ($[Ca^{2+}]_c$) may have diverse effects on growth, differentiation and sporulation. For instances, Ca^{2+} regulates several cell processes such as growth, cell

TH-1227_09610609

proliferation, cell cycle control and cytokinesis in *Saccharomyces cerevisiae*. The deprivation of Ca^{2+} first inhibits the initiation of bud emergence and DNA synthesis and then inhibits S phase and G2/M traverses in *S. cerevisiae* (Iida et al. 1990). In addition, MID-1, a stretch-activated channel protein in *S. cerevisiae*, is required for successful mating (Iida et al. 1994). In *Schizosaccharomyces pombe*, Ca^{2+} ATPase homologue Pmr1p is essential for cell wall integrity and is required for polarized cell growth and cytokinesis by allowing protein glycosylation and the polarized actin distribution to take place normally (Cortés et al. 2004). In addition, deletion of a calcineurin A homologue *ppb1+* in *S. pombe* results in severe morphological and developmental abnormalities. Such strains are sterile and exhibit defects in cytokinesis and cell shape (Yoshida et al. 1994). Calcineurin is the only known protein phosphatase that is dependent upon Ca^{2+} and calmodulin (CaM) for its activity. Calcineurin plays an important role in controlling cell morphology and virulence in most of the pathogenic fungi via dephosphorylation of a transcription factor called Crz1p. Calcineurin dephosphorylates Crz1p upon an increase in $[Ca^{2+}]_c$, allowing its nuclear translocation where it up-regulates the transcription of Ca^{2+} transporters to combat the toxicity of high level of $[Ca^{2+}]_c$ in *A. fumigatus* (Soriani et al. 2008, 2010). One of the Ca^{2+} transporters called PmcA in *A. fumigatus*, which infect human lungs, plays a role in virulence and pathogenicity via Ca^{2+}/ calcineurin signaling pathway (Dinamarco et al. 2012). In another human pathogenic fungus *Crptococcus neoformans,* the vacuolar Ca^{2+} exchanger VCX1 is involved in Ca^{2+} tolerance and virulence through calcineurin; however, CRZ1 homologue has not been identified in this fungus (Kmetzsch et al. 2010). In *Magnaporthe oryzae*, which causes rice blast, deletion of phosphalipase C -1 (MoPLC1) suppresses Ca^{2+} influx causing the fungus defective in developmental steps, including appressorium formation and pathogenicity (Rho et al. 2009). In another plant pathogen, *Fusarium graminearum*, the causal agent of head blight of wheat and barley, Ca^{2+} signaling has been shown to have a role in hyphal growth, sporulation, and fruiting body function (Cavinder and Trail 2012). FIG1, a transmembrane low affinity Ca^{2+} channel protein in *F. graminearum*, plays role in sexual development, and *fig1* deletion causes complete arrest of perithecia formation. In *Gibberella zeae*, two Ca^{2+} channel proteins, MID1 and CCH1 are involved in ascospore discharge (Cavinder 2011; Hallen and Trail 2008). The *cch1*Δ mutant of *G. zeae* displays slower vegetative growth rates, abnormal sexual and ascospore development, and reduced ascospore discharge. Similarly, the *mid1*Δ mutant of *G. zeae* grows slightly slower, discharge ascospores at a slightly higher level, and develops abnormal ascospores with much greater frequency than the

TH-1227_09610609

*cch1*Δ mutants. In *Claviceps purpurea* that infect rye plant, homologue of *S. cerevisiae* MID1, plays a role in vegetative growth, differentiation and pathogenicity on rye. *C. purpurea* loses complete virulence on *mid-1* deletion (Bormann and Tudzynski 2009). In two entomopathogenic fungi, *Beauveria bassiana* and *Metarhizium acridum*, the homologue of Neuronal Calcium Sensor-1, Bbcsa1 and MaNcs1, respectively, plays role in virulence and pathogenicity of the fungus towards insects (Fan et al. 2012; Min and Yueqing 2012). Bbcsa1 participates in pre-penetration or early penetration events during the host infection. Thus, Ca^{2+} signaling is involved in many cellular processes in fungi; however, the detailed understanding about the Ca^{2+} signaling mediated pathway is still lacking in these organisms.

N. crassa has been established as an excellent eukaryotic model organism that can be utilized to investigate the complex Ca^{2+} signaling processes. The genome sequence of *N. crassa* has revealed 48 Ca^{2+} signaling proteins that includes three Ca^{2+} channel proteins, nine Ca^{2+}/cation-ATPases, six recognizable Ca^{2+}/H^{+} exchangers, two novel putative Ca^{2+}/Na^{+} exchangers, four novel phospholipase C-δ subtype (PLC-δ) proteins, 23 Ca^{2+}/calmodulin-regulated proteins, and one calmodulin (Galagan et al. 2003; Borkovich et al. 2004; Zelter et al. 2004; Tamuli et al. 2013). These 48 Ca^{2+} signaling proteins have been briefly described in Chapter 1. In the beginning of my work, information regarding the functions of Ca^{2+} signaling proteins in *N. crassa* was remained limited, mainly come from the studies using mutants of Ca^{2+} signaling genes generated through RIP, gene knockout, or inhibition mediated by RNA interference (RNAi) and antagonists. However, function of majority of Ca^{2+} signaling genes was not known in *N. crassa* or indeed, any other filamentous fungus. I had access to the published genome sequence of *N. crassa* and obtained large numbers of Ca^{2+} signaling knockout mutants. Therefore, I have decided to work on three broad objectives such as (i) to screen *N. crassa* Ca^{2+} signaling knockout mutants to identify the Ca^{2+} signaling genes involved in various cell functions, (ii) to understand the molecular mechanism of selected Ca^{2+} signaling gene by identifying the critical amino acid residues through site-directed mutagenesis approach, and (iii) to study the genetic interactions of selected Ca^{2+} signaling genes to determine their epistatic relationship.

TH-1227_09610609

Chapter 2 is about materials and methods used in my thesis work. I have obtained the Neurospora strains from Fungal Genetic Stock Centre (FGSC), Missouri, Kansas city, MO 64110, USA. Media and procedures for maintenance and crosses were essentially previously described by Davis and De Serres (1970). The detailed methods used such as cloning, PCR, RT-PCR, agarose gel electrophoresis, Southern hybridization etc. are essentially as described by Sambrook and Russell (2001) or as per the manufacturer's protocol.

Chapter 3 describes the screening of Ca^{2+} signaling knockout mutants to identify the Ca^{2+} signaling genes involved in various cell functions. I have shown that ΔNCU04379.2 mutant has a slow growth phenotype and an increased sensitivity to Ca^{2+} and ultraviolet (UV) stress than the wild type. To confirm NCU04379 gene function, I performed complementation analysis. A fragment carrying the NCU04379 gene complemented the slow growth, Ca^{2+} and UV sensitivity phenotype of ΔNCU04379.2 mutant. These results suggest that NCU04379 gene product is involved in growth, Ca^{2+} stress tolerance and UV-induced DNA damage repair pathways (Deka et al. 2011). This is the first report of the involvement of a Ca^{2+} signaling gene in UV-induced DNA damage repair process in *N. crassa*.

Chapter 4 describes the sequence analysis and site-directed mutational analysis of critical amino acid residues of the NCU04379 encoded protein. The NCU04379 gene encodes a Ca^{2+} and/or CaM binding protein of 190 amino acid residues (GenBank accession number EAA28220.1). BLAST analysis using NCU04379 protein sequence as a query sequence against the non-redundant protein databank in NCBI has revealed its sequence similarity to Neuronal Calcium Sensor-1 (NCS-1) homologues from other organisms such as NcsA in *Aspergillus fumigatus*, MgNCS-1 in *Magnaporthe grisea*, Frq1 in *Saccharomyces cerevisiae*, and NCS-1 in *Homo sapiens* (Deka et al. 2011; Tamuli et al. 2011). The NCU04379 encoded protein also possesses a consensus signal for N-terminal myristoylation and four EF-hand Ca^{2+}-binding sites like the NCS-1 homologues in *A. fumigatus*, *Danio rerio*, *H. sapiens*, *M. grisea*, *Mus musculus*, *S. cerevisiae*, *Schizosaccharomyces japonicus*, *S. pombe* and *Xenopus laevis.* A phylogenetic analysis with a subset of NCS-1 homologues from various organisms revealed that NCU04379 product is clustered with the Pezizomycotina clade. These results suggest that NCU04379 gene encodes a homologue of NCS-1 in *N. crassa* (Deka et al. 2011). In *S. cerevisiae*, Frq1 interacts with the target protein phosphatidylinositol-4-OH kinase (Pik1) (Hendricks et al. 1999; Huttner et al. 2003; Strahl et al. 2007).

TH-1227_09610609

To identify the critical amino acid residues of *N. crassa* NCS-1 homologue, I did the site-directed mutagenesis of some important residues of the NCS-1 protein. The N-terminal myristoylation site, more commonly a glycine residue, is the target for the attachment of myristoyl group derived from the myristic acid. The N- myristoylation targets the protein to the membrane and transduces signal downstream. I performed site-directed mutation of the glycine residue at position two of the NCS-1 homologue to alanine (G2A) in order to disrupt its membrane targeting. The G2A mutant of the NCS-1 homologue complements growth and Ca^{2+} sensitivity but the UV sensitivity phenotype of the Δ*ncs-1* mutant is not rescued by the G2A mutant. These results might indicate that the membrane targeting of NCS-1 is not essential for its role in growth, and Ca^{2+} stress tolerance but necessary for its involvement in UV induced DNA damage repair process in *N. crassa*. It was shown that upon binding to Ca^{2+} in the EF hand domains of Frq1 in *S. cerevisiae*, the protein changes its conformation by exposing its N- myristoylation sequence embedded in its hydrophobic pocket and targeted to membrane where it interacts with Pik1 (Strahl et al. 2007). The hydrophobic pocket of Frq1 also contains critical amino acids including the valine residue at position 175 that constitute the binding interface with Pik1 (Strahl et al. 2007). In the *N. crassa* homologue of NCS-1, arginine at position 175 replaces the valine in *S. cerevisiae* Frq1. To understand the functional significance of this arginine residue in NCS-1, I have changed the arginine to alanine (R175A). The *ncs-1*^{R175A} mutant allele complements the growth and Ca^{2+} sensitivity phenotype, and surprisingly, displayed greater UV sensitivity than the Δ*ncs-1* mutant. This might indicate the molecular basis of novelty of the NCS-1 protein for its involvement in UV-induced DNA damage and repair in *N. crassa*. Within the EF hand domain of the *N. crassa* homologue of NCS-1, there is a helix-loop-helix structural unit called EF hand loop formed by a stretch of 12 amino acid residues (D, D/T/I/K, C/D, P/K/G/E, S/S/D/N, G, M/T/K/S, L/I, T/D, K/F/Y/M, A/K/D, E). Ca^{2+} has high affinity for carboxylate oxygen present at negatively charged amino acids aspartate and glutamate. The EF hand loop is rich in negatively charged amino acids that bind Ca^{2+}. The loop's residues contribute individual and identifiable roles to both the stabilization and fold of the protein structure (Gifford et al. 2007). The residue at position 12 of the EF hand loop, mainly glutamate, is important for the stabilization of the open conformation of the protein upon binding to Ca^{2+}. Therefore, I have performed the site-directed mutation of this glutamate, which is present at position 120 of the NCS-1 in *N. crassa*, to glutamine (E120Q). The *ncs-1*^{E120Q} mutant allele has not shown complementation of either

TH-1227_09610609

the growth defect or the Ca^{2+} and UV sensitivity phenotypes of the Δ*ncs-1* mutant. Therefore, these results suggest that Ca^{2+} binding is essential for the NCS-1 function.

Chapter 5 describes the genetic interaction of *ncs-1* with other Ca^{2+} signaling genes that are selected on the basis of exhibiting cell functions similar to the *ncs-1* gene. One of the Ca^{2+} signaling genes, NCU04736 encodes NCA-2, a PMCA type Ca^{2+} ATPase, which plays a major role in pumping Ca^{2+} out of the cell as evidenced by the accumulation of 4-to 10 fold more Ca^{2+} in the Δ*nca-2* mutant. In addition, the Δ*nca-2* mutant grows slowly in Vogel's medium and displays sensitivity to high concentration of Ca^{2+} (Bowman et al. 2011). Another Ca^{2+} signaling gene NCU06703 encodes a stretch-activated Ca^{2+} permeable channel MID-1 that regulates passive flow of Ca^{2+} across the membrane. The absence of MID-1 protein makes the fungus unable to response normally to low extracellular or high intracellular Ca^{2+} levels (Lew et al. 2008). In *S. pombe*, Ncs1p, the homologue of NCS-1, promotes Ca^{2+}-induced closure of Ca^{2+} channel Yam8p, a homologue of MID1. The Ca^{2+}-sensitive phenotype of the *ncs-1* deletion mutant is rescued by a *yam8* deletion, indicating that Ncs1p negatively regulates Yam8p in *S. pombe* by minimizing Ca^{2+}- influx under extreme external conditions (Hamasaki-Katagiri and Ames 2010). However, no information is available regarding the interaction between NCS-1 and MID-1 in *N. crassa*. To understand the genetic interaction among *ncs-1*, *nca-2* and *mid-1* Ca^{2+} signaling genes in *N. crassa*, I have generated the double mutants of these genes and studied their phenotypes. The Δ*ncs-1*Δ*nca-2* double mutant shows distinct swollen sponge-like colony morphology, slow growth phenotype, short aerial hyphae, reduction in carotenoid accumulation, insensitivity to the respiratory byproduct CO_2 and conidial bands in race tube till 72 h. Moreover, the *Δncs-1Δnca-2* double mutant displayed severe sensitivity to Ca^{2+} and UV than their parental single mutants, indicating the negative interaction of *ncs-1* and *nca-2*. In addition, the Δ*ncs-1*Δ*mid-1* double mutant accumulates more carotenoids than the wild-type and the single mutants, produces robust and distinct conidial bands with increased period length of 25.41 ± 0.48 h, which is longer than the *ras-1*^{bd} control that is insensitivity to respiratory byproduct CO_2 and shows a period length of 22.48 ± 0.72; therefore, this result indicates the insensitivity of the Δ*ncs-1*Δ*mid-1*double mutant to respiratory byproduct CO_2. Moreover, in Δ*mid-1* mutant growth is stimulated on the medium supplemented with 0.2 M Ca^{2+} supplement; interestingly, stimulation of the growth is synthetically suppressed in the Δ*ncs-1*Δ*mid-1* double mutant. Besides, Ca^{2+} sensitivity phenotype of the Δ*ncs-1* mutant is not fully rescued by the Δ*mid-1*

TH-1227_09610609

mutant, indicating that the relationship between *ncs-1* and *mid-1* genes are not the same in *N. crassa* as their homologues in *S. pombe*. The UV sensitivity phenotype of the Δ*ncs-1*Δ*mid-1* double mutant is comparable to its single mutants. In Δ*mid-1*Δ*nca-2* double mutant, stimulation of the growth at 0.2 M $CaCl_2$ has been completely disappeared. This could explain the epistasis of the *nca-2* over *mid-1* for Ca^{2+} sensitivity. The Δ*mid-1*Δ*nca-2* double mutant is more tolerant to UV than either of the single mutants. The Δ*mid-1*Δ*nca-2* double mutant also shows more carotenoid production as compared to the wild-type and other single and double mutants tested, and produces distinct conidial bands in race tube with an increased period length of 23.96 ± 0.58 h, indicating its increased insensitivity to respiratory byproduct CO_2. Moreover, the conidial bands in the *Δncs-1Δnca-2*, *Δncs-1Δmid-1*, and *Δmid-1Δnca-2* double mutants are suppressed by the addition of the antioxidant N-acetyl-L-cysteine (NAC) in the medium that scavenges reactive oxygen species (ROS). These results indicate that *ncs-1*, *mid-1*, and *nca-2* gene products synthetically act as negative regulators of circadian regulated conidiation and ROS was possibly increased in the double mutants of these genes. Thus, I have shown that genetic interactions of *ncs-1*, *mid-1*, and *nca-2* regulate multiple cellular processes in *N. crassa* (Deka et al. 2013).

The additional results of my thesis work have been described in appendix. Here, I describe the expression analysis of few selected Ca^{2+} signaling genes. I have studied the relative expression of *ncs-1*, *mid-1*, and *nca-2* genes in response to Ca^{2+} stress using real time PCR analysis. Moreover, I have also studied the relative expressions of the NCU06366 and NCU07952 genes, encode a Ca^{2+}/H^{+} exchanger and the *N. crassa* homologue of Crz1p (GenBank accession number, EAA32849), respectively. The relative expression study indicates a complex interaction of *ncs-1*, *mid-1*, and *nca-2* in response to Ca^{2+} stress tolerance.

TH-1227_09610609

CHAPTER 1

An introduction to Neurospora crassa and calcium signaling

TH-1227_09610609

1.1 Introduction to the model organism *Neurospora crassa*

The ascomycete, filamentous fungus *Neurospora crassa* is used as an ideal model organism for several decades for the study of genetics, biochemistry, and molecular biology. Neurospora is usually referred as orange bread mold and originally discovered and categorized in 1843 as the causative agent of an orange mold infestation in French bakeries (Payen 1843; Perkins 1991). Thereafter, in mid-1920s, Dodge and Shear performed variety of experiments on *Neurospora*. They identified *N. crassa* and *N. sitophila* as heterothallic species with eight-spored asci (Shear and Dodge 1927). During the 1930's, Bernard Dodge together with Carl Lindegren, discovered the segregation patterns of mating type *A* and *a* in *Neuropora* asci. Thus, they developed the genetics of *Neurospora* and made the organism known to geneticists. In 1939, Dodge asserted that "the fungi in their reproduction and inheritance follow exactly the same laws that govern these activities in higher plants and animals" (Dodge 1939; Perkins 1992). In 1941, George Beadle and Edward Tatum introduced the concept of 'one gene, one enzyme' hypothesis using *N. crassa* as an experimental organism (Beadle and Tatum 1941). In 1958, Beadle and Tatum were awarded the Nobel Prize in Physiology or Medicine for their discovery that the characteristic function of the gene was to control the synthesis of a particular enzyme.

As a primary model organism, *N. crassa* has contributed significantly to the understanding of numerous biological processes such as the genome defense, DNA methylation, mitochondrial protein import, circadian rhythms, post-transcriptional gene silencing and DNA repair (Galagan 2003). Thus, till date, diverse researches in *N. crassa* have greatly enriched the knowledge of filamentous fungal life style and of eukaryotes in general. Moreover, *Neurospora* possesses a wide array of environmental sensory capabilities and therefore, serves as an outstanding model organism for investigations of signaling such as signaling mediated by G-protein-coupled receptors (GPCRs), signaling mediated by mitogen-activated protein kinase (MAPK), and signaling mediated by intracellular calcium.

N. crassa is a multicellular haploid organism (Figure 1.1). Its genome size is 43 Mb, divided into seven linkage groups (LG I-VII, size ranges from 4 to 10.3 Mb each) and contains 10,082 protein coding genes. *N. crassa* has a simple, heterothallic, haploid life cycle and depending on growth conditions, it propagates asexually or reproduces sexually (Figure 1.2). The two mating types are determined by alternative DNA sequences called idiomorphs,

TH-1227_09610609

at the mating type locus called *mat A* and *mat a.* Briefly, in the asexual part of the life cycle, conidia are formed following mitosis of the haploid nuclei. Germination and growth of a haploid asexual spore (conidium) results in a mass of branched threads called hyphae, which constitute a colony. Hyphae have no cross walls, therefore, a colony is essentially a single cell containing many haploid nuclei. A colony buds off millions more conidia from aerial hyphae, the multinucleate macroconidia and uninucleate microconidia, which disperse and repeat the asexual cycle upon landing on a suitable if they land on a suitable substrate. The sexual phase is triggered by nitrogen limitation. During the sexual phase, the *mat A* and *mat a* mycelia come into contact and their fusion results in fertilization. After fertilization, the *A* and *a* nuclei do not fuse immediately but proliferate as a dikaryon in specialized structures called ascogenous hyphae. In the final few divisions, nuclei of the opposite mating type are paired and they undergo conjugate divisions (synchronous divisions). The last conjugate division before karyogamy occurs in a binucleate hook-shaped structure called crozier. Nuclei of the opposite mating types fuse during the karyogamy event to form a diploid zygote. The diploid zygote nucleus immediately undergoes two meiotic divisions and a postmeiotic mitosis in the common cytoplasm of the ascus. The resulting eight haploid nuclei are then sequestered into an octad of eight spindle-shaped ascospores, which are held in linear order in the narrow ascus. Ascospores become multinucleate and pigmented on maturation. Several thousands of ascospores are produced in a cross. Ascospores germinate following heat shock and the emerging hyphae resume the vegetative phase of the life cycle.

TH-1227_09610609

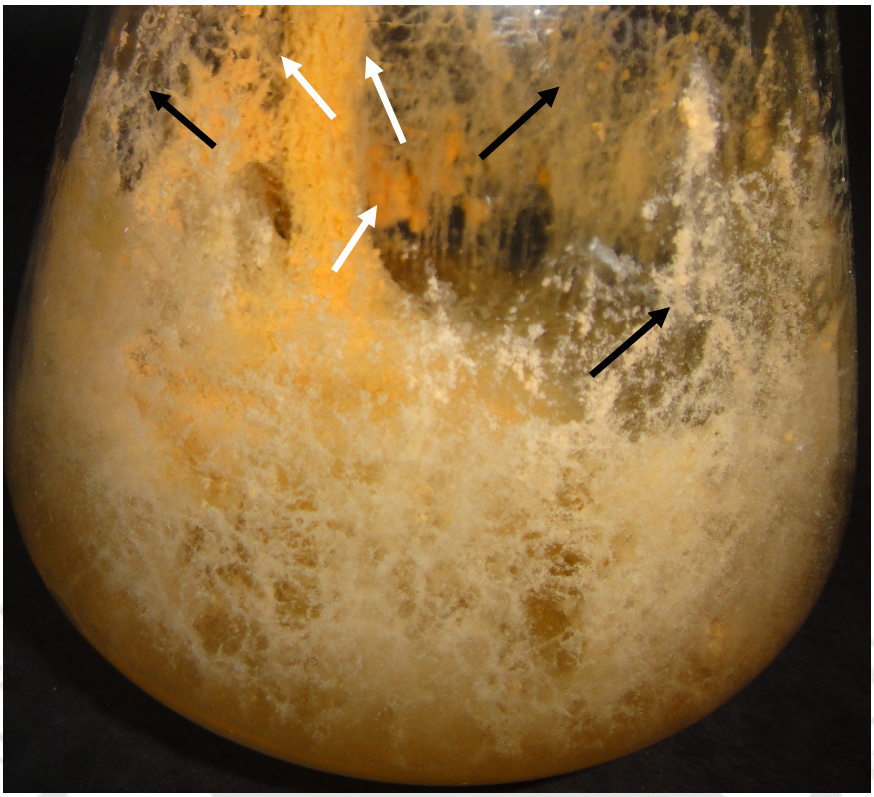

Figure 1.1: Morphology of *Neurospora crassa*. A wild-type strain of *N. crassa* (FGSC 987) was grown on Vogel's glucose agar medium for five days at 30°C in 250 ml conical flask. Black arrows indicate the aerial hyphae that are attached to the walls of the flask growing from the surface of the agar medium. White arrows indicate conidia (macroconidia and microconidia that are indistinguishable in the image) that are produced from aerial hyphae. The deep orange-pigmentation of conidia is due to the accumulation of carotenoid pigment called xanthophyll neurosporaxanthin and various amounts of precursor carotenoids that give characteristic orange colour to conidia and mycelia, and thus whole strain appears orange. Image was taken using a Nikon COOLPIX S6300 digital camera in the *Neurospora* laboratory, Department of Biotechnology, IIT Guwahati.

TH-1227_09610609

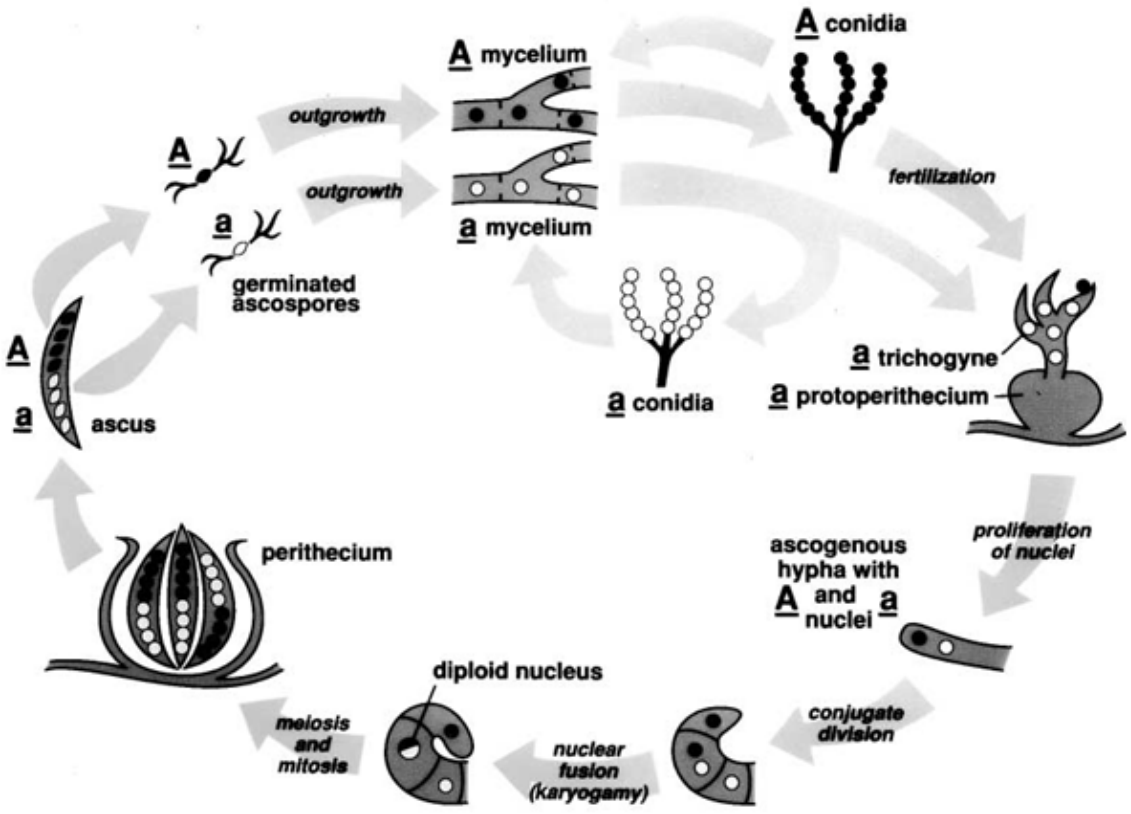

Figure 1.2: The life cycle of a heterothallic fungus *Neurospora crassa*. In the asexual cycle, the vegetative mycelium develops into aerial hyphae and produces conidia, which form new mycelium on germination (A conidia develops into A mycelium and a conidia develops into a mycelium). The sexual cycle is shown with the formation of the protoperithecium (formed in a mycelium in this example), its fertilization via its trichogyne by a conidium of the opposite mating type (A conidia in this example), and the later events culminating in the formation of ascospores. Adapted from Shiu et al. (2001).

In the following part of the Chapter, I discussed the current understanding of calcium signaling in fungi including *N. crassa*.

TH-1227_09610609

1.1.1 Calcium ion is a versatile and a ubiquitous signaling molecule

Calcium ion (Ca^{2+}) is one of the most versatile intracellular second messengers that is involved in regulating wide variety of cellular processes and adaptive responses. A feature that makes Ca^{2+} such a versatile ion in signaling is the ability of the cell to precisely regulate the cellular concentrations of free and sequestered Ca^{2+} both in time and space (Campbell 1983; Berridge et al. 2000; Sanders et al. 2001). But why is Ca^{2+}, the only ion among various inorganic ions (H^+, Na^+, K^+, Mg^{2+}, Ba^{2+}, Zn^{2+}) in the environment acquired a special status? Ca^{2+} was the most abundant ion in igneous rocks present in the earth's hot crust and was unavailable for use by living matter. It was through various chemical and biological reactions during cooling of earth that caused the extracellular free Ca^{2+} levels to rise in the environment (Jaiswal 2001). The rise of Ca^{2+} in the environment put tremendous pressure on the cell as Ca^{2+} at high concentration cause precipitation of the phosphates necessary for the energy transactions in the cell, organellar damage, aggregation of proteins and nucleic acids. These events would cause instant death of the cell. Therefore, it was essential for cells to contain Ca^{2+} in a manner that it was no longer harmful (Jaiswal 2001). This could have been the basis for the selective pressure that led to the evolution of Ca^{2+} pumps and internal Ca^{2+} stores, by which cells could maintain their cytosolic free Ca^{2+} ($[Ca^{2+}]_c$) within the tolerable range. The presence of Ca^{2+} pumps and various Ca^{2+} stores in the cell (vacuoles, endoplasmic reticulum, and mitochondria) could be a feature that contributed to the use of this ion as a messenger (Jaiswal 2001). The ubiquitous role of Ca^{2+} lies in its chemistry that involves its molecular structure, balance state, binding strength, ionization potential, and kinetic parameters in the biological reactions. The Ca^{2+} ion typically exhibits high coordination numbers (6–8) and can accommodate 4-12 oxygen atoms in its primary coordination sphere. The coordination geometry of Ca^{2+} is often irregular (i.e. protein induced) due to its favourable ionic radius (100–120 pm) and its electronic structure (Swain and Amma 1989; Carugo et al. 1993; Jaiswal 2001). Typically, Ca^{2+} ion is coordinated by 6-7 oxygen atoms in a pentagonal bipyramidal manner or in a trigonal manner (Swain and Amma 1989; Figure 1.3). The Ca^{2+} ion has maximum affinity for carboxylate oxygen and interestingly, acidic amino acids like aspartic acid and glutamic acid that contain the carboxylate oxygen occur more frequently in proteins. The Ca^{2+} that flows into the cytoplasm through channels does not remain free and binds to a wide variety of Ca^{2+} binding proteins ranging from channel voltage sensors to DNA binding proteins through a characteristic helix-loop-helix structural motif termed the EF-hand domain (Nakayama and Kretsinger 1994; Clapham 2007; Gifford et al. 2007). In EF hand helix-turn-helix motifs,

TH-1227_09610609

negatively charged oxygen atoms cradle Ca^{2+} within a 12 amino acid loop between two α-helices (Figure 1.4 A). The EF hand containing proteins provide the required coordinate chemistry of Ca^{2+}, the most preferable is the pentagonal bipyramidal geometry (Figure 1.4 B). The capacity of Ca^{2+} to bind and dissociates from a protein is 100-fold or so faster than Mg^{2+} due to its high rate of water exchange of metal aquo-complexes; such a rate (in units of s^{-1} at 25°C) has been found to be 10^8 for Ca^{2+}, 7×10^5 for Mg^{2+} (Ochiai 1991; Jaiswal 2001).

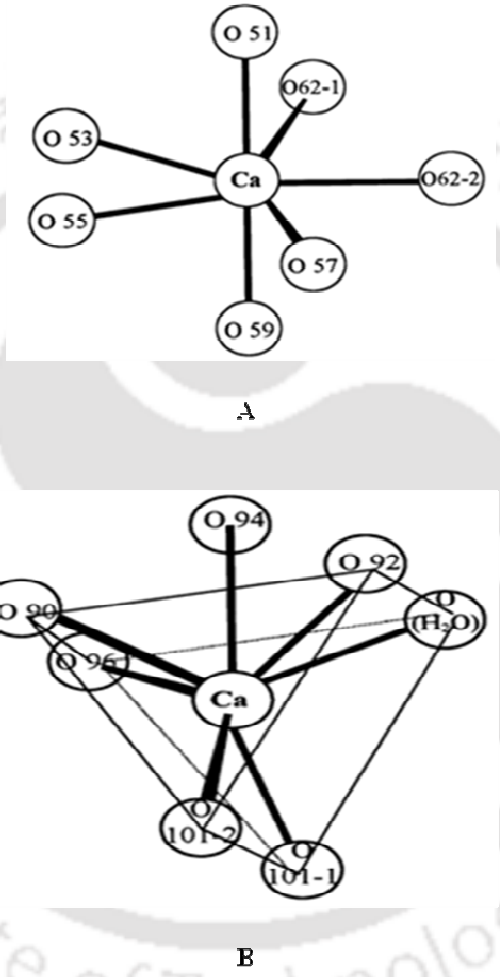

Figure 1.3: The coordination polyhedron of the Ca^{2+} ion. **(A)** Pentagonal bipyramidal coordination geometry of Ca atom in CD domain of a parvalbumin. **(B)** Monocapped trigonal prism in the EF hand site of Ca atom in parvalbumin. Adapted from Swain and Amma (1989).

TH-1227_09610609

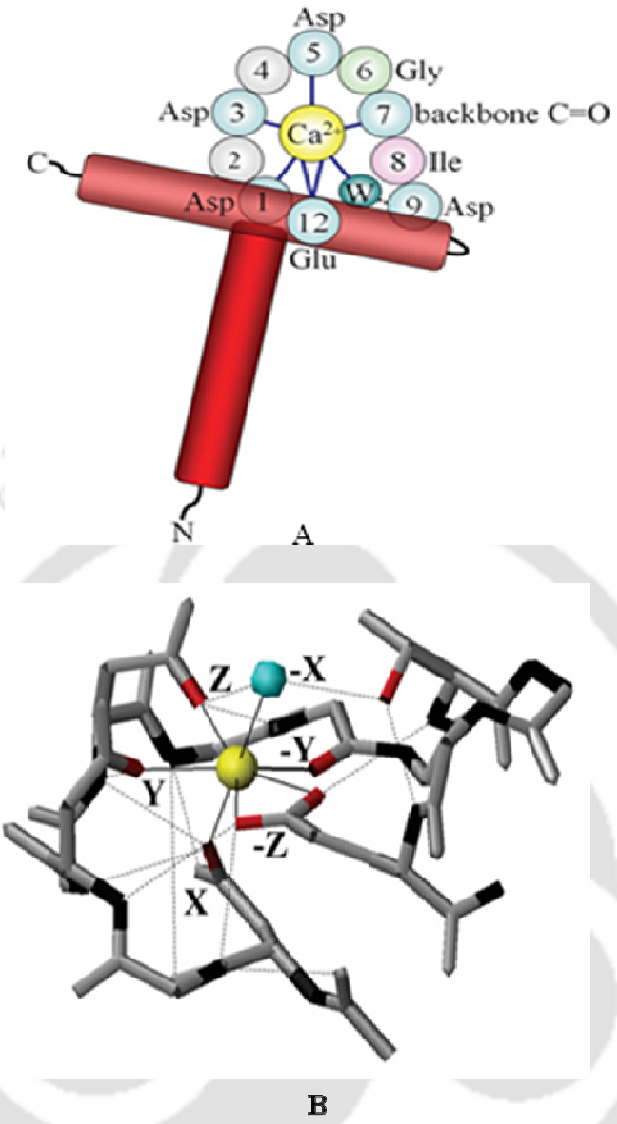

Figure 1.4: The coordination sphere of the EF hand loop. **(A)** A schematic diagram of the Ca^{2+} co-ordination sphere with the two α helices in red, the co-ordinating protein ligands in blue and co-ordinating water molecule (W) in dark blue. Light green corresponds to the conserved glycine residue that provides the bend in the loop. Purple highlights the conserved hydrophobic residue that forms the short *β*-sheet in the paired EF-hand. Most common amino acids found at the critical positions are also indicated. **(B)** Ca^{2+} co-ordination by the canonical EF-hand domain 1 of calmodulin that illustrates both the pentagonal bipyramidal co-ordination of the Ca^{2+} ion (continuous lines) and the extensive hydrogen bonding pattern found in the loop (broken lines). Adapted from Gifford et al. (2007).

TH-1227_09610609

1.1.2 Overview of Ca^{2+} signaling in fungi

Ca^{2+} signaling is an important regulatory mechanism in all eukaryotic cells for a wide variety of cellular processes such as growth, metabolism and differentiation. Therefore, Ca^{2+} signaling process, affects every aspect of a cell's life and death. The control of intracellular Ca^{2+} homeostasis in eukaryotic cells is the result of a strict cooperation among the different cellular compartments and organelles (Cerella et al. 2010). Small changes in $[Ca^{2+}]_c$ levels can activate various Ca^{2+} sensing proteins, which then lead to the induction of various downstream signal transduction pathways. Excess or deregulated $[Ca^{2+}]_c$ is toxic to the cell producing an intrinsic stress leading to cell death (Kaiser and Edelman 1977, 1978; De Leiris and Boucher 1990; Ritcher 1993; Qian et al. 1999; Cerella et al. 2010). Therefore, cellular Ca^{2+} levels are tightly controlled by a diverse set of Ca^{2+} channels, pumps, transporters and calcium binding proteins. The resting level of $[Ca^{2+}]_c$ is kept very low, typically 100-350 nM in fungi (Iida et al. 1990a; Miller et al. 1990; Halachmi 1989), 100-200 nM in plant cells (Gilroy et al. 1987; Johannes et al. 1991) and 100-200 nM in animal cells (Carafoli 1987). To provide for a very fast and effective Ca^{2+}-signaling, the cells use a great amount of energy to maintain almost 20,000-fold Ca^{2+}-gradient between their intracellular (~100 nM) and extracellular (~ 1.2 mM) Ca^{2+} concentrations. To maintain this Ca^{2+} gradient, the cells chelate, compartmentalize, or remove Ca^{2+} from the cytoplasm (Clapham 2007). In fungi, vacuoles are the major storage for intracellular Ca^{2+} (Cornelius and Nakashima 1987; Halachmi and Eilam 1989).

In filamentous fungi, growth pattern and development process are more complex than lower fungi and there is evidence for the involvement of Ca^{2+} in far more physiological processes including cell cycle, circadian rhythms, cytoskeletal organization, hyphal branching, hyphal orientation, hyphal tip growth, infection structure differentiation, sporulation and spore germination (Gadd 1994; Shaw and Hoch 2001). In *Saccharomyces cerevisiae* Ca^{2+} regulates several cell processes such as growth, cell proliferation, cell cycle control and cytokinesis. The deprivation of Ca^{2+} first inhibits the initiation of bud emergence and DNA synthesis and then inhibits S and G2/M traverses (Iida et al. 1990b). A stretch-activated Ca^{2+} channel protein MID-1 in *S. cerevisiae* is required for Ca^{2+} influx for successful mating (Iida et al. 1994). The *mid-1* mutant loses viability after receiving mating pheromones. In *Schizosaccharomyces pombe*, Ca^{2+} ATPase homologue Pmr1p is essential for cell wall integrity and is required for polarized cell growth and cytokinesis by allowing

TH-1227_09610609

protein glycosylation and the polarized actin distribution to take place normally (Cortés et al. 2004). In addition, deletion of a calcineurin A homologue *ppb1+* in *S. pombe* results in severe morphological and developmental abnormalities, such strains are sterile and exhibit defects in cytokinesis and cell shape (Yoshida et al. 1994). Ca^{2+} signaling is also involved in fungal virulence and pathogenicity. One of the Ca^{2+} transporter *pmcA* in *Aspergillus fumigatus*, which infect human lungs, plays a role in virulence and pathogenicity via Ca^{2+}/ calcineurin signaling pathway (Dinamarco et al. 2012). Calcineurin dephosphorylates a transcription factor called Crz1p upon an increase in $[Ca^{2+}]_c$, allowing nuclear translocation of dephosphorylated Crz1p where it upregulates the transcription of Ca^{2+} transporters to combat the toxicity of high level of $[Ca^{2+}]_c$ (Soriani et al. 2008, 2010). In another human pathogenic fungus *Crptococcus neoformans,* the vacuolar Ca^{2+} exchanger VCX1 is involved in Ca^{2+} tolerance and virulence through calcineurin; however, CRZ1 homologue has not been identified in this fungus (Kmetzsch et al. 2010). In *Magnapothe oryzae* that causes rice blast in plants, deletion of phosphalipase C -1 (MoPLC1) suppresses Ca^{2+} influx causing the fungus defective in developmental steps, including appressorium formation and pathogenicity (Rho et al. 2009). In another plant pathogen, *Fusarium graminearum*, the causal agent of head blight of wheat and barley, Ca^{2+} signaling has been shown to have a role in hyphal growth, sporulation, and fruiting body function. FIG1, a transmembrane low affinity Ca^{2+} channel protein in *F. graminearum* plays role in sexual development, and *fig1* deletion causes complete arrest of perithecia formation (Cavinder and Trail 2012. In *Giberella zeae,* two Ca^{2+} channels, MID1 and CCH1 are involved in ascospore discharge (Cavinder et al. 2011; Hallen and Trail 2008). The Δ*cch1* mutant displays slower vegetative growth rates, abnormal sexual and ascospore development, and reduced ascospore discharge. The Δ*mid1* mutant grows slightly slower, discharge ascospores at a slightly higher level and develops abnormal ascospores with much greater frequency than the Δ*cch1* mutants. In *Claviceps purpurea* that infect rye plant, the homologue of *S. cerevisiae* MID1 plays a role in vegetative growth, differentiation and pathogenicity on rye. The *C. purpurea* loses complete virulence on *mid-1* deletion (Bormann and Tudzynski 2009). In two entomopathogenic fungi, *Beauveria bassiana* and *Metarhizium acridum*, the homologue of Neuronal Calcium Sensor-1, Bbcsa1 and MaNcs1 respectively plays role in virulence and pathogenicity of the fungus towards insects (Fan et al. 2012; Min and Yueqing 2012). The Bbcsa1 protein participates in pre-penetration or early penetration events during the host infection. Thus, Ca^{2+} signaling is involved in many cellular processes in fungi; however, the detailed knowledge about the Ca^{2+} signaling mediated pathways is still unknown for any of the fungus.

Ca^{2+} signaling has also been extensively studied in higher organisms including human especially with respect to development and disease. The deregulation of Ca^{2+} mediated signaling was shown to associate with many pathologic conditions. Previous studies had show that defects in recoverin cause degeneration of retina, disruption of the muscle isoform p94 (Calpain III) causes limb girdle muscular distrophy type 2A, and genetic variations in the Ca^{2+} binding C-terminal domain of Calpain 10 favors the onset of type 2 diabetes (Richard et al 1995; Horikawa et al. 2000). In addition, the hearing loss in humans was found to be associated with PMCA2, a Ca^{2+}-ATPase pump, defects (Street et al 1998). Moreover, several neurodegenerative diseases and psychiatric diseases are linked to the dysregulation or subtle alterations in Ca^{2+} signaling pathways such as in Alzhiemer's disease, Schizophrenia and Bipolar disorders (Woods and Padmanabhan 2012, Berridge 2013). The Neuronal calcium sensor-1 (NCS-1), a Ca^{2+} signaling protein interacts with dopamine receptor, was found to be upregulated in Schizophrenic and Bipolar patients (Koh et al 2003). Handley et al. (2010) discovered a single mutation in human NCS-1 substituting R102 for glutamine (R102Q) in a patient suffering from autistic spectrum disorder. The substitution in the NCS-1^{R102A} variant affects the structural and dynamical features of the C-terminal tail of NCS-1, and therefore leads to the loss of the Ca^{2+}-dependent cycling of NCS-1 between cytosol and plasma membrane.

1.1.3 Calcium signaling machinery in *N. crassa*

The filamentous fungus *N. crassa* has been established as an excellent eukaryotic model organism that can be utilized to investigate the complex Ca^{2+} signaling processes. *N. crassa* has 48 Ca^{2+} -signaling proteins that comprises of three Ca^{2+} channel proteins, nine Ca^{2+}/cation-ATPases, six recognizable Ca^{2+}/H^{+} exchangers, two novel putative Ca^{2+}/Na^{+} exchangers, four novel phospholipase C-δ subtype (PLC-δ) proteins, 23 Ca^{2+}/calmodulin-regulated proteins, and one calmodulin (Figure 1.5, Table 1.1; Borkovich et al. 2004; Tamuli et al. 2013). The Ca^{2+} signaling machinery in *N. crassa* is unique in that it lacks receptors for second messengers such as inositol-1,4,5-trisphosphate ($InsP_3$), ryanodine and cyclic ADP ribose (cADPR) that are responsible for Ca^{2+} release from internal stores in other organisms (Berridge et al. 2000; Sanders et al. 2001; Bootman et al. 2001). $InsP_3$ is synthesized by phospholipase C-δ subtype (PLC- δ) proteins. These proteins are identified in Neurospora as well as in other filamentous fungi; however, signaling via $InsP_3$ receptor is still unclear since no recognizable $InsP_3$ receptors have been identified in *Neurospora* (Borkovich et al. 2004).

TH-1227_09610609

In addition, ADP-ribosyl cyclase protein that synthesizes second messengers cADP ribose or NAADP and ryanodine receptor which are the key components of Ca^{2+} release mechanisms in animal cells are not known in *Neurospora* and other fungi. Furthermore, no homologues of either sphingosine kinase that synthesizes the second-messenger sphingosine- 1-phosphate, or the sarcoplasmic reticulum Ca^{2+} release channel, SCaMPER, which is a possible target for sphingolipids could be identified in *N. crassa* (Figure 1.6). In addition, Ca^{2+}/Na^{+} exchangers and Ca^{2+}/H^{+} exchangers are identified in *N. crassa* whereas animals possesses only Ca^{2+}/Na^{+} exchangers and plants possesses only Ca^{2+}/H^{+} exchangers. These notable differences suggest that filamentous fungi might possess novel intracellular Ca^{2+} release mechanisms that remain to be identified. Knowledge about the novel intracellular Ca^{2+} release mechanisms in filamentous fungi might be helpful in identifying novel antifungal targets for drug discovery.

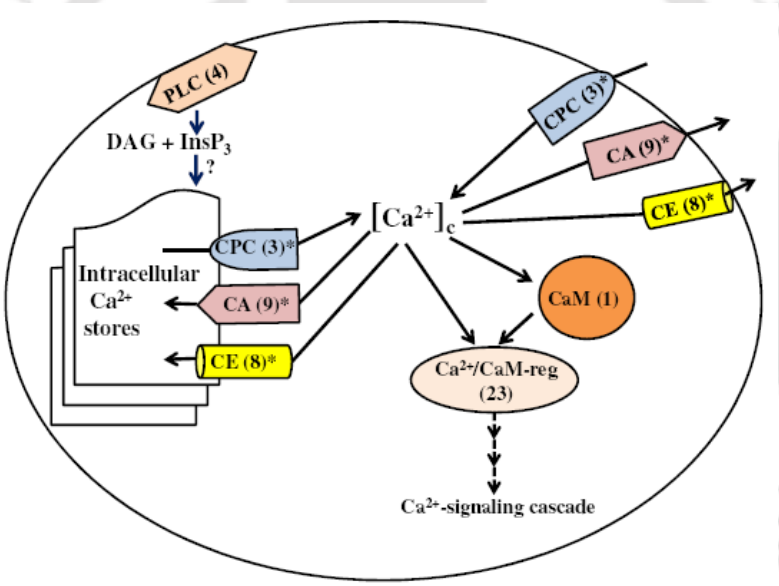

Figure 1.5: Overview of calcium signaling system in *N. crassa*. The Ca^{2+} signaling proteins are CPC, Ca^{2+}-permeable channel; CA, Ca^{2+}-and cation-ATPases; CE, Ca^{2+}/H^{+} and Ca^{2+}/Na^{+} exchanger; CaM, calmodulin; Ca^{2+}/CaM-reg, calcium- and calmodulin regulated; and PLC, phospholipase C. The intracellular second messenger molecules diacylglycerol (DAG) and inositol-1,4,5-trisphosphate ($InsP_3$) are also shown. Minute change in $[Ca^{2+}]_c$ may lead to a Ca^{2+} signaling cascade via Ca^{2+}/CaM-reg proteins. Numbers in parentheses indicate the number of genes identified in that class and asterisk indicates that the location in the plasma membrane and/or organelle membranes are not determined (Galagan et al. 2003; Borkovich et al. 2004; Zelter et al. 2004). Adapted from Tamuli et al. (2013).

TH-1227_09610609

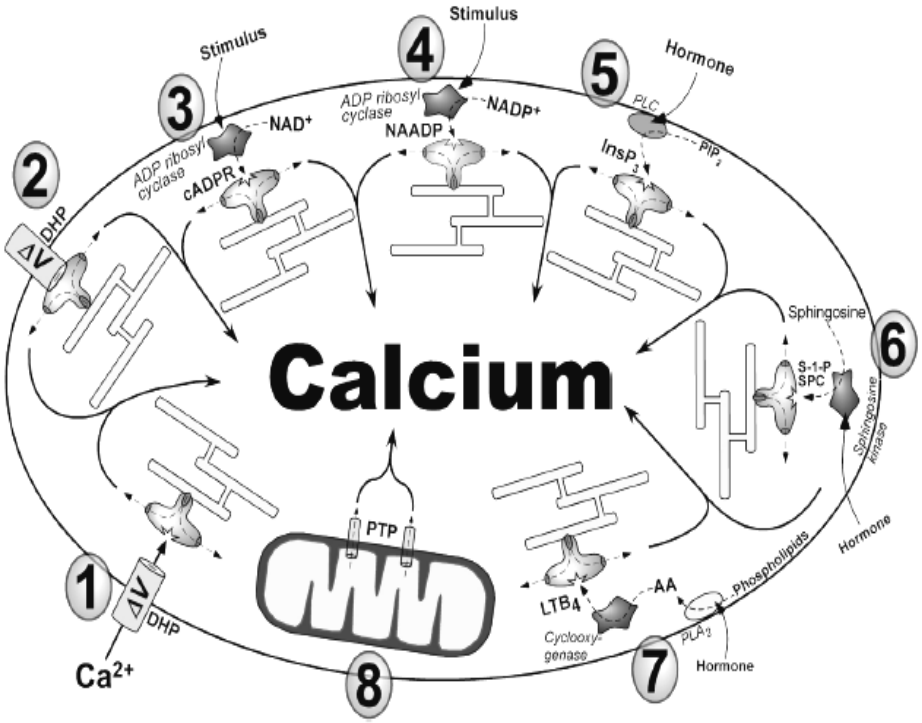

Figure 1.6: Mechanisms of Ca^{2+} release depicting the major pathways for mobilising Ca^{2+} from internal stores. The major pathways are: 1, Ca^{2+}-induced Ca^{2+} release from Ryanodine receptors (RyRs) caused by the influx of Ca^{2+} through Voltage operated Ca^{2+} Channels (VOCCs) on the PM; 2, activation of RyRs by direct protein-protein interaction; 3, cyclic ADP ribose(cADPR)-evoked Ca^{2+}- release; 4, Nicotinic acid adenine dinucleotide phosphate (NAADP)-evoked Ca^{2+} release; 5, $InsP_3$-evoked Ca^{2+}release; 6, Ca^{2+} release evoked by sphingolipids; 7, Leukotriene B4 (LTB4)-evoked Ca^{2+}release; 8, Ca^{2+} release from mitochondrial following activation of the PTP. Adapted from Bootman et al. (2001).

TH-1227_09610609

Table 1.1[a] Calcium signaling proteins in *Neurospora crassa*

S. no.	NCU no.	Name	Type of protein	Best overall (*e*-value; organism; protein name; accession number)
1.	02762.5		Ca^{2+} permeable channel	0; *Verticillium dahlia*; cch1, EGY18507.1
2.	06703.5		Ca^{2+} permeable channel	2*e*-97; *Paracoccidioides brasiliensis*; MID1, EEH23338.1
3.	11680.5[b]		Ca^{2+} permeable channel	0; *Ajellomyces dermatitidis*; Yvc1, EGE78766.1
4.	03305.5	NCA1	Ca^{2+} -ATPase	0; *Trichophyton tonsurans*; SCA-1, EGD96734.1
5.	04736.5	NCA2	Ca^{2+} -ATPase	0; *Magnaporthe oryzae*; Plasma membrane calcium-transporting ATPase 3, EHA56671.1
6.	05154.5	NCA3	Ca^{2+} -ATPase	0; *Glomerella graminicola*; Calcium-translocating P-type ATPase, EFQ29373.1
7.	03292.5	PMR1	Ca^{2+} -ATPase	0; *Uncinocarpus reesii*; PMR1, XP_002541437.1
8.	08147.5	PH-7	Ca^{2+} -ATPase	0; *Glomerella graminicola*; Potassium/sodium efflux P-type ATPase, EFQ36596.1
9.	04898.5		Ca^{2+} -ATPase	0; *Cordyceps militaris* (Cation-transporting ATPase 4, EGX91104.1)
10.	03818.5		Ca^{2+} -ATPase	0; *Verticillium dahliae*; Neo1p, EGY18069.1
11.	07966.5		Cation-ATPase	0; *Trichophyton tonsurans*; Cta3p, EGD97988.1
12.	10143.5[c]		Cation-ATPase	0; *Cordyceps militaris*; ATPase type 13A2, EGX92563.1
13.	07075.5	CAX	Ca^{2+}/H^{+} exchanger	0; *Glomerella graminicola*; Calcium/proton exchanger, EFQ30300.1
14.	00916.5		Ca^{2+}/H^{+} exchanger	2*e*-176; *Aspergillus fumigatus*; Membrane bound cation transporter,

TH-1227_09610609

				XP_001481534.1
15.	00795.5		Ca^{2+}/H^{+} exchanger	1e-149; *Aspergillus niger*; Membrane bound cation transporter, XP_001400827.2
16.	06366.5		Ca^{2+}/H^{+} exchanger	0; *Sclerotinia sclerotiorum*; Ca^{2+}/H^{+} antiporter, XP_001589752.1
17.	07711.5		Ca^{2+}/H^{+} exchanger	4*e*-160; *Trichophyton tonsurans*; Vacuolar calcium ion transporter/H^{+} exchanger, EGD98067.1
18.	05360.5		Ca^{2+}/H^{+} exchanger	0; *Metarhizium anisopliase*; Calcium permease, EFY95914.1
19.	02826.5		Ca^{2+}/Na^{+} exchanger	0; *Verticillium albo-atrum*; Sodium/calcium exchanger protein, XP_003004985.1
20.	08490.5		Ca^{2+}/Na^{+} exchanger	1*e*-83; *Aspergillus niger*; Sodium/calcium transporter, XP_001397155.1
21.	01266.5		Phospholipase C	0; *Sordaria macrospora*; Phosphoinositide-specific phospholipase C, XP_003348116.1
22.	06245.5	PLC-1	Phospholipase C	0; *Glomerella graminicola*; Phosphatidylinositol-specific phospholipase C, EFQ28596.1
23.	11415.5[d]		Phospholipase C	0; *Glomerella graminicola* ; Phosphatidylinositol-specific phospholipase C, EFQ31595.1
24.	02175.5		Phospholipase C	3*e*-125; *Botryotinia fuckeliana*; BcPLC2, CCD34776.1
25.	04120.5	CaM	Calmodulin	1*e*-103; *Gibberella zeae*; CaM, XP_382067.1
26.	03804.5	CNA-1	Calcineurin catalytic subunit	0; *Sordaria macrospora*; Serine/threonine-protein phosphatase 2B catalytic subunit protein, XP_003352213.1

TH-1227_09610609

27.	03833.5	CNB-1	Calcineurin regulatory subunit /variant	2*e*-119; *Trichoderma reesei*; Calcineurin, beta subunit, EGR44907.1
28.	09265.5		Calnexin	0; *Sordaria macrospora*; cnx1, XP_003347545.1)
29.	05225.5[e]		Ca^{2+} and/or CaM binding protein	0; *Magnaporthe oryzae*; Mitochondrial NADH dehydrogenase, EHA47323.1
30.	02115.5		Ca^{2+} and/or CaM binding protein	0; *Magnaporthe oryzae*; EF hand domain-containing protein, EHA48778.1
31.	01564.5		Ca^{2+} and/or CaM binding protein	0; *Magnaporthe oryzae*; Calcium dependent mitochondrial carrier protein, EHA48778.1
32.	06948.5		Ca^{2+} and/or CaM binding protein	2*e*-54; *Mycosphaerella graminicola*; Calcium ion binding, calmodulin, EGP88834.1
33.	04379.5	NCS-1	Ca^{2+} and/or CaM binding protein	4*e*-126; *Grosmannia clavigera*; Neuronal calcium sensor 1, EFX03580.1
34.	02738.5	PEF-1	Ca^{2+} and/or CaM binding protein	2*e*-130; *Verticillium dahliae*; Peflin, EGY21808.1
35.	09871.5		Ca^{2+} and/or CaM binding protein	4*e*-33; *Verticillium dahliae*; Centrin-3, EGY16271.1
36.	01241.5		Ca^{2+} and/or CaM binding protein	0; *Trichoderma reesei*; Mitochondrial carrier protein, EGR44893.1
37.	06347.5		Ca^{2+} and/or CaM binding protein	0; *Sordaria macrospora*; Actin cytoskeleton-regulatory complex protein, XP_003350109.1
38.	06617.5		Ca^{2+} and/or CaM binding protein	7*e*-93; *Verticillium albo-atrum*; Myosin regulatory light chain cdc4, XP_003009631.1
39.	03750.5		Ca^{2+} and/or CaM binding protein	8*e*-74; *Botryotinia fuckeliana*; Calmodulin, XP_001560827.1
40.	08980.5	NDE-1	Ca^{2+} and/or CaM binding protein	0; *Grosmannia clavigera*; Alternative NADH-dehydrogenase, EFX03867.1

TH-1227_09610609

41.	02283.5		Ca^{2+} and/or CaM binding protein	0; *Sordaria macrospora*; Calcium/calmodulin-dependent protein kinase type I, XP_003344498.1
42.	09123.5		Ca^{2+} and/or CaM binding protein	0; *Sporothrix schenckii*; Calcium/calmodulin-dependent kinase, AAV80434.1
43.	02814.5	PRD-4	Ca^{2+} and/or CaM binding protein	0; *Grosmannia clavigera*; Serine/threonine-protein kinase chk2, EFX01629.1
44.	06650.5		Ca^{2+} and/or CaM binding protein	3*e*-61; *Nectria haematococca*; Phospholipase A2, XP_003042542.1
45.	02411.5		Ca^{2+} and/or CaM binding protein	0; *Glomerella graminicola*; Microtubule associated protein, EFQ31793.1
46.	06177.5		Ca^{2+} and/or CaM binding protein	0; *Magnaporthe grisea*; CMKK2, ACM41720.1
47.	04265.5		Ca^{2+} and/or CaM binding protein	7*e*-85; *Bacillus megaterium*; Beta-fructosidase FruA, AEN90524.1
48.	06650.5		Ca^{2+} and/or CaM binding protein	3*e*-61; *Nectria haematococca*; Phospholipase A2, XP_003042542.1

[a]Adapted from Tamuli et al. (2013)

[b]Split from NCU07605.1

[c]Split from NCU01437.1

[d]Split from NCU09655.1

[e]NCU05225.5 (was indicated as NCU08980.1 in Borkovich et al. 2004)

TH-1227_09610609

The *N. crassa* Ca^{2+} signaling proteins are described briefly in the following section.

Ca^{2+} permeable channels

Ca^{2+} permeable channels are homogenously distributed along the hyphae and mediate Ca^{2+} uptake by passive flow of Ca^{2+} across cell membranes into the cytoplasm (Bootman et al. 2001; Zelter et al. 2004). In *N. crassa*, NCU02762, NCU06703, and NCU11680 (changed from NCU07605) genes encode three different Ca^{2+} channel proteins and are classified into group I, II, and III respectively based on the several different activation mechanisms (Zelter et al. 2004). Among these genes, NCU06703 encodes a stretch activated Ca^{2+} permeable channel called MID-1 that plays a role in regulation of ion transport via Ca^{2+} homeostasis (Lew et al. 2008).

Ca^{2+}-and cation-ATPases

Ca^{2+}- and cation-ATPases are located in plasma membrane and organelle membrane. They hydrolyse ATP to catalyse active Ca^{2+}-efflux across biological membranes, and maintain a steep Ca^{2+} gradient across the plasma membrane (Hao et al. 1994; Møller et al. 1996). In *N. crassa*, nine ATPases have been identified, seven of them are Ca^{2+}-and cation-ATPases and remaining two are cation-ATPases. The NCU03305, NCU04736, NCU05154, NCU03292, and NCU08147 genes encode NCA1, NCA2, NCA3, PMR1, and PH-7 proteins, respectively (Benito et al. 2000). The *N. crassa* ATPases are distributed in different branches as revealed by a phylogentic analysis; NCA1 in SERCA (sarcoplasmic reticulum Ca^{2+}), NCA2 and NCA3 in PMCA (plasma membrane Ca^{2+}), PMR1 and PH-7 in ENA (*exitus natru*; Latin, 'exit sodium') branch (Haro et al. 1991; Benito et al. 2000). Strains lacking NCA-1 and NCA-3 have no obvious defects either in growth or distribution of Ca^{2+}. However, lack of NCA-2 results in slow growth, Ca^{2+} sensitivity, and female sterility. Besides, a strain lacking NCA-2 accumulates more Ca^{2+} than the wild type, indicating that it functions in the plasma membrane to pump Ca^{2+} out of the cell (Bowman et al. 2011).

H^+ /Ca^{2+}exchangers

Ca^{2+}-exchangers exchange positive ions across membranes to reduce high $[Ca^{2+}]_c$ to resting level and to transport Ca^{2+}into intracellular Ca^{2+}-stores. The H^+ /Ca^{2+} antiport system in plants accounts for Ca^{2+} accumulation in the vacuole with a minimum H^+:Ca^{2+} stoichiometry of at least three (Blackford et al. 1990). Evidence in *N. crassa* suggest that the ATP-driven H^+/ Ca^{2+} exchange system has a stoichiometric ratio of at least 2 H^+/ Ca^{2+} (Miller

TH-1227_09610609

et al. 1990). *N. crassa* has six Ca^{2+}/H^{+} exchangers encoded by genes NCU07075, NCU00916, NCU00795, NCU06366, NCU07711, and NCU05360. Among these Ca^{2+}/H^{+} exchangers, NCU07075 encodes CAX, and strains lacking *cax* accumulate very little Ca^{2+} in the dense vacuolar fraction (Bowman et al. 2011).

Na^{+}/Ca^{2+} exchangers

The two Na^{+}/Ca^{2+} exchangers, NCU02826 and NCU08490, have been identified in *N. crassa* genome. The major function of the Na^{+}/Ca^{2+} exchangers is to remove Ca^{2+} from the cytoplasm and allow Ca^{2+} entry under special conditions (Lytton et al. 2007).

Phospholipase C-δ subtype

N. crassa possesses four phospholipase C-δ subtype (PLC-δ) proteins. The genes NCU01266, NCU02175, NCU06245, and NCU11415 encode PLC-δ subtype proteins (Galagan et al. 2003; Borkovich et al. 2004). PLC-δ acts on a plasma membrane phospholipid phosphatidylinositol 4, 5-biphosphate (PIP2) to synthesize second messengers inositol-1,4,5-triphosphate ($InsP_3$, also IP_3) and 1,2-diacylglycerol (DAG) (Berridge 1987, 1993). $InsP_3$ induces Ca^{2+} release from vacuoles (Cornelius et al. 1989), and it is present in the lipid extract of *N. crassa* mycelia (Lakin-Thomas 1993). The null mutant of *plc-1*, generated using repeat-induced point mutation (RIP; Selker et al. 1987), grows slowly in a 'spreading colonial' (Garnjobst and Tatum 1967) manner and displays defects in hyphal size, proportion and branching (Gavric et al. 2007). The *plc-1*mutant contains residual PLC activity, indicating redundancy of this enzyme.

Ca^{2+} and/or CaM binding proteins and calmodulin

The effects of changes in intracellular Ca^{2+} levels are mediated primarily by Ca^{2+} and/or CaM binding proteins. They have several conserved domains like N-terminal catalytic domain, EF-hand Ca^{2+}-binding sites, autoinhibitory and overlapping CaM-binding domain. Little is known about Ca^{2+} and/or CaM binding proteins in *N. crassa*. Knockout mutant for the gene NCU09123, a Ca^{2+} and/or CaM binding protein show modest phase delay, a small period lengthening, light-induced phase shifting of the circadian conidiation rhythm, and a transient slow growth phenotype (Yang et al. 2001). Additionally, my colleague Ravi in the lab had shown that crosses homozygous for ΔNCU09123.2 and ΔNCU02283.2 mutant display an intermediate phenotype (produced few hundred ascospores) and a barren

TH-1227_09610609

phenotype (produced very few ascospores; Deka et al 2011; Tamuli et al 2013). Calcineurin is a CaM-dependent protein phosphatase consisting of a catalytic subunit A that binds to CaM (Winkler et al. 1984), and a regulatory subunit B that binds Ca^{2+} (Klee et al. 1979). Conditional expression of the antisense RNA for the *cna-1*, the *N. crassa* catalytic subunit of calcineurin results in extensive hyphal branching, altered hyphal morphology, loss of the apical tip-high Ca^{2+} gradient, and ultimately, growth arrest (Prokisch et al. 1997). Calcineurin B mutant, *cnb-1*, displays an abnormal morphology indicating that calcineurin regulatory subunit B is required for normal vegetative growth in *N. crassa* (Kothe and Free 1998). Another Ca^{2+} and/or CaM binding protein is the NDE-1, also known as the external NADPH dehydrogenase of *N. crassa* mitochondria, contains a Ca^{2+}-binding motif (Melo et al. 1999, 2001; Borkovich et al. 2004; Carneiro et al. 2007). It has been shown *in vitro* that the NADPH oxidation activity of the NDE-1 protein is Ca^{2+}- dependent (Melo et al. 1999, 2001). *N. crassa* possesses a CaM encoded by NCU4120 that appears to be essential for viability and it has possible roles in signal transduction process in circadian clock and activation of chitin synthase (Capelli et al. 1993; Sadakane and Nakashima 1996; Suresh and Subramanyan 1997; Galagan et al. 2003; Borkovich et al. 2004).

1.2 Objectives of this study

Only few Ca^{2+} signaling genes has been studied using either RIP-induced null mutants such as *plc-1*^{rip} (Gavric et al. 2007), *cnb-1* $^{rip-3}$ (Kothe and Free 1998), or RNAi technology such as *cna-1*antisense or by using inhibitors such as CaM antagonists (Sadakane and Nakashima 1996) in *N. crassa*. However, understanding on Ca^{2+}-signaling machinery in *N. crassa* or any other filamentous fungus is largely unknown and majority of the Ca^{2+} signaling genes remain to be studied. I had access to large number of Ca^{2+} signaling knockout mutants in addition to the published genome sequence of *N. crassa*. Therefore, I had decided to work on three broad objectives as given below:

1. To screen *N.crassa* Ca^{2+}-signaling knockout mutants to identify the Ca^{2+}-signaling genes involved in various cell functions,
2. To understand the molecular mechanism of the selected Ca^{2+}-signaling gene, and
3. To study the genetic interactions of selected Ca^{2+}-signaling genes to determine their epistatic relationship.

TH-1227_09610609

CHAPTER 2

Materials and Methods

TH-1227_09610609

2.1 Materials

2.1.1 Chemicals and other materials

Agarose, ethidium bromide, sodium dodecyl sulphate (SDS), cetyltrimethyl ammonium bromide (CTAB), Tween 80, sorbitol, sorbose, fructose, sucrose, bacto-agar, bacto-tryptone, yeast extract, absolute ethanol, Phenol:Chloroform:Isoamyl mixture (25:24:1), β-mercaptoethanol and other general laboratory chemicals and glasswares were procured from various manufacturers such as SRL (Mumbai, India), Merck (Mumbai, India), Himedia (Mumbai, India), Borosil (Mumbai, India), Tarsons (Kolkata, India). Hexane and acetone was purchased from Rankem reagents (Faridabad, India). Hygromycin, glufosinate ammonium sulphate (basta), biotin and Triazol reagent were purchased from the Sigma Aldrich, USA. Sephadex G-50 was from Pharmacia Biotech, Sweden. All restriction enzymes, DNA size markers, and Taq DNA polymerases for PCRs were purchased from New England Biolabs, USA. High fidelity Taq polymerases were purchased from Finzymes (Finland). Custom oligonucleotide primers were purchased from Metabion GmbH, Germany as well as from Integrated DNA Technologies, USA. DNA purification kits were from Qiagen, USA. The Hybond N+ membranes were from Amersham International, UK. The DNA mutiprime labelling kit and radiolabeled nucleotides were from BRIT, INDIA. All other chemicals were purchased from local manufacturers and were of analytical grade.

2.1.2 *Neurospora crassa* strains

(i) *74-OR23-1 A* (FGSC 987) and *OR8-1 a* (FGSC 988)

These are standard Wild-type *N. crassa* laboratory strains. These were obtained from the Fungal Genetics Stock Center (FGSC), University of Missouri, Kansas City, MO 64110.

(ii) Knockout mutants of calcium signaling genes of *N. crassa*

Knockout mutants of calcium signaling genes were obtained from FGSC (Table 1.1)

(iii) *erg-3^{RIP} A* and *erg-3^{RIP} a* strains

The RIP-induced *erg*-3 mutants lack a functional sterol C-14 reductase (Prakash et al. 1999). They have slow growth rate than the wild type, and are female sterile. The *erg-3^{RIP} A* and *erg-3^{RIP} a* strains were kind gift from Dr D. P. Kasbekar, Centre of Cellular and Molecular Biology, Hyderabad.

(iv) Δ*mus53::hph A* (FGSC 10139) and Δ*mus53::hph a* (FGSC 10140) strains

These strains were obtained from the FGSC. The *mus-53* gene encodes a homologue of human DNA ligase 4 (LIG4) that functions in the final step of non homologous end-joining.

TH-1227_09610609

In Δ*mus53* mutant, integration of a foreign DNA segment occurs only at the targeted site and therefore, making them an extremely efficient and safe host for gene targeting (Ishibashi et al. 2006).

(v) Strains generated in this study

Δ*ncs-1*Δ*mus53 a (15)* and Δ*ncs-1*Δ*mus53 A (18)* strains were generated in this study for targeted integration of foreign DNA; *ncs-1*^{G2A} *A (22)*, *ncs-1*^{G2A} *a (20)*, *ncs-1*^{G2A} *a (21)*, *ncs-1*^{R175A} *a (8)*, *ncs-1*^{R175A} *A (20)*, *ncs-1*^{E120Q} *A (5)*, *ncs-1*^{E120Q} *a (9)* for site-directed mutational studies; Δ*ncs-1*Δ*nca-2 a (10)* and Δ*ncs-1*Δ*nca-2 A (5)*, Δ*ncs-1*Δ*mid-1 a (2)* and Δ*ncs-1*Δ*mid-1 A (9)*, Δ*mid-1*Δ*nca-2 a (19)* and Δ*mid-1*Δ*nca-2 A (15)*, Δ*ncs-1*Δ*prd-4 a (55)* and Δ*ncs-1*Δ*prd-4 A (53)* double mutants were generated for genetic interaction studies.

2.1.3 Bacterial strains

Escherichia coli DH5α

The genotype of *E. Coli DH5α* is *SupE*44 *Δlac*U169 (ϕ80*lacZ* ΔM15) *hsdR*17 *recA*1 *end A*1 *gyrA*96 *thi*-1 *relA*1 and is a recombination-deficient amber suppressing strain used for plating and growth of plasmids (Sambrook and Russell 2001). The ϕ80 *lacZ* ΔM15 mutation permits α-complementation with the amino terminus of β-galactosidase encoded in pUC vectors. It was used for all routine transformations, plasmid isolation and selection of recombinants.

2.1.4 Plasmid vectors

(i) pBARGEM7-1

The plasmid vector pBARGEM7-1 is of size 4.5 kb and carries the fungal selectable marker *bar*, polylinker and *lacZ'* sequence including the T7 and SP6 promoters, bacterial selectable marker ampicillin, and pUC origin (FGSC 19; Pall and Brunelli 1993; Figure 2.1). The expression of *bar* gene is under the control of *Aspergillus nidulans trpC* promoter. The *bar* gene encodes a phosphinothricin acetyl transferase that detoxifies the antibiotic basta present in the selection medium and therefore, serves as a selectable marker for fungal transformants. The polylinker region containing the *lacZ`* sequence is subcloned from pGEM7Zf(+) vector. Insertion of DNA fragments into the polylinker region disrupt the function of the *lacZ`* gene and recombinant clone can be screened by blue white selection on the concept of α-complementation (Ullmann et al. 1967).

TH-1227_09610609

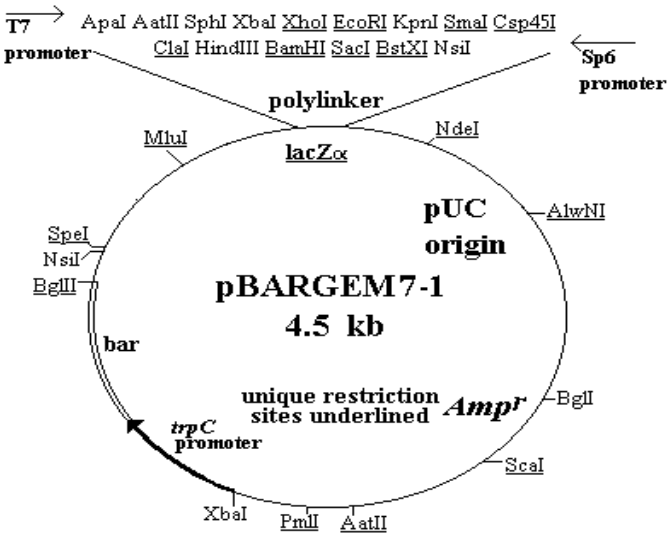

Figure 2.1: Schematic of the pBARGEM7-1 vector. The size of the vector is 4.5 kb. The unique restriction sites are underlined in the polylinker region of *lacZ′* sequence. The plasmid map is adapted from Pall and Brunelli 1993.

(ii) pRS426

The pRS426 is an yeast-type episomal shuttle plasmid vector used for gene cloning in host *Saccharomyces cerevisiae* and *E. Coli*. While in *E. coli*, they replicate from the pMB1 origin of replication from pBR322. They carries polylinker in *lacZ′* sequence, the T7 and T3 promoters, and ampicillin resistance gene for selection with ampicillin in *E. coli*. The *lacZ′* gene encodes the α-peptide of beta-galactosidase, that permits the selection of transformed colonies through blue-white screening. The unique cloning sites present in the polylinker region of the *lacZ′* sequence are *SacI BxtXI SacII EagI NotI SpeI BamHI SmaI EcoRI HindIII ClaI SalI XhoI I KpnI*. For replication in *S. cerevisae*, the pRS426 carries origin of replication from 2 micron circle plasmid along with the REP3 and FRT sequences necessary for high copy propagation. The yeast auxotrophic marker *URA3* is present for selection of transformed yeast. In *S. cerevisiae*, the copy number is about 20 per haploid cell (Figure 2.2). The pRS426 was used as a host vector in generating various knockout mutants of *N. crassa* including knockout mutants of Ca^{2+}-signaling genes through high throughput gene knockout procedure (Colot et al. 2006; described in Chapter 3).

TH-1227_09610609

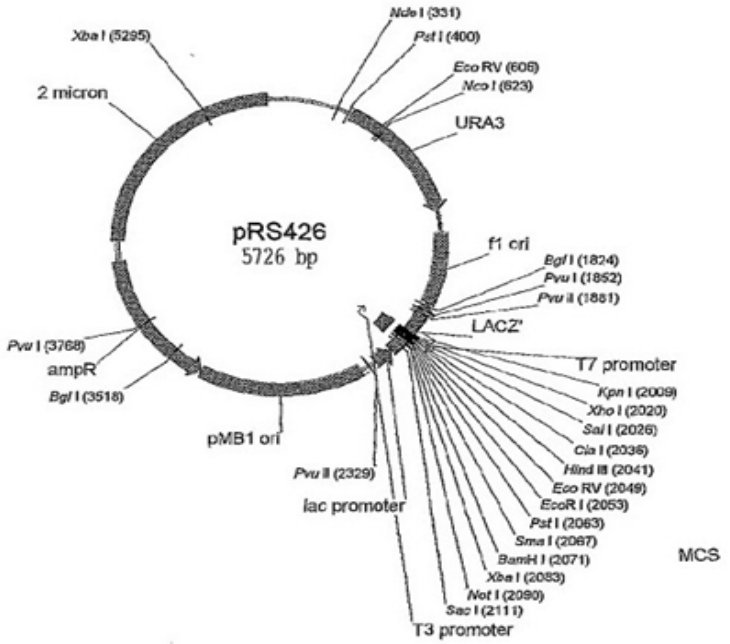

Figure 2.2: Schematic of the pRS426 vector. The size of the vector is 5.726 kb. The unique restriction sites are *SacI BxtXI SacII EagI NotI SpeI BamHI SmaI EcoRI HindIII ClaI SalI XhoI KpnI* are present in the polylinker region of *lacZ'* sequence. The *URA3*, an auxotrophic marker for selection in *S. cerevisae*, and amp^R marker for selection in *E. coli* through blue-white secreening. The plasmid map is available at http://www.creative-biogene.com/pRS426-phagemid-in-E.-coli-vector-VET1104-179-16.html.

2.1.5 Bacterial media, antibiotics and commonly used solutions

Commonly used solutions were prepared essentially as described by Sambrook and Russell 2001.

1. LB (Luria Bertani) broth: 1% bacto-tryptone, 1% sodium chloride, 0.5% bacto- yeast extract, pH 7.0.
2. LB agar: LB broth solidified with 1.5% agar.
3. Terriffic broth: Terrific broth is composed of 1.2% peptone, 2.4% yeast extract, 0.4% glycerol (v/v) and 10% (v/v) of the sterile solution of 0.17 M KH_2PO_4, 0.72 M K_2HPO_4. The solution of 0.17 M KH_2PO_4, 0.72 M K_2HPO_4 was prepared by dissolving 2.31 g of KH_2PO_4 and 12.54 g of K_2HPO_4 in 90 ml of deionized water. After the salts have dissolved, the volume of the solution was adjusted to 100 ml and sterilized by autoclaving.

TH-1227_09610609

4. SOB agar: The media is composed of 0.5% yeast extract, 2% peptone, 10 mM NaCl, 2.5 mM KCl, 10 mM $MgCl_2$, 10 mM $MgSO_4$, 2% agar. The sterile solution of $MgCl_2$ and $MgSO_4$ were added only after sterilizing the media.
5. SOC medium: The media is composed of 0.5% yeast extract, 2% peptone, 10 mM NaCl, 2.5 mM KCl, 10 mM $MgCl_2$, 10 mM $MgSO_4$, 20 mM glucose. The sterile solution of $MgCl_2$, $MgSO_4$ and glucose were added only after sterilizing the media.
6. IPTG (isopropylthio-β-D-galactoside): A 20 % solution of IPTG was prepared by dissolving 2 g of IPTG in 8 ml of sterile water. The volume of the solution was adjusted to 10 ml and sterilized by passing it through a 0.22-µm disposable filter. The solution was dispensed into 1 ml aliquots and stored at -20ºC.
7. X-gal (5 bromo-4-chloro-3-indolyl-B-galactoside): A stock solution of 20 mg/ml X-gal was prepared in dimethylformamide in an amber eppendorf tube to prevent damage by light and stored at -20ºC.
8. 5 M NaCl: Dissolved 29.22 g of NaCl in 80 ml of distilled water, and adjusted the volume to 100 ml. The stock was then sterilized by autoclaving and stored at room temperature.
9. 2 M KCl: Dissolved 14.9 g of KCl in a final volume of 100 ml of distilled water and stored at room temperature.
10. 1 M $MgSO_4$: Dissolved 12 g of $MgSO_4$ in a final volume of 100 ml of distilled water and sterilized by autoclaving.
11. 1 M $MgCl_2$: Dissolved 20.33g of $MgCl_2.6H_2O$ in 80 ml of distilled water, adjusted the volume to 100 ml and sterilized by autoclaving.
12. 10 N NaOH: Dissolved 40 g of NaOH pellet slowly in 80 ml of distilled water, stirring continuously in a plastic beaker placed on ice, adjusted the volume to 100 ml and stored at room temperature.
13. 5 M $CaCl_2.2H_2O$: Amount of 73.5 g of $CaCl_2.2H_2O$ was dissolved in distilled water to a final volume of 100 ml. The solution was sterilized by autoclaving.
14. 0.1% DEPC: DEPC is a Diethylpyrocarbonate. 0.1% DEPC solution was prepared in sterile distilled water and sterilized by autoclaving.
15. 8 M LiCl: Amount of 33.9 g of LiCl was dissolved in a final volume of 100 ml of DEPC treated sterile distilled water and sterilized by autoclaving.
16. 1 M glucose: Amount of 18.016 g of glucose was dissolved in a final volume of 100 ml of distilled water and sterilized by autoclaving.

TH-1227_09610609

17. 1 M Sorbitol: Amount of 18.21 g of sorbitol was dissolved in distilled water to a final volume of 100 ml and sterilized by autoclaving.
18. 5 M Sucrose: Amount of 85.575 g of sucrose was dissolved in distilled water to a final volume of 100 ml and sterilized by autoclaving.
19. Ampicillin: A 1000X stock solution of 100 mg/ml ampicillin was made in sterile double-distilled water and stored in aliquots of 200 µl at -20°C.
20. Hygromycin B (100 mg/ml): A stock solution of 100 mg/ml was prepared by dissolving an amount of 100 mg of hygromycin B in 1 ml of sterile water and stored as aliquots of 200 µl at -20°C.
21. Glufosinate ammonium sulphate (basta;100 mg/ml): A stock solution of 100 mg/ml was prepared by dissolving an amount of 100 mg of basta was dissolved in 1 ml of sterile water and stored as aliquots of 200 µl at -20°C.
22. Ethidium bromide (10 mg/ml): 50 mg of ethidium bromide was dissolved in 5 ml of distilled water to prepare 10 mg/ml stock.
23. 6X Gel-loading Buffer (Type III): A solution of 0.25% (w/v) bromophenol blue, 0.25% (w/v) xylene cyanol FF and 30% glycerol (v/v) was made in sterile water and stored at 4°C.
24. 20% Sodium dodecyl sulfate (SDS): Dissolved 200 g of SDS in 900 ml of distilled water, adjusted pH to 7.2 by adding few drops of concentrated HCl, and adjusted the volume to 1 liter with distilled water.
25. 20X SSC: Amount of 175.3 g of NaCl and 88.2 g of sodium citrate was dissolved in 800 ml of distilled water, adjusted the volume to 1 liter, with distilled water and sterilized by autoclaving.
26. Sodium-phosphate buffer (0.5 M): Amount of 70.98 g of anhydrous sodium-phosphate (Na_2HPO_4) was added to 800 ml of distilled water and adjusted pH to 7.2 with ~ 4 ml of 85% orthophosphoric acid (H_3PO_4). The volume of the solution was adjusted to 1 litre.
27. 1 M Tris: Dissolved 121.1 g of Tris base in 800 ml of distilled water, adjusted pH to the desired value by adding concentrated HCl (~ 70 ml, 60 ml, and 42 ml of concentrated HCl was added for pH 7.4, 7.6, and 8.0, respectively), adjusted the volume to 1 liter with distilled water and sterilized by autoclaving.
28. 0.5 M EDTA (pH 8.0): EDTA is disodium ethylenediaminetetra-acetate.2 H_2O. 186.1g of EDTA was dissolved in 800 ml of distilled water, adjusted pH to 8.0 by NaOH, adjusted volume to 1 liter and sterilized by autoclaving.

TH-1227_09610609

29. 0.5 M EGTA (pH 8.0): EGTA is ethylene glycol bis (β-aminoethyl ether) N, N, N′, N′- tetraacetic acid. Amount of 19.017 g of EGTA was dissolved in 60 ml of sterile water and adjusted pH to 8.0 with NaOH pellets. Final volume was adjusted to 100 ml and sterilized by autoclaving.
30. 10% SDS: Dissolved 10 g of SDS in 90 ml of distilled water, heated to 68ºC and stirred with a magnetic stirrer to assist dissolution. The volume was adjusted to 100 ml and stored at room temperature.
31. RNAase A: Dissolved pancreatic RNAase (DNAase free, Sigma) at a concentration of 10 mg/ml in 10 mM Tris.Cl (pH 7.5), 15 mM NaCl, stored at -20°C.
32. Alkaline lysis Solution I: Amount of 50 mM glucose, 25 mM Tris-Cl (pH 8.0), 10 mM EDTA (pH 8.0) was added from their stock solutions in a final volume of 100 ml distilled water. Sterilized by autoclaving and stored at 4ºC.
33. Alkaline lysis Solution II: Amount of 0.2 N NaOH and 1% SDS were added in a required volume. The solution was freshly prepared just prior to use.
34. Alkaline lysis Solution III: For a volume of 100 ml solution, 60 ml of 5 M potassium acetate, 11.5 ml of glacial acetic acid, and 23.5 ml of distilled water were mixed together. Sterilized by autoclaving and stored at 4ºC
35. 50X TAE: The stock solution of 50X TAE for one liter contains 242 g Tris base, 57.1 ml of glacial acetic acid and 100 ml of 0.5 M EDTA (pH 8.0).
36. 1 X TE: The solution was prepared by adding10 mM Tris-HCl (pH 8.0) and 1 mM EDTA (pH 8.0) from their respective stocks.
37. 10X MOPS electrophoresis buffer: MOPS is a 3[N-Morpholino]Propanesulphonic acid. The stock solution of 10X MOPS for 1 litre contains 41.8 g of MOPS (0.2 M), 20 ml sodium acetate solution (20 mM), and 20 ml EDTA (10 mM). After dissolving, 41.8 g of MOPS in DEPC-treated water, pH was adjusted to 7.0 with 2 N NaOH and then added sodium acetate solution and EDTA in an indicated volume. Solution was filter sterilized using 0.45-µm Millipore filter and stored at room temperature protected from light.
38. Lysis buffer for Neurospora genomic DNA isolation: The lysis buffer contains 10 mM Tris-HCl (pH 7.5), 0.5 M NaCl, 10 mM EDTA, 1% SDS and 1% CTAB.
39. Lysis buffer for Neurospora RNA isolation: The lysis buffer contains 100 mM Tris HCl (pH 8.0), 0.6 M NaCl, 10 mM EDTA (pH 8.0), 4.5 % SDS and 2 % β-mercaptoethanol.

TH-1227_09610609

2.1.6 Solutions for growth, maintenance and crossing of Neurospora strains

Media for culturing Neurospora are prepared essentially as described in Davis and De Serres (1970).

(i) Biotin solution

5 mg of biotin was dissolved in 100 ml of 50% (v/v) ethanol, stored at 4 ^{0}C.

(ii)Trace element solution

Trace element solution was prepared by adding the following compounds successively, with stirring to 95 ml of distilled water.

Citric acid.1H_2O	5.00 g
ZnSO4.7H_2O	5.00 g
Fe $(NH_4)_2 (SO_4)_2$.6H_2O	1.00 g
CuSO4.5H_2O	0.25 g
MnSO4.1H_2O	0.05 g
H_3BO_3	0.05 g
Na_2MoO_4.2H_20	0.05 g

The final volume was adjusted to 100 ml; 1 ml of chloroform was added as a preservative and stored at room temperature.

(iii) Synthetic Media

Vogel's Medium N (Vogel, 1964) was prepared as a 50X-strength solution as follows: To 750 ml of distilled water, the following ingredients were added in order, dissolving each one prior to addition of the next.

Na_3 citrate.5H_2O	150 g
KH_2PO_4	250 g
NH_4NO_3	100 g
$MgSO_4$.7H_2O	10 g
$CaCl_2$.2H_2O (predissolved in 20 ml H_2O)	5 g
Biotin solution	5 ml
Trace element solution	5 ml

The volume of the solution was adjusted to one liter and 3 ml of chloroform was added as a preservative.

(iv) Vogel's glucose medium

Vogel's medium N	1X
Glucose	1.5 % (w/v)

TH-1227_09610609

(v) Vogel's glucose agar medium

Vogel's medium N	1X
Glucose	1.5% (w/v)
Agar	2.0% (w/v)

(vi) 4X Synthetic crossing medium (SCM)

4X strength synthetic crossing medium (SCM) was prepared by adding the following compounds with stirring to 500 ml of water. After adding the following components, the solution was sterilized by autoclaving.

KNO_3	2.0 g
K_2HPO_4	1.4 g
KH_2PO_4	1.0 g
$MgSO_4.7H_2O$	1.0 g
$CaCl_2$	0.2 g
NaCl	0.2 g
Biotin solution	0.2 ml
Trace element solution	0.2 ml

(vii) SCM agar

SCM	1X
Glucose	1.5% (w/v)
Agar	2.0% (w/v)

(viii) 10X FGS

Sorbose	20% (w/v)
Fructose	0.5% (w/v)
Glucose	0.5% (w/v)

(ix) Vogel's sorbose agar medium

FGS	1X
Vogel's medium N	1X
Agar	2.0% (w/v)

(x) Top agar

FGS	1X
Vogel's medium N	1X
Agar	2.8% (w/v)

TH-1227_09610609

(xi) Media for circadian clock study

Glucose	0.1 % (w/v)
Arginine	0.17% (w/v)
Vogel's medium N	1X
Biotin	50 ng/ml
Agar	1.5 % (w/v)

Sterilization

All glassware and plasticware were sterilized by autoclaving at a steam pressure of 15 psi at 120°C for 20 min. Solutions were prepared in double-distilled water and generally sterilized by autoclaving. Heat-sensitive solutions were sterilized by filtering through a sterile 0.45 µm nitrocellulose filter (Millipore). For RNA isolation, all glasswares were first treated with 0.1 % DEPC solution for overnight, dried in oven at 150ºC and sterilized by autoclaving.

2.2 Methods

2.2.1 Growth conditions

Growth and maintenance of the Neurospora strains were essentially as described in Davis and De Serres (1970).

2.2.2 Crossing and ascospore collection

Crosses were performed by confrontation between mycelia inoculated as plugs on synthetic crossing medium in petridishes. Generally, ascospores began to shot within 16-18 days in *N. crassa* crosses. Ascospores were harvested by washing the lids with ~1 ml of sterile water.

2.2.3 Transformation of the *N. crassa* strain by electroporation

The protocol was based on the method described by Margolin et al. (1997). The recipient strain was grown in six to eight 250 ml conical flasks on Vogel's-glucose agar medium for a week at 30°C. The conidia were harvested in sterile water and separated from the mycelium by passing the suspension through cheesecloth attached to a 250 ml conical flask (the mouth of a 250 ml conical flask was covered with cheesecloth and sterilized by autoclaving beforehand). The conidial suspension was taken in a 30 ml Corex tube and centrifuged at 800 rpm for 6 min in a Sorvall HB-4 rotor in 4°C. The conidial mass was

TH-1227_09610609

washed twice in 30 ml water and resuspended in 1 M sorbitol at a concentration of $3x10^9$ spores/ml. About 40 µl of the conidial suspension was mixed with the transforming DNA and the mixture was placed in a pre-chilled 0.2 cm gap sterile electroporation cuvette (BioRad Laboratories, Hercules, CA). Electroporation was performed using a BioRad Gene Pulser apparatus (BioRad Laboratories, Hercules, CA). The conditions for electroporation were 1.5 KV, 25 µF and 600 Ω. The time constant varied from 13 to 15 ms. Immediately after the pulse, 600 µl of chilled 1 M sorbitol was added, kept in ice for 5 min and the transformant conidial suspension was mixed with top agar and plated on a Vogel's-sorbose agar plate supplemented with appropriate antibiotic such as basta at a concentration of 220 µg/ml. Usually about 4-5 transformants were obtained per plate and were 'pickable' under a dissection microscope after 2 days. A control transformation was done without adding DNA to eliminate the possibility of any contamination.

2.2.4 Scoring for antibiotic resistance

Antibiotic resistance was scored by streaking conidia onto 1.5% agar plate's containing Vogel's-sorbose medium and supplemented with the antibiotic. The antibiotics used were hygromycin B (220 µg/ml from 100 mg/ml stock in water), basta (220 µg/ml from 100 mg/ml stock in water).

2.2.5 Isolation of sterols from *N. crassa strains* and analysis by UV spectrophotometry

The *N. crassa* strain of interest was grown in liquid Vogel's glucose medium at 30°C for 3 to 5 days. The mycelial mass was harvested by vacuum filtration and lyophilized. The dried mycelia were ground with glass beads (0.2 mm in diameter) using a mortar and a pestle to a fine powder. About 50 mg of the powdered mycelia was taken in a 1.5 ml microfuge tube and 750 µl each of methanol and chloroform was added to the tube and kept on a rotary shaker overnight. The mycelial mass was removed by centrifugation at 12,000 rpm for 10 minutes. The chloroform-methanol extract which contains the lipids was washed once with 0.9 % NaCl and twice with 2 M KCl to remove the saponifiable lipids. The aqueous and organic phases were separated by centrifugation and the bottom organic phase was transferred to a fresh tube. This step separates the saponifiable lipids from non-saponifiable lipids like sterols. The organic phase, which contains the sterols was air-dried and the sterols were dissolved in about 20 ml of chloroform. This sample was diluted 1: 200 in ethanol and

TH-1227_09610609

its UV absorption spectrum (200 to 300 nm) was recorded in a Cary 100 Bio UV-visible spectrophotometer (Agilent technologies, US) .

2.2.6 Preparation of ultracompetent cells

Ultracompetent cells were prepared essentially as described by Inoue et al. 1990. A single colony of *E. coli DH5α* maintained on a fresh LB agar plate was inoculated into 5 ml of LB and incubated at 37°C at 200 rpm for 16 h. One ml of this overnight culture was inoculated into 100 ml of LB medium and incubated at 18°C at 200 rpm, till the OD_{600} reached 0.750. The culture was chilled on ice and centrifuged at 1,500 g for 15 min at 4°C to pellet the cells. The cells were then resuspended in 32 ml of ice cold Transformation Buffer (TB: 10 mM PIPES of pH 6.7, 15 mM $CaCl_2$, 250 mM KCl, 55 mM $MnCl_2$) and incubated on ice for 10 min. The centrifugation was repeated and the cells were resuspended in 8 ml of TB containing 7% DMSO, distributed into 100 µl aliquots, frozen in liquid nitrogen and stored at -70°C. Ultracompetent cells were used for cloning experiments involving ligation of DNA fragments with blunt-ended termini.

2.2.7 Transformation of ultracompetent *E. coli* cells by heat shock

Competent cells were removed from the -70°C freezer and thawed on ice. Ligated DNA sample (~6 µl) was added to the competent cells and mixed gently. The cells were incubated on ice for 30 min, following which they were subjected to heat shock at 42°C in water bath (JULABO GmbH, Germany) for 90 sec. After the heat shock 600 µl of SOC was added to the cells and the tube was incubated at 37 °C with shaking at 250 rpm for 1 h. The cells were plated on 85 mm SOB agar plates containing 50 µg/ml of ampicillin, 40 µl Xgal (from the stock of 20 mg/ml), and 7 µl IPTG (from the stock of 20% IPTG solution). The plates were incubated at 37°C for overnight and transformants were screened by blue-white selection.

2.2.8 Isolation of nucleic acids

(i) Small-scale isolation of plasmid DNA from bacterial culture

Small-scale or minipreparation of plasmid was made by alkaline lysis with SDS (Sambrook and Russell 2001). Briefly, 5 ml of overnight bacterial culture was centrifuged in microfuge tube for 2 min at 6000 rpm. Pellet was resuspended in 100 µl alkaline lysis

TH-1227_09610609

solution II was added to the bacterial suspension, contents were mixed by inverting the tubes 4-5 times and kept on ice for 10 min. To the viscous bacterial lysate, 150 µl alkaline lysis solution III was added, mixed by inverting the tube and kept on ice for 3-5 min. The tube was centrifuged for 10 min at 12,000 rpm and 4°C. The supernatant was transferred to the fresh microfuge tube and equal volume of Phenol:chloroform:isoamyl alcohol (25:24:1) was added, centrifuged for 10 min at 12,000 rpm and 4°C. The aqueous phase was taken in a fresh microfuge tube (1.5 ml) and plasmid DNA precipitated by adding 1.5 volumes of absolute ethanol. The tube was gently inverted few times and the DNA was pelleted by centrifuging the tube for 10 min at 12,000 rpm. The supernatant was discarded and the pellet was washed with 70% ethanol by centrifuging for 2 min at 12,000 rpm. The traces of ethanol was completely removed and the DNA pellet was allowed to dry at room temperature for 15 min. Finally, the pellet was dissolved in about 30 µl of 1X TE buffer (pH 8.0) and stored at 4ºC.

(ii) Large scale isolation of plasmid DNA from bacterial culture

Large-scale preparation of plasmid DNA (~500 µg) was made by alkaline lysis method (Sambrook and Russell 2001). Briefly, centrifuged overnight (250 ml with antibiotic) at 6,000 rpm for 10 min. The pellet was suspended in 9 ml of alkaline lysis solution I, 1 ml of a freshly prepared solution of 10 mg/ml lysozyme and 20 ml of freshly prepared alkaline lysis solution II. The contents were thoroughly mixed by gently inverting the bottle several times and incubated for 5-10 min at room temperature. 10 ml of alkaline lysis solution III was added to the contents and gently mixed by swirling several times and placed the mixtures on ice for 5-10 min. The bacterial lysate was centrifuged for 15 min at 12,000 rpm at 4°C. The supernatant was transferred to the fresh tube and 0.6 volume of isopropanol was added and stored the tube at room temperature for 10 min. The precipitated nucleic acid was recovered by centrifugation at 12,000 rpm at room temperature and washed once with 70% ethanol. The pellet was dried at room temperature and then dissolved in 200 µl of TE buffer. RNAase A treatment was given to the plasmid solution and then stored at -20°C for further use.

(iii) *Neurospora* genomic DNA isolation

The strain of interest was grown in liquid Vogel's glucose medium at 30°C for 2 to 3 days with shaking at 200 rpm. The mycelial mass was harvested by vacuum filtration and lyophilized. The dried mycelia were ground with glass beads (0.2 µm in diameter) using a

TH-1227_09610609

mortar and a pestle to a fine powder. Approximately, 150 mg of the powdered mycelia was taken in a 1.5 ml microfuge tube and 1 ml of lysis buffer added to it. Complete mixing of the mycelia and lysis buffer was achieved using a pipette tip or a toothpick. The tube was incubated at 65°C for 30 min, followed by centrifugation at 15,000 rpm for 10 min. The supernatant was taken in a fresh microfuge tube and 500 µl of phenol:chloroform:isoamyl alcohol mixture (25:24:1) was added. The tube was rotated in a cell mixer for 15 min and centrifuged at 15,000 rpm for 10 min. The aqueous phase was carefully removed and the phenol:chloroform:isoamyl alcohol treatment repeated. The aqueous phase was taken in a fresh microfuge tube and washed with 600 µl of chloroform to remove the last traces of phenol. The aqueous phase was taken in a fresh tube and genomic DNA precipitated by adding 1.5 volumes of absolute ethanol. The tube was gently inverted few times and the genomic DNA pelleted by centrifuging the tube for 10 min at 15,000 rpm. The supernatant was discarded and the pellet was washed with 70% ethanol by centrifuging for 2 min at 15,000 rpm. The traces of ethanol were completely removed and the genomic DNA pellet was allowed to dry at room temperature for 15 min. Finally, the pellet was dissolved in about 60 µl of 1X TE buffer (pH 8.0) and stored at 4ºC. All centrifugations were carried out at 25ºC.

(iv) *Neurospora* RNA isolation

The conidia of the strain of interest were grown in 250 ml conical flasks in liquid Vogel's glucose medium at 30ºC and 150 rpm for 12 to 16 h. The mycelial mass was harvested by vacuum filtration and immediately frozen in liquid nitrogen. The frozen tissue was ground to a fine powder using a mortar and a pestle. The powder was immediately transferred into a 2 ml microfuge tube containing 0.3 ml TRIzol reagent (Invitrogen, CA) to protect RNA from degradation by RNAase followed by further addition of the mixture of 0.75 ml lysis buffer (0.6 M NaCl, 10 mM EDTA, 100 mM Tris HCl, pH 8.0, 4% SDS) and 0.75 ml phenol (saturated with 0.1 M Tris HCl, pH 8.0). The tube was rotated in a cell mixer for 20 min and centrifuged at 10,000 rpm for 10 min. The upper aqueous phase was carefully removed and transferred to a fresh 2 ml microfuge tube containing an equal volume of phenol (saturated with 0.1 M Tris HCl, pH 8.0). The mixture was vortexed for few seconds and centrifuged for 10 min at10,000 rpm. The upper aqueous phase was transferred to a fresh 2 ml microfuge tube and 0.75 ml of 8 M LiCl was added. The mixture was stored overnight at 4°C for 16-20 h. The next day mixture was vortexed briefly and centrifuge for 10 min at

TH-1227_09610609

10,000 rpm. The pellet was resuspended, which is not always visible, in 0.3 ml double distilled water, mixed with 0.03 ml 3 M Na-acetate (pH 5.2) and 0.75 ml ethanol. The mixture was stored at -20°C for 2 h and centrifuged for 10 min at 10,000 rpm. The supernatant was discarded and the precipitate was washed with 70% ethanol. The RNA pellet was dried in room temperature for 10 to 15 min and re-dissolved in DEPC treated water. The RNA solution was stored at -70°C. The next day RNA sample were analysed in 1.2% agarose gel containing 2.2 M formaldehyde and 1X MOPS solution. Purity of the RNA preparations was assayed by spectrophotometric measurements. The A_{260}/A_{230} and A_{260}/A_{280} ratios were 2 or more, indicating the absence of any protein or polysaccharide contamination.

2.2.9 Quantitation of nucleic acids

The concentration of nucleic acids was estimated by measuring the OD at 260 nm in nanodrop spectrophotometer (eppendorf, Germany). The following empirical relationships were used to calculate the concentrations. An OD of 1 corresponds to ~50 µg/ml for double-stranded DNA, 40 µg/ml for single-stranded DNA and RNA, ~20 µg/ml for single-stranded oligonucleotides. The purity of nucleic acids was estimated by calculating the OD_{260}/OD_{280} ratio. Pure preparations of DNA and RNA have OD_{260}/OD_{280} values of 1.8 and 2.0, respectively.

2.2.10 Polymerase Chain Reaction (PCR)

The routine PCR reaction was carried out using *Taq* DNA polymerase and according to the manufacturer's protocol (*Taq* DNA polymerase with standard *Taq* buffer, Cat no. M0273S, NEB, USA). *Taq* DNA polymerase isolated from *Thermus aquaticus* and has no proofreading ability. Therefore, for subsequent cloning purposes, Phusion™ High-Fidelity DNA polymerase was used (Finzymes, Finland). The enzyme possess proofreading activity (3′-5′ exonuclease activity). The enzyme isolated from *Pyroccocus furiosus* was further processed by Phusion DNA technology to bring a novel *Pyroccocus*-like enzyme with a processivity enhanced domain.

Ordinarily, the PCR conditions were varied with respect to the product size and annealing temperature of the primers. The reaction conditions of PCR using standard *Taq* DNA polymerase were a 2 min denaturation at 95°C followed by 30 cycles of 30 sec denaturation at 95°C, 30 sec annealing at 60°C, and 2 min elongation at 72°C. The high fidelity PCR reaction was carried out according to the manufacturer's protocol (Finzymes,

TH-1227_09610609

Finland). All PCRs were performed in either My Cycler™ thermal cycler (BIO RAD, CA) or Arktik Thermal Cycler (Thermo Fisher Scientific, Finland).

2.2.11 Reverse-transcriptase PCR (RT-PCR) and Real time PCR

(i) RT-PCR

For RT-PCR based gene expression study, total RNA was isolated from the mycelia (grown for two days at 30ºC at 180 rpm) using the procedure as described in Neurospora RNA isolation. cDNA was synthesized from one µg of total RNA template using BioScript™ One Step RT PCR Kit (Bioline, US) that contains ultra-stable Moloney Murine Leukaemia Virus (MMLV) reverse transcriptase (BioScript) for first strand cDNA synthesis. The cycling condition for cDNA synthesis was 42ºC for 30 min. The cDNA template was further subjected to PCR cycling with *N. crassa* gene-specific primers to analyse the expression of specific genes. The PCR amplicons were analysed in 1.2% agarose gel with 100 bp DNA ladder for size comparison of amplicons.

(ii) Real Time PCR

For Real time PCR, total RNA was isolated using the procedure same as described in the protocol for Neurospora RNA isolation. One µg of total RNA was used to synthesize cDNA using Thermo Scientific Verso cDNA synthesis kit (Cat no. AB-1453/B). Real time PCR was performed in triplicate in ABI 7500 Fast Real-Time PCR System (Applied Biosystems, USA) with the SYBR® select master mix (Applied Biosystems, USA) by using 100 ng of cDNA and 10 µM each of primer in a final reaction volume of 12 µl. The PCR cycle was as follows: 95°C for 10 min followed by 40 cycles of 95 °C for 15 s and 60 °C for 1 min. The $2^{-\Delta\Delta Ct}$ relative expression quantification method was used to calculate the fold change of each gene, using the β-tubulin gene as an endogenous control.

2.2.12 Digestion of DNA with restriction endonuclease

For analytical and preparative purposes, plasmid DNA were digested with specific restriction endonucleases up to 5 U of enzyme for 1 µg DNA in a final volume of 20 µl. The reaction was carried out for 3 h using suitable buffers and assay conditions as specified by the manufacturer's. In this study, basically four restriction endonucleases, *SmaI, EcoRI, BamHI,* and *XmnI*, were used with their suitable buffers and temperature conditions. The enzyme was

TH-1227_09610609

heat-inactivated by heating the digested samples at 65°C for 10 min. The digested DNA fragments were analyzed by agarose gel electrophoresis.

2.2.13 Ligation reactions

Ligation reactions were carried out using Quick Ligation™ Kit (NEB, Cat no. M2200S). The 20 µl ligation reaction volume contained 50 ng of a linearized DNA vector, a 3-fold molar excess of insert, 10 µl of 2X ligation buffer (132 mM Tris-HCl, 20 mM $MgCl_2$, 2 mM dithiothreitol, 2 mM ATP, 15% Polyethylene, glycol 6000) and 1 µl Quick T4 DNA ligase enzyme. The ligation was performed for 5 min at 25ºC.

2.2.14 Agarose gel electrophoresis

The DNA samples were loaded with one-sixth the volume of 6X DNA loading dye (0.25% bromophenol blue, 0.25% xylene cyanol, 30% glycerol). Depending upon the size of the fragments to be resolved, the samples were loaded on 0.7% to 1.5% agarose gels cast on 1X TAE containing 0.5 µg/ml ethidium bromide. Electrophoresis was carried out in 1X TAE at 5 V/cm. Standard DNA size markers were run alongside for estimation of DNA fragment sizes. The ethidium bromide stained DNA samples were visualized on a gel doc (Gel Logic 1500 Imaging System). RNA samples were resolved in 1.2% agarose gel containing 2.2 M formaldehyde and 1X MOPS buffer.

2.2.15 Purification of DNA fragments from agarose gels

PCR-amplified DNA subsequently used for cloning, sequencing, and preparation of probes or for transformation was purified from agarose gels using the QIAquick Gel Extraction Kit (Qiagen, Cat no. 28704). The sample containing DNA was resolved on a 1% high purity agarose gel. The DNA bands were visualized on a Gel doc (Gel Logic 1500 Imaging System) and the DNA band to be eluted was excised and transferred to a weighed 1.5 ml centrifuge tube. DNA from the gel slice was eluted according to the instructions provided by the manufacturer.

2.2.16 Preparation of radiolabeled DNA probes by random primer labeling

Double-stranded DNA was radiolabeled using random primers as described by Feinberg and Vogelstein (1983) using a multiprime labelling kit. About 50-100 ng of double-stranded DNA was denatured in a volume of 20 µl by boiling for 5 min and quick chilling on ice. This was followed by the sequential addition of 5 µl of random primers solution, 5 µl of

TH-1227_09610609

10X reaction buffer, 4 µl each of dCTP, dGTP, dTTP, 40 µCi of α-[$_{32}$P]-dATP and 2 units of Klenow enzyme. The reaction volume was made upto 50 µl and the reaction was carried out at 37°C for 1 h. The enzyme was inactivated at 75°C for 10 min and the probe was separated from the unincorporated nucleotides by Sephadex G-50 column chromatography (described below), denatured in boiling water for 5 min and added to the prehybridization solutions.

2.2.17 Sephadex G-50 column chromatography for purification of radiolabeled probe

Sephadex gel filtration column chromatography was employed to separate out unincorporated radionucleotides from DNA solutions. A sterile 1 ml disposable plastic syringe was plugged with sterile glass wool and filled with the Sephadex G-50 slurry previously equilibrated with TE pH 8.0. The column was packed by centrifugation at 1000 rpm for 5 min in a Sorvall HB-4 rotor at room temperature. Then 50 µl of the DNA solution to be purified was loaded and the column was centrifuged at 1000 rpm for 5 min at room temperature to elute the purified DNA.

2.2.18 Southern hybridization

The DNA samples to be hybridized were digested with appropriate restriction enzymes and resolved on 0.8% to 1.5% agarose gels alongside DNA markers. The gel was stained with ethidium bromide, photographed and the DNA was transferred to Hybond N+ membrane by vacuum blotting in a vacuum blotter apparatus (custom made at CCMB, Hyderabad) for 10 min using 0.25 N HCl followed by 1 hour in 0.4 N NaOH. The blot was then rinsed in 2X SSC, and air-dried. Prehybridization was carried out at 65°C for 2 h in 20 ml of 0.5 M sodium-phosphate buffer and 7% SDS. The blot was hybridized at 65°C for 12 h by the addition of denatured radiolabeled probe (prepared by random primer labeling as described above). The blot was then washed using solutions of 100 ml of 2X SSC and 0.5% SDS for 20 min at room temperature, 1X SSC and 0.5% SDS for 20 min at 65°C, and 0.5X SSC and 0.5% SDS for 20 min at 65°C. The hybridized blot was exposed to Fujifilm imaging plate, BAS-IP MS 2025 for ~1 hour and developed using Fujifilm FLA-3000, Fuji Photo Film Co. Ltd., Japan).

TH-1227_09610609

2.3 Databases and Computer software used

(i) *Neurospora crassa* genome database

Genome resources for Neurospora are available at http://www.broad.mit.edu/annotation/genome/neurospora/Home.html. The web site for Fungal Genetics Stock Center is http://www.fgsc.net/

(ii) Basic Local Alignment Search Tool (BLAST)

BLAST program was used to compare nucleotide or protein sequences to sequence databases. This is available at http://blast.ncbi.nlm.nih.gov/Blast.cgi

(iii) Clustal X 1.83

The Clustal X 1.83 software (Thompson et al. 1997) was used for multiple alignments of DNA and protein sequences.

(iv) Conserved Domain Database (CDD)

Conserved Domain Database was used to identify conserved domains in the proteins. This is available at http://www.ncbi.nlm.nih.gov/Structure/cdd/wrpsb.cgi

(v) ExPasy Translate tool

ExPasy Translate tool was used for translating DNA sequences to protein sequences. It is available at http://web.expasy.org/translate/

(vi) Maps sites for restriction enzymes

This was used for restriction analysis of DNA sequences. It is available at http://www.restrictionmapper.org/

(vii) MEGA 4

MEGA 4 software (Tamura et al. 2007) was used to perform phylogenetic analysis.

(viii) Primer3

Primer3 was used for analysis of the secondary structure of oligonucleotide primers. It is available at http:// bioinfo.ut.ee/primer3-0.4.0/

(ix) Site for reverse-complement

To convert a DNA sequence into reverse-complement counterpart, sequence manipulation suite (SMS) software package was used. It is available at http://www.bioinformatics.org/sms/index.html

TH-1227_09610609

CHAPTER 3

Screening of knockout mutants of Neurospora crassa calcium signaling genes and identification of cellular roles of the NCU04379 gene

TH-1227_09610609

3.1 Introduction

The genome analysis of *Neurospora crassa* has revealed ~10,082 protein coding genes including 48 genes that encode Ca^{2+} signaling proteins (Galagan et al. 2003; Borkovich et al. 2004). The *Neurospora* functional genomics project has aimed to generate knockout mutants of all the ~10,082 genes (http://www.dartmouth.edu/~neurosporagenome/knockouts_completed.html) for functional analysis. We have obtained 43 Ca^{2+} signaling knockout mutants from the FGSC. These knockout mutants were generated using a high throughput gene knockout procedure (Colot et al. 2006). The high throughput knockout procedure essentially used a gene targeting cassette that contains an ~1–1.5 kb of 5′ flank of the target ORF followed by the selectable marker *hph* (gene for hygromycin B phosphotransferase) driven by the *trpC* promoter that confers resistance to antibiotic hygromycin (Gritz and Davies 1983; Staben et al. 1989) and an ~1–1.5 kb of 3′ flank of the target ORF (Figure 3.1). This strategy yielded homokaryotic knockouts for only 31 Ca^{2+} -signaling genes, heterokaryotic knockout mutants are available for 12 Ca^{2+} -signaling genes. However, no knockouts are available for five Ca^{2+} -signaling genes, indicating that the initial PCR to generate the knockout cassette did not work or these genes are essential for viability. I had initially obtained 18 Ca^{2+} signaling knockout mutants from the FGSC (Table 3.1) and studied their growth phenotype.

3.2 Results

3.2.1 Growth study of the *N. crassa* knockout mutants of calcium signaling genes

I studied growth behaviour of knockout mutants for 18 Ca^{2+} signaling genes in petridishes (100 mm) diameter containing Vogel's medium. Agar plugs of strains were inoculated at the centre of petridish and colony diameter was measured regularly at 3 h interval for 24 h. The ΔNCU04379.2 mutant displayed a slow growth phenotype (Table 3.2). Therefore, I studied the ΔNCU04379.2 knockout mutant in detail.

TH-1227_09610609

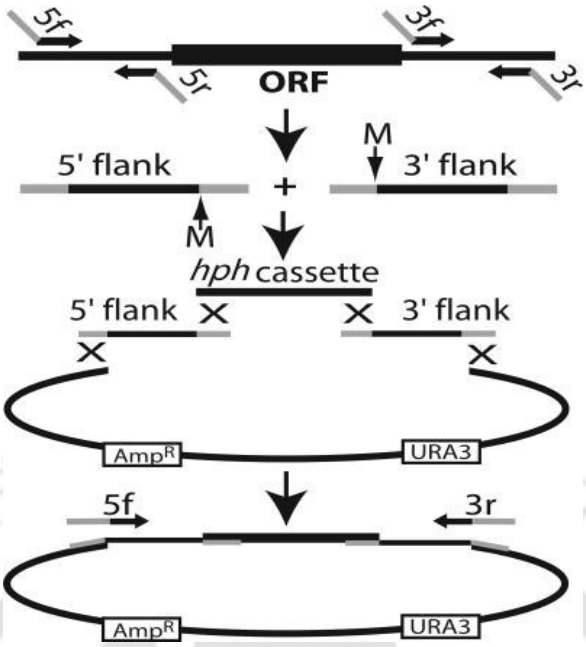

Figure 3.1: Strategy for generating deletion constructs. The 5′ and 3′ flank fragments are amplified separately from the wild-type using primers 5f with 5r and 3f with 3r, respectively. Primers 5r and 3f incorporate *MmeI* sites (M) and have 5′ tails homologous to the *hph* cassette, whereas 5′ tails of 5f and 3r are homologous to the shuttle vector pRS426 (described in Chapter 2). The two flanks are co-transformed into the yeast strain along with the *hph* cassette and a gapped pRS426 vector. Homologous recombination creates the circular construct and the final linear deletion cassette is amplified from the pooled yeast DNA with primers 5f and 3r. The *hph* is transcribed in the antisense direction relative to the transcription of the target gene. Adapted from Colot et al. (2006).

TH-1227_09610609

Table 3.1 List of *N. crassa* knockout mutant strains of Ca^{2+}signaling genes used in this study

S. no.	NCU no. or strain type	FGSC no. (*a*/*A*)	Type of protein	Source
1.	Wild-type	988/987		FGSC
2.	02814.2	11169/11170	Ca^{2+} and/or CaM binding protein	FGSC
3.	06650.2	11246/11247	Ca^{2+} and/or CaM binding protein	FGSC
4.	04379.2	11403/11404	Ca^{2+} and/or CaM binding protein	FGSC
5.	05255.2	11405/11406	Ca^{2+} and/or CaM binding protein	FGSC
6.	06177.2	11537/11536	Ca^{2+} and/or CaM binding protein	FGSC
7.	06948.2	11541/11542	Ca^{2+} and/or CaM binding protein	FGSC
8.	02283.2	12448/12449	Ca^{2+} and/or CaM binding protein	FGSC
9.	09123.2	12548/12547	Ca^{2+} and/or CaM binding protein	FGSC
10.	01564.2	15898/15899	Ca^{2+} and/or CaM binding protein	FGSC
11.	07075.2	11248/11249	Ca^{2+} H^{+} exchanger	FGSC
12.	06366.2	11407/11408	Ca^{2+} /H^{+} exchanger	FGSC
13.	00916.2	11685/11686	Ca^{2+} /H^{+} exchanger	FGSC
14.	00795.2	12376/12375	Ca^{2+} /H^{+} exchanger	FGSC
15.	08147.2	11255/11256	Ca^{2+} -ATPase	FGSC
16.	07966.2	11410/11409	Ca^{2+} -ATPase	FGSC
17.	02826.2	11530/11529	Ca^{2+} -ATPase	FGSC
18.	05154.2	13036/13037	Ca^{2+} -ATPase	FGSC
19.	09655.2	11271/11272	Phospholipase C	FGSC

TH-1227_09610609

Table 3.2 Average growth rate of the *N. crassa* calcium signaling knockout mutants

S. no.	Strain	Average growth rate (cm/h)
1.	Wild-type	0.354
2.	ΔNCU04379.2	0.258
3.	ΔNCU05225.2	0.325
4.	ΔNCU06366.2	0.298
5.	ΔNCU07966.2	0.311
6.	ΔNCU02814.2	0.332
7.	ΔNCU08147.2	0.306
8.	ΔNCU02826.2	0.359
9.	ΔNCU06650.2	0.350
10.	ΔNCU07075.2	0.331
11.	ΔNCU09655.2	0.308
12.	ΔNCU06177.2	0.326
13.	ΔNCU06948.2	0.309
14.	ΔNCU00916.2	0.374
15.	ΔNCU0795.2	0.339
16.	ΔNCU02283.2	0.363
17.	ΔNCU09123.2	0.320
18.	ΔNCU05154.2	0.328
19.	ΔNCU01564.2	0.343

TH-1227_09610609

3.2.2 The ΔNCU04379.2 mutant displayed a slow growth rate

The growth behaviour of the ΔNCU04379.2 mutant was further studied using standard race tube assay (Ryan et al. 1943; Ryan 1950). The race tube is a hollow glass tube about ~30 cm long and ~13 mm in diameter, bent upward (~45º) at both ends in order to hold the media. The linear growth of strains can be better studied for 3 days (~72 h) in this long tube. Agar plugs of the wild-type and ΔNCU04379.2 mutant were inoculated at one end of the race tube containing 13 ml of Vogel's glucose agar medium, and incubated at 30ºC for 72 h (till growth front reaches the other end of the race tube). The hyphal growth front was marked periodically at an interval of 12 h for 72 h and the distance of the hyphal growth front from the inoculation point was plotted against time (Figure 3.2; Table 3.3). The average growth rates of the wild-type and ΔNCU04379.2 mutant strains were 0.357 ± 0.106 and 0.263 ± 0.076 cm h^{-1}, respectively (n = 3).

3.2.2.1 The slow growth phenotype of the ΔNCU04379.2 mutant was not due to a defect in ergosterol biosynthesis

Ergosterol is a major constituent of fungal plasma membrane synthesized from a central metabolite acetyl CoA (Paltauf et al. 1992; Parks and Casey 1995). The ergosterol biosynthesis pathway is catalyzed by several enzymes. In Neurospora, *erg-3* gene encodes sterol C-14 reductase that catalyses the reduction of the $\Delta^{14, 15}$ double bond in intermediates in the sterol biosynthesis pathway using NADPH as a cofactor (Prakash et al. 1999). The RIP-induced *erg-3* mutant grows slowly due to a defect in ergosterol biosynthesis (Prakash et al. 1999). To test if the slow growth phenotype of the ΔNCU04379.2 mutant was due to a defect in ergosterol biosynthesis, I had analysed the ergosterol profiles of the wild-type and ΔNCU04379.2 mutant. Ergosterol has UV absorption maxima at 272, 282, and 293 nm whereas sterols from the *erg-3* mutant absorb maximally at ~250 nm, typical of $\Delta^{8, 14}$ sterols, indicating absence of ergosterol in the *erg-3* mutant (Prakash et al. 1999). UV spectra analysis of sterols isolated from the wild-type and ΔNCU04379.2 mutant suggested no defect in sterol biosynthesis in the ΔNCU04379.2 mutant and showed intense peak at 272, 282, and 293 nm (Figure 3.3). Thus, it was concluded that slow growth phenotype of the ΔNCU04379.2 mutant was not due to a defect in ergosterol biosynthesis.

TH-1227_09610609

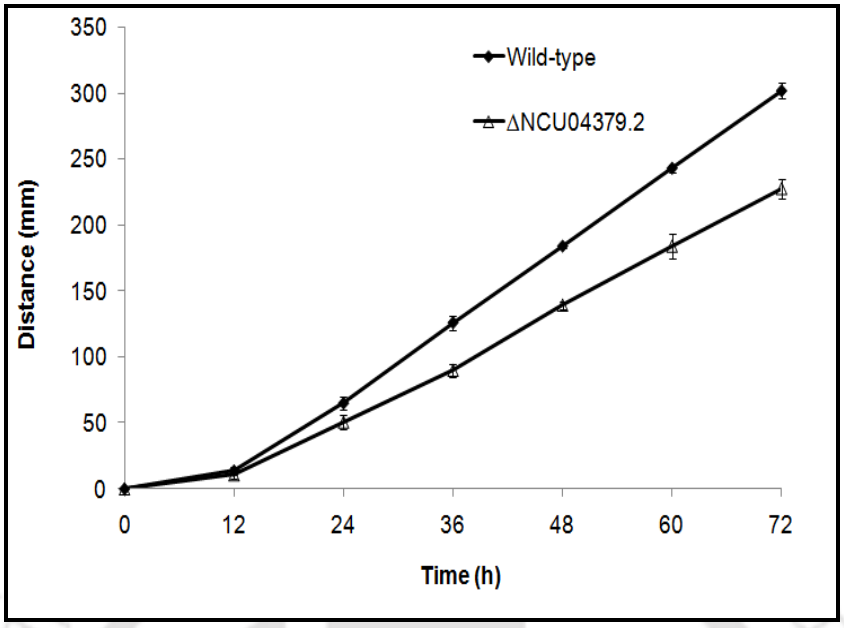

Figure 3.2: Growth phenotype of the wild-type and the ΔNCU04379.2 mutant. The Apical growth of the wild-type and ΔNCU04379.2 mutant strains were measured at 30ºC using 'race tubes' over a period of 72 h containing Vogel's glucose medium. Error bars indicate the standard errors calculated from the data for three independent experiments. The ΔNCU04379.2 mutant grows slowly in compare to the wild-type. The average growth rate of the wild-type and the ΔNCU04379.2 are 0.357 ± 0.106 cm h^{-1}, and 0.267 ± 0.076 cm h^{-1}, respectively.

Table 3.3 Apical growth of the *N. crassa* wild-type and ΔNCU04379.2 mutant in race tube

Strain	Distance (mm) in race tube at the indicated time interval						
	0 h	**12 h**	**24 h**	**36 h**	**48 h**	**60 h**	**72 h**
Wild-type	0	20 ± 5	73 ± 6	134 ± 5	197 ± 3	262 ± 3	322 ± 3
ΔNCU04379.2	0	15 ± 5	53 ± 6	97 ± 4	146 ± 3	193 ± 9	241 ± 7

TH-1227_09610609

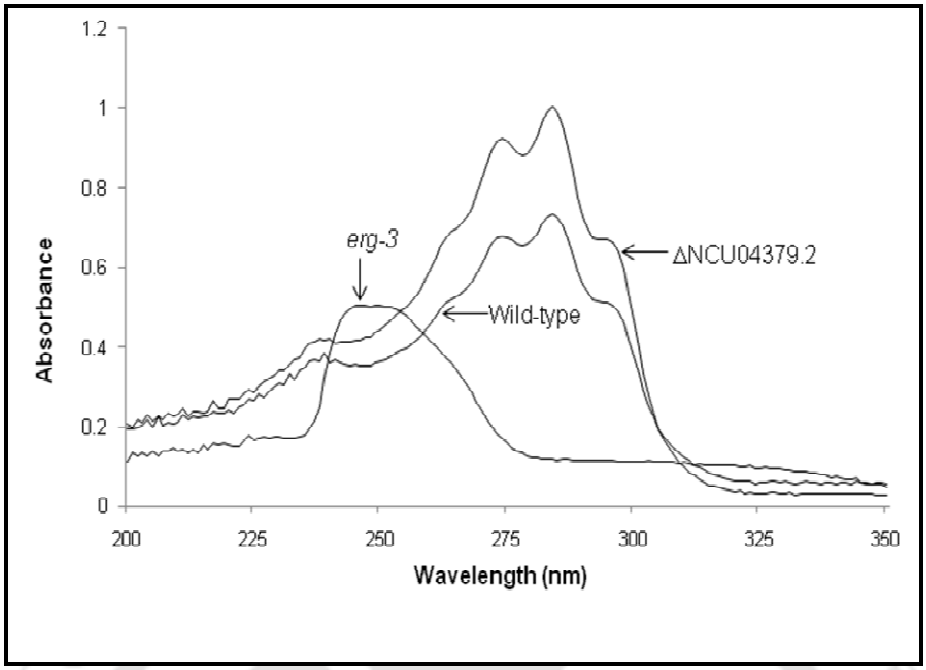

Figure 3.3: Ergosterol profiles in the wild-type, ΔNCU04379.2 and *erg-3* null mutant. Profile of the sterols extracted from the wild-type, ΔNCU04379.2, and the *erg-3* mutant were analyzed by UV spectrophotometry. Ergosterol has UV absorption maxima at 272, 282, and 293 nm whereas the *erg-3* mutant sterols absorb maximally at ~250 nm, typical of $\Delta^{8,14}$ sterols, indicating absence of ergosterol in the *erg-3* mutant. Ergosterol is present in the wild-type and the ΔNCU04379.2 mutant.

TH-1227_09610609

3.2.3 Calcium sensitivity analysis

3.2.3.1 The ΔNCU04379.2 mutant was hypersensitive to $CaCl_2$ stress

The cytosolic free Ca^{2+} ($[Ca^{2+}]_c$) and the Ca^{2+}gradient in fungal hyphae plays an important role in establishing and maintaining apical organization, morphogenesis and growth (Jackson and Heath 1993). To test the effect of Ca^{2+} on growth, I did the growth analysis of the wild-type and ΔNCU04379.2 mutant on medium supplemented with various concentrations of $CaCl_2$ (0, 0.2, 0.3, and 0.4 M). The ΔNCU04379.2 mutant showed severe growth defect on medium supplemented with 0.3 M and 0.4 M $CaCl_2$ (Figure 3.4 A). The average colony growth rate was calculated by plotting colony growth rate against different concentrations of $CaCl_2$. The ΔNCU04379.2 mutant displayed a lower colony growth rate than the wild-type (Figure 3.4 B, Table 3.4). Therefore, I concluded that the ΔNCU04379.2 mutant is hypersensitive to $CaCl_2$ stress.

3.2.3.2 The $CaCl_2$ hypersensitivity of the ΔNCU04379.2 mutant was not due to a mere osmotic effect

High concentration of salts also gives rise to osmotic stress that may inhibit growth. In eukaryotes, Ca^{2+} acts as one of the primary regulators of osmotic stress. Intracellular Ca^{2+} levels rise during hypo-osmotic and hyper-osmotic stresses (Kader and Lindberg 2010). To determine whether Ca^{2+} sensitivity phenotype of the ΔNCU04379.2 mutant was specific to $CaCl_2$ stress or due to an osmotic effect, I studied the effect of NaCl (Figure 3.5, Table 3.5) and sucrose (Figure 3.6, Table 3.6) at various concentrations on the growth of the mutant. I found that the ΔNCU04379.2 mutant was not sensitive to either NaCl or sucrose stress. These results suggested that sensitivity of the ΔNCU04379.2 mutant was specific to $CaCl_2$ stress and not due to a mere osmotic effect.

3.2.3.3 Effect of Ca^{2+} deprivation on growth

In order to test the effect of Ca^{2+} deprivation, the wild-type and ΔNCU04379.2 mutant strains were grown on Vogel's glucose agar media with various concentrations of EGTA that has high affinity and selectivity for free Ca^{2+} (Tsien 1980). The decrease of EGTA, and the corresponding increase of Ca^{2+} levels, revealed the higher Ca^{2+}-sensitivity of the ΔNCU04379.2 mutant relative to wild type (Figure 3.7). This suggested that the $CaCl_2$ sensitivity phenotype of the ΔNCU04379.2 mutant was selectively for the Ca^{2+}.

TH-1227_09610609

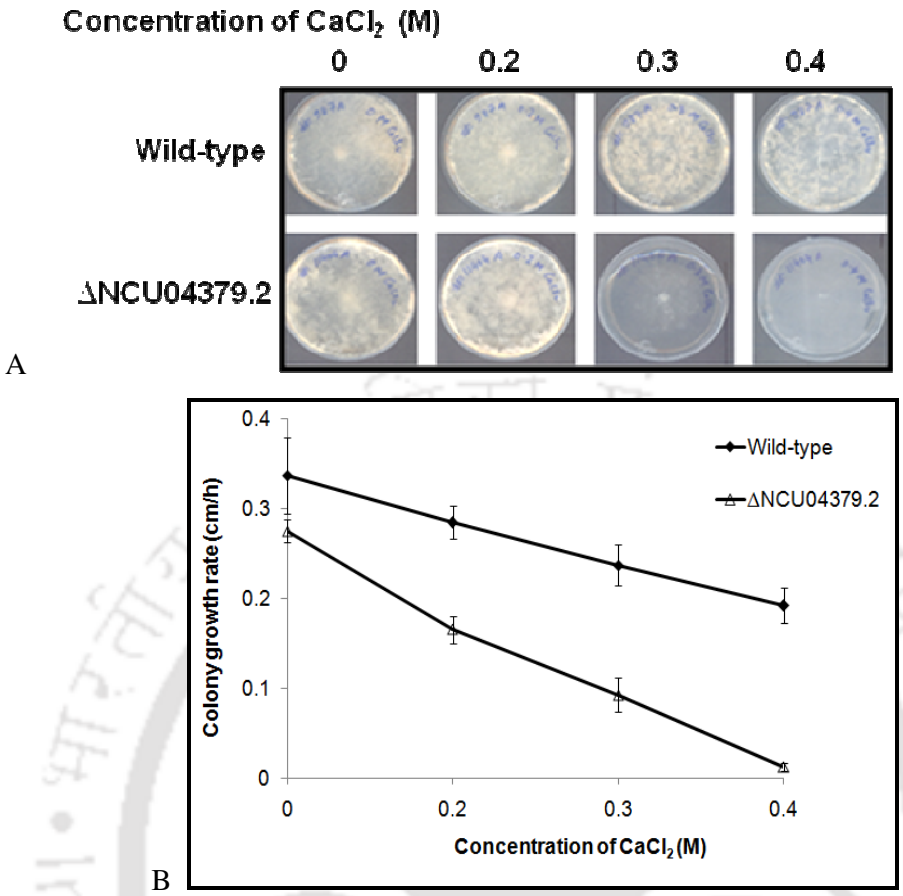

Figure 3.4: Effect of $CaCl_2$ stress on the growth of the wild-type and ΔNCU04379.2 mutant. **(A)** Growth of the wild-type and ΔNCU04379.2 mutant in petridishes containing Vogel's glucose medium supplemented with various concentrations of $CaCl_2$ (0 M, 0.2 M, 0.3 M, 0.4 M). Plates were incubated at 30ºC for 24 h. **(B)** Colony growth rate (cm/h) of the wild-type and ΔNCU04379.2 mutant in petridishes containing Vogel's glucose medium supplemented with various concentrations of $CaCl_2$. Error bars indicate the standard errors calculated from the data for three independent experiments.

Table 3.4 Average colony growth rate of the wild-type and ΔNCU04379.2 mutant at various concentrations of $CaCl_2$

Strain	Average growth rate (cm/h) at various concentrations of $CaCl_2$ (M)			
	0	**0.2**	**0.3**	**0.4**
Wild-type	0.336 ± 0.042	0.284 ± 0.018	0.236 ± 0.022	0.191 ± 0.019
ΔNCU04379.2	0.274 ± 0.012	0.165 ± 0.015	0.092 ± 0.018	0.012 ± 0.004

TH-1227_09610609

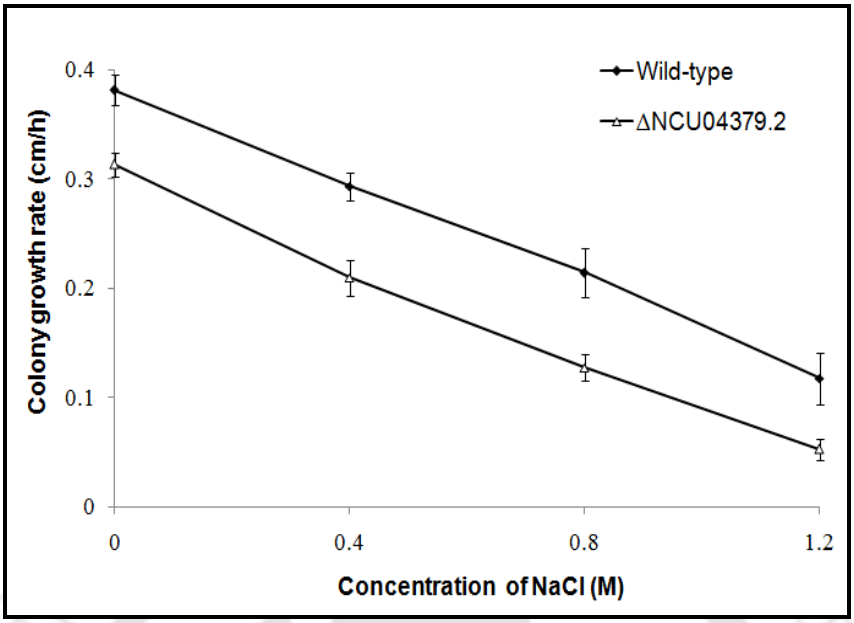

Figure 3.5: Effect of NaCl on the growth of the wild-type and ΔNCU04379.2 mutant. Colony growth rate (cm/h) of the wild-type and ΔNCU04379.2 mutant on Vogel's glucose medium supplemented with various concentrations of NaCl (0.4 M, 0.8 M, and 1.2 M). Error bars indicate the standard errors calculated from the data for three independent experiments.

Table 3.5 Average colony growth rate of the wild-type and ΔNCU04379.2 mutant at various concentrations of NaCl

Strain	Average growth rate (cm/h) at various concentration of NaCl (M)			
	0	**0.4**	**0.8**	**1.2**
Wild-type	0.381 ± 0.013	0.293 ± 0.012	0.214 ± 0.023	0.117 ± 0.023
ΔNCU04379.2	0.313 ± 0.010	0.209 ± 0.016	0.127 ± 0.012	0.052 ± 0.010

TH-1227_09610609

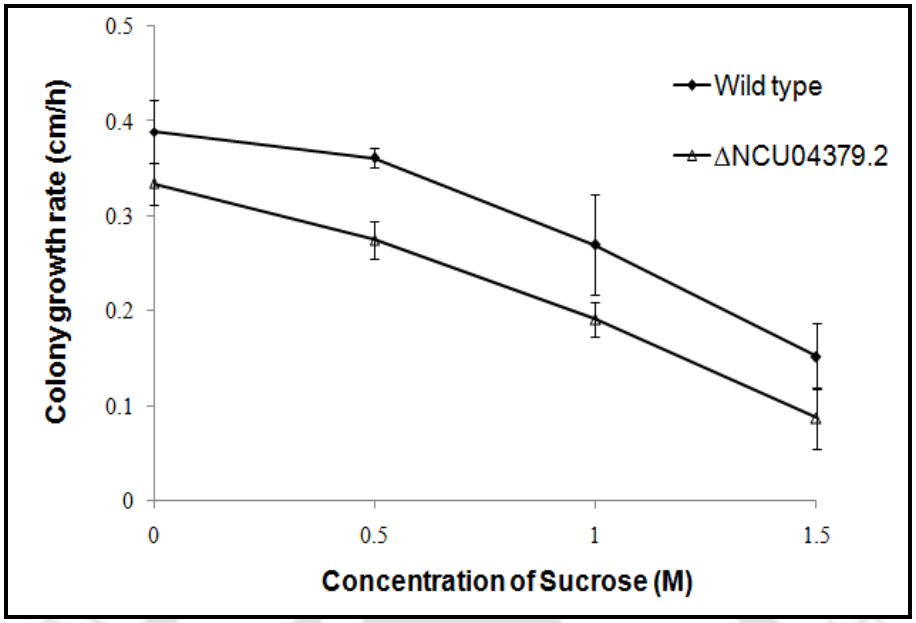

Figure 3.6: Effect of sucrose on the growth of the wild-type and ΔNCU04379.2 mutant. Colony growth rate (cm/h) of the wild-type and ΔNCU04379 on Vogel's glucose medium supplemented with various concentrations of sucrose (0.5, 1, and 1.5 M). Error bars indicate the standard errors calculated from the data for three independent experiments.

Table 3.6 Average colony growth rate of the wild-type and ΔNCU04379.2 mutant at various concentrations of sucrose

Strain	**Average growth rate (cm/h) at the various concentration of sucrose (M)**			
	0	**0.5**	**1**	**1.5**
Wild-type	0.389 ± 0.033	0.361 ± 0.012	0.27 ± 0.052	0.152 ± 0.034
ΔNCU04379.2	0.334 ± 0.022	0.275 ± 0.019	0.191 ± 0.017	0.087 ± 0.031

TH-1227_09610609

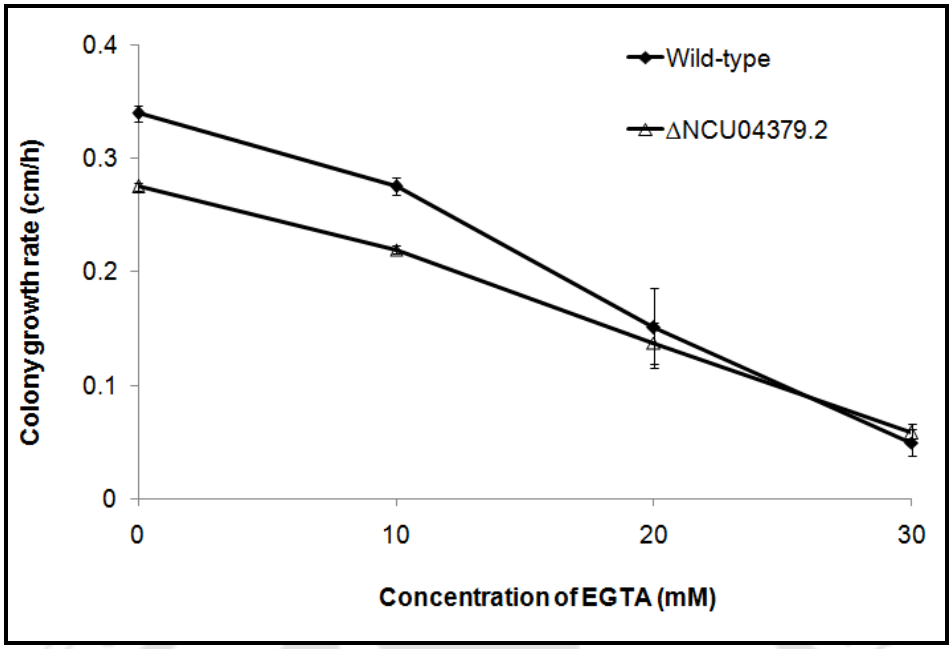

Figure 3.7: Effect of EGTA on the growth of the wild-type and ΔNCU04379.2 mutant. Colony growth rate (cm/h) of the wild-type, and ΔNCU04379.2 mutant were measured at various concentrations of EGTA (10, 20, and 30 mM). Error bars indicate the standard errors calculated from the data for three independent experiments.

TH-1227_09610609

3.2.4 UV survival assay

3.2.4.1 The ΔNCU04379.2 mutant showed an increased sensitivity to UV-irradiation

One of the versatile Ca^{2+} signaling proteins, Ca^{2+}-modulated protein CaM plays a crucial role in DNA repair, DNA synthesis and proliferation in both CHO and human cell lines (Chard 1987; Mirzayans et al. 1995). The sensitivity of the ΔNCU04379.2 mutant to Ca^{2+} stress prompted me to test if ultraviolet (UV) stress has any effect on this strain. I assayed UV-sensitivity of the ΔNCU04379.2 mutant qualitatively and quantitatively. For qualitative analysis, conidia were grown on Vogel's glucose agar media for seven days, harvested, washed with sterile water, and finally re-suspended in sterile water. A conidial suspension of ~1 x 10^6 conidia/ml was further diluted and ~10^5, 10^4, 10^3, 10^2, and 10^1 conidia were spotted on Vogel's sorbose agar medium and irradiated with UV doses of 100, 200 and 300 J/m^2 in a UVC 500 crosslinker (Hoefer, UK). For quantitative analysis, ~1000 conidia were plated on the Vogel's sorbose agar medium and irradiated with the same UV doses. The results of the spot test (Figure 3.8 A) and the UV dose-response curves (Figure 3.8 B) revealed an increased sensitivity of the ΔNCU04379.2 mutant to UV-irradiation. The *upr-1(34-97-3)* mutant strain was used to compare the relative UV sensitivity phenotypes. The relative UV sensitivity of the ΔNCU04379.2 mutant was less than the *upr-1* mutant. This result indicates that the NCU04379 gene plays a role in UV-survival.

TH-1227_09610609

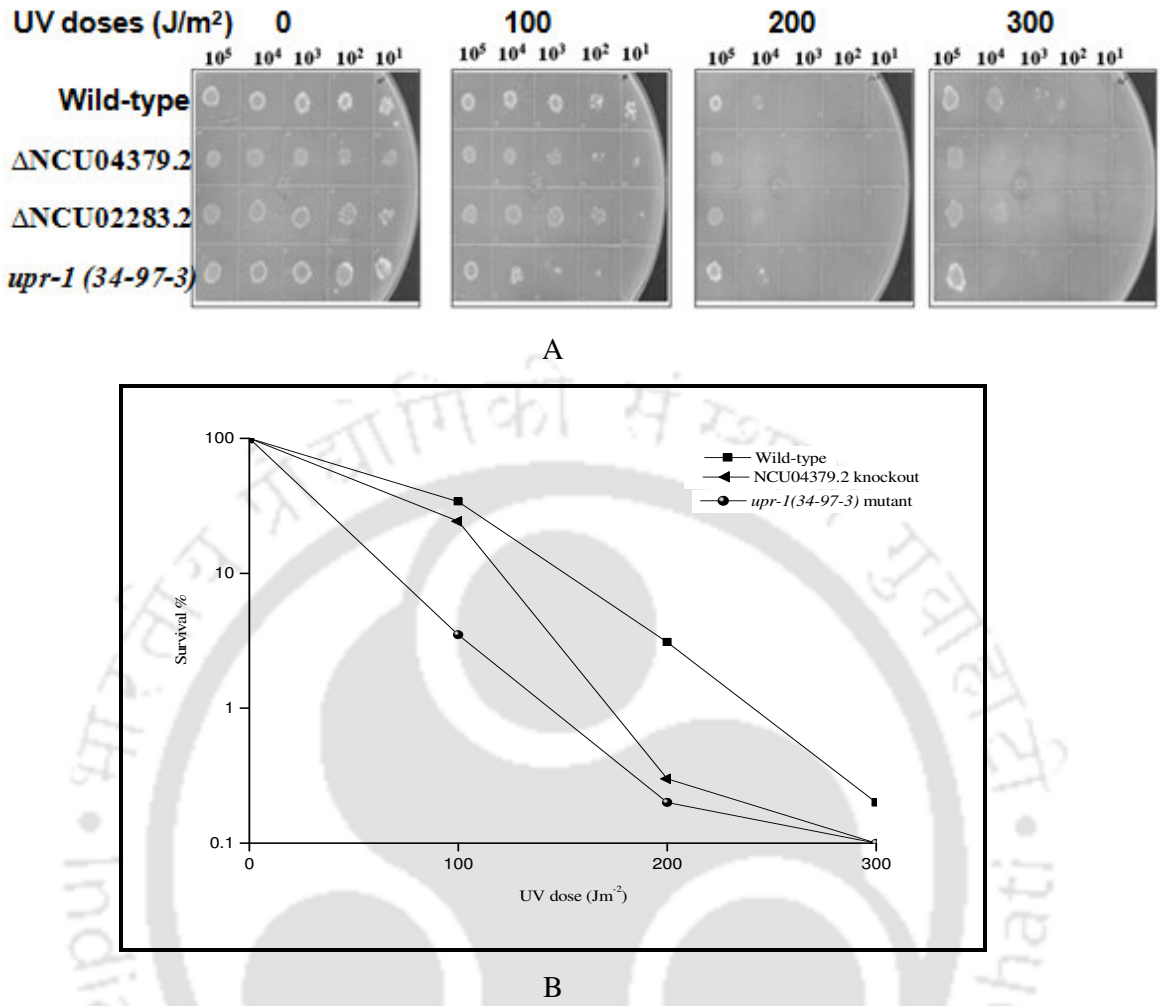

Figure 3.8: Effect of UV irradiation on the survival of the wild-type and ΔNCU04379.2 mutant. **(A)** Qualitative analysis of UV sensitivity. Approximately 10^5,10^4, 10^3, 10^2 and 10^1 conidia were spotted from left to right on agar plates and irradiated with the indicated UV doses. The *upr-1(34-97-3)* strain was previously generated (Tamuli et al. 2006) and used as a reference strain to compare the relative UV sensitivity of the ΔNCU04379.2 mutant. **(B)** Quantitative assay to determine the UV sensitivity of the wild-type, ΔNCU04379.2, and the *upr-1(34-97-3)* strain. Each data point represents the mean of at least three independent experiments.

TH-1227_09610609

3.2.5 Cloning of the NCU04379 fragment from the wild-type for complementation analysis

The oligonucleotide primer pairs NCU04379-5F (Table 3.7; entry 1) and NCU04379-3R (Table 3.7, entry 2) were used to PCR amplify a fragment of ~3972 bp that contains the of NCU04379 gene from the wild-type strain (Figure 3.9 A). The sequences of the primers NCU04379-5F and NCU04379-3R were obtained from the FGSC primer list for the knockouts (http://www.dartmouth.edu/~neurosporagenome/primers.html). PCRs were performed using custom oligonucleotide primers (Integrated Genome Technology, USA), and Phusion™ high fidelity DNA polymerase (Finnzymes, Finland). The PCR reaction condition used were 30 sec initial denaturation at 98ºC followed by 25 cycles of 10 sec denaturation at 98ºC, 30 sec annealing at 60ºC and 3 min elongation at 72ºC. The final extension was at 72 ºC for 10 min. The size of the PCR amplified product was ~3.972 kb (Figure 3.9 B). The PCR product of the NCU04379 fragment was purified from agarose gel using quick gel extraction kit (Qiagen, CA), cloned into the *SmaI* site of the pBARGEM7-1 vector and transformed into the *E. coli DH5α* ultra-competent cells. The transformants were initially selected by blue-white screening. The plasmids were isolated from the white colonies and clone that showed plasmid shift was used further to confirm the correct insert fragment (Figure 3.9 C). The recombinant plasmid, designated as pRD-1, was confirmed by restriction digestion using *BamHI* and *EcoRI* enzymes (Figure 3.9 D).

3.2.6 Transformation of the pRD-1 construct into the ΔNCU04379.2 mutant

Transformation of the pRD-1 construct into the ΔNCU04379.2 mutant was done by electroporation. The detail procedure of transformation in *N. crassa* was described in Chapter 2. Transformants were selected on the sorbose plate containing antibiotic basta (220 µg/ml). Out of three initial transformants, two transformants were basta resistant. One of the initial heterokaryotic transformant, designated as HT-1, was confirmed by Southern hybridization. For performing Southern hybridization, the *Xmn1* restriction enzyme was used to digest the genomic DNA isolated from the strains. The 3.972 kb fragment containing the NCU04379 gene was used as a probe in Southern hybridization. The restriction enzyme *Xmn I* has two cut sites (X2 and X3) within the probe region, therefore, *Xmn I* digestion results in three fragments of size 645, 1860, and 2175 bp in the wild-type; the NCU04379 knockout has only one *Xmn I* cut site within the probe region (X3), and thus, results only two fragments of size 645 and 3856 bp (Figure 3.10 A, B). The Southern analysis confirmed that the

TH-1227_09610609

integration of the NCU04379 transgene is ectopic in the transformant strain HT-1. The heterokaryotic transformant HT-1 was further crossed with opposite mating type of the ΔNCU04379.2 mutant to obtain homokaryotic progenies. In addition, PCR analysis, using primer pairs NCU04379-5F and 5HPHR (Table 3.7, entries 1, 3), was performed to verify the presence of the ΔNCU04379.2 mutant allele in the transformant progenies. Amplification of the knockout allele in the homokaryotic transformant progenies also supported that the integration of NCU04379 transgene in the ΔNCU04379.2 mutant strain is ectopic (Figure 3.11 A, B). In addition, RT-PCR analysis, using primers 6NCU04379-F forward (Table 3.7, entry 4) and 7NCU04379-R reverse (Table 3.7, entry 5), confirmed the expression of NCU04379 transgene in the homokaryotic transformant (Figure 3.12).

Table 3.7 Primers used for complementation studies of the ΔNCU04379.2 mutant

S. no.	Primer	Sequence (5′→3′)	Reference/source
1.	NCU04379-5F	GCTCGAAAGTTTAGTCCTGG	FGSC
2.	NCU04379-3R	CCCAGTAACGTCTCTTTTGC	FGSC
3.	5HPHR	ATCCACTTAACGTTACTGAAATC	This study
4.	6NCU04379-F	AGCTCGAGCGTGATAAGCTG	This study
5.	7NCU04379-R	AGGGCGGATACGATTGTCTC	This study
6.	NcTUB1f	AAC TTA CAA GAT GGC AGA GC	This study
7.	NcTUB1r	AAG GGG TCA CTA CAC TGA GGG	This study

3.2.7 Complementation of the ΔNCU04379.2 mutant

I tested three homokaryotic transformants carrying the NCU04379 transgene for their ability to complement the growth, $CaCl_2$ and UV sensitivity phenotypes of the ΔNCU04379.2 mutant. The homokaryotic transformants were found to complement the slow growth (Figure 3.13, Table 3.8), $CaCl_2$ sensitivity (Figure 3.14 A, B; Table 3.9), $CaCl_2$ deprivation by EGTA (Figure 3.15) and UV sensitivity (Figure 3.16 A, B) phenotypes of the ΔNCU04379.2 mutant. Therefore, I concluded that NCU04379 gene plays a role in growth, Ca^{2+} stress tolerance and UV survival in *N. crassa*.

TH-1227_09610609

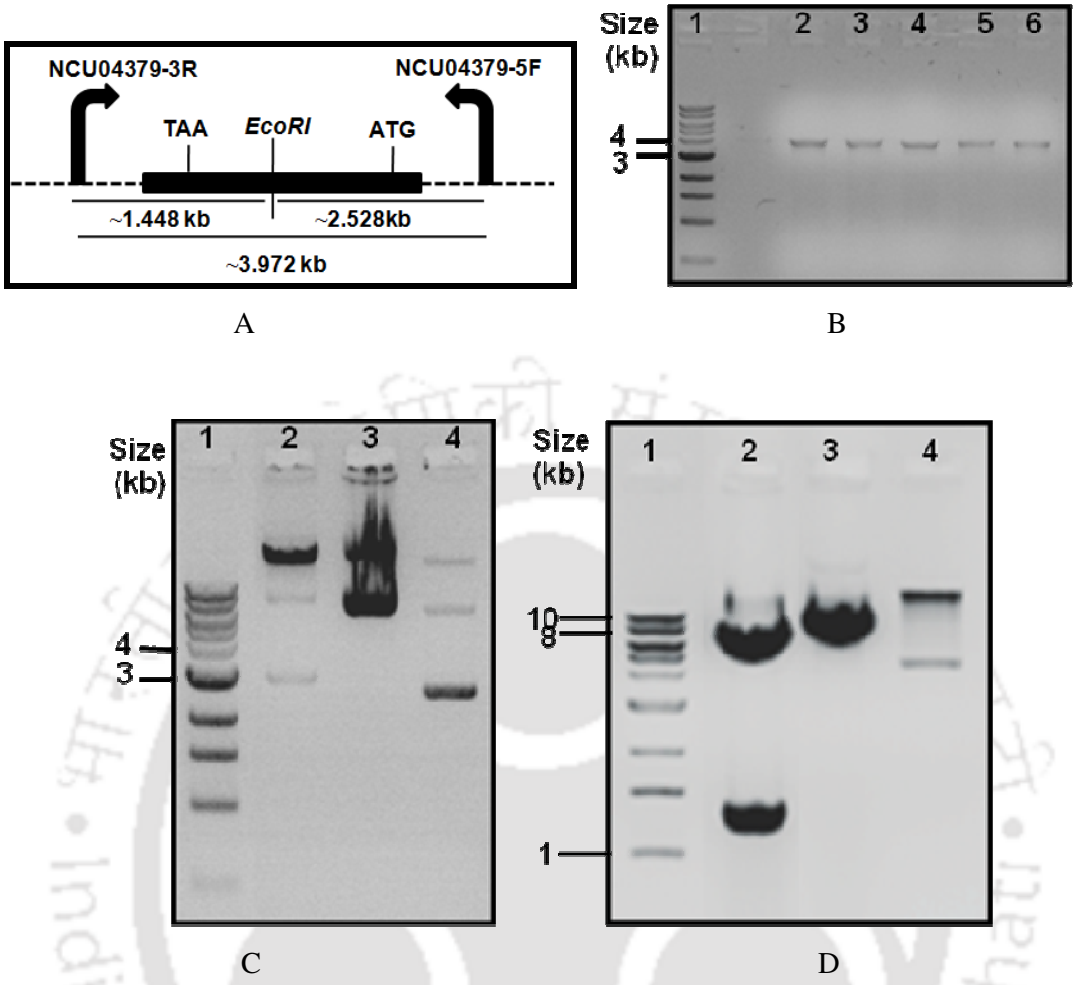

Figure 3.9: Cloning of NCU04379 fragment from the wild-type for complementation analysis. **(A)** The primer pairs NCU04379-5F and NCU04379-3R, used to amplify the NCU04379 fragment (~3.972 kb in size) from the wild-type, are indicated. The relative positions of the start (ATG) and the stop (TAA) codons and the *EcoRI* restriction site are shown. The distance of the *EcoRI* site, ~1.448 kb and ~2.528 kb, respectively, from the NCU04379-3R and NCU04379-5F primers are also shown. The size of the PCR amplified product is shown below. **(B)** Agarose gel electrophoresis of the NCU04379 fragment (~3.972 kb in size) amplified from the wild-type, resolved in lanes 2 to 6; lane 1, 1 kb DNA ladder (NEB). **(C)** Agarose gel electrophoresis of the plasmid isolated from *E. coli DH5α* transformants; lane 1, 1 kb DNA ladder (NEB); lane 2, pBARGEM7-1 vector (uncut); lane 3, the plasmid shift indicates the ligation of the insert in the pBARGEM7-1 vector, and designated as pRD-1; lane 4, another plasmid isolate did not show any plasmid shift. **(D)** Restriction digestion analysis of the pRD-1 construct. The pRD-1 construct was digested with *EcoRI* and *BamHI* restriction enzymes and resolved in 0.8% agarose gel; lane 1, 1 kb

TH-1227_09610609

DNA ladder (NEB); lane 2, *EcoRI* digestion releases two fragments of different sizes, ~1.448 kb and ~6 kb from the pRD-1 construct; Lane 3, *BamHI* digestion resulted in linearization of the pRD-1 construct of size 8.472 kb.

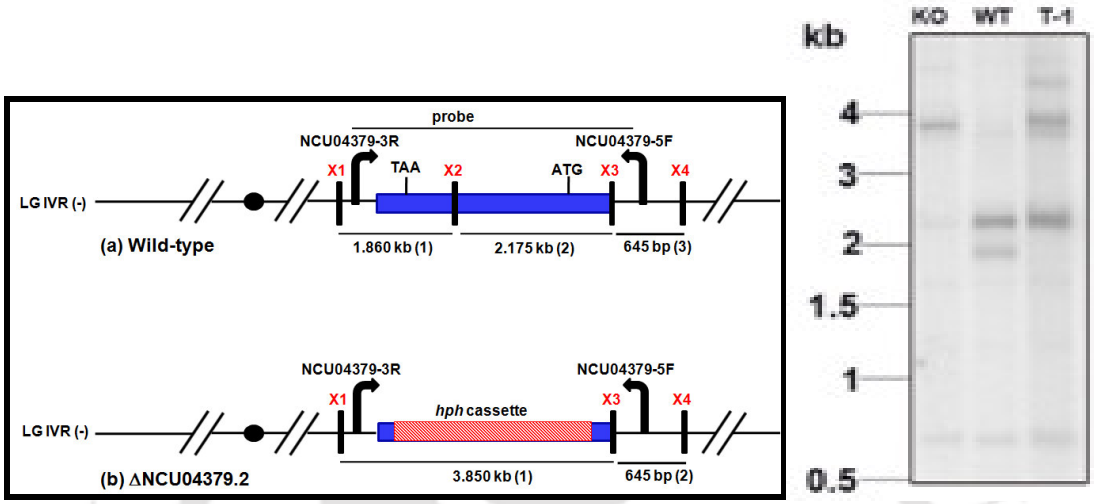

Figure 3.10: Confirmation of the ΔNCU04379.2 mutant and the pRD-1 transformants by Southern hybridization. **(A)** Schematic representation to illustrate the fragments generated in the Southern hybridization. Position of the *Xmn1* restriction enzyme cut sites (X1, X2, X3 and X4) in the locus region of the NCU04379 gene in the wild-type (a) and corresponding region in the ΔNCU04379.2 mutant (b). The 3.972 kb NCU04379 fragment, PCR amplified using primers NCU04379-5F and NCU04379-3R, was used as probe to hybridize the Southern blot. The *Xmn I* enzyme has two cut sites (X2 and X3) within the probe region that result in three fragments of size 645,1860, and 2175 bp in the wild-type, the knockout has only one cut site within the probe region (X3) that results only two fragments of size 645 and 3856 bp. **(B)** Southern analysis to confirm the ΔNCU04379.2 mutant and pRD-1 transformant. Genomic DNA of the ΔNCU04379.2 mutant (KO), the wild-type (WT), and the pRD-1 heterokaryotic transformant (T-1) were digested with *Xmn I* and probed with a 3972 bp NCU04379 fragment amplified from the wild-type using the primers NCU04379-5F and NCU04379-3R (Table 3.6, entries 1, 2). Three fragments of size 645,1860, and 2175 bp were appeared in the wild-type (WT) due to the presence of two cut sites within the probe, the knockout (KO) has only one cut site within the probe region and thus resulted in two fragments of size 645 and 3856 bp. The 2175 bp fragment, specific for the wild-type, is restored in the transformant (T-1).

TH-1227_09610609

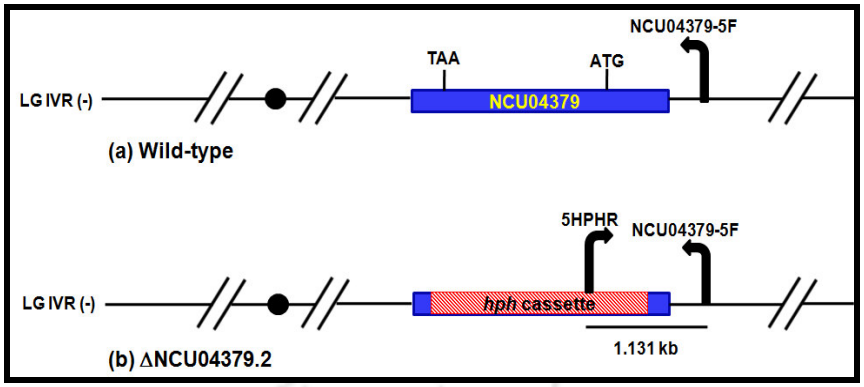

A

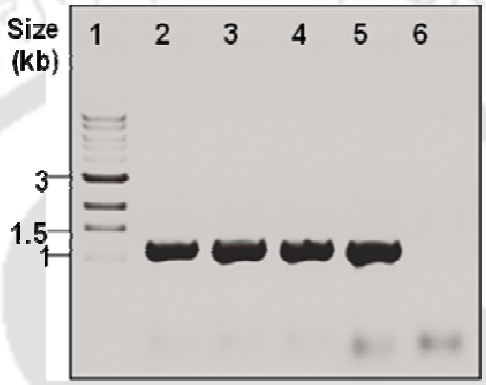

B

Figure 3.11: Verification of the ΔNCU04379.2 mutant allele in the strains transformed with pRD-1 construct. **(A)** Schematics of the NCU04379 gene in the wild-type (a) and the ΔNCU04379.2 mutant allele (b) are shown relative to the location on the linkage group. The position of NCU04379-5F forward (Table 3.7, entry 1) and the 5HPHR reverse (Table 3.7, entry 3) primers are shown. The 5HPHR is specific for the *hph* cassette used to generate the ΔNCU04379.2 mutant (Colot et al. 2006). Primers NCU04379-5F forward and 5HPHR are used to amplify a specific PCR product of size ~1.131 kb to verify the ΔNCU04379.2 mutant allele. **(B)** Verification of the ΔNCU04379.2 mutant allele in the homokaryotic transformants by PCR using primers NCU04379-5F and 5HPHR. PCR products were resolved in a 0.8% agarose gel; lane 1, 1 kb DNA ladder (NEB); lane 2, PCR amplification verifying the presence of the knockout allele (~1.131 kb in size) in the ΔNCU04379.2 mutant (control); lanes 3, 4, and 5, PCR amplification to verify the ΔNCU04379.2 mutant allele (~1.131 kb in size) in the homokaryotic transformants HoP-7, HoP-10, and HoP-6, respectively; lane 6, wild-type control (no PCR product as target sequence for the 5HPHR primer is absent in the wild-type).

TH-1227_09610609

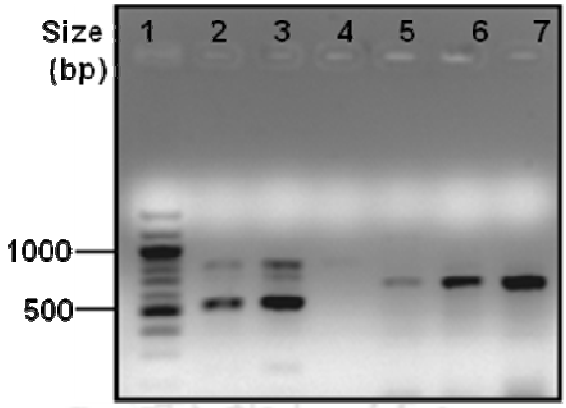

Figure 3.12: Verification of the expression of NCU04379 gene in the pRD-1 homokaryotic transformant. RT-PCR using primers NCU04379-6F and NCU04379-7R (Table 3.6, entries 4, 5), and RNA isolated from the wild-type, ΔNCU04379.2 mutant and the homokaryotic transformant-10. Amplification of a ~529 bp fragment confirms the expression of the NCU04379 gene. The RT-PCR products were resolved in a 1.2% agarose gel; lane 1, 100 bp ladder (NEB); lane 2, NCU04379 expression in the wild-type (control); lane 3, NCU04379 expression the homokaryotic transformant-10; lane 4, ΔNCU04379.2 mutant (control); lanes 5, 6, and 7, β-tubulin control expression (~651 bp in size) in the wild-type, homokaryotic transformant-10, and the ΔNCU04379.2 mutant, respectively, using primers NcTUB1f and NcTUB1r.

TH-1227_09610609

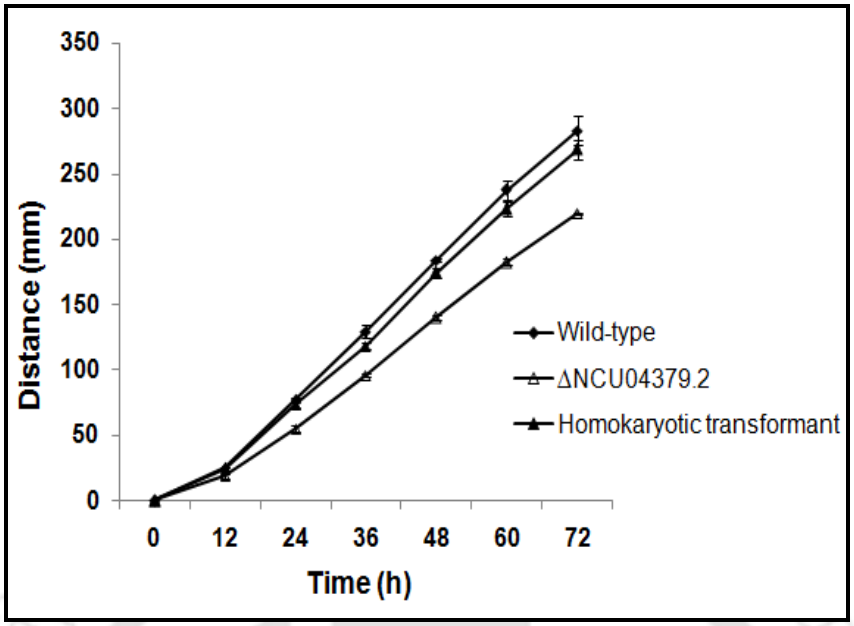

Figure 3.13: Complementation of the slow growth phenotype of the ΔNCU04379.2 mutant. Agar plug of the wild-type, the ΔNCU04379.2 mutant and the homokaryotic transformant were inoculated at one end of the race tube and incubated at 30°C till the growth front reaches the other end of the race tube (72 h). The homokaryotic transformant carrying the NCU04379 transgene showed growth rate similar to the wild-type. Error bars indicate the standard errors calculated from the data for three independent experiments.

Table 3.8 Apical growth of the wild-type, ΔNCU04379.2 mutant and homokaryotic transformant in race tube

Strain	Distance (mm) in race tube at the indicated time interval						
	0 h	**12 h**	**24 h**	**36 h**	**48 h**	**60 h**	**72 h**
Wild type	0	25 ± 3	77 ± 2	129 ± 5	184 ± 1	237± 7	283 ± 11
ΔNCU04379.2	0	19 ± 2	55 ± 3	96 ± 1	140 ± 2	182 ± 3	220 ± 1
Homokaryotic transformant	0	24 ± 2	73 ± 2	118 ± 2	174 ± 3	223 ± 5	268 ± 8

TH-1227_09610609

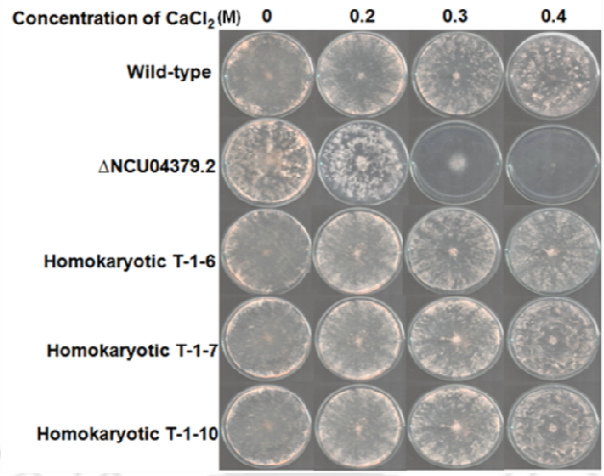

A

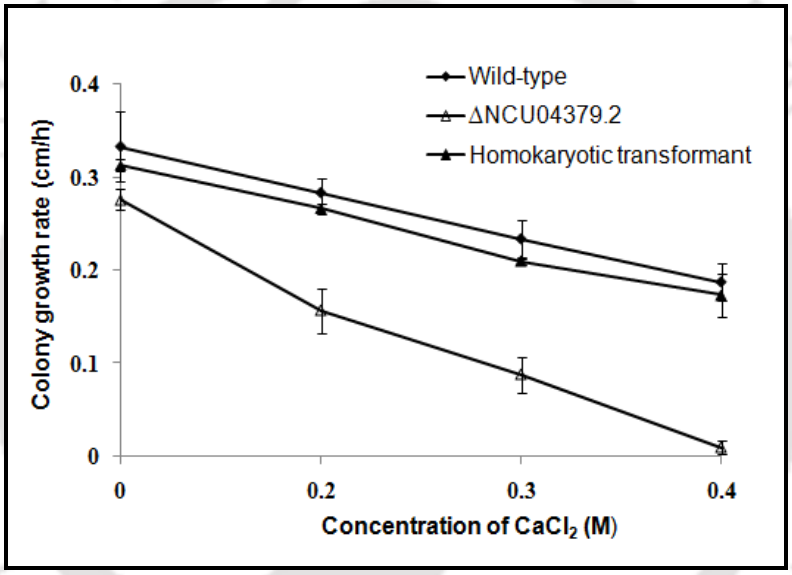

B

Figure 3.14: Complementation of the calcium sensitivity phenotype of the ΔNCU04379.2 mutant. **(A)** Conidia of the wild-type, the ΔNCU04379.2 mutant and the homokaryotic transformants were inoculated in the center of petridishes (100 mm diameter) containing Vogel's glucose agar medium supplemented with indicated concentrations of $CaCl_2$ and incubated at 30°C for 2 days. The homokaryotic transformants (T-1-6, T-1-7, T-1-10) carrying the NCU04379 transgene showed growth similar to the wild-type on medium supplemented with $CaCl_2$. **(B)** Average colony growth rate of wild-type, the ΔNCU04379.2 mutant and the homokaryotic transformants were plotted against different concentrations of $CaCl_2$. The homokaryotic transformants (T-1-6, T-1-7, T-1-10) carrying the NCU04379 transgene displayed growth rates similar to the wild-type. Error bars indicate the standard errors calculated from the data for three independent experiments.

TH-1227_09610609

Table 3.9 Average colony growth rate of the wild-type, ΔNCU04379.2 mutant and homokaryotic transformant at various concentrations of $CaCl_2$

Strain	Average growth rate (cm/h) at various concentrations of $CaCl_2$ (M)			
	0	**0.2**	**0.3**	**0.4**
Wild-type	0.339 ± 0.041	0.283 ± 0.018	0.228 ± 0.021	0.185 ± 0.022
ΔNCU04379.2	0.279 ± 0.010	0.153 ± 0.026	0.084 ± 0.019	0.012 ± 0.007
Homokaryotic transformant	0.312 ± 0.004	0.271 ± 0.01	0.213 ± 0.007	0.178 ± 0.021

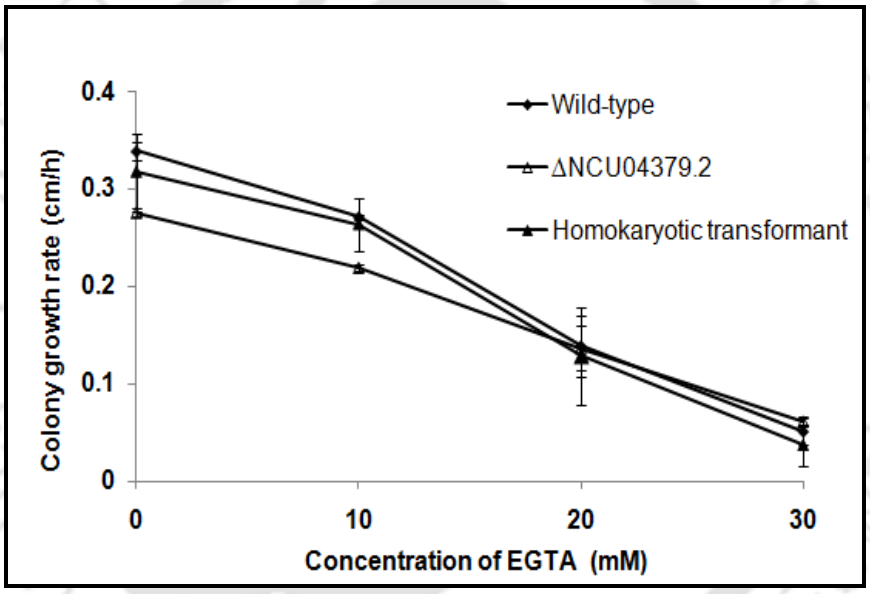

Figure 3.15: Complementation of the effect of EGTA on the ΔNCU04379.2 mutant. Average colony growth rate of the wild-type, the ΔNCU04379.2 mutant and the homokaryotic transformant strains were plotted against different concentrations of EGTA. The homokaryotic transformants (T-1-6, T-1-7, T-1-10) carrying the NCU04379 transgene displayed growth rates similar to the wild-type on the medium supplemented with EGTA. Error bars indicate the standard errors calculated from the data for three independent experiments.

TH-1227_09610609

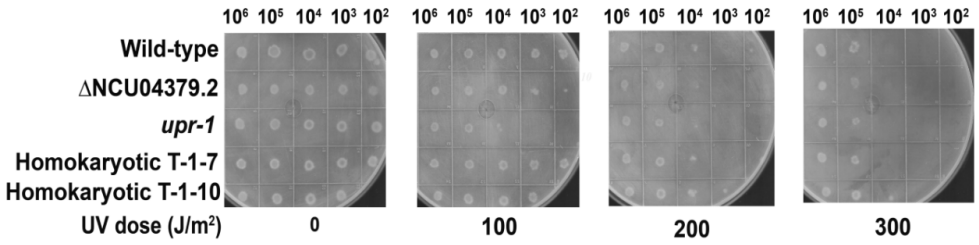

A

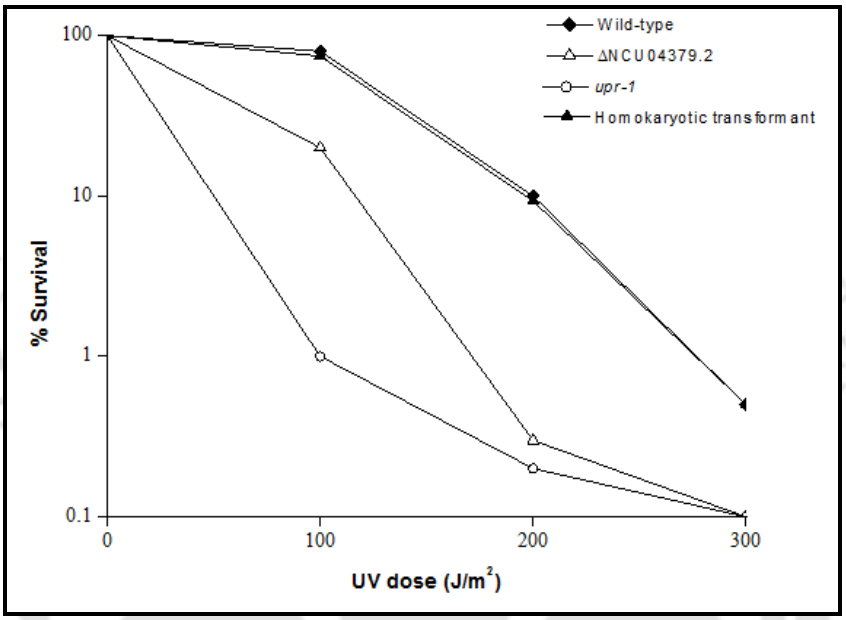

B

Figure 3.16: Complementation of the UV sensitivity phenotype of the ΔNCU04379.2 mutant. (A) Qualitative analysis of the UV sensitivity phenotype. Approximately 10^5, 10^4, 10^3, 10^2, 10^1 conidia of the wild-type, the ΔNCU04379.2 mutant, the *upr-1* mutant, and the homokaryotic transformants (homokaryotic T-1-7and 10) were spotted from left to right on the Vogel's sorbose agar plates, irradiated with the indicated UV doses, and grown at 30°C for 3 days in dark. The ΔNCU04379.2 mutant was more sensitive to UV irradiation than the wild-type, and the homokaryotic transformant strains (T-1-7and 10) carrying the NCU04379 transgene displayed UV sensitivity similar to the wild-type. **(B)** Quantitative analysis of UV sensitivity by calculating the percent survival of the colonies on irradiation to UV doses. Approximately 10^3 conidia of the wild-type, the ΔNCU04379.2 mutant, the *upr-1* mutant, and the homokaryotic transformants (Homokaryotic T-1-7and 10) were plated onVogel's sorbose agar plate and irradiated with different doses of UV. Percent survival was obtained by dividing the number of colonies from plates irradiated with UV by the number of colonies on plates with no UV irradiation (control). The homokaryotic transformant carrying the

TH-1227_09610609

NCU04379 transgene displayed UV sensitivity similar to the wild-type. Each data point represents the mean of at least three indepented experiments.

3.3 Discussion

The ΔNCU04379.2 mutant showed a slow growth phenotype and an increased sensitivity to Ca^{2+} and UV stress than the wild-type (Figures 3.2, 3.4 and 3.8, respectively). A fragment carrying the NCU04379 gene complements the slow growth, Ca^{2+} and UV sensitivity phenotypes of the ΔNCU04379.2 mutant (Figures 3.13, 3.14 and 3.16, respectively). These results suggested that the NCU04379 gene product is involved in growth, Ca^{2+} stress tolerance and UV-induced DNA damage repair pathways (Deka et al. 2011). This is the first report demonstrating the involvement of Ca^{2+} signaling gene in UV-induced DNA damage and repair in *N. crassa*.

A part of this chapter was published in Genetica (Deka et al. 2011) and presented in International Workshop on "Biology of Yeasts and Filamentous Fungi, 2009", held at Centre for Cellular and Molecular Biology, Hyderabad, India. In the next Chapter, I describe the sequence and site directed mutational analysis of the NCU04379 encoded protein to identify its homologues and critical amino acid residues necessary for its cell functions, respectively.

TH-1227_09610609

CHAPTER 4

Identification of NCU04379 as the Neurospora crassa homologue of Neuronal Calcium Sensor-1 and its site-directed mutational analysis

TH-1227_09610609

4.1 Introduction

In the previous Chapter, I described the role of NCU04379 gene in growth, Ca^{2+} stress tolerance, and UV survival. Information regarding the NCU04379 gene location and protein sequence was obtained from *Neurospora* genome database (version 2; http://www.broadinstitute.org/annotation/genome/neurospora/MultiHome.html). The NCU04379 gene is genetically mapped in supercontig four from position 3562633 to 3565030 (- strand) at the right arm of Linkage group IV (LG IVR). The NCU04379 sequence was used as a query sequence in a BLAST search to identify its homologues. In addition, site-directed mutational analysis of the NCU04379 gene was performed to identify critical amino acid residues necessary for its cellular functions. This Chapter describes the sequence and site-directed mutational analysis of NCU04379.

4.2 Results

4.2.1 NCU04379 gene encodes a homologue of Neuronal Calcium Sensor-1 (NCS-1)

The sequence analysis of NCU04379 was performed using the BLAST tool (Altschul et al. 1990) of NCBI. Homologue protein sequences were selected on the basis of *e*-values, % identities and gaps (Table 4.1). The protein sequences were aligned with ClustalX 1.83 (Thompson et al. 1997) and transferred to GeneDoc for visualization (Figure 4.1; Nicholas et al. 1997). The Conserved Domain Database (CCD; Marchler-Bauer and Bryant 2004; Marchler-Bauer et al. 2009) was used to identify conserved domains in the protein. The sequence analysis revealed that NCU04379 gene encodes a Ca^{2+} and/or CaM binding protein of 190 amino acid residues (GenBank accession number EAA28220.1) that showed sequence similarity to the *Aspergillus fumigatus*, *Magnaporthe grisea*, *Saccharomyces cerevisiae*, and *Homo sapiens* NCS-1 homologues (91, 92, 59, and 66% identity; 95, 97, 79, and 82% similarity; *e*-values 9e-96, 8e-96, 4e-64, and 2e-68, respectively). The NCU04379 encoded protein also possesses a consensus signal for N-terminal myristoylation and four EF-hand Ca^{2+}-binding sites like the NCS-1 homologues in *A. fumigatus*, *Danio rerio*, *H. sapiens*, *M. grisea*, *Mus musculus*, *S. cerevisiae*, *Schizosaccharomyces japonicus*, *Schizosaccharomyces pombe*, and *Xenopus laevis* (Figures 4.1, 4.2). Phylogenetic tree was constructed from the alignment using the minimum-evolution method (Rzhetsky and Nei 1992), 500 bootstrap replications as test of phylogeny (Felsenstein 1985) and the software MEGA4 (Tamura et al. 2007). In a phylogenetic analysis with a subset of NCS-1 homologues from various organisms, NCU04379 product was clustered with the Pezizomycotina clade (Figure 4.3). These results indicated that NCU04379 gene encodes a homologue of Neuronal Calcium

TH-1227_09610609

Sensor 1(NCS-1) in *N. crassa*. The NCS-1 protein belongs to a family of Neuronal Calcium Sensor proteins (Burgoyne and Weiss 2001).

Table 4.1 Summary of BLAST analysis using NCU04379 protein as a query

Organism	protein	*e*-value	Identity (%)	Similarity (%)
Magnaporthe grisea	Mg-NCS-1	8e-96	92	95
Aspergillus fumigatus	NcsA	9e-96	91	94
Schizosaccharomyces japonicus	Ncs1	7e-108	79	91
Schizosaccharomyces pombe	Ncs1p	8e-106	78	90
Danio rerio	NCS-1	2e-87	66	82
Homo sapiens	NCS-1	2e-68	66	82
Mus musculus	freq	2e-68	66	82
Xenopus laevis	Xfreq	3e-93	65	82
Saccharomyces cerevisiae	Frq1	4e-64	59	79

TH-1227_09610609

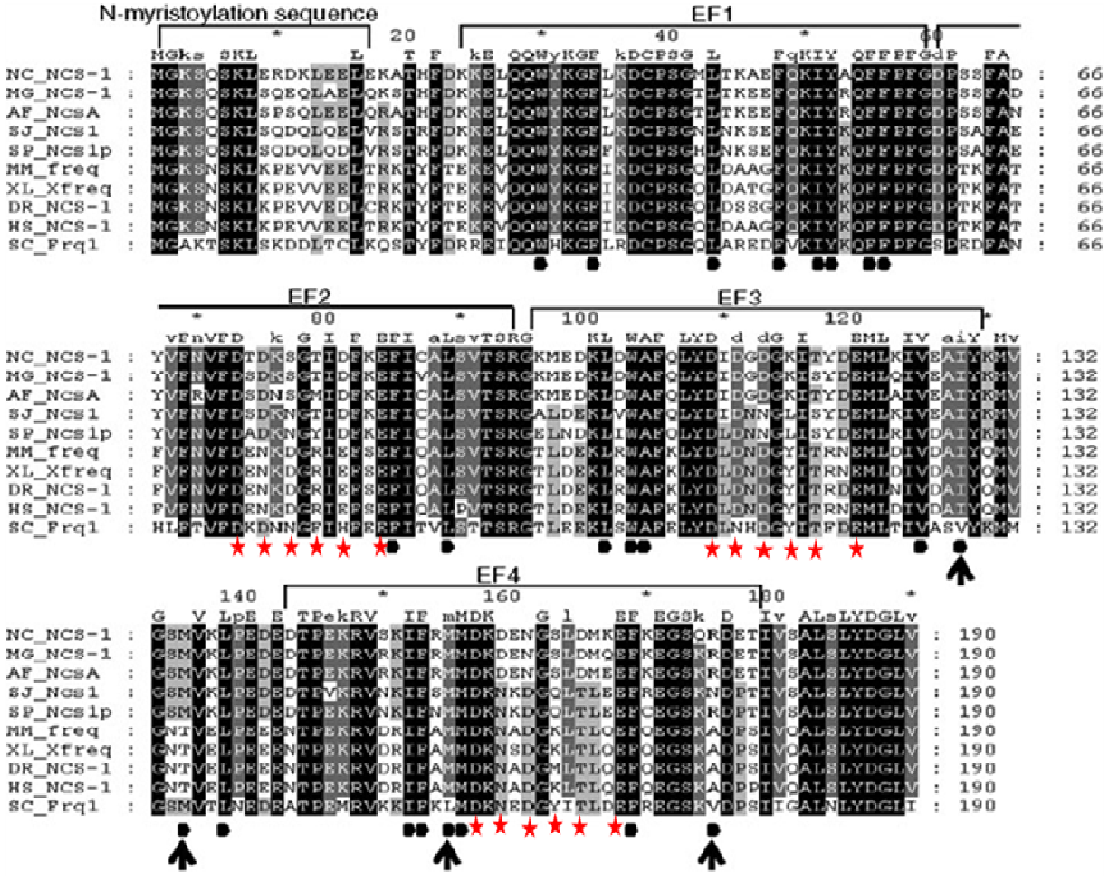

Figure 4.1: Sequence alignment of NCS-1 homologues. The positions of the N-terminal myristoylation sequence and the four EF-hands (EF1, EF2, EF3, and EF4) along with the consensus sequence of the alignment (above the sequences) are shown. Solid circles below the Frq1 sequence indicate the hydrophobic residues that constitute the binding interface with the target peptide of the Frq1 (Strahl et al. 2007), and the arrow heads indicate residues that are found altered in other sequences in the alignment. Asterisk marks (red) below the Frq1 sequence indicate the amino acid residues that provide oxygen ligands for Ca^{2+} coordination. AF, *Aspergillus fumigatus*; DR, *Danio rerio*; HS, *Homo sapiens*; MG, *Magnaporthe grisea*; MM, *Mus musculus*; NC, *Neurospora crassa*; SC, *Saccharomyces cerevisiae*; SJ, *Schizosaccharomyces japonicus*; SP, *Schizosaccharomyces pombe*; XL, *Xenopus laevis*. Conserved amino acids are shown in black, dark gray, and light gray indicating 100%, 80%, and 60% sequence similarities, respectively.

TH-1227_09610609

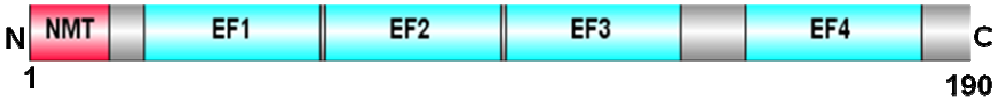

Figure 4.2: Domain organization of *N. crassa* homologue of NCS-1. The *N. crassa* homologue of NCS-1 is 190 amino acid residues in length, contains an N-terminal myristoylation sequence (NMT) and four EF hand domains (EF1, EF2, EF3, and EF4).

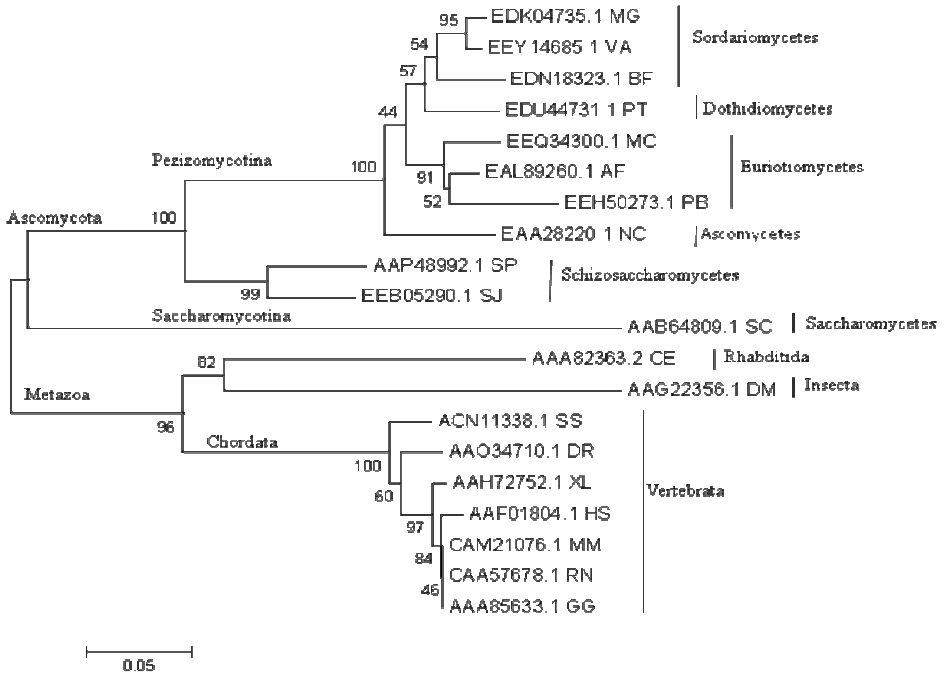

Figure 4.3: Phylogenetic analysis of NCS-1 homologues from fungi to mammals. Phylogenetic analysis of the frequenin/NCS-1 proteins fungi to mammals using the minimum-evolution method, 500 bootstrap replications (bootstrap values are indicated in the point at nodes) as test of phylogeny, and the software MEGA4. Frequenin/NCS-1 proteins are described by Genbank accession number, organism, and class; MG, *Magnaporthe grisea*; VA, *Verticillium albo-atrum*; BF, *Botryotina fuckeliana*; PT, *Pyrenophora tritici-repentis*; MC, *Microsporum canis*; AF, *Aspergillus fumigatus*; PB, *Paracoccidioides brasiliensis*; NC, *Neurospora crassa*; SP, *Schizosaccharomyces pombe*; SJ, *Schizosaccharomyces japonicus*; SC, *Saccharomyces cerevisiae*; CE, *Caenorhabditis elegans*; DM, *Drosophila Melanogaster*; SS, *Salmo salar*; DR, *Danio rerio*; XL, *Xenopus laevis*; HS, *Homo sapiens*; MM, *Mus musculus*; RN, *Rattus norvegicus*; GG, *Gallus gallus.* Phylum is indicated at major clades. Bar indicates scale of genetic distances.

TH-1227_09610609

4.2.2 Cloning of *N. crassa* homologue of *ncs-1* gene from the wild-type for site-directed mutational analysis

4.2.2.1 Double-joint polymerase chain reaction (DJ-PCR)

The Double-joint polymerase chain reaction (DJ-PCR) technique (Yu et al. 2004) was used to make a construct for targeted integration in the genome without laborious sub cloning steps. The construct (pRD-2) that was used for site-directed mutational analysis of *N. crassa* homologue of NCS-1 protein contain the 5´ flank of the *ncs-1* gene, *bar* cassette as a selectable marker and the target *ncs-1* gene (Figure 4.4). The *bar* gene was transcribed in the antisense direction of the *ncs-1* gene. This pRD-2 construct was generated essentially using a DJ-PCR technique that is based on PCR-mediated ligation of the individual fragments. PCRs of 5´ flank of the *ncs-1* gene, *bar* cassette, and the target *ncs-1* gene were carried out using custom made primers (Table 4.2), Phusion™ high fidelity DNA polymerase (Finzymes, Finland) in a total reaction volume of 50 µl unless mentioned otherwise.

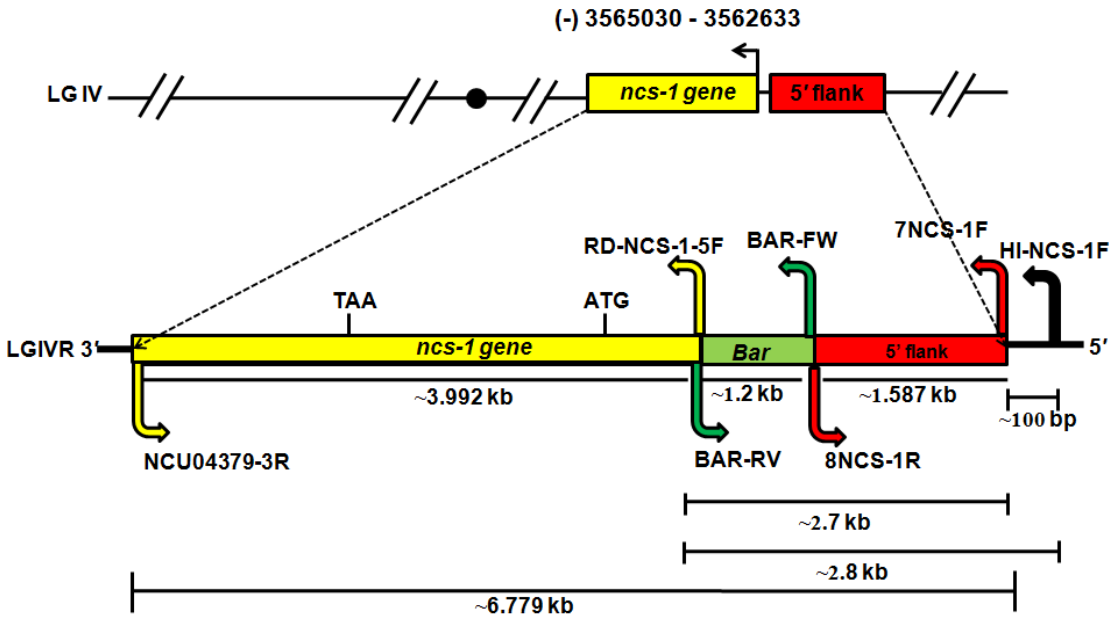

Figure 4.4: Schematic of the pRD-2 construct. PCR-mediated ligation of the 5′ flank of the *ncs-1* gene followed by the *bar* selectable marker and the functional *ncs-1* gene (shaded in red, green, and yellow, respectively) has resulted in an engineered insert of size ~6.779 kb, which then ligated into the *SmaI* site of the pRS426 vector to yield the pRD-2 construct. The relative genomic position of the *ncs-1*gene along with its 5′ flank fragment and the engineered insert are shown in top and bottom, respectively. The relative position of the start

TH-1227_09610609

(ATG) and stop (TAA) codons, the primers (arrow heads indicate the 5′→3′ direction), size of the fragments, distance of the HI-NCS-1F primer from the 5′ flank, and size of the engineered construct are shown. The direction of transcription of *ncs-1* gene is shown in the top, the *bar* gene is transcribed in the antisense direction of the *ncs-1* gene in the engineered construct.

Table 4.2 Primers used for site-directed mutational analysis

S. no.	Primer	Sequence (5′→ 3′)	Source
[a]1.	RD 5NCS-1-5F	CATCTTCTGTCGAGTCTAGAGCT CGAAAGTTTAGTCCTGG	This study
2.	NCU04379-3R	CCCAGTAACGTCTCTTTTGC	FGSC
3.	7NCS-1 F	CTGTGTCCAACAGAACGGTC	This study
[b]4.	8NCS-1 R	CATAGTACCGAGAAACTAGTTGC GCTCGATGTCAAACAGC	This study
5.	BAR-FW	ACTAGTTTCTCGGTACTATG	Larrando et al. 2009
6.	BAR- RV	TCTAGACTCGACAGAAGATG	Larrando et al. 2009
7.	HI-NCS-1F	GTCTCAGCATGAAAGTCGTC	This study
8.	NCS-1(G2A)-F	TCACGATTTGGCCATTTTCGG	This study
9.	NCS-1(G2A)-R	TCACGATTTGGCCATTTTCGG	This study
10.	NCS-1(R175A)-F	GGGCAGCCAGGCCGACGAGACA	This study
11.	NCS-1(R175A)-R	TGTCTCGTCGGCCTGGCTGCCC	This study
12.	NCS-1(E120Q)-F	CACCTACGACCAGATGCTCAA	This study
13.	NCS-1(E120Q)-R	TTGAGCATCTGGTCGTAGGTG	This study
14.	6NCU04379-F	AGCTCGAGCGTGATAAGCTG	This study
15.	7NCU04379-R	AGGGCGGATACGATTGTCTC	This study

[a]1, nucleotides underlined in the RD 5NCS-1-5F primer sequence is the reverse complement of BAR-RV

[b]2, nucleotides underlined in the 8NCS-1 R primer sequence is the reverse complement of BAR-FW

TH-1227_09610609

The DJ-PCR was performed essentially using three steps. Briefly, step 1 was the first round PCRs of the 5′ flank of the *ncs-1* gene, the *bar* cassette and the *ncs-1* gene (Figure 4.5 A). The 5′ flank of the *ncs-1* gene was amplified, using primers 7NCS-1 F and 8NCS-1 R, from the template DNA of the wild-type (Table 4.2, entries 3, 4). The reverse primer 8NCS-1 R carries 20 bases of homologous sequence that overlaps with one end (3′ end) of the *bar* cassette or reverse complement of the BAR-FW primer. The PCR reaction condition used were 2 min of initial denaturation at 98ºC followed by 30 cycles of 5 sec denaturation at 98ºC, 10 sec annealing at 60ºC with temperature increment of 0.3ºC at every cycle and 1min 30 sec elongation at 72ºC. The final extension was for 10 min at 72ºC. The size of the 5′ flank amplicon was ~1.587 kb. The *bar* cassette was amplified from the pBARGEM7-1 vector using the primers BAR-FW and BAR-RV (Table 4.2, entries 5, 6). The PCR reaction condition used were 2 min initial denaturation at 98ºC followed by 30 cycles of 5 sec denaturation at 98ºC, 10 sec annealing at 48.2ºC with temperature increment of 0.2ºC at every cycle and 50 sec elongation at 72ºC. The final extension was for 10 min at 72ºC. The size of the *bar* amplicon was ~1.2 kb. The target *ncs-1* gene was amplified from the wild-type genomic DNA using the primers RD-NCS-1 5F and NCU04379-3R (Table 4.2, entries 1, 2). The RD-NCS-1 5F forward primer carries the 20 bases of homologous sequence that overlaps with another end (5′ end) of the *bar* cassette or reverse complement of the BAR-RV primer. The PCR reaction condition used were 2 min initial denaturation at 98ºC followed by 30 cycles of 5 sec denaturation at 98ºC, 10 sec annealing at 60ºC with temperature increment of 0.3ºC at every cycle and 2 min 30 sec elongation at 72ºC. The final extension was for 10 min at 72ºC. The size of the *ncs-1* amplicon was ~3.992 kb.

The second round of PCR in step 2 was the assembly reaction of the amplified individual fragments generated in step 1. The amplified products of step 1 were purified using QIAquick Gel Extraction Kit (QIAGEN, CA). Subsequently, 100 ng each of the 5′ flank and the *bar* cassette were mixed in 0.2 ml PCR tube (mix 1); similarly, 100 ng each of the *ncs-1* gene and the *bar* cassette were mixed in another PCR tube (mix 2). The PCR reaction was carried out to join the fragments of mix 1 and mix 2 with Phusion™ high fidelity DNA polymerase without using primer in a 25 µl reaction volume. The PCR cycling parameter were 2 min initial denaturation at 98ºC followed by 15 cycles of 5 sec denaturation at 98ºC, 30 sec annealing at 60ºC and 3 min elongation at 72ºC. The final extension was for 10 min at 72ºC.

The third round of PCR in step 3 was the amplification of the joined fragments in step 2 to generate the final product (Figure 4.5 B). Approximately 200 ng (2 µl) of the raw

TH-1227_09610609

product each from mix 1 and mix 2 were mixed in a separate PCR tube. The PCR was performed using primers 7NCS-1F and NCU04379-3R (Table 4.2, entry 3, 2) in a 25 µl reaction mixture. The PCR cycling parameter was 2 min initial denaturation at 98ºC followed by 30 cycles of 5 sec denaturation at 98ºC, 30 sec annealing at 60ºC and 6.5 min elongation at 72ºC. The final extension was for 10 min at 72ºC. The size of the final product was ~6.779 kb.

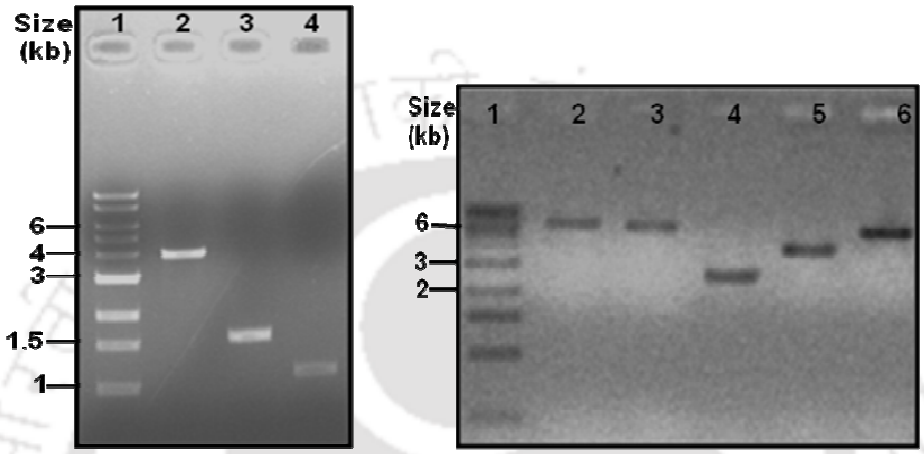

Figure 4.5: Cloning of the *N. crassa* homologue of *ncs-1* gene from the wild-type for site-directed mutational analysis. **(A)** Amplification of individual fragments. Primers that are used to amplify the respective fragments are shown in Figure 4.4. PCR products were resolved in 0.8% agarose gel; lane 1, 1 kb DNA ladder (NEB); lane 2, PCR amplicon of the fragment of size ~3.992 kb that contains the *ncs-1* gene (using primers RD-NCS-1-5F and NCU04379-3R); lane 3, PCR amplicon of the 5′ flank which is of size ~1.587 kb of the *ncs-1* gene (using primers 7NCS-1F and 8NCS-1R); lane 4, PCR amplicon of the selectable marker *bar* cassette of ~1.2 kb in size (using primers BAR-FW and BAR-RV). **(B)** Double joint PCR for joining the individual fragments. PCR products were resolved in 0.8% agarose gel; lane 1, 1 kb DNA ladder (NEB); lanes 2 and 3, PCR of the full length construct of ~6.779 kb generated after joining all the three individual fragments (using primers 7NCS-1F and NCU04379-3R); lane 4, control PCR amplicon generated after joining the *bar* cassette and the 5′ flank (~2.7 kb); lane 5, control PCR amplicon of the functional *ncs-1* gene (~3.992 kb); lane 6, pRS426 vector digested with the *Sma I* enzyme (~5.7 kb).

TH-1227_09610609

4.2.2.2 Cloning of the final double joint PCR product carrying *ncs-1* gene in the pRS426 vector

The final double joint PCR product of size ~6.779 kb was cloned into the *SmaI* site of the pRS426 vector. The ligation reaction was carried out using Quick Ligation™ Kit (NEB, UK) and according to manufacturer's protocol. Additionally, the ligated product was further digested with the *Sma I* restriction enzyme to linearize the self ligated vector. Finally, the ligated product was transformed into the *E. coli DH5α* ultra competent cells and transformants were selected on SOB agar containing ampicillin. The plasmids were isolated from the transformants (Figure 4.6 A) and the plasmid construct, designated as pRD-2-B-*ncs-1*, containing the final engineered product of DJ-PCR was identified. The pRD-2-B-*ncs-1* construct was verified by PCR analysis (Figure 4.6 B).

4.2.3 Transformation of the pRD-2-B-*ncs-1* construct into the Δ*ncs-1*Δ*mus 53 a (15)* strain

The recombinant construct pRD-2-B-*ncs-1* was transformed into the Δ*ncs-1*Δ*mus53 a (15)* strain by electroporation (as described in chapter 2) and selected on Vogel's sorbose plate containing basta (220 µg/ml). One of the initial heterokaryotic transformant, designated as HT-1, was verified by PCR using the forward primer HI-NCS-1F (Table 4.2, entry 8) specific for the homologous integration of the recombinant construct and the reverse primer BAR-RV specific (Table 4.2, entry 7) for the *bar* cassette ligated in the construct. The initial heterokaryotic transformant HT-1 was crossed with the Δ*ncs-1 A* mutant strain to isolate the homokaryotic transformants. From this cross, ten homokaryotic progenies were isolated and screened for basta resistance (basta^R). One of the basta^R homokaryotic transformant, designated as HoP-3, was verified by PCR using primers HI-NCS-1F and BAR-RV, and used for further analysis (Figure 4.6 C). The HoP-3 strain displayed growth, Ca^{2+} and and UV sensitivity phenotypes like the wild-type (results were similar to the homokaryotic transformants described in Chapter 3). Thus, the pRD-2-B-*ncs-1* construct complemented the Δ*ncs-1* mutant.

TH-1227_09610609

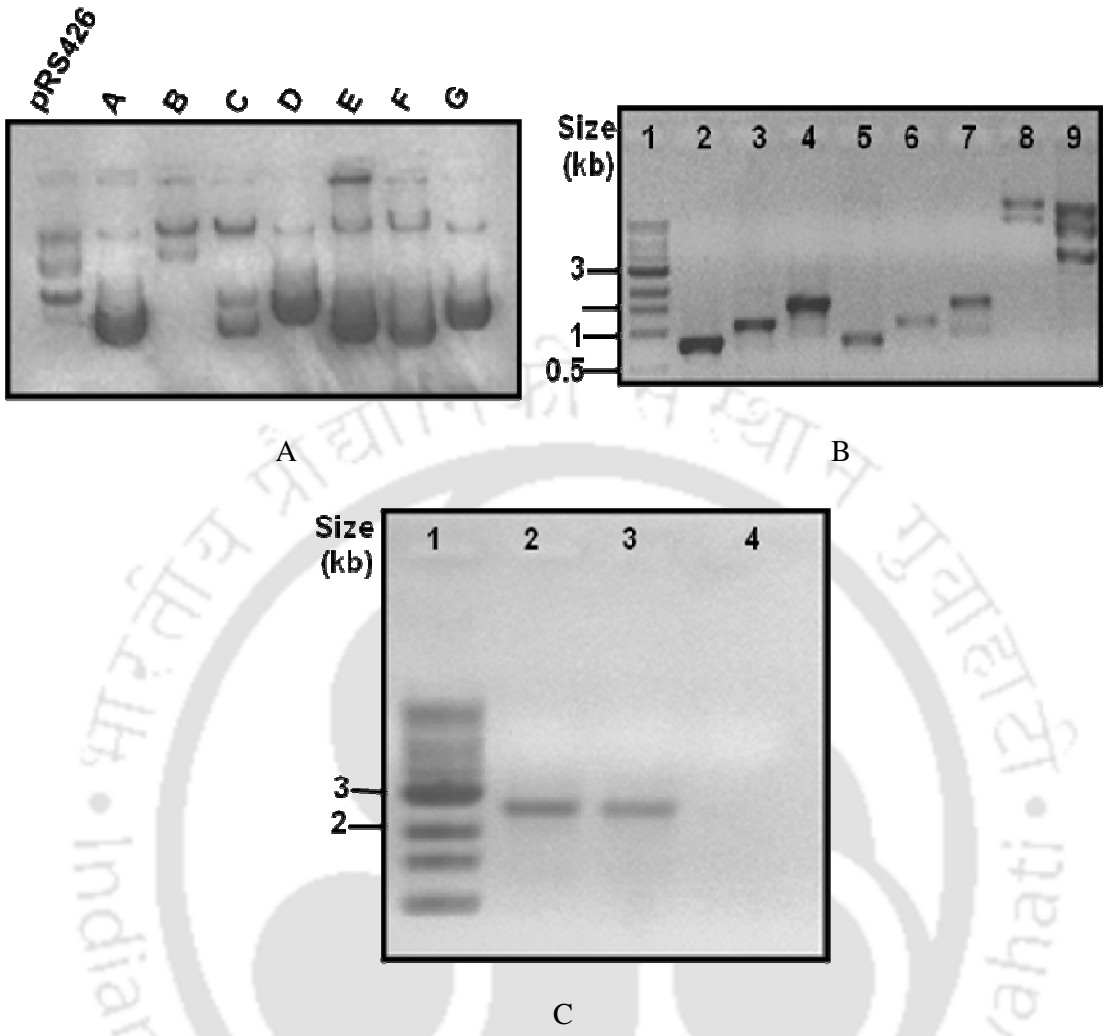

Figure 4.6: Confirmation of clones constructed for site-directed mutational analysis. **(A)** Agarose gel electrophoresis (0.8% agarose) of pRS426 vector (uncut) and clones (A to G) to screen the clone containing the full length insert of *ncs-1* of size ~6.779 kb that is ligated into the *SmaI* site of the pRS426 vector. The plasmid shift was observed for the clone B (Sl. No. 3 from the left) that was designated as pRD-2-B-*ncs-1* and selected for further analysis. **(B)** PCR of the plasmid pRD-2-B-*ncs-1* for verification of the ligation of all the desired fragments. PCR products were resolved in 0.8% agarose gel; lane 1, 1 kb DNA ladder (NEB); lanes 2, 3, and 4, indicate PCR amplicon of a segment of the *ncs-1* ORF (~811 bp) using primers 6NCU04379-F and 7NCU04379-R, *bar* cassette (~1.2 kb) using primers BAR-FW and BAR-RV and the 5′ flank of *ncs-1* gene (~1.587 kb) using primers 7NCS-1F and 8NCS-1R, respectively; lane 5, control PCR of a segment of the *ncs-1* ORF (~811 bp) from the wild-type; lane 6, control PCR amplification of the *bar* gene (~1.2 kb) from the pBARGEM7-1 vector; lane 7, control PCR of the 5'flank (~1.587 kb) of *ncs-1* gene from the

TH-1227_09610609

wild-type; lane 8, uncut clone pRD-2-B loading control (~12.479 kb); lane 9, pRS426 vector loading control (~5.7 kb). **(C)** PCR verification of the *N. crassa* strains transformed with the plasmid construct pRD-2-B-*ncs-1*. PCR products were resolved in 0.8% agarose gel; lane 1, 1 kb DNA ladder (NEB); lanes 2 and 3, PCR product (~2.8 kb) obtained using the template DNA from the heterokaryotic transformant HT-1-Δ*ncs-1*Δ*mus53 a (15)* and the homokaryotic transformant HoP-3-Δ*ncs-1*Δ*mus53 a (15)*, respectively, using primers Bar-RV and HI-NCS-1F. The BAR-RV reverse primer is specific for the *bar* cassette. HI-NCS-1F forward primer, which is ~100 bp upstream of the 5' flank of the *ncs-1* gene, is used to confirm the targeted integration at homologous position (described in Figure 4.4).

4.2.4 Site-directed mutational analysis of *N. crassa* homologue of NCS-1

To identify critical amino acid residues of *N. crassa* NCS-1 homologue, I performed site-directed mutational analysis for some of the selected amino acid residues of the NCS-1 protein. The amino acid residues selected for site-directed mutational analysis were glycine at position 2, arginine at position 175 and glutamate at position 120 (Figure 4.7). The site-directed mutations of the *ncs-1* were performed using the pRD-2-B-*ncs-1* construct. The procedure for generating the site-directed mutations was essentially as described in QuickChange® II site-directed mutagenesis protocol (Stratagene, CA). The mutational PCR reactions were performed using mutagenic primer pairs containing the desired mutation and Phusion™ High-Fidelity DNA Polymerase (Finzymes, Finland). The PCR cycling parameters were 2 min initial denaturation at 98ºC followed by 25 cycles of 10 sec denaturation at 98ºC, 15 sec annealing at 60ºC and 7 min elongation at 72ºC. The final extension was for 15 min at 72ºC. The PCR generates a mutated plasmid containing staggered nicks. The PCR products were digested with *Dpn I* restriction enzyme to digest the parental methylated and hemimethylated DNA template (unmutated) and then transformed into the *E. coli DH5α* ultracompetent cells for nick repair. The transformant colonies were selected on SOB-ampicillin plate and plasmids were isolated. The desired mutation in the respective plasmid construct was confirmed by DNA sequencing.

The glycine at position 2 is the site for N-terminal myristoylation (Figures 4.1, 4.7). Myristoylation is an irreversible, co-translational protein modification catalysed by enzyme N-myristoyltransferase (EC 2.3.1.97; McIlhinney 1998, Podell and Gribskov 2004). Protein N-myristoylation is found in fungi, higher eukaryotes and viruses that involves the covalent attachment of myristoyl group (derived from myristic acid) via an amide bond to the alpha-

TH-1227_09610609

amino group of an N-terminal glycine residue exposed during co-translational N-terminal methionine removal (Podell and Gribskov 2004). This modification alters the lipophilicity of the target protein and facilitates its interaction with membranes, thereby affecting its subcellular localization or the hydrophobic domains of other proteins for transducing signal downstream (Resh 1999; Olsen and Kaarsholm 2000; Batistic et al. 2008; Benetka et al. 2008). I performed a point mutation that changes a glycine codon GGC to an alanine codon GCC (changed nucleotide is underlined) for generating G2A mutation in the *ncs-1* ORF using the mutagenic primer pairs NCS-1(G2A)-F and NCS-1(G2A)-R (Table 4.2, entries 8, 9). The G2A mutation was confirmed by DNA sequencing (Figures 4.8, 4.9) and the construct carrying G2A mutation was designated as pRD-2-B-*ncs-1*^{G2A}. The G2A mutation is known to disrupt the N-terminal myristoylation of the protein (Dizhoor et al. 1993; Klenchin et al. 1995; Ames et al. 1997; Ishitani et al. 2000).

The arginine at position 175 of the *N. crassa* NCS-1 is located in the hydrophobic pocket of the protein (Figure 4.1, 4.7). In *S. cerevisiae*, Frq1, homologue of *N. crassa* NCS-1, interacts with the phosphatidylinositol-4-OH kinase (Pik1; Strahl et al. 2007). It was shown that upon binding to Ca^{2+} in the EF hand domains of Frq1 in *S. cerevisiae*, the protein changes its conformation by exposing its N-terminal myristoylation sequence embedded in its hydrophobic pocket and targeted to the membrane where it interacts with Pik1 through interactions between amino acids residing in its hydrophobic pocket. The valine residue at position 175 within the hydrophobic pocket of Frq1 is an important residue for its interaction with Pik1 (Huttner et al. 2003; Strahl et al. 2007). In case of the *N. crassa* NCS-1 homologue protein, arginine residue is present at position 175 unlike the valine in Frq1 of *S. cerevisiae* (Figure 4.1). I performed two point mutations that changes a arginine codon CGC to an alanine codon GCC (changed nucleotides are underlined) for generating R175A mutation in the *ncs-1* ORF using the mutagenic primer pairs NCS-1(R175A)-F and NCS-1(R175A)-R (Table 4.2, entries 10, 11). The R175A mutation was confirmed by sequencing (Figures 4.10, 4.11) and the construct carrying R175A mutation was designated as pRD-2-B-*ncs-1*^{R175A}.

The glutamate at position 120 of the *N. crassa* NCS-1 protein is located in the Ca^{2+} binding site of the third EF hand domain (EF3; Figures 4.1, 4.7). The EF hand domain contains a characteristic helix-loop-helix structural unit called as EF hand loop or Ca^{2+} binding loop, formed by a stretch of 12 amino acid residues (D, D/T/I/K, C/D, P/K/G/E, S/S/D/N, G, M/T/K/S, L/I, T/D, K/F/Y/M, A/K/D, E). This loop is formed by a sequence

TH-1227_09610609

of 12 amino acids rich in acidic residues that provide oxygen ligands for Ca^{2+} coordination in pentagonal bipyramidal geometry (Figure 1.2). The residues in the loop at positions 1(+*x*), 3(+*y*), 5(+*z*), 7(-*y*), 9(-*x*) and 12(-*z*) coordinate with Ca^{2+} by providing oxygen ligands (Gifford et al. 2007). The substitutions in the *z* position of the EF hand loop decrease the affinity for Ca^{2+} by about 1000-fold (Strynadka and James, 1989; Moncrief et al. 1990). The four EF hands domains are present in *N. crassa* homologue of NCS-1, out of which, the first EF hand domain (EF1) is non-functional and incapable of binding Ca^{2+}. The EF1 of NCS-1 is non-functional due to lack of acidic side chains necessary for providing oxygen for Ca^{2+} coordination, presence of lysine at +*x* position and cysteine-proline in the Ca^{2+} binding loop region that disrupts the flexibility of the loop (Burgoyne and Weiss 2001; Muralidhar et al. 2004; Gifford et al. 2007). The EF2, EF3 and EF4 domains of *N. crassa* NCS-1 protein have appeared functional and capable of binding Ca^{2+} based on its sequence analysis. The glutamate residue at position 12 (-*z*) of the EF hand loop is important for both the structure and the function of the loop (Gifford et al. 2007). Binding of Ca^{2+} ions to the EF hand loop is a sequential process with the EF3 filled first or EF3 binds to Ca^{2+} first (Permyakov et al. 2000). In one of the Ca^{2+} binding protein recoverin that belongs to the NCS protein subfamily, the E121Q substitution in the EF3 completely abolishes the high Ca^{2+} affinity of recoverin (Permyakov et al. 2000; Burgoyne and Weiss, 2001). Therefore, I performed a point mutation in the EF3 domain of *N. crassa* NCS-1 protein. The glutamate codon GAG was changed to glutamine codon CAG (changed nucleotide is underlined) for generating E120Q mutation using the mutagenic primer pairs NCS-1(E120Q)-F and NCS-1(E120Q)-R (Table 4.2, entries 12, 13). The E120Q mutation was confirmed by DNA sequencing (Figures 4.12, 4.13) and the construct carrying E120Q mutation was designated as pRD-2-B-*ncs-1* ^{E120Q}.

TH-1227_09610609

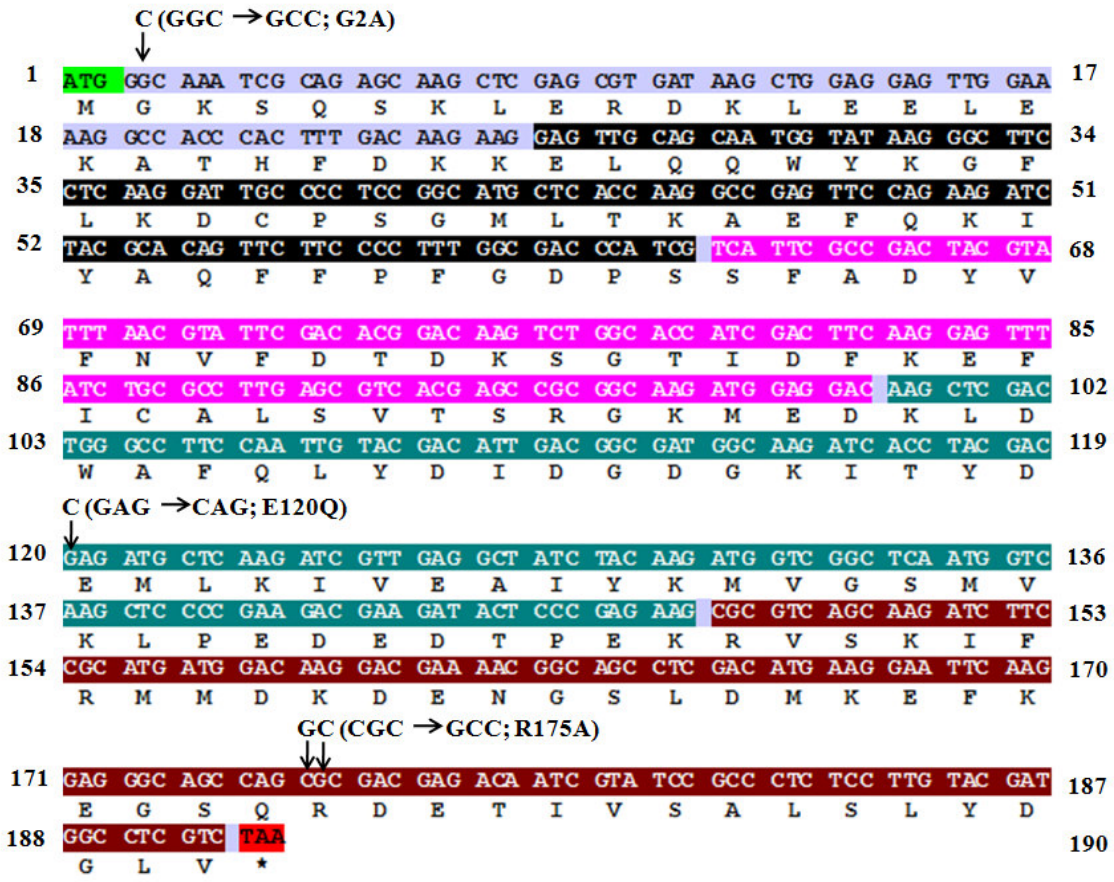

Figure 4.7: Translated sequence of *N. crassa* homologue of NCS-1 including its nucleotide sequence. Translate tool available from the ExPASy bioinformatics Resource Portal (http://web.expasy.org/translate/) was used to translate the nucleotide sequence to a protein sequence. Black, pink, blue, and brown shaded regions are EF hand domain 1 (EF1), EF hand domain 2 (EF2), EF hand domain 3 (EF3), and EF hand domain 4 (EF4), respectively. The codons, targeted for site-directed mutations, are also shown. Glycine residue at position two is the target for N-terminal myristoylation that assist in membrane attachment of the protein. Glycine residue is mutated to alanine by changing the triplet codon GGC to GCC (G2A). Glutamate residue at position 120 (within the EF hand loop 3, and the 12th amino acid of the loop) is mutated to glutamine by changing the triplet codon GAG to CAG (E120Q). Arginine residue at position 175 of the hydrophobic pocket of the protein is mutated to alanine through CGC to GCC alteration (R175A). Arginine residue at position 175 is replaced with valine in one of the NCS-1 homologue protein called Frq1 in *S. cerevisiae* and interacts with the residue of phosphatidylinositol-4-kinase (Pik-1), target of Frq1 (Strahl et al. 2007).

TH-1227_09610609

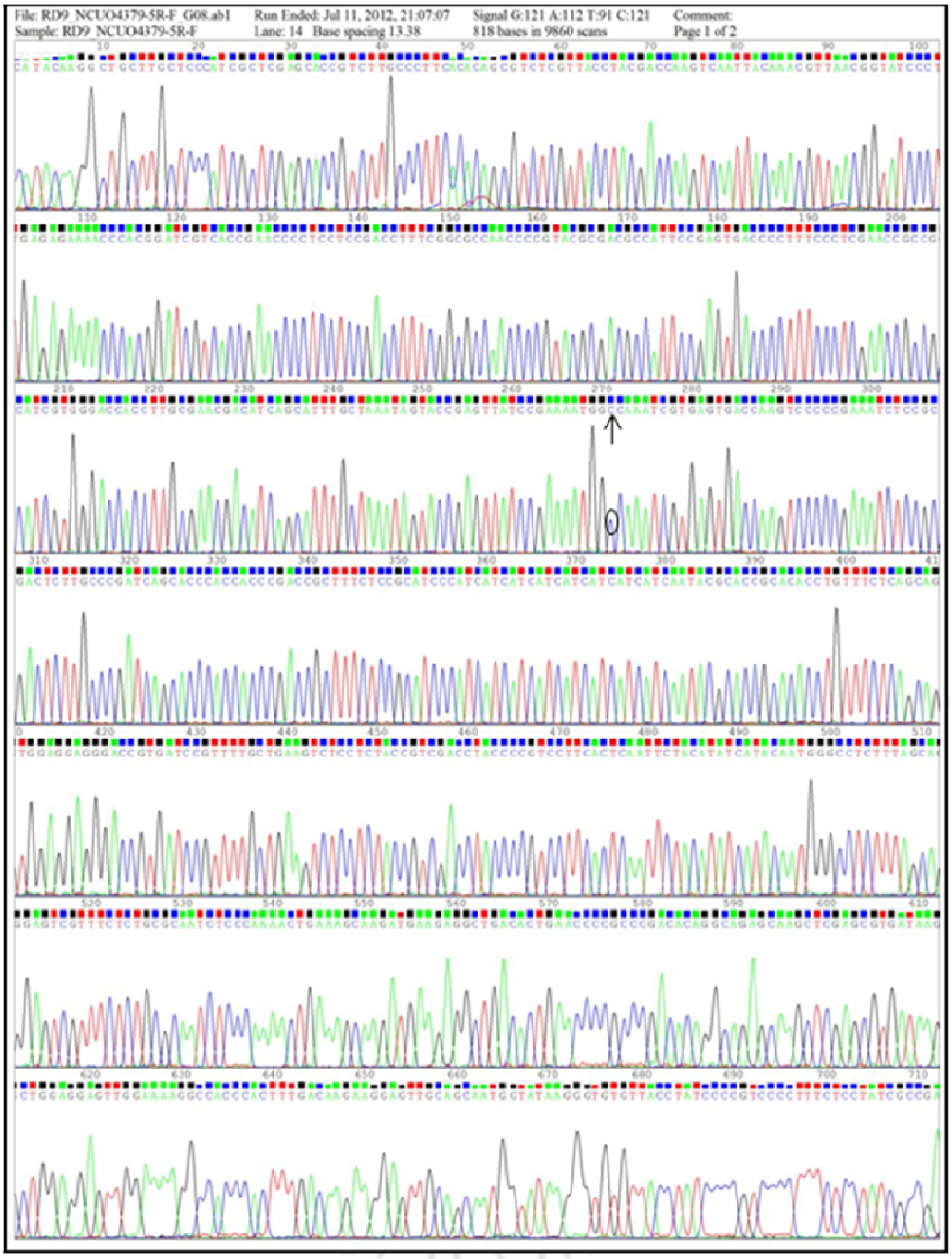

Figure 4.8: Chromatogram profile of the *ncs-1*^{G2A} mutant allele generated by partial sequencing of the pRD-2-B-*ncs-1*^{G2A} construct. The point mutation in the triplet codon GGC to GCC changes glycine to alanine in the NCS-1 protein. The position of point mutation is shown using an unfilled circle in the chromatogram and a black arrow head in the corresponding sequence.

TH-1227_09610609

```
NCS1        GCTTACCGAGTCTGCTACTTGAACTATCCTATCGGCCGACGACAATATAAATCCACCATA
RD2-G2A     ------------------------------------------------------------CATA
                                                                       ****

NCS1        CAAGGCTGCTTGCTCCCATCGCTCGAGCACCGTCTTGCCCTTCACACAGCGTCTCGTTAC
RD2-G2A     CAAGGCTGCTTGCTCCCATCGCTCGAGCACCGTCTTGCCCTTCACACAGCGTCTCGTTAC
            ************************************************************

NCS1        CTACGACCAAGTCAATTACAAACGTTAACGGTATCCCTGAGAGAAAACCCACGGATCGTC
RD2-G2A     CTACGACCAAGTCAATTACAAACGTTAACGGTATCCCTGAGAGAAAACCCACGGATCGTC
            ************************************************************

NCS1        ACCGAACCCCTCCTCCGACCTTTCGGCGCCAACCCCGTACGCGACGCCATTCCGAGTGAC
RD2-G2A     ACCGAACCCCTCCTCCGACCTTTCGGCGCCAACCCCGTACGCGACGCCATTCCGAGTGAC
            ************************************************************

NCS1        CCCTTTCCCTCGAACCGCCGCATCGTGGGACCACCTTGCGAACGACATCAGCATTTGCTA
RD2-G2A     CCCTTTCCCTCGAACCGCCGCATCGTGGGACCACCTTGCGAACGACATCAGCATTTGCTA
            ************************************************************

NCS1        AATAGTACCGAGTTATCCGAAAATGGGCAAATCGTGAGTGACCAAGTCCCCCGAAATCTC
RD2-G2A     AATAGTACCGAGTTATCCGAAAATGGCCAAATCGTGAGTGACCAAGTCCCCCGAAATCTC
            ************************ ********************************

NCS1        CGCGACTCTTGCCCGATCAGCACCCACCACCCGACCGCTTTCTCCGCATCCCATCATCAT
RD2-G2A     CGCGACTCTTGCCCGATCAGCACCCACCACCCGACCGCTTTCTCCGCATCCCATCATCAT
            ************************************************************

NCS1        CATCATCATCATCATCAATACGCACCGCACACCTGTTTCTCAGCAGTGGAGGAGGGACCG
RD2-G2A     CATCATCATCATCATCAATACGCACCGCACACCTGTTTCTCAGCAGTGGAGGAGGGACCG
            ************************************************************

NCS1        TGATCCGTTTTGCTGAAGTCTCCTCTACCGTCGACCTACCCCGTCCTTCACTCAATTCTA
RD2-G2A     TGATCCGTTTTGCTGAAGTCTCCTCTACCGTCGACCTACCCCGTCCTTCACTCAATTCTA
            ************************************************************

ncs1        CATATCATACAATGGGCCTCTTTAGCAGGAGTCGTTTCTCTGCGCAATCTCCCAAAACTG
RD2-G2A     CATATCATACAATGGGCCTCTTTAGCAGGAGTCGTTTCTCTGCGCAATCTCCCAAAACTG
            ************************************************************
```

Figure 4.9: Confirmation of the G2A mutation in the pRD-2-B-*ncs-1*^{G2A} construct.
Partial sequence of the pRD-2-B-*ncs-1*^{G2A} construct was aligned with the sequence of *ncs-1* wild-type allele using the ClustalW. Asterisks below the alignment indicate the identical nucleotide. Absence of asterisk below the unmatched nucleotide (indicated with a pink shade) in the alignment confirmed the mutation (the triplet codon GGC to GCC) that changes the amino acid residue glycine to alanine at position 2 (G2A) of the NCS-1 protein (the partial sequence of the pRD-2-B-*ncs-1*^{G2A} was translated using the translate tool of ExPASy and aligned with the sequence of NCS-1 using the ClustalW to verify the amino acid changed). The start codon ATG is shaded with green.

TH-1227_09610609

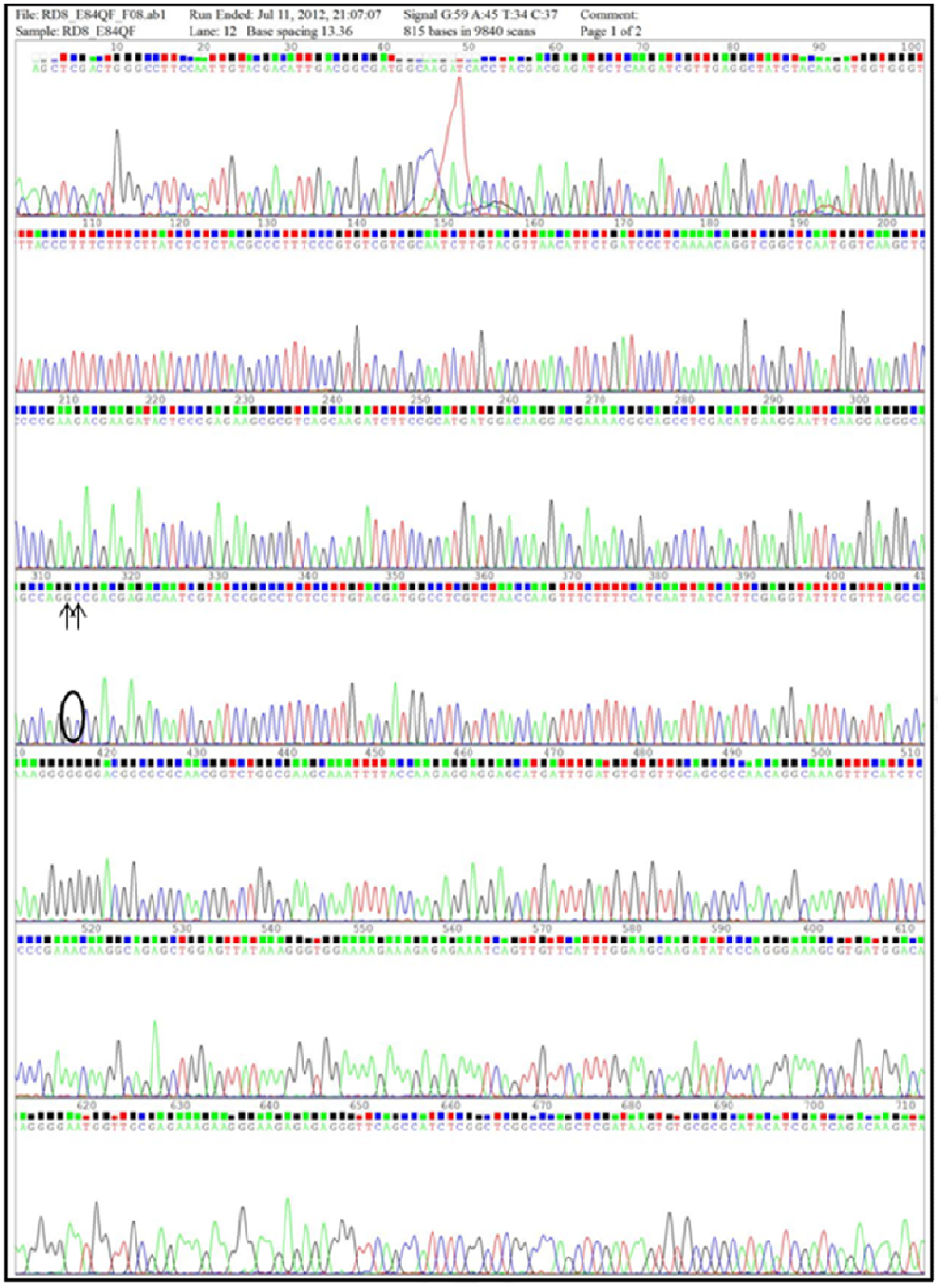

Figure 4.10: Chromatogram profile of the *ncs-1*^{R175A} mutant allele generated by partial sequencing of the pRD-2-B-*ncs-1*^{R175A} construct. The point mutations in the triplet codon CGC to GCC change arginine to alanine in the NCS-1 protein. The positions of two point mutations are shown using an unfilled circle in the chromatogram and black arrows in the corresponding sequence.

TH-1227_09610609

```
NCS1            CGACTTCAAGGAGTTTATCTGCGCCTTGAGCGTCACGAGCCGCGGCAAGATGGAGGACAA
RD2-R175A       ----------------------------------------------------------A
                                                                           *

NCS1            GCTCGACTGGGCCTTCCAATTGTACGACATTGACGGCGATGGCAAGATCACCTACGACGA
RD2-R175A       GCTCGACTGGGCCTTCCAATTGTACGACATTGACGGCGATGGCAAGATCACCTACGACGA
                ************************************************************

NCS1            GATGCTCAAGATCGTTGAGGCTATCTACAAGATGGTGGGTTTACCCTTTCTTTCTTATCT
RD2-R175A       GATGCTCAAGATCGTTGAGGCTATCTACAAGATGGTGGGTTTACCCTTTCTTTCTTATCT
                ************************************************************

NCS1            CTCTACGCCCTTTCCCGTGTCGTCGCAATCTTGTACGTTAACATTCTGATCCCTCAAAAC
RD2-R175A       CTCTACGCCCTTTCCCGTGTCGTCGCAATCTTGTACGTTAACATTCTGATCCCTCAAAAC
                ************************************************************

NCS1            AGGTCGGCTCAATGGTCAAGCTCCCCGAAGACGAAGATACTCCCGAGAAGCGCGTCAGCA
RD2-R175A       AGGTCGGCTCAATGGTCAAGCTCCCCGAAGACGAAGATACTCCCGAGAAGCGCGTCAGCA
                ************************************************************

NCS1            AGATCTTCCGCATGATGGACAAGGACGAAAACGGCAGCCTCGACATGAAGGAATTCAAGG
RD2-R175A       AGATCTTCCGCATGATGGACAAGGACGAAAACGGCAGCCTCGACATGAAGGAATTCAAGG
                ************************************************************

NCS1            AGGGCAGCCAGCGCGACGAGACAATCGTATCCGCCCT----------------------
RD2-R175A       AGGGCAGCCAGGCCGACGAGACAATCGTATCCGCCCTCTCCTTGTACGATGGCCTCGTCT

                **********  ************************
```

Figure 4.11: Confirmation of the R175A mutation in the pRD-2-B-*ncs-1*^{R175A} construct. Partial sequence of the pRD-2-B-*ncs-1*^{R175A} construct was aligned with the sequence of *ncs-1* allele using the ClustalW. Asterisks below the alignment indicate the identical nucleotide. Absence of asterisk below the unmatched nucleotide (indicated with pink shades) in the alignment confirmed the changed nucleotide of the triplet codon CGC to GCC that changes the amino acid residue arginine to alanine at position 175 (R175A) of the NCS-1 protein (the partial sequence of the pRD-2-B-*ncs-1*^{R175A} was translated using the translate tool of ExPASy and aligned with the sequence of NCS-1 using the ClustalW to verify the amino acid changed).

TH-1227_09610609

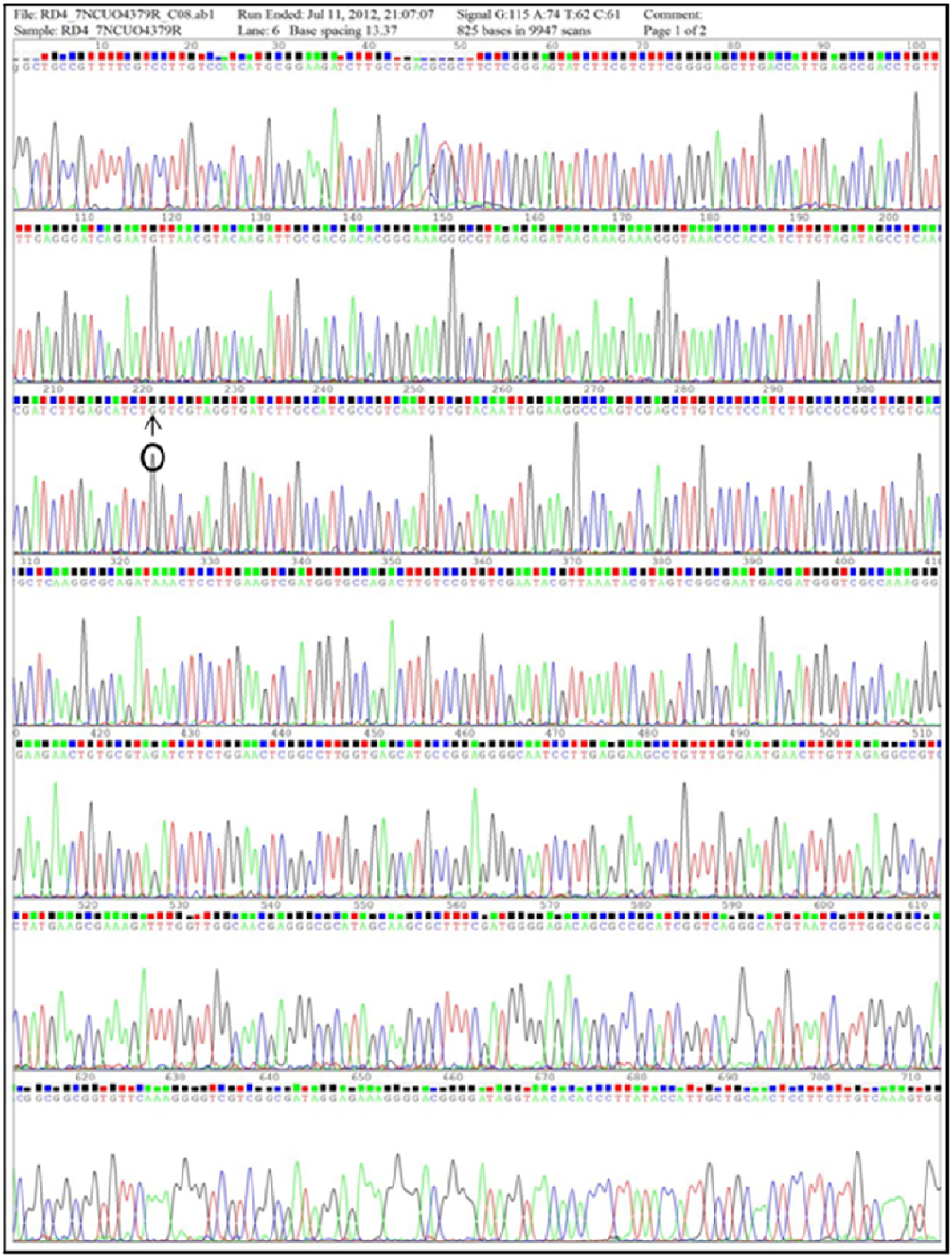

Figure 4.12: Chromatogram profile of the *ncs-1*^{E120Q} mutant allele generated by partial sequencing of the pRD-2-B-*ncs-1*^{E120Q} construct. The point mutation in the triplet codon GAG to CAG (or CTC to GTC) changes glutamate to glutamine in the NCS-1 protein. The position of the point mutation is shown using an unfilled circle in the chromatogram and a black arrow head in the corresponding sequence.

```
NCS1            ------CGACTTCAAGGAGTTTATCTGCGCCTTGAGCGTCACGAGCCGCGGCAAGATGGA
RD2-E120Q       CACCATCGACTTCAAGGAGTTTATCTGCGCCTTGAGCGTCACGAGCCGCGGCAAGATGGA
                      **************************************************

NCS1            GGACAAGCTCGACTGGGCCTTCCAATTGTACGACATTGACGGCGATGGCAAGATCACCTA
RD2-E120Q       GGACAAGCTCGACTGGGCCTTCCAATTGTACGACATTGACGGCGATGGCAAGATCACCTA
                ************************************************************

NCS1            CGACGAGATGCTCAAGATCGTTGAGGCTATCTACAAGATGGTGGGTTTACCCTTTCTTTC
RD2-E120Q       CGACCAGATGCTCAAGATCGTTGAGGCTATCTACAAGATGGTGGGTTTACCCTTTCTTTC
                **** ********************************************************

NCS1            TTATCTCTCTACGCCCTTTCCCGTGTCGTCGCAATCTTGTACGTTAACATTCTGATCCCT
RD2-E120Q       TTATCTCTCTACGCCCTTTCCCGTGTCGTCGCAATCTTGTACGTTAACATTCTGATCCCT
                ************************************************************

NCS1            CAAAACAGGTCGGCTCAATGGTCAAGCTCCCCGAAGACGAAGATACTCCCGAGAAGCGCG
RD2-E120Q       CAAAACAGGTCGGCTCAATGGTCAAGCTCCCCGAAGACGAAGATACTCCCGAGAAGCGCG
                ************************************************************

NCS1            TCAGCAAGATCTTCCGCATGATGGACAAGGACGAAAACGGCAGCCTCGACATGAAGGAAT
RD2-E120Q       TCAGCAAGATCTTCCGCATGATGGACAAGGACGAAAACGGCAGCC--------------
```

Figure 4.13: Confirmation of the E120Q mutation in pRD-2-B-*ncs-1*^{E120Q} construct. Partial sequence of the pRD-2-*ncs-1*^{E120Q} construct was aligned with the sequence of *ncs-1* allele using the ClustalW. Asterisks below the alignment indicate the identical nucleotide. Absence of asterisk below the unmatched nucleotide (indicated with pink shade) in the alignment confirmed the changed nucleotide of the triplet codon GAG to CAG that changes the amino acid residue glutamate to glutamine at position 120 (E120Q) of the NCS-1 protein (the partial sequence of the pRD-2-*ncs-1*^{E120Q} was translated using the translate tool of ExPASy and aligned with the sequence of NCS-1 using the ClustalW to verify the amino acid changed).

4.2.5 Transformation of pRD-2-B-*ncs-1*^{G2A}, pRD-2-B- *ncs-1*^{R175A} and pRD-2-B-*ncs-1*^{E120Q} constructs into the Δ*ncs-1*Δ*mus53 a (15)* strain

The pRD-2- B-*ncs-1*^{G2A}, pRD-2-B-*ncs-1*^{R175A}, and pRD-2-B-*ncs-1*^{E120Q} were transformed into the Δ*ncs-1*Δ*mus53 a (15)* strain by electroporation (as described in chapter 2) and transformants were selected on Vogel's sorbose plate containing basta (220 µg/ml). The homologous integration of the constructs in the initial heterokaryotic transformants was verified by PCR analysis using the primer pairs HI-NCS-1F and BAR-RV (Table 4.2, entries 7, 6). The HI-NCS-1F primer target sequence is 100 bp upstream of the 5´flank of *ncs-1* gene and the BAR-RV is specific for the *bar* cassette of the construct (Figure 4.4). The initial heterokaryotic transformants, which showed the PCR band for targeted integration, were used further to generate the homokaryotic transformants by crossing with the Δ*ncs-1 A* strain**.** The homokaryotic transformants of pRD-2-B-*ncs-1*^{G2A}, pRD-2-B-*ncs-1*^{R175A}, and pRD-2-B-*ncs-1*^{E120Q} were initially screened for basta resistance (basta^{R}) and basta^{R} progenies

TH-1227_09610609

were used further for verification of homologous integration by PCR analysis (Figures 4.14-4.16). Thus, at least two homokaryotic transformant progenies were isolated for each of the *ncs-1*^{G2A}, *ncs-1*^{R175A}, and *ncs-1*^{E120Q} allele and used for further studies.

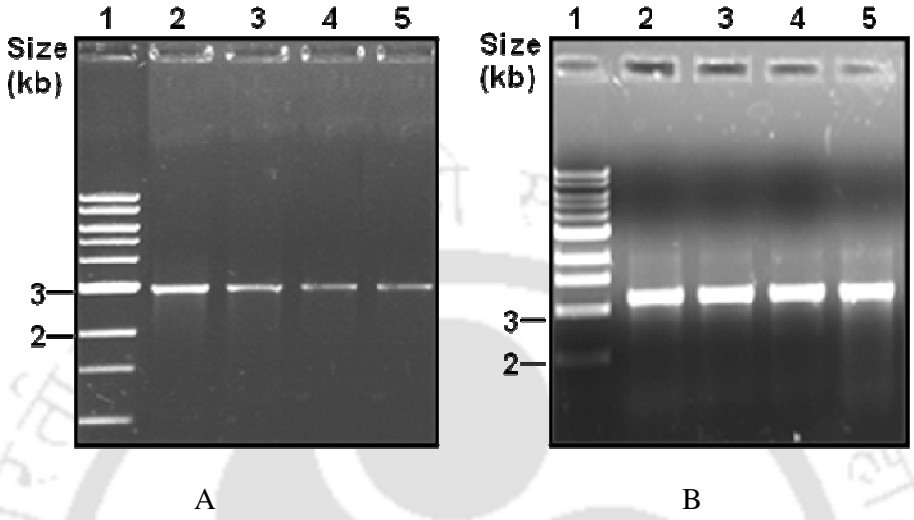

Figure 4.14: Verification of the pRD-2-B-*ncs-1*^{G2A} transformants by PCR. **(A)** PCR from the genomic DNA isolated from the *Δncs-1Δmus53 a (15)* strains transformed with the pRD-2-B-*ncs-1*^{G2A} construct. Primer pairs BAR-RV and HI-NCS-1F specific for the *bar* cassette and ~100 bp upstream of the 5' flank of *ncs-1* gene, respectively, were used to confirm the homologous integration of the construct as described in Figure 4.4. The PCR amplicon of size ~2.8 kb indicates homologous integration of the construct. PCR products were resolved in 1% agarose gel; lane 1, 1 kb DNA ladder (NEB); lane 2, pRD-2-B-*ncs-1*^{G2A} heterokaryotic transformant 1 (HT-1); lanes 3, 4, and 5, pRD-2-B-*ncs-1*^{G2A} homokaryotic isolates designated as Hop-20, Hop-21, and Hop-22, respectively. **(B)** Verification of the presence of part of *ncs-1* ORF in the transformants. PCR from the genomic DNA isolated from the wild-type, and pRD-2-B-*ncs-1*^{G2A} homokaryotic isolates Hop-20, Hop-21, and Hop-22 using primer pairs NCS-1(G2A)-F and 7NCU04379-R (Table 4.2, entry 8, 15) produces the amplicons of size ~1.146 kb indicating presence of *ncs-1* ORF. Lane 1, 1 kb DNA ladder (NEB); lane 2, PCR amplicon from the wild-type template; lanes 3, 4 and 5, PCR amplicons from the template of pRD-2-B-*ncs-1*^{G2A} homokaryotic transformants Hop-20, Hop-21, and Hop-22 , respectively.

TH-1227_09610609

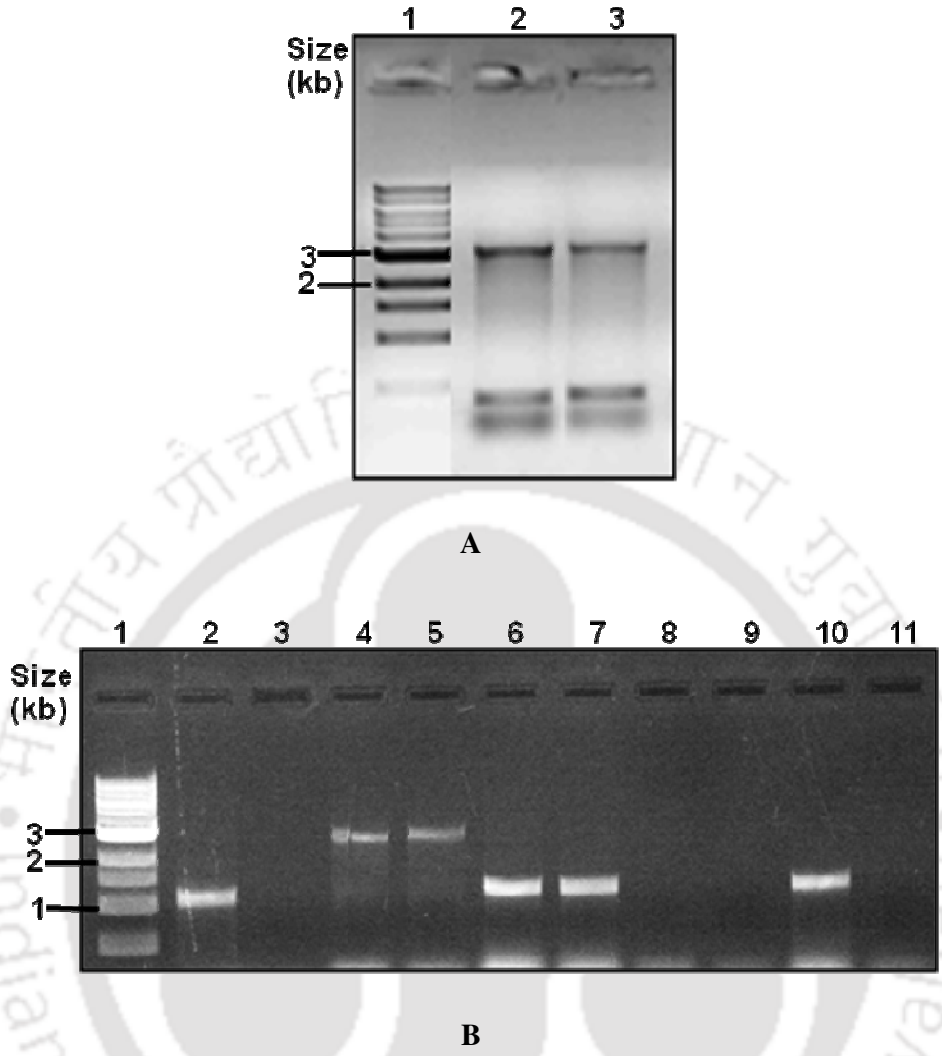

Figure 4.15: Verification of the pRD-2-B-*ncs-1*^{R175A} transformants by PCR. **(A)** PCR from the genomic DNA isolated from heterokaryotic transformants of the *Δncs-1Δmus53 a (15)* strain transformed with the pRD-2-B-*ncs-1*^{R175A} construct. Lane 1, 1 kb DNA ladder (NEB); lanes 2, 3, PCRs of heterokaryotic transformants one (HT-1) and two (HT-2) isolated from the *Δncs-1Δmus53 a (15)* recipient strain, respectively. Primer pairs BarRV and HI-NCS-1F were used in the PCR reactions to confirm the homologous integration (~2.8 kb) of pRD-2-B-*ncs-1*^{R175A} construct in the *Δncs-1Δmus53 a (15)* recipient strain. **(B)** PCRs to verify the homokaryotic isolates of the pRD-2-*ncs-1*^{R175A} transformants (homokaryotic isolates from cross of HT-1x Δ*ncs-1A*). Lane 1,1 kb DNA ladder (NEB); lane 2, PCR of the *bar* gene (~1.2 kb) from the HT-1- *Δncs-1Δmus53 a (15)* using primers BAR-FW and BAR-RV; lane 3, control PCR for the *bar* gene using the *Δncs-1Δmus53 a (15)* template DNA (no product); lanes 4 and 5, PCRs of the homokaryotic isolates designated as HoP-8 and HoP-20

TH-1227_09610609

using primers BarRV and HI-NCS-1F to confirm the homologous integration (~2.8 kb); lanes 6 and 7, PCR for the intact *ncs-1* gene (~1.132 Kb) using primers NCS-1(G2A)-F and NCS-1(R175A)-R, and template DNA of HoP-8 and HoP-20, respectively; lanes 8 and 9, control PCRs using primers BAR-RV and HI-NCS-1F using the template DNA from the wild-type and *Δncs-1Δmus53 a (15)* strains (no product); lane 10, control PCR using primers NCS-1(G2A)-F and NCS-1(R175A)-R for the *ncs-1* gene using the wild-type template DNA (~1.132 Kb); lane 11- control PCR using NCS-1(G2A)-F and NCS 1(R175A)-R primers for the *ncs-1* using the template DNA of the *Δncs-1Δmus53 a (15)* strain (no product). Primers are described in Table 4.2.

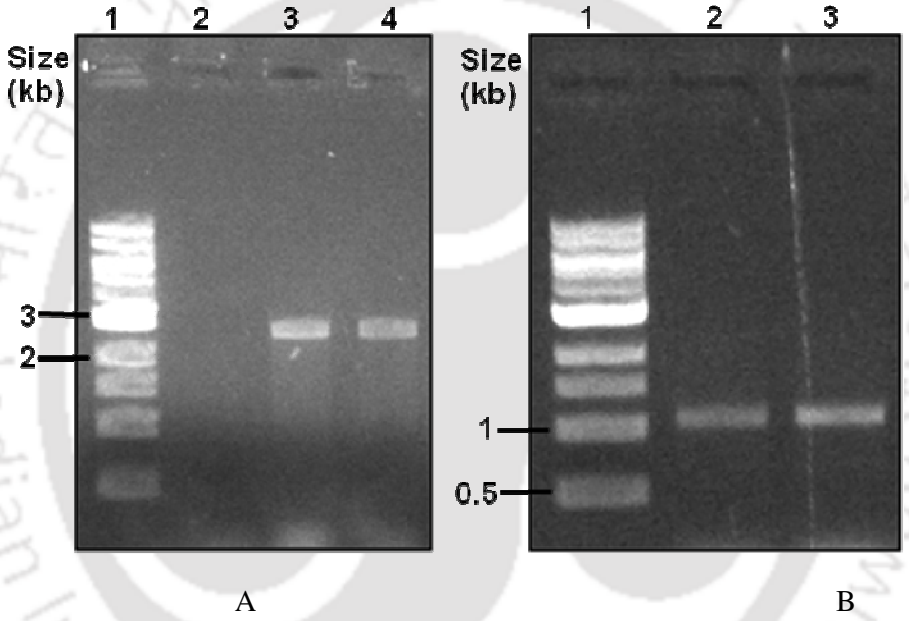

Figure 4.16: Verification of the *ncs-1*^{E120Q} transformants by PCR. (A) PCR from the genomic DNA isolated from the *Δncs-1Δmus53* strains transformed with the pRD-2-*ncs-1*^{E120Q} construct. Primers BAR-RV and HI-NCS-1F specific for the *bar* and upstream of the 5' flank of *ncs-1* gene, respectively, were used to confirm the homologous integration of the construct as described in Figure 4.4 A. The PCR amplicon of size ~2.8 kb indicates homologous integration of the construct. PCR products were resolved in a 0.8 % agarose gel; lane 1, 1 kb DNA ladder (NEB); lane 2, control PCR reaction using the template DNA from the *Δncs-1Δmus53 a (15)*; lane 3, *ncs-1*^{E120Q} heterokaryotic transformant 4 (HT-4); lanes 4, *ncs-1*^{E120Q} homokaryotic isolate designated as Hop-5. **(B)** Verification of presence of the intact *ncs-1* gene in the transformants. PCR from the genomic DNA isolated from *ncs-1*^{E120Q} homokaryotic isolates using primers NCS-1(G2A)-F and 7NCU04379-R, specific for the *ncs-*

TH-1227_09610609

1 gene, produced the amplicons of size ~1.146 indicating presence of the intact *ncs-1* gene; lane 1, 1 kb DNA ladder (NEB); lane 2, wild-type; lane 3, homokaryotic isolate HoP-5. Primers are described in Table 4.2.

4.2.6 The *ncs-1*^{G2A} mutant displayed growth phenotype like the wild-type

Agar plugs of the wild-type, Δ*ncs-1*, *ncs-1::bar*, *ncs-1*^{G2A} strains were inoculated at one end of the race tube containing 13 ml Vogel's glucose agar, and incubated at 30ºC till growth front reaches the other end of the race tube (n=3). Growth front was marked periodically at a regular interval of 12 h for 72 h and distance was plotted against time (Figure 4.17, Table 4.3) to obtain the linear growth rate. The average growth rate of the *ncs-1*^{G2A} mutant was comparable to the wild-type; thus, the *ncs-1*^{G2A} mutant complemented the slow growth phenotype of the Δ*ncs-1* mutant. This result suggested that N-myristoylation of NCS-1 and its subsequent membrane targeting is not essential for its role in growth.

TH-1227_09610609

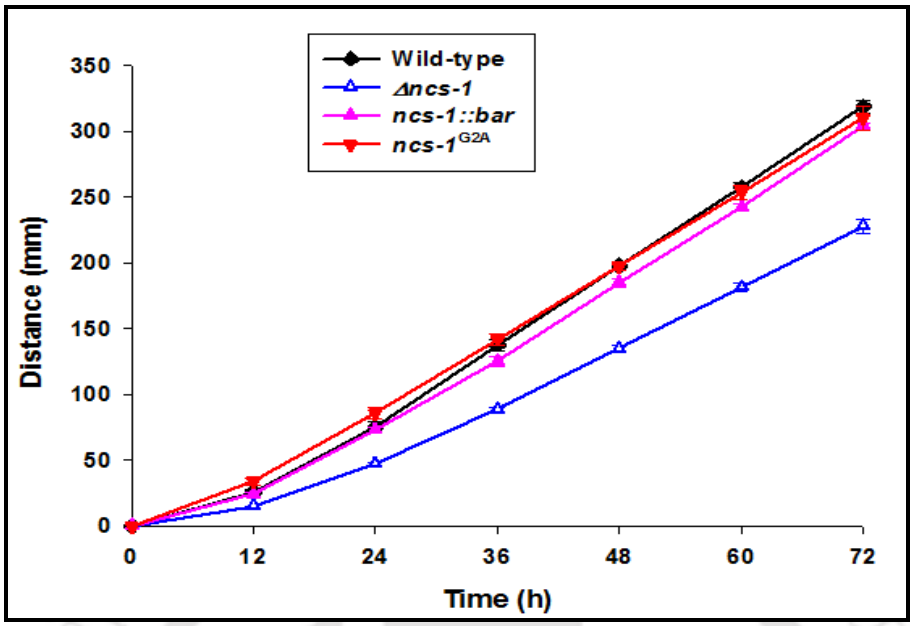

Figure 4.17: Growth phenotype of the *ncs-1*^{G2A} mutant. The wild-type, the Δ*ncs-1* mutant, the *ncs-1::bar* homokaryotic transformant, and the *ncs-1*^{G2A} mutant strains were inoculated at one end of the race tube and incubated at 30°C for 72 h. The *ncs-1*^{G2A} mutant allele complemented the growth defect of the Δ*ncs-1* mutant.

Table 4.3 Apical growth of the wild-type, Δ*ncs-1* mutant, *ncs-1::bar* homokaryotic transformant, and *ncs-1*^{G2A} mutant strains in the race tube

Strain	Distance in race tube (mm) at the indicated time interval (h)						
	0	**12**	**24**	**36**	**48**	**60**	**72**
Wild-type	0	26 ± 1.7	75.6 ± 3.7	137.6 ± 4	197.6 ± 3.5	257.3 ± 3.7	318 ± 4.9
Δ*ncs-1*	0	15 ± 0	47.3 ± 1.1	88.6 ± 1.1	135 ± 2	181.3 ± 3	228 ± 5.2
ncs-1::bar	0	24.3 ± 1.6	73.2 ± 2.3	125.2 ± 3.9	185 ± 3	242.3 ± 2.5	304.3 ± 2.0
ncs-1^{G2A}	0	34.2 ± 2.7	85.9 ± 3.9	141.9 ± 3.9	197.3 ± 3	253.8 ± 5.5	310.4 ± 9.1

TH-1227_09610609

4.2.7 The *ncs-1*^{G2A} mutant displayed a faster growth in absence of extracellular Ca^{2+} and tolerates to high Ca^{2+} stress like the wild-type

To test the effect of Ca^{2+} on growth of the *ncs-1*^{G2A} mutant, I did the growth analysis of mutant on medium supplemented with various concentration of $CaCl_2$. Colony diameter of the mutant and the control strains used was marked at a regular interval of 3 h for 24 h. The *ncs-1*^{G2A} mutant displayed faster growth than the wild-type in Vogel's glucose medium lacking Ca^{2+}, and Ca^{2+} sensitivity phenotype of the *ncs-1*^{G2A} mutant was like the wild-type (Figure 4.18, Table 4.4). Therefore, *ncs-1*^{G2A} mutant complemented the Ca^{2+} sensitivity phenotype of the Δ*ncs-1* mutant. This result suggested that the N-myristoylation mediated membrane targeting of NCS-1 is not essential for its role in Ca^{2+} stress tolerance.

4.2.8 The *ncs-1*^{G2A} mutant showed an increased sensitivity to UV irradiation like the Δ*ncs-1* mutant

To test the effect of UV stress, ~10^3 conidia were plated on the Vogel's sorbose agar medium and irradiated with different doses of UV. The *ncs-1*^{G2A} mutant showed UV sensitivity phenotype like the Δ*ncs-1* mutant (Figure 4.19, Table 4.5) suggesting that the N-myristoylation mediated membrane targeting of NCS-1 is essential for its role in UV induced DNA damage repair.

TH-1227_09610609

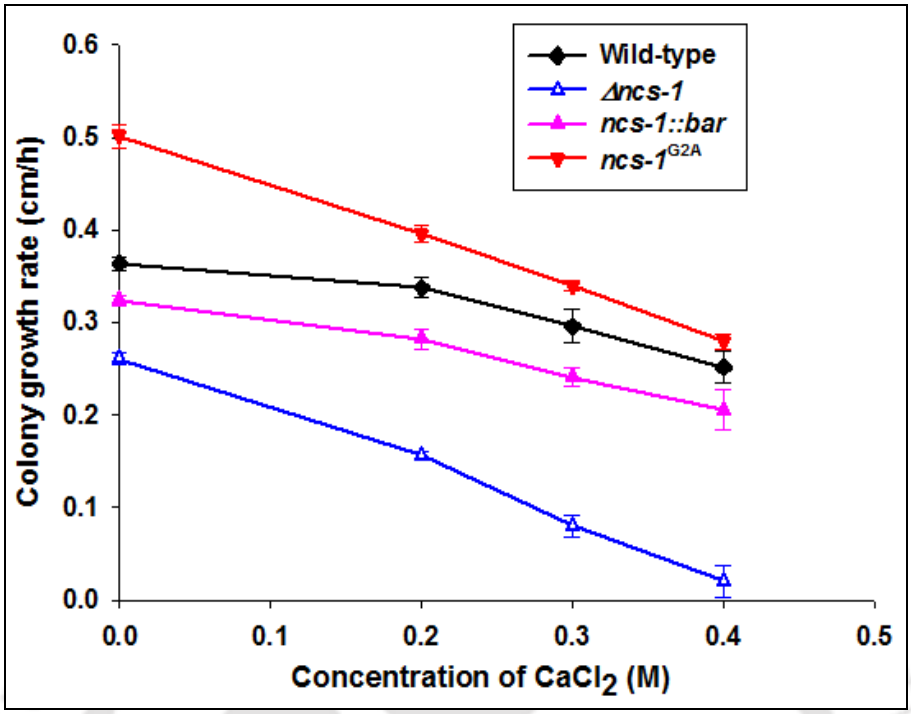

Figure 4.18: Effect of calcium stress on the growth of the *ncs-1*^{G2A} mutant. Conidia of the wild-type, the Δ*ncs-1* mutant, the *ncs-1::bar* homokaryotic transformant, and the *ncs-1*^{G2A} mutant strains were inoculated at the center of petridishes containing indicated amount of $CaCl_2$. Colony diameter of the strains was measured at a regular interval of 3 h for 24 h. Average colony growth rates were plotted against different concentrations of $CaCl_2$. The *ncs-1*^{G2A} mutant allele complemented the sensitivity of the Δ*ncs-1* mutant to $CaCl_2$ stress and displayed a faster colony growth rate in the medium without $CaCl_2$.

Table 4.4 Average colony growth rate of the wild-type, Δ*ncs-1* mutant, *ncs-1::bar* homokaryotic transformant, and the *ncs-1*^{G2A} mutant strains at various concentrations of $CaCl_2$

Strain	Colony growth rate (cm/h) at various concentrations of $CaCl_2$ (M)			
	0	**0.2**	**0.3**	**0.4**
Wild-type	0.363 ± 0.007	0.337± 0.018	0.295 ± 0.018	0.251 ± 0.016
Δ*ncs-1*	0.260 ± 0.006	0.156 ± 0.004	0.08± 0.010	0.02 ± 0.017
ncs-1::bar	0.323 ± 0.005	0.282 ± 0.010	0.241± 0.010	0.185 ± 0.02
ncs-1^{G2A}	0.5 ± 0.012	0.395 ± 0.008	0.339 ± 0.005	0.279 ± 0.008

TH-1227_09610609

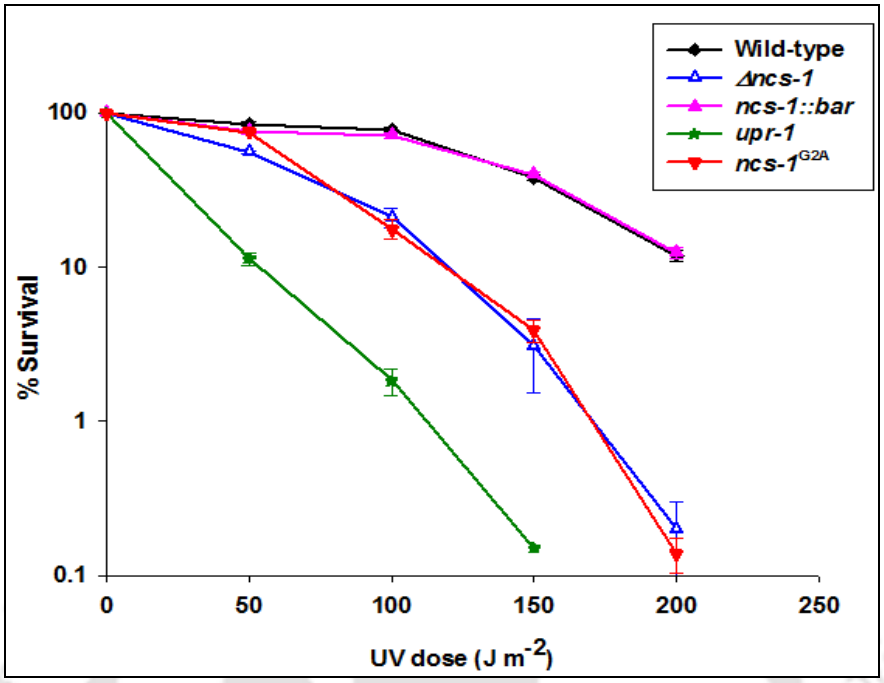

Figure 4.19: Dose response curves showing the relative UV-sensitivity of the *ncs-1*^{G2A} mutant. Approximately 10^3 conidia of the wild-type, the Δ*ncs-1* mutant, the *ncs-1::bar* homokaryotic transformant, and the *ncs-1*^{G2A} mutant strains were plated in petridishes (150 mm diameter) containing Vogel's sorbose agar medium and irradiated with various UV doses. Percent survival was obtained by dividing the number of colonies from plates irradiated with UV dose by the number of colonies on plates with no UV irradiation (control). The *ncs-1*^{G2A} mutant allele did not complement the UV-sensitivity phenotype of the Δ*ncs-1* mutant.

Table 4.5 Relative UV-sensitivity of the of the wild-type, Δ*ncs-1* mutant, *ncs-1::bar* homokaryotic transformant, *ncs-1*^{G2A} mutant, and *upr-1* mutant strains

Strain	% Survival at indicated doses of UV irradiation (J m^{-2})				
	0	**50**	**100**	**150**	**200**
Wild-type	100	84.8 ± 2.3	78.2 ± 1.9	38.3 ± 1.7	11.9 ± 1
Δ*ncs-1*	100	55.7 ± 1.1	21.1 ± 2.9	3.1 ± 1.5	0.2 ± 0.1
ncs-1::bar	100	76.6 ± 2.9	71.4 ± 1.4	40 ± 1.4	12.4 ± 1
ncs-1^{G2A}	100	75.3 ± 1	17.66 ± 2.5	3 ± 0.6	0.1 ± 0.03
upr-1	100	11.3 ± 1	1.8 ± 0.3	0.15 ± 0	0

TH-1227_09610609

4.2.9 The *ncs-1*^{R175A} mutant showed growth and Ca^{2+} stress tolerance like the wild-type

Agar plugs of the wild-type, Δ*ncs-1*, *ncs-1::bar*, *ncs-1*^{R175A} strains were inoculated at one end of the race tube containing 13 ml Vogel's glucose agar, and incubated at 30ºC till growth front reaches the other end of the race tube (n=3). Growth front was marked periodically at a regular interval of 12 h for 72 h and distance was plotted against time (Figure 4.20, Table 4.6) to obtain the linear growth rate. The average growth rate of the *ncs-1*^{R175A} mutant was comparable to the wild-type; thus, the *ncs-1*^{R175A} mutant complemented the growth defect of the Δ*ncs-1* mutant.

To test the effect of Ca^{2+} on growth of *ncs-1*^{R175A} mutant, I did growth analysis of the mutant on medium supplemented with various concentrations of $CaCl_2$. The *ncs-1*^{R175A} mutant had grown faster than the wild-type on Vogel's glucose medium lacking Ca^{2+}, and showed growth rate similar to the wild-type on medium supplemented with various concentrations of $CaCl_2$. Thus, the *ncs-1*^{R175A} mutant complemented the Ca^{2+} sensitivity phenotype of Δ*ncs*-1 mutant (Figure 4.21, Table 4.7).

4.2.10 The *ncs-1*^{R175A} mutant showed an increased sensitivity to UV irradiation than the Δ*ncs-1* mutant.

To test the effect of UV stress, ~10^3 viable conidia were plated on the Vogel's sorbose agar medium and irradiated with different doses of UV (Figure 4.22, Table 4.8). The *ncs-1*^{R175A} mutant displayed greater UV sensitivity phenotype than the Δ*ncs-1* mutant. This result indicated that *ncs-1*^{R175A} mutant possibly acts in a dominant negative manner. Furthermore, the replacement of valine at 175 with arginine in the *N. crassa* homologue of NCS-1 might explain its novel role in UV-induced DNA damage repair process.

TH-1227_09610609

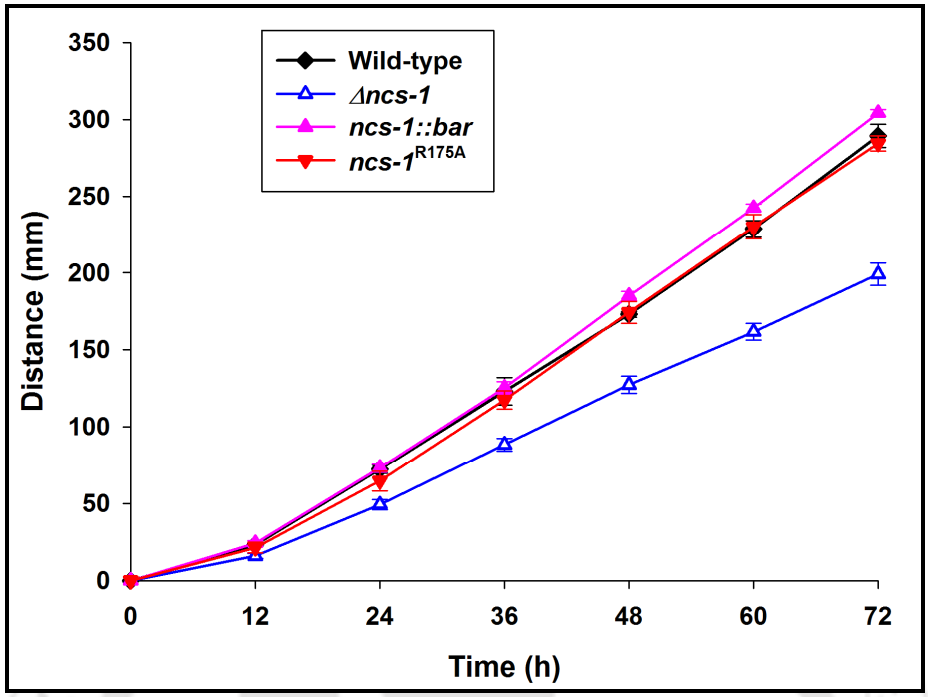

Figure 4.20: Growth phenotype of the *ncs-1*^{R175A} mutant. The wild-type, the Δ*ncs-1* mutant, the *ncs-1::bar* homokaryotic transformant, and the *ncs-1*^{R175A} mutant strains were inoculated at one end of the race tube and incubated at 30°C for 72 h. The *ncs-1*^{R175A} mutant allele complemented the growth defect of the Δ*ncs-1* mutant.

Table 4.6 Apical growth of the wild-type, Δ*ncs-1*mutant, *ncs-1::bar* homokaryotic transformant, and *ncs-1*^{R175A} mutant in the race tube

Strain	Distance in race tube (mm) at indicated time interval						
	0	12	24	36	48	60	72
Wild-type	0	23.3 ± 1.5	72.3 ± 2.5	123 ± 8.8	173.6 ± 1.7	228.6 ± 5.5	289 ± 7.5
Δ*ncs-1*	0	16 ± 1.7	49.3 ± 3.2	88.3 ± 4.1	127.3 ± 5.5	161. ± 5.5	199 ± 7.2
ncs-1::bar	0	24.3 ± 1.6	73.2 ± 2.3	125.2 ± 3.9	185 ± 3	242.3 ± 2.5	304.3 ± 2.0
ncs-1^{R175A}	0	21.3 ± 3.5	64.6 ± 6.4	117.3 ± 5.8	174.3 ± 7.0	230.8 ± 8	284.3 ± 5.0

TH-1227_09610609

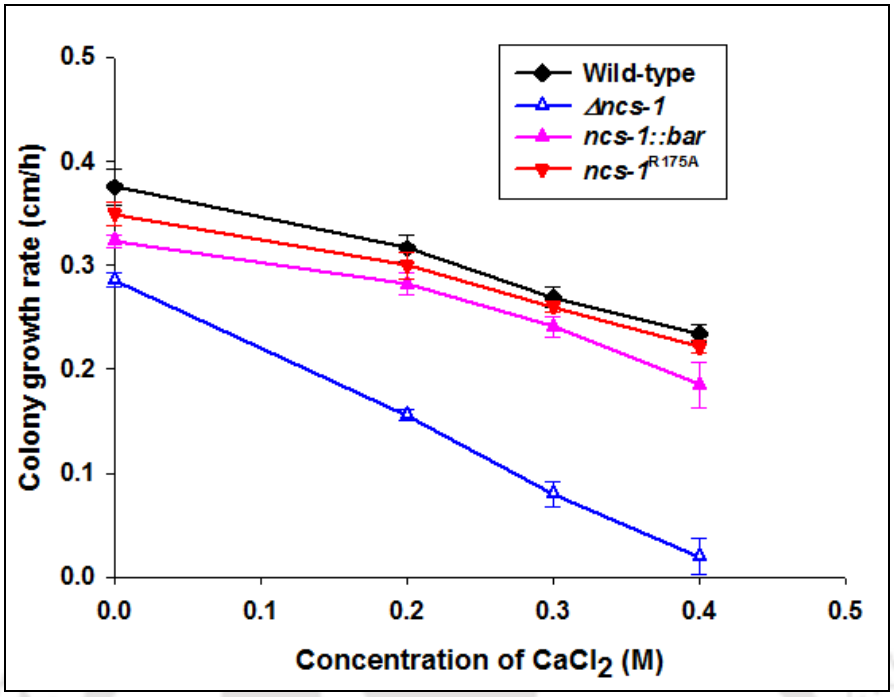

Figure 4.21: Effect of calcium stress on growth of the *ncs-1*^{R175A} mutant. Conidia of the wild-type, the Δ*ncs-1* mutant, the *ncs-1::bar* homokaryotic transformant, and the *ncs-1*^{R175A} mutant strains were inoculated at the center of petridishes containing medium supplemented with various amounts of $CaCl_2$. Colony diameter of strains was measured at a regular interval of 3 h for 24 h. Average colony growth rates were plotted against different concentrations of $CaCl_2$. The *ncs-1*^{R175A} mutant allele complemented the sensitivity of the Δ*ncs-1* mutant to $CaCl_2$ stress.

Table 4.7 Average colony growth rate of the wild-type, the Δ*ncs-1* mutant, the *ncs-1::bar* homokaryotic transformant, and the *ncs-1*^{R175A} mutant strains at various concentrations of $CaCl_2$

Strain	Colony growth rate (cm/h) at various concentrations of $CaCl_2$ (M)			
	0	**0.2**	**0.3**	**0.4**
Wild-type	0.375 ± 0.01	0.316± 0.013	0.269 ± 0.01	0.234 ± 0.008
Δ*ncs-1*	0.285 ± 0.006	0.156 ± 0.049	0.08 ± 0.011	0.02 ± 0.017
ncs-1::bar	0.323 ± 0.005	0.282 ± 0.010	0.241± 0.010	0.185 ± 0.02
ncs-1^{R175A}	0.349 ± 0.011	0.300 ± 0.012	0.260 ± 0.005	0.221 ± 0.005

TH-1227_09610609

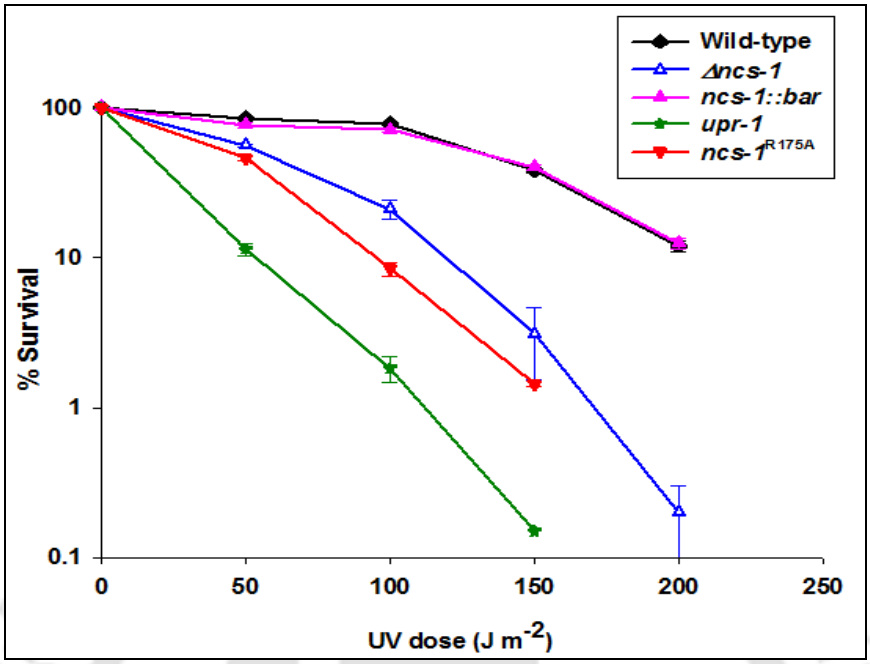

Figure 4.22: Dose response curves showing relative UV-sensitivity of the *ncs-1*^{R175A} mutant. Approximately 10^3 conidia of the wild-type, the Δ*ncs-1* mutant, the *ncs-1::bar* homokaryotic transformant, and the *ncs-1*^{R175A} mutant strains were plated on Vogel's sorbose agar (in petridishes of 150 mm diameter) and irradiated with various UV doses. Percent survival was obtained by dividing the number of colonies from plates irradiated with UV dose by the number of colonies on plates with no UV exposure (control). The *ncs-1*^{R175A} mutant allele did not complement UV-sensitivity phenotype of the Δ*ncs-1* mutant.

Table 4.8 Relative UV- sensitivity of the of the wild-type, Δ*ncs-1* mutant, *ncs-1::bar* homokaryotic transformant, *ncs-1*^{R175A} mutant, and *upr-1* mutant strains.

Strain	% Survival in various doses of UV irradiation (J m^{-2})				
	0	**50**	**100**	**150**	**200**
Wild-type	100	84.8 ± 2.3	78.2 ± 1.9	38.3 ± 1.7	11.9 ± 1
Δ*ncs-1*	100	55.7 ± 1.1	21.1 ± 2.9	3.1 ± 1.5	0.2 ± 0.1
ncs-1::bar	100	76.6 ± 2.9	71.4 ± 1.4	40 ± 1.4	12.4 ± 1
ncs-1^{R175A}	100	46.1 ± 2.1	8.4 ± 0.8	1.4 ± 0.0	0.0 ± 0.00
upr-1	100	11.3 ± 1	1.8 ± 0.3	0.15 ± 0	0

TH-1227_09610609

4.2.11 The *ncs-1*^{E120Q} mutant showed slow growth, sensitivity to Ca^{2+} and UV stress like the Δ*ncs-1* mutant

The *ncs-1*^{E120Q} mutant did not complement the growth, Ca^{2+} sensitivity, and UV sensitivity phenotypes of the Δ*ncs-1* mutant. The growth rate of *ncs-1*^{E120Q} mutant was lower than the Δ*ncs-1* mutant indicating that *ncs-1*^{E120Q} mutant affect more severely on growth than the Δ*ncs-1* mutant (Figure 4.23, Table 4.9). The *ncs-1*^{E120Q} mutant was sensitive to Ca^{2+} and UV stress like the Δ*ncs-1* mutant (Figures 4.24, 4.25; Tables 4.10, 4.11). Therefore, these results suggested that glutamate at the position 120 of EF3 is critical for NCS-1 functions and ablating the function of this Ca^{2+}-binding residue impairs the NCS-1 function.

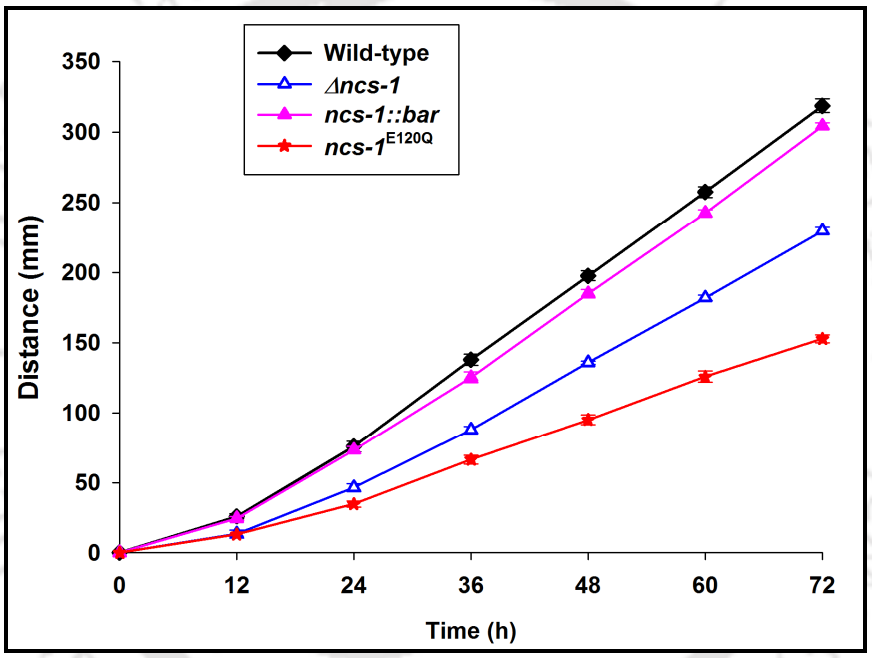

Figure 4.23 Growth phenotype of the *ncs-1*^{E120Q} mutant. The wild-type, the Δ*ncs-1* mutant, the *ncs-1::bar* homokaryotic transformant, and the *ncs-1*^{E120Q} mutant strains were inoculated at one end of the race tube and incubated at 30°C for 72 h. The *ncs-1*^{E120Q} mutant displayed a lower growth rate than the Δ*ncs-1* mutant. Therefore, growth defect in the *ncs-1*^{E120Q} mutant was more severe than the Δ*ncs-1* mutant.

TH-1227_09610609

Table 4.9 Apical growth of the wild-type, Δ*ncs-1*mutant, *ncs-1::bar* homokaryotic transformant, and *ncs-1*^{E120Q} mutant strains in the race tube

Strain	Distance in race tube (mm) at the indicated time interval						
	0	12	24	36	48	60	72
Wild-type	0	26 ± 1.73	75.6 ± 3.7	137.6 ± 4.0	197.6 ± 3.5	257.3 ± 3.7	318.6 ± 4.9
Δ*ncs-1*	0	13.3 ± 2.8	46.3 ± 2.8	87.6 ± 2.5	135.6 ± 1.1	182 ± 2	229 ± 2.5
ncs-1::bar	0	24.3 ± 1.6	73.2 ± 2.3	125.2 ± 3.9	185 ± 3	242.3 ± 2.5	304.3 ± 2.0
ncs-1^{E120Q}	0	13 ± 0	34.6 ± 2	66.3 ± 3.2	95 ± 3.4	125.6 ± 4	152.6 ± 2.8

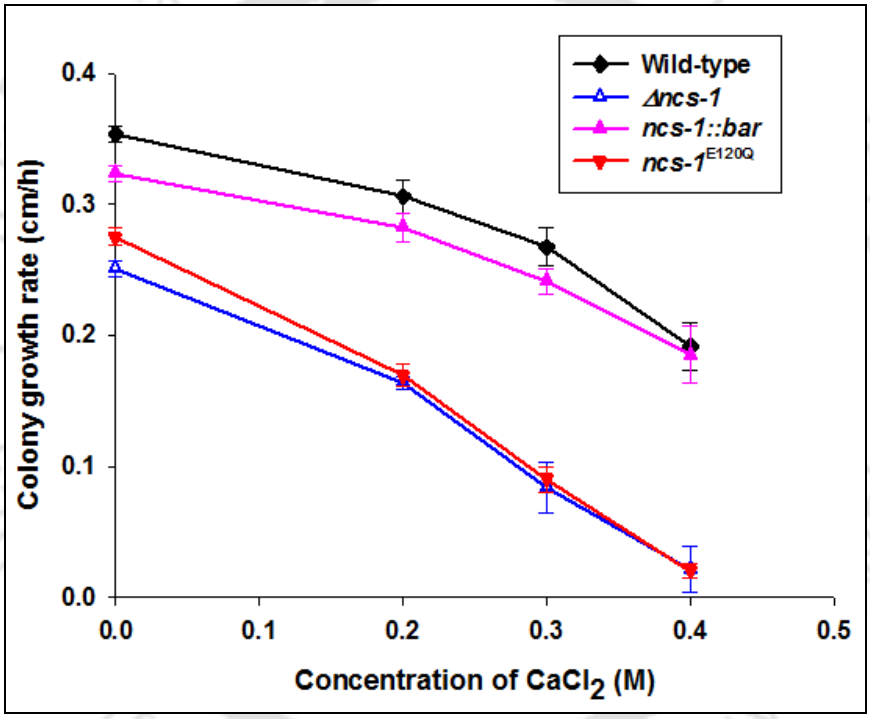

Figure 4.24: Effect of calcium stress on the growth of *ncs-1*^{E120Q} mutant. Conidia of the wild-type, the Δ*ncs-1* mutant, the *ncs-1::bar* homokaryotic transformant, and the *ncs-1*^{E120Q} mutant strains were inoculated at the center of petridishes containing various amounts of $CaCl_2$. Colony diameter of strains was measured at a regular interval of 3 h for 24 h. Average colony growth rates were plotted against different concentrations of $CaCl_2$. The *ncs-1*^{E120Q} mutant showed sensitivity to $CaCl_2$ stress like the Δ*ncs-1* mutant. Therefore, the *ncs-1*^{E120Q} mutant allele did not complement the calcium sensitivity phenotype of the Δ*ncs-1* mutant.

TH-1227_09610609

Table 4.10 Average colony growth rate of the wild-type, the Δ*ncs-1* mutant, the *ncs-1::bar* homokaryotic transformant, and the *ncs-1*^{E120Q} mutant strains at various concentrations $CaCl_2$

Strain	Colony growth rate (cm/h) at various concentrations of $CaCl_2$ (M)			
	0	**0.2**	**0.3**	**0.4**
Wild-type	0.353 ± 0.005	0.305± 0.012	0.267 ± 0.014	0.191 ± 0.018
Δ*ncs-1*	0.286 ± 0.006	0.163 ± 0.049	0.117 ± 0.011	0.047 ± 0.017
ncs-1::bar	0.323 ± 0.005	0.282 ± 0.010	0.241± 0.010	0.185 ± 0.020
ncs-1^{E120Q}	0.274 ± 0.006	0.169 ± 0.008	0.102 ± 0.009	0.047 ± 0.005

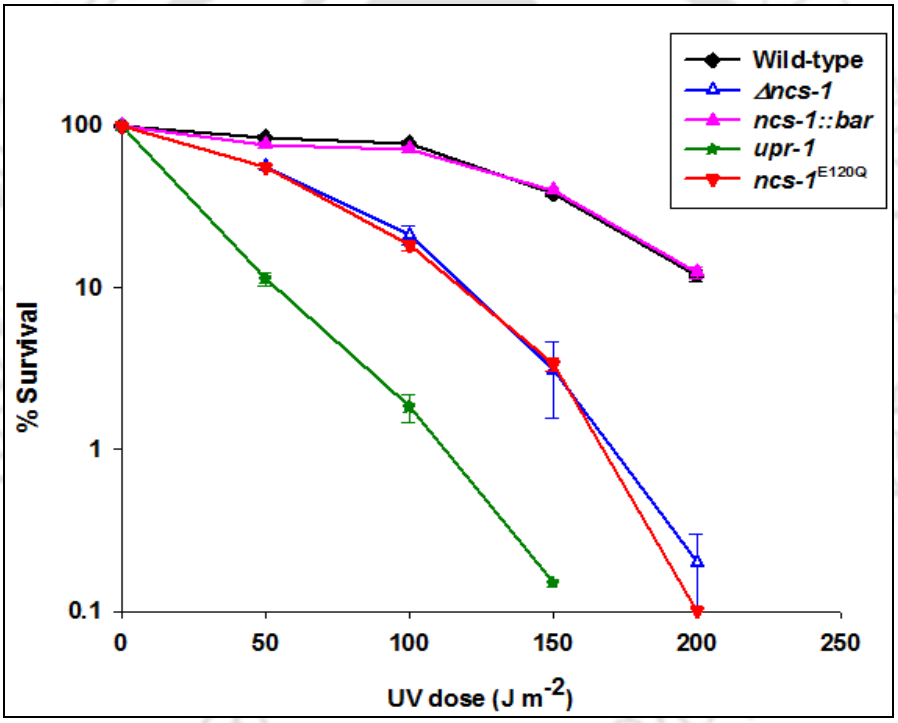

Figure 4.25: **Dose response curves showing relative UV-sensitivity of the *ncs-1*^{E120Q} mutant.** Approximately 10^3 conidia of wild-type, the Δ*ncs-1* mutant, the *ncs-1::bar* homokaryotic transformant, and the *ncs-1*^{E120Q} mutant strains were plated on Vogel's sorbose agar medium (in petridishes of 150 mm diameter) and irradiated with various UV doses. Percent survival was obtained by dividing the number of colonies from plates irradiated with UV dose by the number of colonies on plates with no UV exposure (control). The *ncs-1*^{E120Q} mutant showed UV-sensitivity phenotype like the Δ*ncs-1* mutant. Therefore, *ncs-1*^{E120Q} mutant allele did not complement UV-sensitivity phenotype of the Δ*ncs-1* mutant.

TH-1227_09610609

Table 4.11 Relative UV-sensitivity of the of the wild-type, Δ*ncs-1* mutant, *ncs-1::bar* homokaryotic transformant, *ncs-1*^{E120Q} mutant, and *upr-1* mutant strains

Strain	% Survival in various doses of UV irradiation (J m^{-2})				
	0	**50**	**100**	**150**	**200**
Wild-type	100	84.8 ± 2.3	78.2 ± 1.9	38.3 ± 1.7	11.9 ± 1
Δ*ncs-1*	100	55.7 ± 1.1	21.1 ± 2.9	3.1 ± 1.5	0.2 ± 0.1
ncs-1::bar	100	76.6 ± 2.9	71.4 ± 1.4	40 ± 1.4	12.4 ± 1
ncs-1^{E120Q}	100	55.7 ± 0.8	18.2 ± 1.3	3.3 ± 0.2	0.1 ± 0.00
upr-1	100	11.3 ± 1	1.8 ± 0.3	0.15 ± 0	0

4.3 Discussion

The sequence analysis revealed that NCU04379 gene encodes a Ca^{2+} and/or CaM binding protein of 190 amino acid residues that shows sequence similarity to the homologues of Neuronal Calcium Sensor-1 (NCS-1) from *M. grisea, A. fumigatus*, *S. japonicus, S. pombe*, *D. rerio*, *H. sapiens*, *M. musculus*, *X. Laevis,* and *S. cerevisiae* (92, 91, 79, 78, 66, 66, 66, 65, and 59% identity; 95, 94, 91, 90, 82, 82, 82, 82, and 79% similarity; *e*-values 6e-121, 1e-121, 7e-108, 8e-106, 2e-87, 2e-68, 3e-93, and 4e-64, respectively). Therefore, the NCU04379 encodes a *N. crassa* homologue of NCS-1. The functions of NCS-1 orthologues were previously identified in *S. cerevisiae, M. grisea, A. fumigatus, S. pombe, D. melanogaster*, and *H. sapiens.* In *S. cerevisiae*, Frq1, the NCS-1 homologue, was found essential for cell growth and viability (Hendricks et al. 1999). The spores of *frq1*Δ null mutants were inviable and growth was stopped after three or four divisions. The Frq1 protein, upon Ca^{2+} binding, changes its conformation and exposes its N-myristoyl group through which the protein physically associates with the N-terminus of phosphatidylinositol-4-OH kinase (Pik1) and contribute to optimal function of Pik1 by assisting with its membrane attachment (Huttner et al. 2003). In *M. grisea*, null-mutants for *ncs-1* like gene, *Mg-ncs-1*, showed normal growth and pathogenicity similar to their parental strains, but high concentrations of Ca^{2+} and acidic conditions suppressed their growth (Saitoh et al. 2003). In *S. pombe*, *ncs1*Δ mutant showed nutrition-insensitive sexual development and Ca^{2+} sensitivity at high concentrations of Ca^{2+} (Hamasaki-Katagiri et al. 2004). The starvation independent sexual development in *ncs1*Δ of *S. pombe* was suppressed by exogenous cAMP suggesting the involvement of Ncs1p in the adenylate cyclase pathway switched on by a glucose-sensing G-coupled receptor Git3p (Welton and Hoffman 2000). Thus, in contrast to the lethal null phenotype of the budding

TH-1227_09610609

yeast homolog Frq1, the *ncs1* gene in fission yeast was found non-essential for vegetative growth. In *A. fumigatus*, Δ*ncsA* mutant was more resistant to $CaCl_2$ and sensitive to EGTA suggesting the involvement of NcsA, the NCS-1 homologue, in Ca^{2+} metabolism. Moreover, NcsA was found to support the expression of ion pumps *pmcA* and *pmcB* regulating Ca^{2+} metabolism in the cytoplasm. NcsA was also found to be involved in sterol distribution and polar establishment in the tip of *A. fumigatus* (Mota Ju´nior et al. 2008). In *Drosophila*, Frequenin modulates Ca^{2+} entry through a functional interaction with voltage-gated Ca^{2+} -channel subunit. This regulates neurotransmission release and nerve terminal outgrowth (Dason et al. 2009). In mammals, NCS-1 is involved in anti-apoptotic mechanism in adult motor neurons. It was found to be a novel survival-promoting factor in bilateral dorsal motor nucleus of vagus neurons in adult rats. Overexpression of NCS-1 rendered cultured neurons more tolerant to cell death caused by several kinds of stressors whereas the dominant-negative mutant (E120Q) accelerated the cell death (Nakamura et al. 2006). In *Danio rerio*, *ncs-1a* gene encoding NCS-1 is required for semicircular canal formation. The knockdown of *ncs-1a* blocks normal development of non-sensory components of semicircular canals (Petko et al. 2009). In *Caenorhabditis elegans*, proper calcium signaling via NCS-1 is essential for associative learning and memory (Gomez et al. 2001).

The knockout mutant of *N. crassa* homologue of NCS-1 displayed slow growth rate and hypersensitivity to Ca^{2+} stress (Figures 3.2, 3.4, discussed in Chapter 3) which was in contrast to the phenotype of *A. fumigatus* Δ*ncsA* mutant that showed resistance to Ca^{2+} stress. This result suggested that homologues of NCS-1 in *N. crassa* and *A. fumigatus* functions differently with regard to Ca^{2+} metabolism. Additionally, UV-sensitivity of the ΔNCU04379.2 mutant strain (Figure 3.8, discussed in Chapter 3) uncovered a novel function of *N. crassa* homologue of NCS-1. This suggested the involvement of *N. crassa* homologue of NCS-1 in UV-induced DNA damage repair process. UV light absorption may cause DNA damage primarily through formation of cyclobutane pyrimidine dimers (CPD; Lippke et al. 1981) and pyrimidine (6–4) pyrimidone photoproducts (6–4PP; Mitchell and Nairn 1989) leading to induction of DNA repair mechanisms or apoptosis (Lo et al. 2005). It was also reported that overexpression of CaM activates H2AX mediated DNA repair after irradiation and the CaM protein antagonists fully or partially block double-stranded DNA repair in human cells (Wang et al. 2000; Herman et al. 2002; Smallwood et al. 2009).

TH-1227_09610609

The site-directed mutational analysis revealed that N-myristoylation in *N. crassa* homologue of NCS-1 is not essential for its growth and Ca^{2+} stress tolerance since *ncs-1*^{G2A} mutant complemented the slow growth and Ca^{2+} sensitivity phenotypes of the Δ*ncs-1* mutant (Figures 4.17, 4.18). However, the *ncs-1*^{G2A} mutant showed an increased sensitivity to UV like the Δ*ncs-1* mutant (Figure 4.19). This result suggested that the N-myristoylation mediated membrane targeting is essential for the NCS-1 role in UV induced DNA damage repair in *N. crassa*. The R175A mutation in the hydrophobic pocket of *N. crassa* homologue of NCS-1 complemented growth defect and Ca^{2+} sensitivity phenotypes of the Δ*ncs-1* mutant (Figure 4.20, 4.21). However, the *ncs-1*^{R175A} mutant was more sensitive to UV than the Δ*ncs-1* mutant (Figure 4.22). This could indicate the molecular basis of the novelty of the NCS-1 protein for its involvement in UV-induced DNA damage and repair process in *N. crassa.* The E120Q mutation in the EF3 domain was found to be very critical for NCS-1 functions in *N. crassa* since *ncs-1*^{E120Q} mutant did not complement the slow growth, Ca^{2+} and UV sensitivity phenotypes of the Δ*ncs-1* mutant (Figures 4.23, 4.24, 4.25). In addition, *ncs-1*^{E120Q} mutant displayed slow growth rate that was much lower than the Δ*ncs-1* mutant indicating the dominant negative effect of *ncs-1*^{E120Q} allele in growth.

Thus, this Chapter describes sequence analysis that identified NCU04379 gene as a homologue of NCS-1. In addition, site-directed mutational analysis had identified three critical residues of NCS-1 in *N. crassa*. A part of this Chapter was published in Journal of Basic Microbiology (Tamuli et al. 2011) and in Genetica (Deka et al. 2011). Genetic interaction of *ncs-1* will be discussed in the next Chapter.

TH-1227_09610609

CHAPTER 5

Genetic interaction of Neurospora crassa homologue of Neuronal Calcium Sensor-1

TH-1227_09610609

5.1 Introduction

In the previous Chapter, I described the role of *N. crassa* homologue of NCS-1 in growth, Ca^{2+} stress tolerance, and UV survival (Deka et al. 2011). However, mechanism of NCS-1 functions remains unknown in *N. crassa.* In order to gain deeper insight into the mechanism of NCS-1 functions, I have studied the epistatic relationship of NCS-1 with two other selected Ca^{2+}signaling genes. These genes are selected based on their involvement in controlling $[Ca^{2+}]_c$ in *N. crassa* and related fungi. One of such gene, the *nca-2* (NCU04736.2, FGSC13071 A), encodes a PMCA type Ca^{2+}-ATPase that plays a major role in pumping Ca^{2+} out of the cell and the Δ*nca-2* knockout mutant shows sensitivity to high concentration of extracellular Ca^{2+} (Bowman et al. 2011). The mechanosensitive Ca^{2+} -permeable channel MID-1 (NCU06703.2, FGSC 11708 A and 11707 a) in *N. crassa* plays a role in regulation of ion transport via Ca^{2+} homeostasis and signaling and that the Δ*mid-1* mutant exhibits poorer growth in low extracellular Ca^{2+}(Lew et al. 2008). In *S. pombe*, Ncs1p, the homologue of NCS-1, promotes Ca^{2+}-induced closure of Yam8p Ca^{2+} channel, a homologue of the MID-1 (Hamasaki-Katagiri and Ames 2010). Interestingly, the Ca^{2+}-sensitive phenotype of the *ncs1* deletion mutant is rescued by a *yam8* deletion, indicating that Ncs1p negatively regulates Yam8p in *S. pombe* minimizing Ca^{2+}-influx under extreme external conditions (Hamasaki-Katagiri and Ames 2010). However, no information is available regarding the interaction between NCS-1 and MID-1 in *N. crassa*. In this Chapter, I describe the genetic interaction of *ncs-1*, *mid-1*, and *nca-2* based on the phenotypic analysis of the double mutants.

5.2 Results

5.2.1 Genetic location of the *ncs-1*, *mid-1*, and *nca-2* genes

The locus information of the *ncs-1*, *mid-1*, and *nca-2* was obtained from the *N. crassa* genetic and physical maps of genes (http://www.bioinf.leeds.ac.uk/~gen6ar/newgenelist/genes/physical_maps.htm; Figure 5.1) The *ncs-1* gene is physically mapped in the supercontig four (NC4) from position 3562633 to 3565030 (- strand) at the right arm of the Linkage group IV (LGIVR). The *mid-1* gene is physically mapped in the supercontig five (NC5) from position 4334909 to 4337478 (+ strand) at the right arm of the Linkage group V (LGVR). The *nca-2* gene is physically mapped in the supercontig six (NC6) from position 615195 to 620621 (+ strand) at the left arm of the Linkage group VI (LGVIL).

TH-1227_09610609

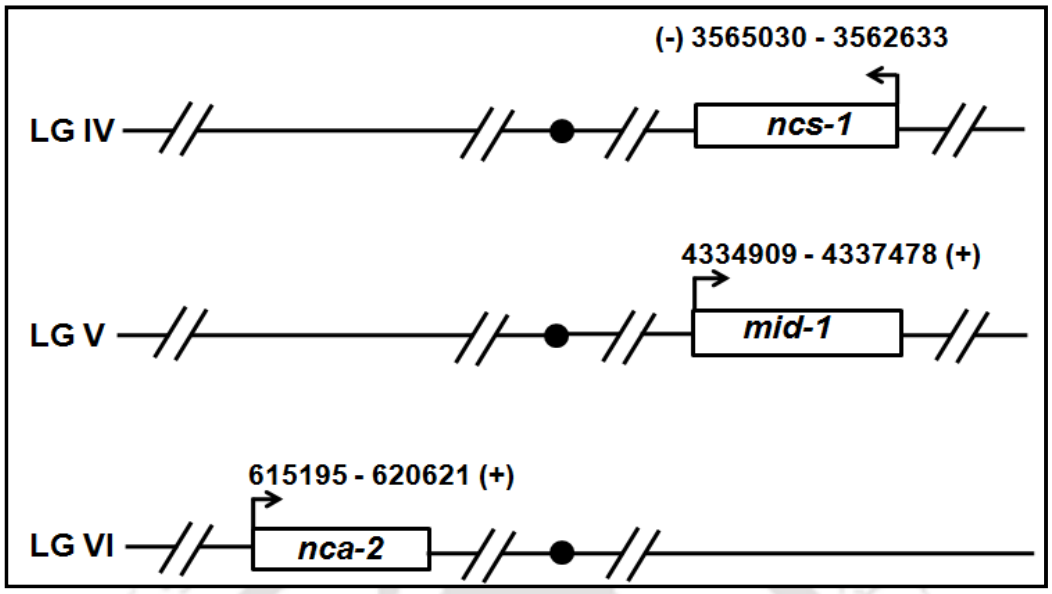

Figure 5.1: Schematics of *ncs-1*, *mid-1*, and *nca-2* genes showing their chromosomal location. The *ncs-1* gene is located on the linkage group IV at the right side of the centromere (LGIVR). The *mid-1* gene is located on the linkage group V at the right side of the centromere (LGVR). The *nca-2* gene is located on the linkage group VI at the left side of the centromere (LGVIL). The arrows indicate direction of transcription relative to for the each gene. The numbers, shown with respect to the transcribed strand (- or +), indicate position of ORF (in 5´→3´ direction of transcription) of the respective gene in the physical map of each gene. Solid circles indicate the centromere in each line.

5.2.2 Generation of the Δ*ncs-1*Δ*nca-2*, Δ*ncs-1*Δ*mid-1*, and Δ*mid-1*Δ*nca-2* double mutants

The single knockout mutants were generated and confirmed by the *N. crassa* genome project (http://www.dartmouth.edu/~neurosporagenome/proj_overview.html) and also verified in independent works (Colot et al. 2006; Lew et al. 2008; Bowman et al. 2011; Deka et al. 2011). The Δ*ncs-1*Δ*nca-2*, Δ*ncs-1*Δ*mid-1*, and Δ*mid-1*Δ*nca-2* double mutants were generated by crossing the respective single mutants of opposite mating type. The f_1 progenies were screened for Hyg^R phenotype and followed by PCR analysis. The Δ*ncs-1* was verified by using HI-NCS-1F forward primer (Table 4.1, entry 8) and 5HPHR reverse primer (Table 3.7, entry 3). The Δ*nca-2* was verified by using HI-NCU04736-F 5′-GTCCCATGGATTCCATACCA -3′ forward primer specific for upstream of the open reading frame (ORF) of *nca-2* gene and 5HPHR reverse primer. Similarly, the Δ*mid-1* was

TH-1227_09610609

verified by using HI-NCU06703- F 5′-CCAAGGCTTATGCCGTCATC -3′ forward primer specific for upstream of the ORF of *mid-1* gene and 5HPHR reverse primer. The PCR reaction condition used were 2 min initial denaturation at 95ºC followed by 30 cycles of 30 sec denaturation at 95ºC, 30 sec annealing at 60ºC and 2 min 50 sec elongation at 72ºC. The final extension was for 10 min at 72ºC. Amplification of the PCR products of size ~2.89, 2.089, and 2.023 kb, respectively, verified the presence of the Δ*ncs-1*, Δ*nca-2*, and Δ*mid-1* alleles in the respective mutants (Figure 5.2).

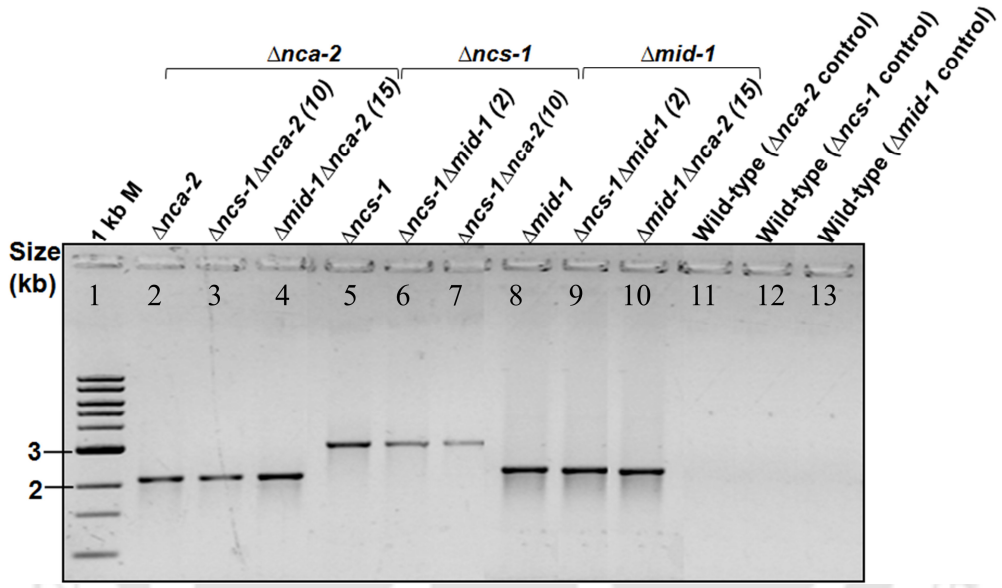

Figure 5.2: Verification of double mutants using PCR. The Δ*ncs-1*Δ*nca-2*, Δ*ncs-1*Δ*mid-1*, and Δ*mid-1*Δ*nca-2* double mutants were verified by using the forward primers HI-NCS-1F 5′-GTCTCAGCATGAAAGTCGTC-3′, HI-NCU06703-F 5′-CCAAGGCTTATGCCGTCATC-3′, and HI-NCU04736-F 5′-GTCCCATGGATTCCATACCA-3′ specific for upstream of the open reading frame of genes *ncs-1*, *mid-1*, and *nca-2*, respectively, and with the common reverse primer 5HPHR (Table 3.7, entry 3) that is specific for the *hph* cassette used to generate the knockout mutants. PCR products were resolved in a 0.8% agarose gel; lane 1,1 kb DNA ladder (NEB); lanes 2, 3 and 4, PCR products which is of size ~2.089 kb for the *nca-2* knockout allele in Δ*nca-2*, Δ*ncs-1*Δ*nca-2*, Δ*mid-1*Δ*nca-2* mutants, respectively; lanes 5, 6 and 7, PCR products which is of size ~2.89 kb for the *ncs-1* knockout allele in Δ*ncs-1*, Δ*ncs-1*Δ*nca-2*, Δ*ncs-1*Δ*mid-1* mutants, respectively; Lanes 8, 9 and 10, PCR products which is of size ~2.023 kb for *mid-1* knockout allele in Δ*mid-1*, Δ*ncs-1*Δ*mid-1,* Δ*nca-2*Δ*mid-1,* respectively; lanes 11, 12 and 13, control

TH-1227_09610609

PCR using the wild-type template for each of the three knockout allele (indicated in parenthesis) using allele specific primer pairs. For the double mutants, the number in the parenthesis indicates the laboratory strain reference number.

5.2.3 The Δ*ncs-1*Δ*nca-2* double mutant showed novel colony morphology

The wild-type, Δ*ncs-1*, Δ*mid-1*, Δ*nca-2*, Δ*ncs-1*Δ*nca-2*, Δ*ncs-1*Δ*mid-1*, and Δ*mid-1*Δ*nca-2* double mutants were grown in 250 ml conical flasks containing 50 ml Vogel's glucose agar medium. The cultures were incubated at 30ºC for five days. The Δ*ncs-1*Δ*nca-2* double mutant showed a characteristic swollen sponge-like colony with reduced aerial hyphae and this phenotype was different from either of the parental single mutants and the wild-type (Figure 5.3 A). However, the Δ*ncs-1*Δ*mid-1* and Δ*mid-1*Δ*nca-2* double mutants did not show any distinct morphological phenotype (Figures 5.3 B, 5.3 C). Furthermore, to test the growth of aerial hyphae of the double mutants, ~1 x10^6 conidia of the mutants and the wild-type were inoculated in the Vogel's minimal medium and incubated at 30ºC in dark for three days followed by exposure to light for one day. The average length of the aerial hyphae of the Δ*ncs-1*Δ*nca*-2 double mutant was ~1.2 ± 0.2 cm (n=3) that was significantly shorter than the other strains, including its parental single mutants, Δ*mid-1* mutant, the other two double mutants, and the wild-type (Figure 5.4, Table 5.1).

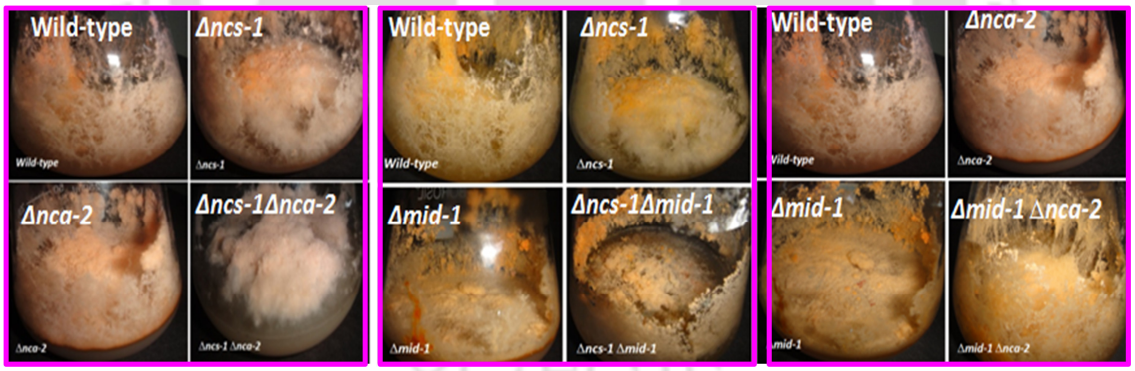

A B C

Figure 5.3: Morphology of the wild-type, single and double mutant strains grown in 250 ml flasks for 5 days at 30ºC. (A) The Δ*ncs-1*Δ*nca-2* double mutant displayed a swollen sponge-like growth and reduced aerial hyphae, which is different from its parental mutants and the wild-type. **(B)** The Δ*ncs-1*Δ*mid-1* double mutant displayed colony morphology and aerial hyphae like the wild-type. **(C)** The Δ*nca-2*Δ*mid-1* double mutant displayed colony morphology and aerial hyphae like the wild-type.

TH-1227_09610609

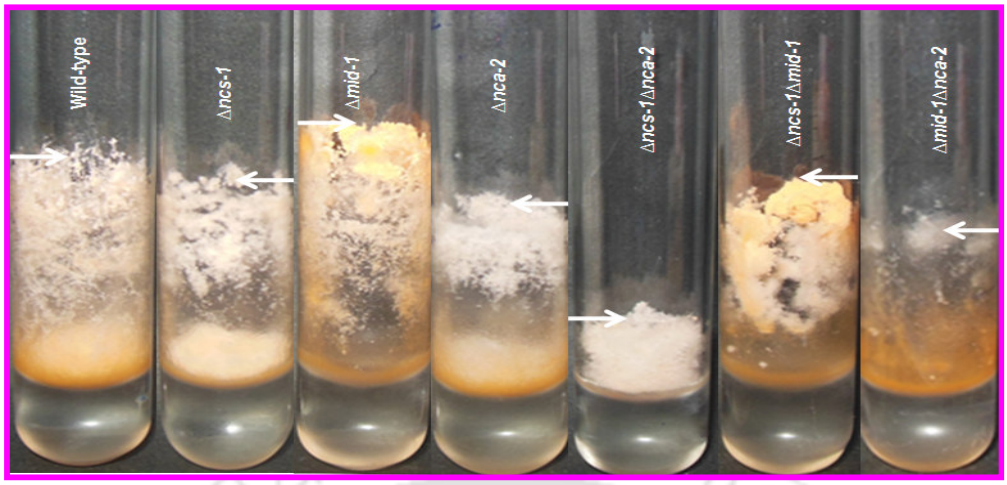

Figure 5.4: Aerial hyphae of the wild-type, single and double mutant strains. All the strains were cultured in test tubes containing standingVogel's liquid minimal medium and incubated at 30°C in darkness for 3 days followed by light for 24 h**.** The edges of aerial hyphae are indicated by white arrows.

Table 5.1 Average height of aerial hyphae of wild-type, single and double mutant strains cultured in test tubes

Strain	Average height (cm) of aerial hyphae (n = 3)
Wild-type	4.7 ± 0.25
Δ*ncs-1*	3.4 ± 0.20
Δ*mid-1*	5 ± 0.23
Δ*nca-2*	3.2 ± 0.13
Δ*ncs-1*Δ*nca-2*	1.2 ± 0.2
Δ*ncs-1*Δ*mid-1*	3.3 ± 0.15
Δ*mid-1*Δ*nca-2*	3.4 ± 0.16

TH-1227_09610609

5.2.4 The Δ*ncs-1*Δ*nca-2*, Δ*ncs-1*Δ*mid-1*, and Δ*mid-1*Δ*nca-2* double mutants showed slow growth phenotype

The growth rate of the double mutants was studied using standard race tube assay (same as described in Chapter 3) and incubated at 30ºC. The hyphal growth fronts were marked at regular interval of 12 h for 72 h and plotted the distance against time (Figure 5.5, Table 5.2) to obtain the linear growth rate. The average growth rates followed the order wild-type > Δ*nca-2* > Δ*ncs-1* > Δ*ncs-1*Δ*nca-2* > Δ*mid-1*Δ*nca-2* ≅ Δ*mid-1* > Δ*ncs-1*Δ*mid-1* (Table 5.3). Growth rates for both Δ*ncs-1*Δ*nca-2* and Δ*ncs-1*Δ*mid-1* double mutants were lower than their parental single mutants.

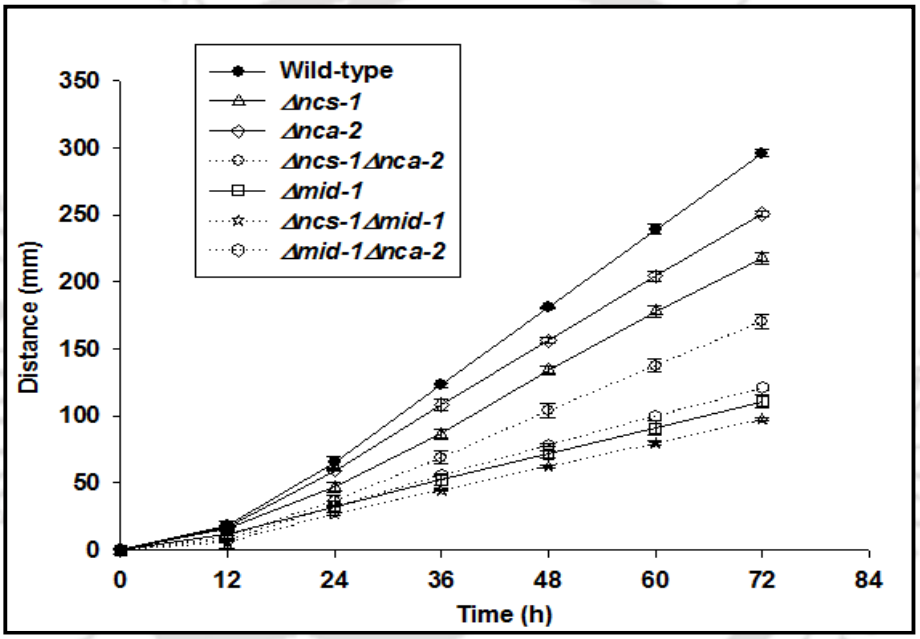

Figure 5.5: Growth phenotypes of the wild-type, single and the double mutant strains. Apical growth rates of the wild-type and mutant strains were measured using race tubes and plotted against the indicated time interval. Error bars show the standard errors calculated from the data for three independent experiments.

TH-1227_09610609

Table 5.2 Apical growth of the wild-type, single and double mutant strains in race tube

Strain	Distance (mm)in the race tube at the indicated time interval (h)						
	0	**12**	**24**	**36**	**48**	**60**	**72**
Wild type	0	19 ± 3	66 ± 2	124 ± 2	183 ± 3	243 ± 5	300 ± 7
Δ*ncs-1*	0	15 ± 2	46 ± 3	86± 4	132 ± 6	178 ± 4	219± 5
Δ*nca-2*	0	18 ± 1	57 ± 2	105 ± 3	152 ± 5	198 ± 7	243 ± 10
Δ*mid-1*	0	11 ± 2	32 ± 3	53 ± 3	72 ± 2	90 ± 4	110 ± 4
Δ*ncs-1*Δ*nca-2*	0	10 ± 0	37 ± 4	69 ± 5	105 ± 5	138 ± 5	171 ± 5
Δ*ncs-1*Δ*mid-1*	0	9 ± 1	27 ± 9	45 ± 1	63 ± 1	80 ± 2	98 ± 1
Δ*mid-1*Δ*nca-2*	0	8 ± 1	33 ± 1	56 ± 0	78 ± 1	100 ± 0	121 ± 0

Table 5.3 Average growth rate (cm h^{-1}) of the wild-type, single and double mutant strains

Strain	Average growth rate (cm h^{-1})
Wild-type	0.327 ± 0.099
Δ*ncs-1*	0.239 ± 0.067
Δ*nca-2*	0.276 ± 0.072
Δ*mid-1*	0.137 ± 0.022
Δ*ncs-1*Δ*nca-2*	0.185 ± 0.058
Δ*ncs-1*Δ*mid-1*	0.117 ± 0.022
Δ*mid-1*Δ*nca-2*	0.142 ± 0.039

TH-1227_09610609

5.2.5 Carotenoid accumulation was affected in the Δ*ncs-1*Δ*nca-2*, Δ*ncs-1*Δ*mid-1*, and Δ*mid-1*Δ*nca-2* double mutants

To test for carotenoid accumulation, ~1 X 10^6 conidia of wild-type and mutant strains were inoculated into flasks containing 25 ml of Vogel's liquid minimal medium supplemented with 0.2% Tween 80 as a wetting agent to avoid conidiation (Zalokar1954). These cultures were incubated initially in continuous darkness at 30ºC for 48 h and then exposed to cool-white light at 22ºC for 24 h (illuminated with two fluorescent bulbs (Philips Lifemax Tube light TL-D 18W/54, Philips, Kolkata, India), 18 W, 6500 K, 1015 lumens). Mycelia were then filtered, lyophilized, and powdered with mortar and pestle. Acetone and hexane were used in consecutive extractions of total carotenoid from 50 mg of lyophilized sample. Total carotenoid content of the wild-type and mutant strains were calculated by measuring the maximum absorbance value at 470 nm and using the formula:
Total carotenoid content (µg/g) = [Total absorbance x Total volume of extract (1ml) x 10^4] / [Absorption coefficient (2500) x Sample weight (g)] (Rodriguez-Amaya and Kimura 2004). The carotenoid profile in Vogel's minimal medium followed the order Δ*mid-1*Δ*nca-2* > Δ*ncs-1* Δ*mid-1* > Δ*mid-1* > Δ*ncs-1* > Δ*nca-2* > wild-type ≅ *Δncs-1Δnca-2* (Figure 5.6, Table 5.4). Thus, except the *Δncs-1Δnca-2* double mutant, the other mutants produced more carotenoid than the wild-type suggesting that products of these genes negatively affect carotenoid accumulation.

TH-1227_09610609

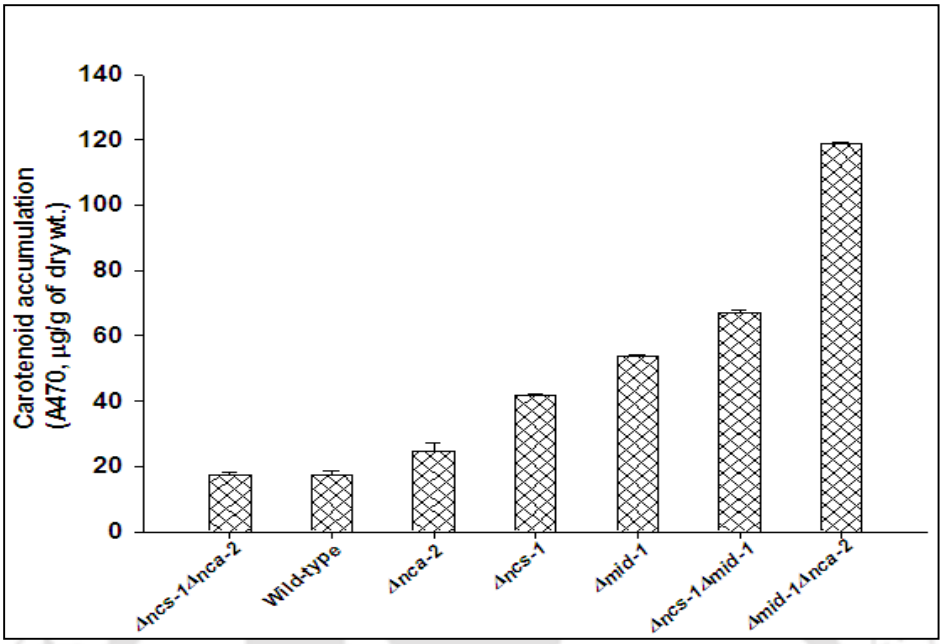

Figure 5.6: Total carotenoid contents of the wild-type, single and double mutant strains. Carotenoid extracted from the indicated *N. crassa* strains grown in Vogel's sucrose minimal medium are expressed as µg carotenoid/g of dry weight. Error bars show the standard errors calculated from the data for three independent experiments

Table 5.4 Quantification of carotenoid in wild-type, single and double mutant strains

Strain	Amount of carotenoid (µg/g dry wt) accumulation (A_{470})
Wild-type	17.3400 ± 1.128
Δ*ncs-1*	41.9267 ± 0.493
Δ*nca-2*	24.5667 ± 2.596
Δmid-1	53.9533 ± 0.064
Δ*ncs-1*Δ*nca-2*	17.5900 ± 0.453
Δ*ncs-1*Δ*mid-1*	67.2267 ± 0.456
Δ*mid-1*Δ*nca-2*	118.6867 ± 0.792

TH-1227_09610609

5.2.6 The Δ*ncs-1*Δ*nca-2* double mutant was hypersensitive to Ca^{2+} and UV stress

The *Δncs-1* and*Δnca-2* mutants were shown sensitive to Ca^{2+} stress (Deka et al. 2011; Bowman et al. 2011). In addition, growth of the *Δmid-1* mutant was inhibited at low extracellular or elevated intracellular Ca^{2+} (Lew et al. 2008). To test if Ca^{2+} stress tolerance is affected by the interactions of*ncs-1*, *mid-1*, and *nca-2*, I studied sensitivity of the mutants to various concentrations of $CaCl_2$. The Ca^{2+} stress tolerance followed the order *Δmid-1* > wild-type > Δ*ncs-1*Δ*mid-1* > Δ*nca-2* > Δ*ncs-1* > Δ*mid-1*Δ*nca-2* > Δ*ncs-1*Δ*nca-2* (Figure5.7, Table 5.5). The growth of the *Δmid-1* mutant was stimulated ~83.8% at 0.2 M $CaCl_2$ concentration. Interestingly, growth stimulation of the *Δmid-1* mutant at 0.2 M $CaCl_2$ was suppressed by the Δ*ncs-1* and Δ*nca-2* mutations. The growth stimulation was only ~34% in the *Δncs-1Δmid-1* double mutant and fully disappeared in the Δ*mid-1*Δ*nca-2* double mutant. In the *Δncs-1Δmid-1* double mutant, the suppression of growth at 0.2 M $CaCl_2$ stress suggested the epistasis of *ncs-1* over *mid-1* for Ca^{2+} sensitivity. In addition, the Δ*mid-1*Δ*nca-2* double mutant did not show growth stimulation at 0.2 M $CaCl_2$ suggesting the epistasis of the *nca-2* over *mid-1* for Ca^{2+} sensitivity. In epistatic relationship, mutation at one locus masks the effects of mutation at the second locus (Cordell 2002; Gavric and Griffiths 2003; Phillips 2008). The Ca^{2+}-sensitivity phenotype was aggravated in the *Δncs-1Δnca-2* double mutant, suggesting that negative interaction of *ncs-1* and *nca-2* plays a critical role in reducing hazardous amount of $[Ca^{2+}]_c$. The Ca^{2+}-permeable channels regulate passive inflow of Ca^{2+} into the cell, whereas the Ca^{2+}-ATPases reduce the $[Ca^{2+}]_c$ by active pumping of Ca^{2+} into internal stores or efflux of Ca^{2+} from the cell (Møller et al. 1996; Zelter et al. 2004). It is possible that NCS-1 is also involved in decreasing $[Ca^{2+}]_c$ by stimulating Ca^{2+}-efflux.

The null mutant of the *N. crassa* homologue of *ncs-1* was previously found sensitive to UV (Deka et al. 2011). I tested the sensitivity of the double mutants and their parental single mutants to UV irradiation. The Δ*mid-1*and Δ*nca-2* mutants showed an increased sensitivity to UV; however, the Δ*mid-1*Δ*nca-2* double mutant was more tolerant to UV than either of the parental single mutants. The Δ*ncs-1*Δ*nca-2* double mutant showed severe sensitivity to UV; however, the UV sensitivity of the Δ*ncs-1*Δ*mid-1* double mutantwas comparable to the parental single mutants (Figure 5.8). Therefore, these results suggested that interactions of *mid-1*with *nca-2* and *ncs-1* with *nca-2* affect the UV survival in a negative and positive manner, respectively, in *N. crassa*.

TH-1227_09610609

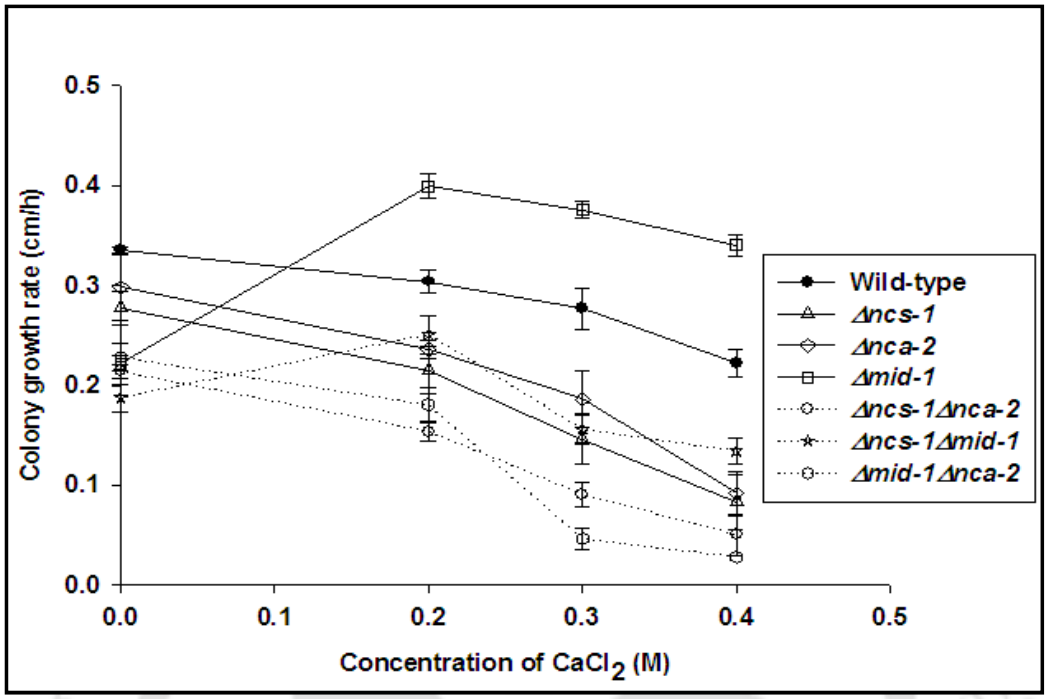

Figure 5.7: Effect of Ca^{2+} stress on the growth of wild-type, single and double mutant strains. Colony diameter (cm h^{-1}) of the indicated *N. crassa* strains were measured at regular intervals and plotted against various concentrations of $CaCl_2$. Standard errors calculated from the data for three independent experiments are shown using error bars.

Table 5.5 Average colony growth rate of the wild-type, single and double mutant strains at different concentrations of $CaCl_2$ (M)

Strain	Average colony growth rate (cm h^{-1}) at different concentrations of $CaCl_2$ (M)			
	0	**0.2**	**0.3**	**0.4**
Wild-type	0.359 ± 0.009	0.327 ± 0.009	0.288 ± 0.018	0.241 ± 0.013
Δ*ncs-1*	0.289 ± 0.018	0.218 ± 0.017	0.122 ± 0.022	0.074 ± 0.029
Δ*nca-2*	0.309 ± 0.028	0.239 ± 0.007	0.187 ± 0.024	0.095 ± 0.013
Δ*mid-1*	0.216 ± 0.011	0.397 ± 0.010	0.385 ± 0.009	0.335 ± 0.016
Δ*ncs-1*Δ*nca-2*	0.213 ± 0.007	0.153 ± 0.009	0.091 ± 0.012	0.05 ± 0.020
Δ*ncs-1*Δ*mid-1*	0.187 ± 0.013	0.251 ± 0.019	0.156 ± 0.015	0.134 ± 0.013
Δ*mid-1*Δ*nca-2*	0.227 ± 0.013	0.180 ± 0.018	0.046 ± 0.010	0.028 ± 0.000

TH-1227_09610609

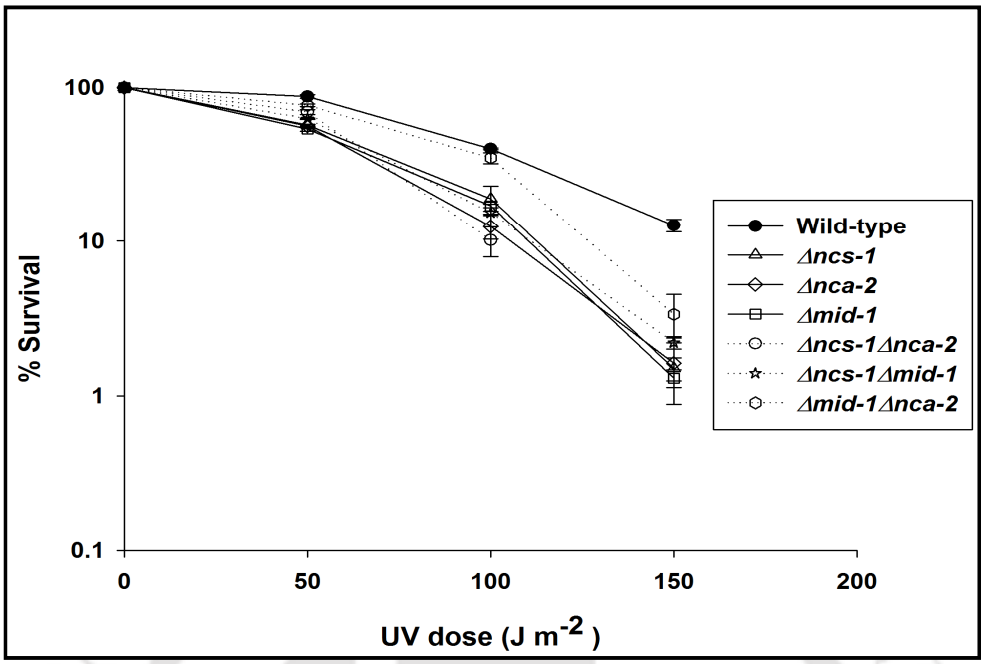

Figure 5.8: Dose response curves showing relative UV-sensitivity of the wild-type, single and double mutant strains. Approximately 10^3 conidia of the wild-type, single and double mutantstrains were plated on Vogel's sorbose agar medium (in petridishes of 150 mm diameter) and irradiated with various UV doses. Percent survival was obtained by dividing the number of colonies from plates irradiated with UV dose by the number of colonies on plates with no UV exposure (control).

Table 5.6 Relative UV-sensitivity of the wild-type, single and double mutant strains

Strain	Percent survival at indicated UV doses (J m^{-2})			
	0	**50**	**100**	**150**
Wild-type	100	87.3 ± 2.08	40 ± 0.577	12.6 ± 1.1577
Δ*ncs-1*	100	56.9 ± 0.90	18.9 ± 3.9	1.5 ± 0.25
Δ*nca-2*	100	56.3 ± 1.15	12.48 ± 2.18	1.62 ± 0.74
Δ*mid-1*	100	53.6 ± 1.52	17 ± 0.5	1.3 ± 0.17
Δ*ncs-1* Δ*nca-2*	100	69.3 ± 2.51	10.1 ± 2.22	0
Δ*ncs-1* Δ*mid-1*	100	62.6 ± 0.57	15.3 ± 0.35	2.2 ± 0.2
Δ*mid-1* Δ*nca-2*	100	76.5 ± 1.36	34.8 ± 2.84	3.36 ± 1.15

TH-1227_09610609

5.2.7 The *Δncs-1Δnca-2*, *Δncs-1Δmid-1*, and *Δmid-1Δnca-2* double mutants showed a decreased sensitivity to the respiratory by-product CO_2 and produced conidial bands

The analysis of the knockout mutants for the genes *ncs-1*, *mid-1*, and *nca-2* has suggested their involvement in stress tolerance. Therefore, I tested the hypothesis that these mutants, either alone or in combination, could also tolerate the stress generated due to the accumulation of the respiratory by-product CO_2. The conidiation of the wild-type in a race tube is suppressed due to accumulation of CO_2. However, conidiation persists despite the CO_2 accumulation in a race tube in the *band* (*bd*) mutant *ras-1*^{bd} that carries a T79I point mutation in *ras-1*; therefore, the *ras-1*^{bd} mutant is used in circadian rhythm studies (Sargent and Kaltenborn 1972; Belden et al. 2007). The wild-type, *ras-1*^{bd} mutant, single and double mutants were inoculated at one end of the race tubes and kept at 25ºC under light for 24 h. After 24 h, the growth front was marked and race tubes were transferred to continuous darkness. After every 24 h, growth front was marked under red safe light (Table 5.7). I found that both *Δncs-1Δmid-1* and *Δmid-1Δnca-2* double mutants produced distinct conidial bands with an increased period length of 25.41 ± 0.48 h and 23.96 ± 0.58 h, respectively, without introducing the *ras-1*^{bd} allele (Figure 5.9 A). The *ras-1*^{bd} control showed a period length of 22.48 ± 0.72. The *Δncs-1Δnca-2* double mutant showed a less robust effect and produced distinct conidial bands up to 72 h (Figure 5.9 A). To test if the conidial bands were produced due to an increased level of reactive oxygen species (ROS), I supplemented race tube medium with antioxidant N-acetyl-L-cysteine (NAC) to deplete ROS. Conidial bands were suppressed in the double mutants on addition of 10 mM NAC (Figure 5.9 B); however, NAC at 30 mM caused growth arrest, indicating a toxic effect at high concentration (Figure 5.9C). In summary, *Δncs-1Δnca-2*, *Δncs-1Δmid-1*, and *Δmid-1Δnca-2* double mutants showed lesser sensitivity than their parental single mutants and the wild-type to the respiratory by-product CO_2 and produced conidial bands, which was possibly due to an increased ROS level in these double mutants. Thus, the finding that *Δncs-1Δnca-2*, *Δncs-1Δmid-1*, and *Δmid-1Δnca-2* double mutants produced distinct conidial bands under conditions normally unfavourable for conidiation in race tube, suggested that the products of these genes synthetically act as negative regulators, possibly in a parallel pathway of circadian regulated conidiation.

TH-1227_09610609

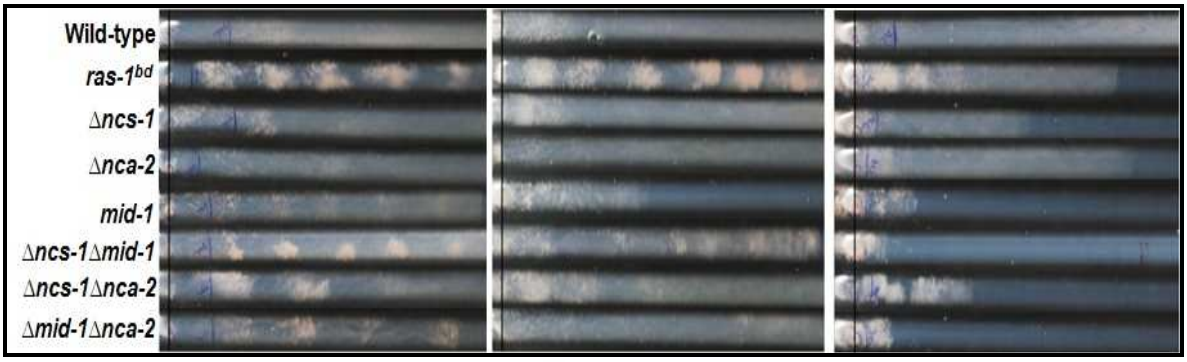

Figure 5.9: Circadian regulated conidiation. (A) The *Δncs-1Δmid-1* and *Δmid-1Δnca-2* double mutants produced distinct conidial bands at regular intervals in race tubes. In the *Δncs-1Δnca-2* double mutant, bands were distinct till 72 h. **(B)** Rhythmic conidiation patterns of the *Δncs-1Δmid-1* and *Δmid-1Δnca-2* double mutants were suppressed in the medium supplemented with 10 mM NAC. **(C)** Growth defects of the *N. crassa* strains in the medium supplemented with 30 mM NAC.

Table 5.7 Apical growth and distance of consecutive conidial bands of the wild-type, single and double mutant strains in race tubes in absence of NAC

Strain	Distance (cm) of the apical growth front from the inoculation point in the indicated time interval (h; n=3)					Distance (cm) of consecutive conidial bands from the inoculation point in the indicated time interval (h; n=3)			
	24	**48**	**72**	**96**	**120**	**24 -48**	**48 -72**	**72-96**	**96 -120**
ras-1^{bd}	2.6	6.4	10.2	14	17.3	4.2	7.6	11.1	14.8
	2.5	5.8	9.1	12.3	16.3	4	7.1	10.3	13.5
	2.9	6.4	9.7	13.2	17.6	4.4	7.5	10.5	13.6
Wild-type	5.5	13.9	22.6	32					
	6.5	15.7	26.4	37					
	5.6	15.7	25.4	33					
Δ*ncs-1*	3.3	9.3	17.5	24	32				
	4.8	11.3	18.3	25.4	32.9				
	4.4	12.3	20.4	27.8	37				
Δ*nca-2*	6.5	14.6	23.3	32.2					
	3.4	9.9	18.4	26.6					
	5.6	15.7	24.4	32.9					
Δ*mid-1*	2.7	5.9	8.7	11.8					

TH-1227_09610609

	2.6	5.5	8.4	11.4					
	2.4	5.4	8.2	11.3					
Δncs-1Δnca-2	3.3	8.1	12.9	17.3	21.9	5.7	9.7		
	3.7	9.9	16.1	23	27	6.1	9.1		
	4.1	10.5	16.4	22.5	28.8	7	11.3		
Δncs-1Δmid-1	2	5	7.9	11	14	3.2	6.4	9.4	12.4
	2.3	5.9	9.6	13	16.8	5.5	9.3	12.7	16.6
	2.2	5.2	7.9	11	14.7	4.8	8.1	10.9	14
Δnca-2Δmid-1	2.5	7	11	14.9	19.4	5.7	9.7	13.7	18.5
	2.8	7.2	11.2	15.1	19.4	6.1	9.1	13.8	18.2
	2.7	7.7	11.8	15.8	19.8	7	11.3	15.1	19.5

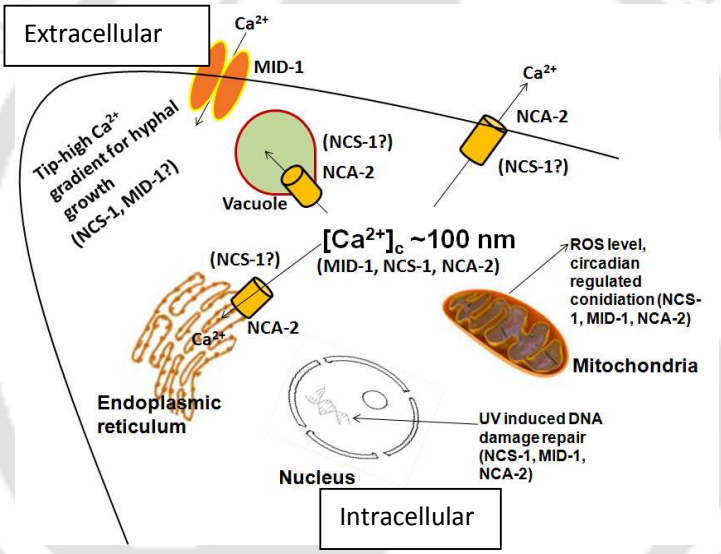

Figure 5.10: Model showing the cellular role of NCS-1, MID-1, and NCA-2. MID-1 is involved in passive influx of Ca^{2+}, and NCA-2 is involved in reducing $[Ca^{2+}]_c$. The NCS-1 also possibly assist reducing $[Ca^{2+}]_c$. Therefore, all these three Ca^{2+} signaling proteins are play a role in maintaining a constant $[Ca^{2+}]_c$ level, which is about 100 nM. NCS-1, MID-1 and NCA-2 are also involved individually or synthetically in UV-induced DNA damage repair, regulation of ROS level and circadian regulated conidiation. In addition, NCS-1 and MID-1 are possibly involved in maintaining tip-high Ca^{2+} gradient necessary for hyphal growth. The location of shown Ca^{2+} signaling proteins are as per the available published data and question mark indicate localisation yet to be identified.

TH-1227_09610609

5.3 Discussion

The Δ*ncs-1* Δ*nca-2*, Δ*ncs-1*Δ*mid-1*, and Δ*mid-1*Δ*nca-2* double mutants were generated by crossing single mutant strains of opposite mating type and phenotypes of the double mutants were studied to determine genetic interaction of the *ncs-1*, *mid-1*, and *nca-2* genes in *N. crassa*. The Δ*ncs-1* Δ*nca-2* double mutant showed novel colony morphology (Figure 5.3). Moreover, the Δ*ncs-1* Δ*nca-2* double mutant displayed reduced aerial hyphae, slow growth rate, reduced carotenoid accumulation, increased sensitivity to Ca^{2+} and UV stress, and decreased sensitivity to CO_2 in race tube than either of the parental mutants (Figures 5.4-5.9). These results consistently suggested for negative genetic interaction of *ncs-1* with *nca-2*. The phenotype of the Δ*ncs-1*Δ*nca-2* double mutant was aggravated possibly due to simultaneous knockdown of the compensatory pathway. The Δ*ncs-1*Δ*mid-1* double mutant showed aerial hyphae like the Δ*ncs-1* mutant (Figure 5.4). However, the Δ*ncs-1*Δ*mid-1* double mutant had lower growth rates, and more carotenoid accumulation than either of the parental single mutants (Figures 5.5, 5.6). Besides, the Δ*ncs-1*Δ*mid-1* double mutant displayed an intermediate Ca^{2+} sensitivity, and similar UV sensitivity in comparison to the parental single mutants (Figures 5.7, 5.8). The Δ*ncs-1*Δ*mid-1* double mutant also produced conidial bands in race tube even in the presence of the accumulated CO_2 that was suppressed when the medium was supplemented with NAC (Figure 5.9). The Δ*mid-1*Δ*nca-2* double mutant showed aerial hyphae like the Δ*nca-2* mutant, growth rate similar to the Δ*mid-1* mutant; however, its carotenoid accumulation was more than either of the parental single mutants (Figures 5.4-5.6). Moreover, stimulation of the growth rate of the *Δmid-1* mutant on medium containing $CaCl_2$ supplement was completely abolished in the *Δnca-2* background and Δ*mid-1* Δ*nca-2* double mutant was hypersensitive to Ca^{2+} (Figure 5.7). Besides, the Δ*mid-1*Δ*nca-2* double mutant was more tolerant to UV and less sensitive to CO_2 accumulation in race tube than the single mutants (Figures 5.8, 5.9). These results suggested that unlike the case for *ncs-1* with *nca-2*, the interactions of *ncs-1* with *mid-1* and *mid-1* with *nca-2* are complex. In addition, *ncs-1* mutation did not show any effect in the knockout background of another Ca^{2+}-signaling gene NCU02814 (*prd-4*) for growth, Ca^{2+} and UV stress, and period length, therefore, ruling out the hypothesis that Ca^{2+}-signaling genes randomly interact or similar genetic interactions exists between any of the Ca^{2+}-signaling gene pair.

The genetic interaction studies also suggested the involvement of *ncs-1*, *mid-1*, and *nca-2* genes in carotenoid accumulation. I found that carotenoid accumulation was consistently increased in presence of the Δ*mid-1* mutation and reached a peak of about six-

TH-1227_09610609

fold high in the Δ*mid-1*Δ*nca-2* mutant (Figure 5.6). Carotenoid accumulation was also increased in the *Δncs-1* and *Δnca-2* mutants; however, surprisingly, carotenoid accumulation in the *Δncs-1Δnca-2* double mutant was like the wild-type. In *N. crassa*, biochemical synthesis of carotenoid pigments involves sequential enzymatic conversion of isopentenyl pyrophosphate (IPP) to geranylgeranyl pyrophosphate (GGPP), GGPP to phytoene (a colorless 40-carbon compound), and phytoene to carotenoid pigments, catalyzed by the enzymes GGPP synthetase, phytoenesynthetase, and phytoene dehydrogenase, respectively (Harding et al. 1969; Porter and Spurgeon 1979). Accumulation of xanthophyll neurosporaxanthin and variable amounts of precursor carotenoid cause characteristic orange pigmentation of conidia and mycelia in *N. crassa* (De Fabo et al. 1976; Harding and Turner 1981; Nelson et al. 1989; Carattoli et al. 1991; Barba-Ostria et al. 2011; Dı´az-Sa´nchez et al. 2011). The GGPP synthetase, phytoenesynthetase, and phytoene dehydrogenase are encoded by *albino* (*al*) genes *al-3*, *al-2*, and *al-1*, respectively, and these genes are regulated by the *white collar-1* (*wc-1*) gene that mediates a blue light induction process (Harding and Turner 1981; Nelson et al. 1989). In addition to these previously identified regulators, this genetic interaction studies suggested involvement of Ca^{2+} signaling pathway in modulating carotenoid biosynthesis.

The Ca^{2+} sensitivity phenotype of the Δ*ncs-1* mutant was not fully rescued by the Δ*mid-1* mutation like their homologues in *S. pombe* (Hamasaki-Katagiri and Ames 2010; Figure 5.7). Moreover, Δ*mid-1* mutation did not rescue the defect in aerial hyphae development in the Δ*ncs-1* mutant. This might indicate functional differences of NCS-1 and MID-1 homologues in *N. crassa* and *S. pombe*. The UV sensitivity studies revealed that, in addition to the previously identified *ncs-1* gene, *mid-1*and *nca-2* also play a role in UV-induced DNA damage repair process (Figure 5.8). Moreover, genetic interactions of *mid-1* with *nca-2* and *ncs-1* with *nca-2* affect the UV survival in a negative and positive manner, respectively, in *N. crassa*. In addition, *Δncs-1Δnca-2*, *Δncs-1Δmid-1*, and *Δmid-1Δnca-2* double mutants showed lesser sensitivity to the respiratory by-product CO_2 and produced conidial bands, which was possibly due to an increased ROS level, unlike their parental single mutants and the wild-type (Figure 5.9; Table 5.7).

These results suggested that complex genetic interactions of *ncs-1*, *mid-1*, and *nca-2* regulate multiple cell functions in *N. crassa*. A model summarizing the cell functions of NCS-1, MID-1 and NCA-2 are shown in figure 5.10. A part of this chapter was published in Journal of Genetics (Deka and Tamuli 2013).

TH-1227_09610609

ADDITIONAL WORK

TH-1227_09610609

A.1 Expression analysis of *N. crassa ncs-1*, *nca-2*, *mid-1*, *crz1*, and *NCU06366* genes in response to Ca^{2+} stress

The genetic interaction studies of the *ncs-1*, *nca-2*, and *mid-1* genes suggested their complex interaction pattern, particularly, in response to the Ca^{2+} stress. I performed real time PCR analysis to determine the relative expression level of *ncs-1*, *mid-1*, and *nca-2* genes in response to Ca^{2+} stress in *N. crassa*. In addition, I also studied the relative expressions of the NCU06366 and NCU07952 genes, encode a Ca^{2+}/H^{+} exchanger and the *N. crassa* homologue of Crz1p (GenBank accession number, EAA32849), respectively. The function of Crz1p, a zinc finger transcription factor, was extensively studied in *S. cerevisiae*, *S. pombe, Torulaspora delbrueckii, Candida albicans, A. fumigatus*, and *A. nidulans* (Cyert 2003; Hirayama et al. 2003 Hernandez-Lopez et al. 2006; Karababa et al. 2006; Soriani et al. 2008; Spielvogel et al. 2008). In response to high level of $[Ca^{2+}]_c$, cytoplasmically localized Crz1p is dephosphorylated by calcineurin (a Ca^{2+}-dependent phosphatase) and results in nuclear translocation of dephosphorylated Crz1p. The nuclear-localized Crz1p then activates the expression of genes possessing the 5′-GNGGC(G/T)CA-3′ consensus sequence for the calcineurin-dependent response elements (CDREs) in their promoters (Matheos et al. 1997; Serrano et al. 2002; Stathopoulos and Cyert 1997). The *A. fumigatus ΔcrzA* null mutant shows altered expression of Ca^{2+} transporters *pmcA* and *pmcC*, homologues of *PMC1* in *S. cerevisiae* (Dinamarco et al. 2012). The CrzA protein upregulates the *pmcA* and *pmcC* mRNA expression by binding to their promoter regions in response to high Ca^{2+} stress in *A. fumigatus* (Soriani et al. 2008; Soriani et al. 2010; Dinamarco et al. 2012). In *N. crassa*, *nca-2* is a homologue of the *PMC1* in *S. cerevisiae* and functions to pump Ca^{2+} out of the cell (Bowmann et al. 2009, 2011). However, interaction between *nca-2* and the *crz1p* homologue has remained unclear in *N. crassa*.

I studied the relative expression of *ncs-1*, *nca-2*, *mid-1*, *crz1*, and *NCU06366* genes in the wild-type and the Δ*ncs-1* mutant, when grown in Vogel's glucose medium (VGM, contains 0.68 mM $CaCl_2$) and VGM supplemented with 0.2 M $CaCl_2$ (Figure A1). The standard VGM that contains 0.68 mM Ca^{2+} was used as control medium. The standard VGM was supplemented with $CaCl_2$ at a concentration of 0.2 M to induce Ca^{2+} stress response, this concentration was selected so that the *Δncs-1* mutant could grow and produce enough mycelial mass for RNA isolation. Relative expressions of the *ncs-1*, *nca-2*, and *mid-1* genes in the control VGM medium and the medium supplemented with 0.2 M $CaCl_2$ were compared. The forward (F) and reverse

TH-1227_09610609

(R) primer pairs that were used to determine expression of target genes are shown in Table A.1. The fold change in expressions of all the genes were considered as one in VGM lacking $CaCl_2$ (0 M $CaCl_2$), normalized to the expression level of endogenous *β-tubulin*, and relative expression level of genes were compared using $2^{-\Delta\Delta Ct}$ method.

Table A.1 Primers used in the real time PCR analysis

S. no.	Primer	Target gene	Sequence (5′→ 3′)	Source
1.	RT-NCU04379-F	*ncs-1*	CAGTTCTTCCCCTTTGGCGA	This study
2.	RT-NCU04379-R	*ncs-1*	CGAGCTTGTCCTCCATCTTG	This study
3.	RT-NCU04736-F	*nca-2*	GAGATGACTCCTCTCCAGTC	This study
4.	RT-NCU04736-R	*nca-2*	GGAGTGTGCTGTGATTTGGG	This study
5.	RT-NCU06703-F	*mid-1*	GCTCGCGGATCGATGAGTTT	This study
6.	RT-NCU06703-R	*mid-1*	ATTGAACCCCTTCTGGCCAG	This study
7.	RT-NCU06366-F	*NCU06366*	CCGCTGTCTTGCTCATCATC	This study
8.	RT-NCU06366-R	*NCU06366*	GATCAGAGTGAGGCGATGAC	This study
9.	RT-NCU07952-F	*crz1*	GATGTCTCTTCGGTAGCCCA	This study
10.	RT-NCU07952-R	*crz1*	CGTCCGACAGACTGAAGTTG	This study
11.	RT-NCU04054-F	*β-tubulin*	TTGAGGACCAGATGCGCAAC	This study
12.	RT-NCU04054-R	*β-tubulin*	TTGAAGAGCTCCTGGATGGC	This study

In the wild-type, the fold change in expression profile followed the order *ncs-1* (~7.5-fold) > *NCU06366* (~4.7-fold) > *nca-2* (~1.8-fold) ≅ *crz1* (~1.7-fold) in VGM (contains 0.68 mM $CaCl_2$) as compared to expressions of respective genes in VGM lacking $CaCl_2$ (0 M $CaCl_2$); however, the *mid-1* expression showed no-fold change in expression. In the Δ*ncs-1* mutant, expression of both *nca-2* and *crz1* were reduced by ~1.5-fold, *NCU06366* expression was reduced by ~3.7-fold, and *mid-1* showed ~1-fold increased expression in comparison to the wild-type. Therefore, in summary, *nca-2*, *crz1*, and *NCU06366* expressions were reduced, while *mid-1* expression showed slight increase in the Δ*ncs-1* mutant.

In VGM supplemented with 0.2 M $CaCl_2$, the *ncs-1*, *nca-2*, and *mid-1* showed fold change in expressions that were different than that of VGM (Figure A1, b). In the wild-type, the fold change in expression followed the order *nca-2* (~15-fold) > *crz1*(~8.6-fold) > *NCU06366* (~4.9-

fold) > *ncs-1* (~1.6-fold) in VGM containing 0.2 M $CaCl_2$ as compared to expressions of respective genes in VGM lacking $CaCl_2$ (0 M $CaCl_2$). In the Δ*ncs-1* mutant, the fold change in expression followed the order *nca-2* (~5.8-fold) > *crz1* (~3.6-fold) > NCU06366 (~4.8-fold) > *mid-1* (~2.6-fold) as compared to expressions of respective genes in VGM lacking $CaCl_2$ (0 M $CaCl_2$). Therefore, in the Δ*ncs-1* mutant background, ~9.2-fold and ~5-fold reduction in expression of *nca-2* and *crz1*, respectively, were observed in comparison to their expression in the wild-type (Figure A.1, b). However, in the Δ*ncs-1* mutant, expression of the *mid-1* was increased by ~2-fold relative to its expression in wild-type.

These results indicate that in *N. crassa*, expression of *nca-2* is possibly dependent on expression of *crz1* and $CaCl_2$ as in *A. fumigatus* and *ncs-1* expression is possibly necessary for expression of *crz1* that in turn modulates the *nca-2* expression. In addition, expression of *nca-2* (~13.4-fold) was ~11.8-fold higher than *ncs-1* (~1.6-fold) in the wild-type in VGM supplemented with 0.2 M $CaCl_2$. These results indicate for the negative interaction between *ncs-1* and *nca-2* and expression of *ncs-1* is possibly inhibited by high amount of extracellular Ca^{2+}. The *ncs-1* is highly expressed in VGM (contains 0.68 mM $CaCl_2$). Therefore, it could be hypothesized that NCS-1 might activate its target to initiate cellular communication and growth of *N. crassa*. This hypothesis has been supported further by a recent finding, which showed that *N. crassa* homologue of NCS-1 protein (also called CSE1) plays an important role in germling communication and fusion in a Ca^{2+} dependent manner (Palma-Guerro et al. 2013). Thus, the expression analysis provided additional evidences in support of the complex genetic interactions among the *ncs-1*, *mid-1*, and *nca-2*.

TH-1227_09610609

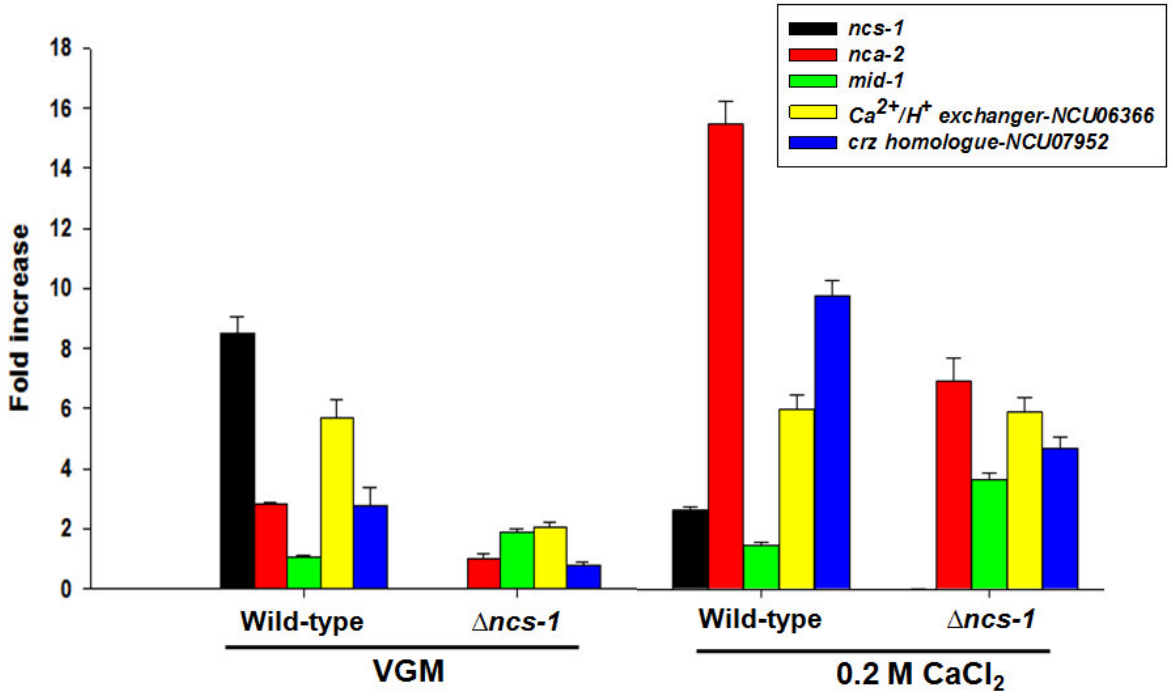

Figure A.1: Average fold change in expression of *ncs-1, mid-1, nca-2*, NCU06366-Ca^{2+}/H^{+} exchanger and the *N. crassa* homologue of *crz1* genes. The fold change in expressions of all the genes (fold change in VGM lacking $CaCl_2$ was considered as one) were normalized to the expression level of endogenous *β-tubulin*, and relative expression level of genes were compared using $2^{-\Delta\Delta Ct}$ method. Fold change in expression of the genes indicated were determined for wild-type and *Δncs-1* mutant strains grown for 30 minutes in VGM that contains 0.68 mM $CaCl_2$ (a), and in VGM medium supplemented with 0.2 M $CaCl_2$ (b). Standard errors calculated from three independent experiments are shown using error bars.

TH-1227_09610609

Conclusion and future perspectives

TH-1227_09610609

Major conclusions of the study

In this work, I have studied the cellular roles of Ca^{2+} signaling genes in *Neurospora crassa* using knockout mutant strains. I have shown that NCU04379 gene is involved in growth, calcium (Ca^{2+}) stress tolerance and ultraviolet (UV) survival. This is the first report demonstrating the involvement of Ca^{2+} signaling gene in UV-induced DNA damage and repair process in *N. crassa*. The sequence analysis has revealed that NCU04379 encodes a protein of 190 amino acid residues that shows sequence similarity to the homologues of Neuronal Calcium Sensor-1 (NCS-1). Moreover, the NCU04379 encoded protein is found to be highly conserved from fungi to mammals and contain consensus sequence for N-terminal myristoylation (NMT), and four EF hand domains (EF1, EF2, EF3, and EF4) for Ca^{2+} binding. Therefore, NCU04379 encodes a homologue of NCS-1 in *N. crassa*.

I performed site-directed mutational analysis to identify critical residues of NCS-1 homologue in *N. crassa*. The glycine to alanine mutation in the N-myristoylation site (G2A) impaired NCS-1 function for UV survival, indicating that N-myristoylation is essential for NCS-1 function in UV induced DNA damage and repair process. The arginine to alanine mutation (R175A) in the hydrophobic pocket of NCS-1 resulted in an increased UV sensitivity in the *ncs-1*^{R175} mutant than the Δ*ncs-1* mutant, suggesting that arginine 175 plays a critical role UV survival and this could explain the molecular basis of *N. crassa* homologue of NCS-1 for its novel involvement in UV-induced DNA damage repair process. The glutamate to glutamine mutation in the Ca^{2+} binding site (E120Q) of the EF hand domain 3, completely abolished NCS-1 functions in growth, Ca^{2+}stress tolerance, and UV survival; these results suggested that Ca^{2+} binding is essential for functions of NCS-1 in *N. crassa*. Thus, site-directed mutational analysis identified three critical amino residues in the NCS-1 homologue of *N. crassa*.

In addition, Δ*ncs-1*Δ*nca-2*, Δ*ncs-1*Δ*mid-1*, and Δ*mid-1*Δ*nca-2* double mutants were generated to study genetic interaction among *ncs-1*, *mid-1*, and *nca-2* genes in *N. crassa*. The *mid-1* and *nca-2* genes encode a Ca^{2+}-permeable channel and a Ca^{2+}-ATPase, respectively. Studies on the double mutants revealed that these genes synthetically regulate growth, aerial hyphae development, carotenoid accumulation, Ca^{2+} stress tolerance, sensitivity to the respiratory by-product CO_2, and UV survival. In addition to the previously identified *ncs-1* gene, *mid-1*and *nca-2* genes also play a role in UV-induced DNA damage repair process as revealed by

TH-1227_09610609

the UV sensitivity analysis. Therefore, a complex genetic interaction of *ncs-1*, *mid-1*, and *nca-2* genes regulate multiple cell functions in *N. crassa*. Moreover, expression profile of *ncs-1*, *mid-1* and *nca-2* in response to Ca^{2+} stress also supported that synthetic interaction of these genes play a role in Ca^{2+} stress tolerance.

Future perspectives

Future directions will be to understand the NCS-1 localization and its molecular targets in response to various stress conditions in *N. crassa* to understand its functional pathway. This might be achieved by fluorescence tagging of the NCS-1 protein. Moreover, Nuclear Magnetic Resonance (NMR) and X-ray crystallography studies will help us in understanding the structure-function relationship of *N. crassa* NCS-1 homologue protein.

TH-1227_09610609

References

TH-1227_09610609

Altschul SF, Gish W, Miller W, Myers EW, Lipman DJ (1990) Basic local alignment search tool. J Mol Biol 215:403-410

Ames JB, Ishima R, Tanaka T, Gordon JI, Stryer L, Ikura M (1997) Molecular mechanics of calcium-myristoyl switches. Nature 389:198-202

Barba-Ostria C, Lledías F, Georgellis D (2011) The *Neurospora crassa* DCC-1 Protein, a putative histidine kinase, is required for normal sexual and asexual development and carotenogenesis. Eukaryot Cell 10:1733-1739

Batistic O, Sorek N, Schültke S, Yalovsky S, Kudla J (2008) Dual fatty acyl modification determines the localization and plasma membrane targeting of CBL/CIPK Ca^{2+} signaling complexes in Arabidopsis. Plant Cell 20:1346-1362

Beadle GW, Tatum EL (1941) Genetic control of chemical reactions in *Neurospora*. Proc Natl Acad Sci 27:499-506

Belden WJ, Larrondo LF, Froehlich AC, Shi M, Chen CH, Loros JJ, Dunlap JC (2007) The band mutation in *Neurospora crassa* is a dominant allele of *ras-1* implicating RAS signaling in circadian output. Genes Dev 21:1494-1505

Benetka W, Mehlmer N, Maurer-Stroh S, Sammer M, Koranda M, Neumüller R, Betschinger J, Knoblich JA, Teige M, Eisenhaber F (2008) Experimental testing of predicted myristoylation targets involved in asymmetric cell division and calcium-dependent signalling. Cell Cycle 7:3709-3719

Benito B, Garciadeblas B, Rodriguez-Navarro A (2000) Molecular cloning of the calcium and sodium ATPases in *Neurospora crassa*. Mol Microbiol 35:1079-1088

Berridge MJ (1987) Inositol trisphosphate and diacylglycerol: two interacting second messengers. Annu Rev Biochem 56:159-193

TH-1227_09610609

Berridge MJ (1993) Inositol trisphosphate and calcium signalling. Nature 361:315-325
Berridge MJ, Lipp P, Bootman MD (2000) The versatility and universality of calcium signaling. Nat Rev Mol Cell Biol 1:11-21

Berridge MJ (2013) Dysregulation of neural calcium signalling in Alzheimer disease, bipolar disorder and schizophrenia. Prion 6:1–12

Blackford S, Rea PA, Sanders D (1990) Voltage sensitivity of H^+/Ca^{2+}antiport in higher plant tonoplast suggests a role in vacuolar calcium accumulation. J Biol Chem 265:9617-9620

Bootman MD, Collins TJ, Peppiatt CM, Prothero LS, Mac- Kenzie L, De Smet P, Travers M, Tovey SC, Seo JT, Berridge MJ, Ciccolini F, Lipp P (2001) Calcium signaling-an overview. Semin Cell Dev Biol 12:3-10

Borkovich KA, Alex LA, Yarden O, Freitag M, Turner GE, Read ND, Seiler S, Bell-Pedersen D, Paietta J, Plesofsky N, Plamann M, Goodrich-Tanrikulu M, Schulte U, Mannhaupt G, Nargang FE, Radford A, Selitrennikoff C, Galagan JE, Dunlap JC, Loros JJ, Catcheside D, Inoue H, Aramayo R, Polymenis M, Selker EU, Sachs MS, Marzluf GA, Paulsen I, Davis R, Ebbole DJ, Zelter A, Kalkman ER, O'Rourke R, Bowring F, Yeadon J, Ishii C, Suzuki K, Sakai W, Pratt R (2004) Lessons from the genome sequence of *Neurospora crassa*: tracing the path from genomic blueprint to multicellular organism. Microbiol Mol Biol Rev 68:1-108

Bormann J, Tudzynski P (2009) Deletion of Mid1, a putative stretch-activated calcium channel in *Claviceps purpurea*, affects vegetative growth, cell wall synthesis and virulence. Microbiology 155:3922-3933

Bowman BJ, Abreu S, Margolles-Clark E, Draskovic M, Bowman EJ (2011) Role of four calcium transport proteins, encoded by *nca-1*, *nca-2*, *nca-3*, and *cax*, in maintaining intracellular calcium levels in *Neurospora crassa*. Eukaryot Cell 10:654-661

Burgoyne RD, Weiss JL (2001) The neuronal calcium sensor family of Ca^{2+}-binding proteins. Biochem J 353:1-12

TH-1227_09610609

Campbell AK (1983) Intracellular Calcium: its universal role as regulator. John Wiley and Sons:Chichester, pp 556

Capelli N, van Tuinen D, Ortega Perez R, Arrighi JF, Turian G (1993) Molecular cloning of a cDNA encoding calmodulin from *Neurospora crassa*. FEBS Lett 321:63-68

Carafoli E (1987) Intracellular calcium homeostasis. Annu Rev Biochem 56:395-433

Carattoli A, Romano N, Ballarioj P, Morelli G, Macino G (1991) The *Neurospora crassa* carotenoid biosynthetic gene (Albino 3) reveals highly conserved regions among prenyltransferases. J Biol Chem 266:5854-5859

Carneiro P, Duarte M, Videira A (2007) The external alternative NAD(P)H dehydrogenase NDE3 is localized both in the mitochondria and in the cytoplasm of *Neurospora crassa*. J Mol Biol 368:1114-1121

Carugo O, Djinovic K, Rizzi M (1993) Comparison of co-ordinative behaviour of calcium(II) and magnesium(II) from crystallographic data. J Chem Soc Dalton Trans:2127–2135

Cavinder B, Hamam A, Lew RR, Trail F (2011) Mid1, a mechanosensitive calcium ion channel, affects growth, development, and ascospore discharge in the filamentous fungus *Gibberella zeae*. Eukaryot Cell 6:832-841

Cavinder B, Trail F (2012) Role of Fig1, a component of the low-affinity calcium uptake system, in growth and sexual development of filamentous fungi. Eukaryot Cell 8:978-988

Cerella C, Diederich M, Ghibelli L (2010) The dual role of calcium as messenger and stressor in cell damage, death, and survival. Int J Cell Biol 2010:546163

Chard PA (1987) DNA repair in human cells: methods for the determination of calmodulin involvement. Methods Enzymol 139:715-730

TH-1227_09610609

Clapham DE (2007) Calcium signaling. Cell 131:1047-1058

Colot HV, Park G, Turner GE, Ringelberg C, Crew CM, Litvinkova L, Weiss RL, Borkovich KA, Dunlap JC (2006) A high throughput gene knockout procedure for Neurospora reveals functions for multiple transcription factors. Proc Natl Acad Sci USA 103:10352-10357

Cordell HJ (2002) Epistasis: what it means, what it doesn't mean, and statistical methods to detect it in humans. Hum Mol Genet 11:2463-2468

Cornelius G, Nakashima H (1987) Vacuoles play a decisive role in calcium homeostasis in *Neurospora crassa*. J Gen Microbiol 133:2341-2347

Cornelius G, Gebauer G, Techel D (1989) Inositol trisphosphate induces calcium release from *Neurospora crassa* vacuoles. Biochem Biophys Res Commun 162:852-856

Cortés JC, Katoh-Fukui R, Moto K, Ribas JC and Ishiguro J (2004) *Schizosaccharomyces pombe* Pmr1p is required for polarized cell growth and essential for cell wall integrity and is cytokinesis. Eukaryot Cell 3:1124 1135

Cyert MS (2003) Calcineurin signaling in *Saccharomyces cerevisiae*: how yeast go crazy in response to stress. Biochem Biophys Res Commun 311:1143-1150

Dason JS, Romero-Pozuelo J, Marin L, Iyengar BG, Klose MK, Ferrús A, Atwood HL (2009) Frequenin/NCS-1 and the Ca^{2+}-channel alpha1-subunit co-regulate synaptic transmission and nerve-terminal growth. J Cell Sci 122:4109-4121

Davis RH, De Serres FJ (1970) Genetic and microbiological research techniques for *Neurospora crassa*. Methods Enzymol 17:79-143

Deka R, Kumar R, Tamuli R (2011) *Neurospora crassa* homologue of Neuronal Calcium Sensor-1 has a role in growth, calcium stress tolerance, and ultraviolet survival. Genetica 139: 885-894

Deka R, Tamuli R (2013) *Neurospora crassa ncs-1*, *mid-1* and *nca-2* double-mutant phenotypes suggest diverse interaction among three Ca^{2+}-regulating gene products. J Genet 92

TH-1227_09610609

De Fabo EC, Harding RW, Shropshire W (1976) Action spectrum between 260 and 800 nanometers for the photoinduction of carotenoid biosynthesis in *Neurospora crassa*. Plant Physiol 57:440-445

De Leiris J, Boucher F (1990) Ischemic myocardial cell necrosis: calcium overload or oxygen free-radicals? Rev Port Cardiol 9:153-158

Díaz-Sánchez V, Estrada AF, Trautmann D, Limón MC, Al-Babili S, Avalos J (2011) Analysis of *al-2* mutations in *Neurospora*. PLoS One 6:e21948

Dinamarco TM, Frietas FZ, Almeido RS (2012) Functional characterization of an *Aspergillus fumigatus* calcium transporter (PmcA) that is essential for fungal infection. PLos One 7: e37591

Dizhoor AM, Chen CK, Olshevskaya E, Sinelnikova VV, Phillipov P, Hurley JB (1993) Role of the acylated amino terminus of recoverin in $Ca(2^{+})$-dependent membrane interaction. Science 259:829-832

Dodge BO (1939) Some problems in the genetics of the fungi. Science 90:379-85

Fan Y, Ortiz-Urquiza A, Kudia RA, Keyhani NO (2012) A fungal homologue of neuronal calcium sensor-1, Bbcsa1, regulates extracellular acidification and contributes to virulence in the entomopathogenic fungus *Beauveria bassiana*. Microbiology 158:1843-1845

Felsenstein J (1985) Confidence limits on phylogenies: an approach using the bootstrap. Evolution 39:783-791

Feinberg AP, Vogelstein B (1983) A Technique for radiolabeling DNA restriction endonuclease fragments to high specific activity. Anal Biochem 132:136

Gadd GM (1994) Signal transduction in fungi. In: Gow NAR, GaddGM (eds) The growing fungus. Chapman & Hall, London, 183-210

TH-1227_09610609

Galagan JE, Calvo SE, Borkovich KA, Selker EU, Read ND, Jaffe D, FitzHugh W, Ma LJ, Smirnov S, Purcell S, Rehman B, Elkins T, Engels R, Wang S, Nielsen CB, Butler J, Endrizzi M, Qui D, Ianakiev P, Bell-Pedersen D, Nelson MA, Werner-Washburne M, Selitrennikoff CP, Kinsey JA, Braun EL, Zelter A, Schulte U, Kothe GO, Jedd G, Mewes W, Staben C, Marcotte E, Greenberg D, Roy A, Foley K, Naylor J, Stange-Thomann N, Barrett R, Gnerre S, Kamal M, Kamvysselis M, Mauceli E, Bielke C, Rudd S, Frishman D, Krystofova S, Rasmussen C, Metzenberg RL, Perkins DD, Kroken S, Cogoni C, Macino G, Catcheside D, Li W, Pratt RJ, Osmani SA, DeSouza CP, Glass L, Orbach MJ, Berglund JA, Voelker R, Yarden O, Plamann M, Seiler S, Dunlap J, Radford A, Aramayo R, Natvig DO, Alex LA, Mannhaupt G, Ebbole DJ, Freitag M, Paulsen I, Sachs MS, Lander ES, Nusbaum C, Birren B, Calvo SE, Borkovich KA, Selker EU, Read ND, et al (2003) The genome sequence of the filamentous fungus *Neurospora crassa*. Nature 422:859-868

Garnjobst L, Tatum EL (1967) A survey of new morphological mutants in *Neurospora crassa*. Genetics 57:579-604

Gavric O, Griffiths AJ (2003) Interaction of mutations affecting tip growth and branching in Neurospora. Fungal Genet Biol 40:261-270

Gavric O, dos Santos DB, Griffiths A (2007) Mutation and divergence of the phospholipase C gene in *Neurospora crassa*. Fungal Genet Biol 44:242-249

Gifford JL, Walsh MP, Vogel HJ (2007) Structures and metal-ion-binding properties of the Ca^{2+} binding helix–loop–helix EF-hand motifs. Biochem J 405:199-221

Gilroy S, Blowers DP, Terewavas AJ (1987) Calcium: a regulation system emerges in plant cells. Development 100:181-184

Gomez M, De Castro E, Guarin E, Sasakura H, Kuhara A, Mori I, Bartfai T, Bargmann CI, Nef P (2001) Ca^{2+} signaling via the neuronal calcium sensor-1 regulates associative learning and memory in *C. elegans*. Neuron 30:241-248

Gritz L, Davies J (1983) Plasmid-encoded hygromycin B resistance: the sequence of hygromycin B phosphotransferase gene and its expression in Escherichia coli and *Saccharomyces cerevisiae*. Gene 25**:**179-188

TH-1227_09610609

Halachmi D, Eilam Y (1989) Cytostolic and vacuolar Ca^{2+} concentrations in yeast measured with Ca^{2+}-sensitive dye Indo-1. FEBS Lett 256:55-61

Hallen HE, Trail F (2008) The L-type calcium ion channel cch1 affects ascospore discharge and mycelial growth in the filamentous fungus *Gibberella zeae* (anamorph Fusarium graminearum). Eukaryot Cell 7:415-424

Hamasaki-Katagiri N, Molchanova T, Takeda K, Ames JB (2004) Fission yeast homolog of neuronal calcium sensor-1 (Ncs1p) regulates sporulation and confers calcium tolerance. J Biol Chem 279:12744-12754

Hamasaki-Katagiri N, Ames JB (2010) Neuronal calcium sensor-1 (Ncs1p) is up-regulated by calcineurin to promote Ca^{2+} tolerance in fission yeast. J Biol Chem 285:4405-4414

Handley TW, Lian LY, Haynes LP, Burgoyne RD (2010) Structural and Functional Deficits in a Neuronal Calcium Sensor-1 Mutant Identified in a Case of Autistic Spectrum Disorder. PLoS ONE **5**, e10534

Hao L, Rigaud JL, Inesi G (1994) Ca^{+}/H^{+} counter transport and electrogenecity in proteoliposomes containing erythrocyte plasma membrane Ca^{2+}-ATPase and exogenous lipids. J Biol Chem 269:14268-14275

Harding RW, Huang PC, Mitchell HK (1969) Photochemical studies of the carotenoid biosynthetic pathway in *Neurospora crassa*. Arch Biochem Biophys 129:696-707

Harding RW, Turner RV (1981) Photoregulation of the Carotenoid Biosynthetic Pathway in Albino and White Collar Mutants of *Neurospora crassa*. Plant Physiol 68**:**745-749

Haro R, Garciadeblas B, Rodríguez-Navarro A (1991) A novel P-type ATPase from yeast involved in sodium transport. FEBS Lett 291:189-191

Hendricks KB, Wang BQ, Schnieders EA, Thorner J (1999) Yeast homologue of neuronal frequenin is a regulator of phosphatidylinositol-4-OH kinase. Nat Cell Biol 1:234-241

TH-1227_09610609

Herman M, Ori Y, Chagnac A, Weinstein T, Korzets A, Zevin D, Malachi T, GafterU (2002) DNA repair in mononuclear cells: role of serine/threonine phosphatases. J Lab Clin Med 140:255-262

Hernandez-Lopez MJ, Panadero J, Prieto JA, Randez-Gil F (2006) Regulation of salt tolerance by *Torulaspora delbrueckii* calcineurin target Crz1p. Eukaryotic Cell 5:469–479

Hirayama S, Sugiura R, Lu Y, Maeda T, Kawagishi K, Yokoyama M, Tohda H, Giga-Hama Y, Shuntoh H, Kuno T (2003) Zinc finger protein Prz1 regulates Ca^{2+} but not Cl^- homeostasis in fission yeast. Identification of distinct branches of calcineurin signaling pathway in fission yeast. J Biol Chem 278**:**18078-18084

Horikawa Y, Oda N, Cox NJ, Li X, Orho-Melander M, Hara M, Hinokio Y, Lindner TH, Mashima H, Schwarz PE, del Bosque-Plata L, Horikawa Y, Oda Y, Yoshiuchi I, Colilla S, Polonsky KS, Wei S, Concannon P, Iwasaki N, Schulze J, Baier LJ, Bogardus C, Groop L, Boerwinkle E, Hanis CL, Bell GI (2000) Genetic variation in the gene encoding calpain-10 is associated with type 2 diabetes mellitus. Nat Genet 26:163-175

Huttner IG, Strahl T, Osawa M, King DS, Ames JB, Thorner J (2003) Molecular interactions of yeast frequenin (frq1) with the phosphatidylinositol 4-kinase isoform, Pik1. J Biol Chem 278:4862-4874

Iida H, Yagawa Y, Anraku Y (1990a) Essential role for induced Ca^{2+} influx followed by $[Ca^{2+}]_i$ rise in maintaining viability of yeast cells late in the mating pheromone response pathway. J Biol Chem 265:13391-13399

Iida H, Sakaguchi S, Yagawa Y, Anraku Y (1990b) Cell cycle control by Ca^{2+} in *Saccharomyces cerevisiae.* J Biol Chem 265:21216-21222

Iida H, Nakamura H, Ono T, Okumura MS, Anraku Y (1994) MID1, a novel *Saccharomyces cerevisiae* gene encoding a plasma membrane protein, is required for Ca^{2+} influx and mating. Mol Cell Biol 14:8259-8271

Inoue H, Nojima H, Okayama H (1990) High efficiency transformation of *E. coli* with plasmids. Gene 96:23-28

TH-1227_09610609

Ishibashi K, Suzuki K, Ando Y, Takakura C, Inoue H (2006) Nonhomologous chromosomal integration of foreign DNA is completely dependent on MUS-53 (human Lig4 homolog) in Neurospora. Proc Natl Acad Sci USA 103:14871-14876

Ishitani M, Liu J, Halfter U, Kim CS, Shi W, Zhu JK (2000) SOS3 function in plant salt tolerance requires N-myristoylation and calcium binding. Plant Cell 12:1667-1678

Jackson SL, Heath IB (1993) Roles of calcium ions in hyphal tip growth. Microbiol Rev 57:367-382

Jaiswal JK (2001) Calcium- how and why? J Biosci 26:357–363

Johannes E, Brosnan J, Sanders D (1991) Calcium channels and signal transduction in plant cells. BioEssays 13:331-336

Kader MA, Lindberg S (2010) Cytosolic calcium and pH signaling in plants under salinity stress. Plant Signal Behav 5:233-238

Kaiser N, Edelman IS (1977) Calcium dependence of glucocorticoid induced lymphocytolysis. Proc Natl Acad Sci USA 74:638-642

Kaiser N, Edelman IS (1978) Calcium dependence of ionophore A23187 induced lymphocyte cytotoxicity. Cancer Res 38:3599-3603

Karababa M, Valentino E, Pardini G, Coste AT, Bille J, Sanglard D (2006) CRZ1, a target of the calcineurin pathway in *Candida albicans*. Mol Microbiol 59: 1429-1451

Klee CB, Crouch TH, Krinks MH (1979) Calcineurin: a calcium- and calmodulin-binding protein of the nervous system. Proc Natl Acad Sci USA 76:6270-6273

TH-1227_09610609

Klenchin VA, Calvert PD, Bownds MD (1995) Inhibition of rhodopsin kinase by recoverin. Further evidence for a negative feedback system in phototransduction. J Biol Chem 270:16147-16152

Kmetzsch L, Staats CC, Simon E, Fonseca FL, de Oliveira DL, Sobrino L, Rodrigues J, Leal AL, Nimrichter L, Rodrigues ML, Schrank A, Vainstein MH (2010) The vacuolar Ca^{2+} exchanger Vcx1 is involved in calcineurin-dependent Ca^{2+} tolerance and virulence in *Cryptococcus neoformans*. Eukaryot Cell 9:1798-1805

Koh PO, Undie AS, Kabbani N, Levenson R, Goldman-Rakic PS, Lidow MS (2003) Up-regulation of neuronal calcium sensor-1 (NCS-1) in the prefrontal cortex of schizophrenic and bipolar patients. PNAS 100: 313-317

Kothe GO, Free SJ (1998) Calcineurin subunit B is required for normal vegetative growth in *Neurospora crassa*. Fungal Genet Biol 23:248-258

Lakin-Thomas PL (1993) Effects of inositol starvation on the levels of inositol phosphates and inositol lipids in *Neurospora crassa*. Biochem J 292:805-811

Larrondo LF, Colot HV, Baker CL, Loros JJ, Dunlap JC (2009) Fungal functional genomics: tunable knockout-knock-in expression and tagging strategies. Eukaryot Cell 8:800-804

Lew RR, Abbas Z, Anderca MI, Free SJ (2008) Phenotype of a mechanosensitive channel mutant, *mid-1*, in a filamentous fungus, *Neurospora crassa.* Eukaryot Cell 7:647-655

Lippke JA, Gordon LK, Brash DE, Haseltine WA (1981) Distribution of UV light-induced damage in a defined sequence of human DNA: detection of alkaline-sensitive lesions at pyrimidine nucleoside-cytidine sequences. Proc Natl Acad Sci USA 78:3388-3392

Lo HL, Nakajima S, Ma L, Walter B, Yasui A, Ethell DW, Owen LB (2005) Differential biologic effects of CPD and 6–4PP UV induced DNA damage on the induction of apoptosis and cellcycle arrest. BMC Cancer 5:135

Lytton J (2007) Na^{+}/Ca^{2+} exchangers: three mammalian gene families control Ca^{2+} transport. Biochem J 406:365-382

Matheos DP, Kingsbury TJ, Ahsan US, Cunningham KW (1997) Tcn1p/Crz1p, a calcineurin-dependent transcription factor that differentially regulates gene expression in *Saccharomyces cerevisiae*. Genes Dev 11:3445-3458

Marchler-Bauer A, Bryant SH (2004) CD-Search: protein domain annotations on the fly. Nucleic Acids Res 32(Web server issue):W327–W331

Marchler-Bauer A, Anderson JB, Chitsaz F, Derbyshire MK, DeWeese-Scott C, Fong JH, Geer LY, Geer RC, Gonzales NR, Gwadz M, He S, Hurwitz DI, Jackson JD, Ke Z, Lanczycki CJ, Liebert CA, Liu C, Lu F, Lu S, Marchler GH, Mullokandov M, Song JS, Tasneem A, Thanki N, Yamashita RA, Zhang D, Zhang N, Bryant SH (2009) CDD: specific functional annotation with the Conserved Domain Database. Nucleic Acids Res 37 (Database issue):D205–D210

Margolin BS, Freitag M, Selker EU (1997) Improved plasmids for gene targeting at the *his-3* locus of *Neurospora crassa* by electoporation. Fungal Genet Newsl 44**:**34-36

McIlhinney RA (1998) Membrane targeting via protein N-myristoylation. Methods Mol Biol 88:211-25

Melo AM, Duarte M, Videira A (1999) Primary structure and characterisation of a 64 kDa NADH dehydrogenase from the inner membrane of *Neurospora crassa* mitochondria. Biochim Biophys Acta 1412:282-287

Melo AM, Duarte M, Moller IM, Prokisch H, Dolan PL, Pinto L, Nelson MA, Videira A (2001) The external calcium-dependent NADPH dehydrogenase from *Neurospora crassa* mitochondria. J Biol Chem 276:3947-3951

Miller AJ, Vogg G, Saunders D (1990) Cytostolic calcium homeostasis in fungi: roles of plasma membrane transport and intracellular sequestration of calcium. Proc Natl Acad Sci USA 87:9348-9352

TH-1227_09610609

Min LI, Yueqing CAO (2012) Cloning of MaNcs1 Gene and Its Role in Pathogenicity of Metarhizium acridum. Chin J Appl Environ Biol 18: 240-244

Mirzayans R, Famulski KS, Enns L, Fraser M, Paterson MC (1995) Characterization of the signal transduction pathway mediating gamma ray-induced inhibition of DNA synthesis in human cells: indirect evidence for involvement of calmodulin but not protein kinase C nor p53. Oncogene 11:1597-1605

Mitchell DL, Nairn RS (1989) The biology of the (6–4) photoproduct. Photochem Photobiol 49:805–819

Møller JV, Juul B, le Maire M (1996) Structural organization, ion transport, and energy transduction of P-type ATPases. Biochim Biophys Acta 1286:1-51

Moncrief ND, Kretsinger RH, Goodman M (1990) Evolution of EF-hand calcium-modulated Proteins. I. Relationships based on amino acid sequences. J Mol Evol 30:522-62

Mota Júnior AO, Malavazi I, Soriani FM, Heinekamp T, Jacobsen I, Brakhage AA, Savoldi M, Goldman MH, da Silva Ferreira ME, Goldman GH (2008) Molecular characterization of the *Aspergillus fumigatus* NCS-1 homologue, NcsA. Mol Genet Genomics 280:483-95

Muralidhar D, Kunjachen Jobby M, Jeromin A, Roder J, Thomas F, Sharma Y (2004) Calcium and chlorpromazine binding to the EF-hand peptides of neuronal calcium sensor-1. Peptides 25:909-917

Nakayama S, Kretsinger RH (1994) Evolution of the EF-hand family of proteins. Annu Rev Biophys Biomol Struct 23:473–507

Nakamura TY, Jeromin A, Smith G, Kurushima H, Koga H, Nakabeppu Y, Wakabayashi S, Nabekura J (2006) Novel role of neuronal Ca^{2+} sensor-1 as a survival factor up-regulated in injured neurons. J Cell Biol 172:1081-1091

Nelson MA, Morelli G, Carattoli A, Romano N, Macino G (1989) Molecular cloning of a *Neurospora crassa* carotenoid biosynthetic gene (albino-3) regulated by blue light and the products of the white collar genes. Mol Cell Biol 9:1271-1276

TH-1227_09610609

Nicholas KB, Nicholas HB, Deerfield DW (1997) GeneDoc: analysis and visualization of genetic variation. EMBnet News 4:1-4

Ochiai E (1991) Why Calcium? J Chem Edu 68**:**10-12

Olsen HB, Kaarsholm NC (2000) Structural effects of protein lipidation as revealed by LysB29-myristoyl, des (B30) insulin. Biochemistry 39:11893-900

Pall ML, Brunelli JP (1993) A series of six compact fungal transformation vectors containing polylinkers with multiple unique restriction sites. Fungal Genet Newslett 40: 59-62

Paltauf F, Kohlwein S, Henry SA (1992) Regulation and compartmentalization of lipid synthesis in yeast. The Molecular and Cellular Biology of the yeast *Saccharomyces*: Gene Expression 2:415-500

Palma-Guerrero J, Hall CR, Kowbel D, Welch J, Taylor JW, Brem RB, Glass NL (2013) Genome wide association identifies novel Loci involved in fungal communication. PLoS Genet 9:e10036691

Parks LW, Casey WM (1995) Physiological implications of sterol biosynthesis in yeast. Annu Rev Microbiol 49:95-116

Payen A (1843) Extrain d'un rapport addresse' a' M. Le Marechal Duc de Dalmatie, Ministre de la Guerre, President du Conseil, sur une alteration extraordinaire du pain du munition. Ann Chim Phys 9**:**5–21

Perkins DD (1991) The first published scientific study of *Neurospora*, including a description of photoinduction of carotenoids. Fungal Genet Newsl 38:64–65

Perkins DD (1992) Neurospora: the organism behind the molecular revolution. Genetics 130:687-701

TH-1227_09610609

Permyakov SE, Cherskaya AM, Senin II, Zargarov AA, Shulga-Morskoy SV, Alekseev AM, Zinchenko DV, Lipkin VM, Philippov PP, Uversky VN, Permyakov EA (2000) Effects of mutations in the calcium-binding sites of recoverin on its calcium affinity: evidence for successive filling of the calcium binding sites. Protein Eng 13:783-790

Petko JA, Kabbani N, Frey C, Woll M, Hickey K, Craig M, Canfield VA, Levenson R (2009) Proteomic and functional analysis of NCS-1 binding proteins reveals novel signaling pathways required for inner ear development in zebrafish. BMC Neurosci 10:10-27.

Phillips PC (2008) Epistasis--the essential role of gene interactions in the structure and evolution of genetic systems. Nat Rev Genet 9:855-867

Podell S, Gribskov M (2004) Predicting N-terminal myristoylation sites in plant proteins. BMC Genomics 5:37

Porter JW, Spurgeon SL (1979) Enzymatic synthesis of carotenes. Pure Appl Chem 51 449-481

Prakash A, Sengupta S, Aparna K, Kasbekar DP (1999) The *erg-3* (sterol D14, 15-reductase) gene of *Neurospora crassa*: generation of null mutants by repeat-induced point mutation and complementation by proteins chimeric for human lamin B receptorsequences. Microbiology 145:1443-1451

Prokisch H, Yarden O, Dieminger M, Tropschug M, Barthelmess IB (1997) Impairment of calcineurin function in *Neurospora crassa* reveals its essential role in hyphal growth, morphology and maintenance of the apical Ca^{2+} gradient. Mol Gen Genet 256:104-114

Qian T, Herman B, Lemasters JJ (1999) The mitochondrial permeability transition mediates both necrotic and apoptotic death of hepatocytes exposed to Br-A23187. Toxicol appl Pharmacol 154:117–125

Resh MD (1999) Fatty acylation of proteins: new insights into membrane targeting of myristoylated and palmitoylated proteins. Biochim Biophys Acta 1451:1-16

Rho HS, Jeon J, Lee YH (2009) Phospholipase C-mediated calcium signalling is required for fungal development and pathogenicity in *Magnaporthe oryzae*. Mol Plant Pathol 10:337-346

TH-1227_09610609

Richard I, Broux O, Allamand V, Fougerousse F, Chiannilkulchai N, Bourg N, Brenguier L, Devaud C, Pasturaud P, Roudaut C, et al (1995) Mutations in the proteolytic enzyme calpain 3 cause limb-girdle muscular dystrophy type 2A. Cell 81:27-40

Richter C (1993) Pro-oxidants and mitochondrial Ca^{2+}: their relationship to apoptosis and oncogenesis. FEBS Lett 325:104–107

Rodriguez-Amaya DB, Kimura M (2004) Harvestplus handbook for carotenoid analysis. *HarvestPlus Technical Monograph 2*, International Food Policy Research Institute (IFPRI) and International Center for Tropical Agriculture (CIAT), Washington, DC

Ryan FJ, Beadle GW, Tatum EL (1943) The tube method of measuring the growth rate of Neurospora. Am J Bot 30:784-799

Ryan FJ (1950) Selected methods of Neurospora genetics. Methods Med Res 3:51–75

Rzhetsky A, Nei M (1992) Statistical properties of the ordinary leastsquares, generalized least-squares, and minimum-evolution methods of phylogenetic inference. J Mol Evol 35:367-375

Sadakane Y, Nakashima H (1996) Light-induced phase shifting of the circadian conidiation rhythm is inhibited by calmodulin antagonists in *Neurospora crassa*. J Biol Rhythms 11:234-240

Saitoh K, Arie T, Teraoka T, Yamaguchi I, Kamakura T (2003) Targeted gene disruption of the neuronal calcium sensor 1 homologue in rice blast fungus, *Magnaporthe grisea*. Biosci Biotechnol Biochem 67:651-653

Sambrook J, Russell DW (2001) Molecular cloning, a laboratory manual (Third Edition), Volume 1, 2 and 3. Cold Spring Harbor Laboratory Press, New York

Sanders D, Pelloux J, Brownlee C and Harper JF (2001) Calcium at the crossroads of signaling. Plant Cell 14:S401–S417

TH-1227_09610609

Sargent ML, Kaltenborn SH (1972) Effects of medium composition and carbon dioxide on circadian conidiation in *Neurospora*. Plant Physiol 50:171-175

Selker EU, Cambareri EB, Jensen BC, Haack KR (1987) Rearrangement of duplicated DNA in specialized cells of *Neurospora*. Cell 51:741-752

Serrano R, Ruiz A, Bernal D, Chambers JR, Ariño J (2002) The transcriptionalresponse to alkaline pH in *Saccharomyces cerevisiae*: evidence for calcium-mediated signalling. Mol Microbiol 46:1319-1333

Shaw BD, Hoch HC (2001) Biology of the fungal cell. In: Howard RJ, Gow NAR (eds) The mycota VIII. Springer, Berlin, 73-89

Shear CL, Dodge BO (1927) Life histories and heterothallism of the red bread-mold fungi of the *Monilia sitophila* group. J Agric Res 34**:**1019-1042

Shiu PK, Raju NB, Zickler D, Metzenberg RL (2001) Meiotic silencing by unpaired DNA. Cell 107:905-916

Smallwood HS, Lopez-Ferrer D, Eberlein PE, Watson DJ, Squier TC (2009) Calmodulin mediates DNA repair pathways involving H2AX in response to low-dose radiation exposure of RAW 264.7 macrophages. Chem Res Toxicol 22:460-470

Soriani FM, Malavazi I, da Silva Ferreira ME, Savoldi M, Von Zeska Kress MR, de Souza Goldman MH, Loss O, Bignell E, Goldman GH (2008) Functional characterization of *Aspergillus fumigatus* CRZ1 homologue, CrzA. Mol Microbiol 67:1274-1291

Soriani FM, Malavazi I, Savoldi M, Espeso E, Dinamarco TM, Bernardes LA, Ferreira ME, Goldman MH, Goldman GH (2010) Identification of possible targets of the *Aspergillus fumigatus* CRZ1 homologue, CrzA. BMC Microbiol 10:12

TH-1227_09610609

Spielvogel A, Findon H, Arst HN, Araújo-Bazán L, Hernández-Ortíz P, Stahl U, Meyer V, Espeso EA (2008) Two zinc finger transcription factors, CrzA and SltA, are involved in cation homoeostasis and detoxification in *Aspergillus nidulans*. Biochem J 3:419-429

Staben C, Jensen B, Singer M, Pollock J, Schechtman M , Kinsey J, Selker E (1989) Use of a bacterial Hygromycin B resistance gene as a dominant selectable marker in *Neurospora crassa* transformation. Fungal Genet Newsl 36:79-81

Stathopoulos AM, Cyert MS (1997) Calcineurin acts through the CRZ1/TCN1-encoded transcription factor to regulate gene expression in yeast. Genes Dev 24:3432-3444

Strahl T, Huttner IG, Lusin JD, Osawa M, King D, Thorner J, Ames JB (2007) Structural insights into activation of phosphatidylinositol 4-kinase (Pik1) by yeast frequenin (Frq1). J Biol Chem 282:30949-30959

Street VA, McKee-Johnson JW, Fonseca RC, Tempel BL, Noben-Trauth K (1998) Mutations in a plasma membrane Ca^{2+}-ATPase gene cause deafness in deafwaddler mice. Nat Genet 19:390-394

Strynadka NC, James MN (1989) Crystal structures of the helix-loop-helix calcium-binding proteins. Annu Rev Biochem 58:951-998

Suresh K, Subramanyam C (1997) A putative role for calmodulin in the activation of *Neurospora crassa* chitin synthase. FEMS Microbiol Lett 150:95-100
Swain AL, Amma EL (1989) The coordination polyhedron of Ca^{2+}, Cd^{2+} in parvalbumin. Inorg Chim Acta 163:5-7

Tamuli R, Kumar R, Deka R (2011) Cellular roles of neuronal calcium sensor-1 and calcium/calmodulin-dependent kinases in fungi. J Basic Microbiol 51:120-128

Tamuli R, Kumar R, Srivastava DA, Deka R (2013) Calcium signaling. In: Kasbekar DP, McCluskey K (eds.), Neurospora: Genomics and Molecular Biology, 1st edn. Caister Academic Press, Norfolk, UK, pp 209-226

TH-1227_09610609

Tamura K, Dudley J, Nei M, Kumar S (2007) MEGA4: molecular evolutionary genetics analysis (MEGA) software version 4.0. Mol Biol Evol 24:1596-1599

Thompson JD, Gibson TJ, Plewniak F, Jeanmougin F, Higgins DG (1997) The CLUSTAL-X windows interface: flexible strategies for multiple sequence alignment aided by quality analysis tools. Nucleic Acids Res 25:4876-4882

Tsien RY (1980) New calcium indicators and buffers with high selectivity against magnesium and protons: design, synthesis, and properties of prototype structures. Biochem 19:2396-2404

Ullmann A, Jacob E, Monod J (1967) Characterization by in vitro complementation of a peptide corresponding to an operator-proximal segment of the beta-galactosidase structural gene of *Escherichia coli.* J Mol Biol 24**:** 339-343

Vogel HJ (1964) Distribution of lysine pathways among fungi: evolutionary implications. Am. Naturalist 98:435-436

Wang Y, Mallya SM, Sikpi MO (2000) Calmodulin antagonists and cAMP inhibit ionizing-radiation-enhancement of double-strand break repair in human cells. Mutat Res 460:29-39

Welton RM, Hoffman CS (2000) Glucose monitoring in fission yeast via the Gpa2 galpha, the git5 Gbeta and the git3 putative glucose receptor. Genetics 156:513-521

Winkler MA, Merat DL, Tallant EA, Hawkins S, Cheung WY (1984) Catalytic site of calmodulin-dependent protein phosphatase from bovine brain resides in subunit A. Proc Natl Acad Sci USA 81:3054-3058

Woods NK, Padmanabhan J (2012) Neuronal calcium signaling and Alzheimer's disease. Adv Exp Med Biol 740:1193-1217

Yang Y, Cheng P, Zhi G, Liu Y (2001) Identification of a calcium/calmodulin-dependent protein kinase that phosphorylates the *Neurospora* circadian clock protein FREQUENCY. J Biol Chem 276:41064-41072

TH-1227_09610609

Yoshida T, Takashi T, Yanagida M (1994) A calcineurin-like gene *ppb1+* in fission yeast: mutant defects in cytokinesis, cell polarity, mating and spindle pole body positioning. J Cell Sci 107:1725-1735

Yu JH, Hamari Z, Han KH, Seo JA, Reyes-Domínguez Y, Scazzocchio C (2004) Double-joint PCR: a PCR-based molecular tool for gene manipulations in filamentous fungi. Fungal Genet Biol 41:973-981

Zalokar M (1954) Studies on biosynthesis of carotenoids in *Neurospora crassa*. Arch Biochem Biophys 50:71-80

Zelter A, Bencina M, Bowman BJ,Yarden O, Read ND (2004) A comparative genomic analysis of the calcium signaling machinery in *Neurospora crassa*, *Magnaporthe grisea,* and *Saccharomyces cerevisiae*. Fungal Genet Biol 41:827-841

TH-1227_09610609

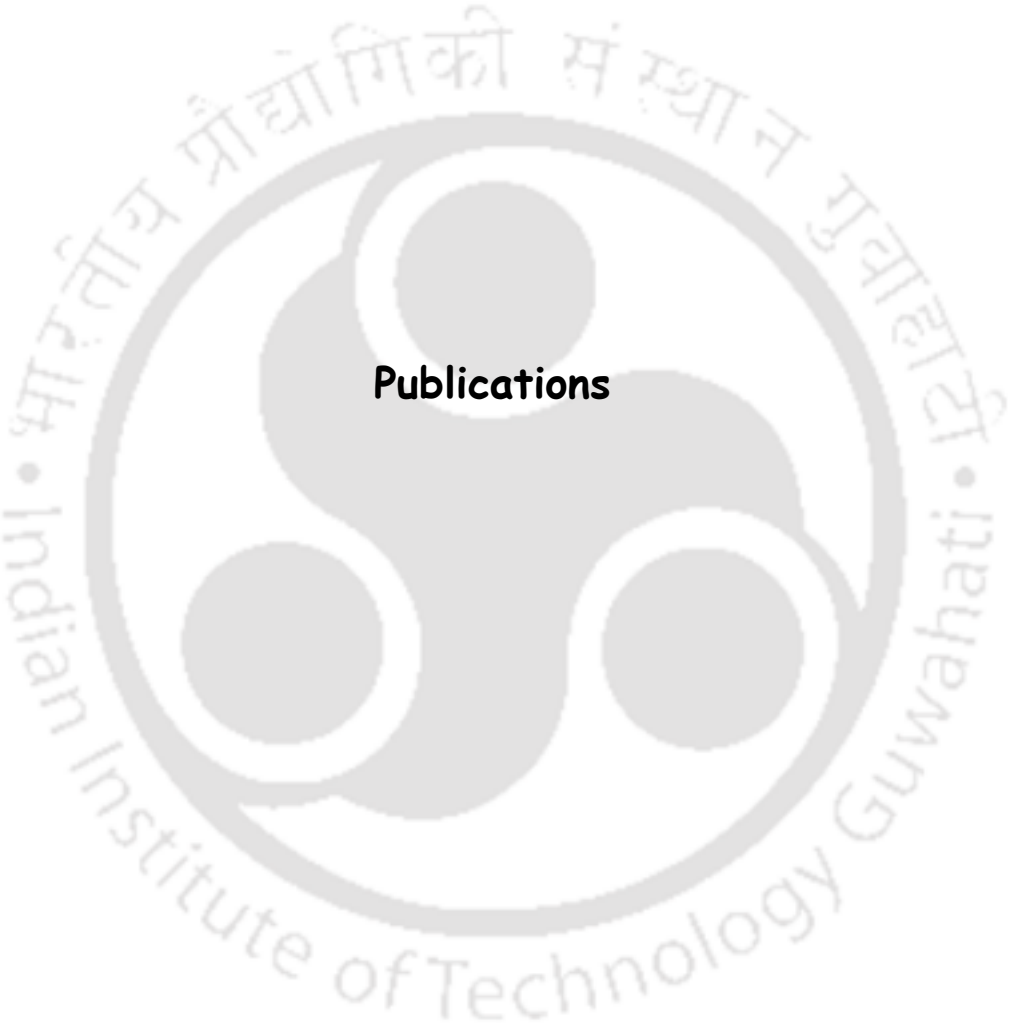

Publications

TH-1227_09610609

Publications in peer reviewed Journals/book:

1. **Deka R**, Tamuli R (2013) *Neurospora crassa ncs-1*, *mid-1*, and *nca-2* double mutant phenotypes suggest diverse interaction among three Ca^{2+}- regulating gene products. J Genetics 9 (in press)
2. Tamuli R, Kumar R, Srivastava DA, **Deka R** (2013) Calcium signaling. In Neurospora: Genomics and Molecular Biology (ed. D. P. Kasbekar and K. McCluskey), pp. 35-57. Caister Academic Press, Norfolk, UK
3. ***Deka R**, Kumar R, Tamuli R (2011) *Neurospora crassa* homologue of Neuronal Calcium Sensor-1 has a role in growth, calcium stress tolerance, and ultraviolet survival. Genetica 139:885-894
4. *Tamuli R, Kumar R, **Deka R** (2011) Cellular roles of Neuronal Calcium Sensor-1and calcium/calmodulin-dependent kinases in fungi. J Basic Microbiol 51:120-128

*These two publications have been cited in "Palma-Guerrero J, Hall CR, Kowbel D, Welch J, Taylor JW, Brem RB, Glass NL. Genome wide association identifies novel Loci involved in fungal communication. PLoS Genet. 2013 Aug; 9(8):e10036691"

Conferences:

1. **Deka R**, Kumar R, Gedela R, Sarma U, Srivastava DA, Tamuli R (2011) Calcium signaling in *Neurospora crassa*. Cell Signaling Networks 2011, Merida, Mexico, 22-27
2. **Deka R**, Tamuli R (2011) Cellular roles of the *Neurospora crassa* neuronal calcium sensor-1 homologue. World Congress on Biotechnology-2011, Hyderabad, India 21-23 March.
3. **Deka R**, Kumar R, Gedela R, Tamuli R (2011) Investigating cellular functions of the calcium signaling genes in *Neurospora crassa*. World Congress on Biotechnology-2011, Hyderabad, India.
4. Tamuli R, Srivastava DA, Kumar R, **Deka** R, Mahor D (2011) Genetics of calcium signaling machinery in *Neurospora crassa*. Comparative genomics of eukaryotic microorganisms: understanding the complexity of diversity, Sant Feliu de Guixols, Spain.

TH-1227_09610609

5. **Deka** R, Kumar R, Tamuli R (2010) Calcium signaling genes in *Neurospora crassa*. Neurospora 2010 Meeting, Asilomar, USA.
6. **Deka** R, Kumar R, Mandrawalia R, Tamuli R (2009) Genetic analysis of calcium signaling genes in *Neurospora crassa*. International Workshop on "Biology of Yeasts and Filamentous Fungi", Indo-U.S. Science and Technology Forum, Centre for Cellular and Molecular Biology, Hyderabad, India, 11-14 December.

TH-1227_09610609

REPRINTS OF PUBLICATIONS

TH-1227_09610609

© Indian Academy of Sciences

RESEARCH NOTE

Neurospora crassa ncs-1, *mid-1* and *nca-2* double-mutant phenotypes suggest diverse interaction among three Ca^{2+}-regulating gene products

REKHA DEKA and RANJAN TAMULI*

Department of Biotechnology, Indian Institute of Technology Guwahati, Guwahati 781 039, India

[Deka R. and Tamuli R. 2013 *Neurospora crassa ncs-1*, *mid-1* and *nca-2* double-mutant phenotypes suggest diverse interaction among three Ca^{2+}-regulating gene products. *J. Genet.* **92**, xx–xx]

Introduction

The calcium (Ca^{2+}) signalling system in the filamentous fungus *Neurospora crassa* is unique and significantly different from that in plants and animals, mainly with regard to the second messenger systems involved in Ca^{2+}-release from internal stores (Galagan *et al.* 2003). The complex Ca^{2+} signalling system in *N. crassa* contains 48 Ca^{2+} signalling proteins including a Ca^{2+} and/or CaM binding protein called neuronal calcium sensor-1 (NCS-1), a Ca^{2+}-permeable channel MID-1 and a PMCA-type Ca^{2+}-ATPase NCA-2 (Zelter *et al.* 2004; Tamuli *et al.* 2013). Here, we show that *ncs-1*, *mid-1* and *nca-2* interactions affect growth, carotenoid accumulation, Ca^{2+} stress tolerance, ultraviolet (UV) survival and circadian-regulated conidiation in *N. crassa*.

The *N. crassa* homologue of NCS-1 has a role in growth, Ca^{2+} stress tolerance and UV survival (Deka *et al.* 2011; Tamuli *et al.* 2011). MID-1 is necessary for Ca^{2+}-homeostasis in *N. crassa* (Lew *et al.* 2008). Mid-1 in *Gibberella zeae* has a role in growth, development and ascospore discharge (Cavinder *et al.* 2011). NCA-2 is responsible for adaptation to stress conditions and functions to pump Ca^{2+} out of the cell in *N. crassa* (Benito *et al.* 2000; Bowman *et al.* 2011).

In *Schizosaccharomyces pombe*, Ncs1p, the homologue of NCS-1, promotes Ca^{2+}-induced closure of Yam8p Ca^{2+} channel, a homologue of the MID1 (Hamasaki-Katagiri and Ames 2010). The Ca^{2+}-sensitive phenotype of the *ncs1* deletion mutant is rescued by a *yam8* deletion, indicating that Ncs1p negatively regulates Yam8p in *S. pombe* (Hamasaki-Katagiri and Ames 2010). However, no information is available regarding the interaction between homologues of Ncs1p and Yam8p in *Neurospora*. In addition, previous studies had indicated NCS-1 and NCA-2 roles in controlling Ca^{2+} levels in *N. crassa*; however, relationship between these two proteins remained unknown. Here, we study *ncs-1*, *mid-1* and *nca-2* mutations, suggesting their proteins interact to regulate various cell functions.

Materials and methods

Strains, growth, assay for Ca^{2+} and UV sensitivity

The *N. crassa* wild-type strains 74-OR23-1 *A* (FGSC 987) and OR8-1 *a* (FGSC 988), *ras-1^{bd}A* (FGSC 1858), *ras-1^{bd}a* (FGSC 1859); and the Ca^{2+}-signalling knockout mutants, Δ*NCU04379.2::hph A* (FGSC 11404), Δ*NCU04379.2::hph a* (FGSC 11403), Δ*NCU06703.2::hph A* (FGSC 11708), Δ*NCU06703.2::hph a* (FGSC 11707), Δ*NCU04736.2::hph A* (FGSC 13071) were obtained from the Fungal Genetics Stock Center (FGSC, Kansas, USA) (McCluskey 2003). The *NCU04379*, *NCU06703* and *NCU04736* genes encode the *N. crassa* homologue of NCS-1 (Deka *et al.* 2011), MID-1 (Lew *et al.* 2008) and NCA-2 (Bowman *et al.* 2009), respectively. The Δ*ncs-1*Δ*nca-2*, Δ*ncs-1*Δ*mid-1* and Δ*mid-1*Δ*nca-2* double mutants were generated by crossing the single mutant strains of opposite mating types and mutant alleles were confirmed by the PCR analysis of f_1 progeny (figure 1 in electronic supplementary material at http://www.ias.ac.in/jgenet/). A minimum of two strains were generated for each of the double mutants. Growth, crossing and maintenance of *Neurospora* strains were essentially as described by Davis and De Serres (1970). Ca^{2+} and UV sensitivity assays were performed as previously described (Deka *et al.* 2011).

*For correspondence. E-mail: ranjantamuli@iitg.ernet.in; ranjan.tam@gmail.com.

This article is dedicated to the memory of Akan Tamuli and Aita Tamuli in appreciation for their encouragement, inspiration and kindness.

Keywords. Ca^{2+} signalling; circadian-regulated conidiation; neuronal calcium sensor-1; mechanosensitive channel MID-1; Ca^{2+}-ATPase NCA-2; ultraviolet survival.

Carotenoid accumulation

To test for carotenoid accumulation, ~1 × 10^6 wild type and mutant strains spores were inoculated into flasks containing 25 mL of Vogel's liquid medium supplemented with 0.2% Tween 80 as a wetting agent to avoid conidiation (Zalokar 1954). The cultures were incubated initially in continuous darkness at 30°C for 48 h and then exposed to cool-white light at 22°C for 24 h (illuminated with two fluorescent bulbs (Philips Lifemax Tubelight TL-D 18W/54, Philips, Kolkata, India), 18 W, 6500 K, 1015 lumens). Mycelia were then filtered, lyophilized and powdered with mortar and pestle. Acetone and hexane were used in consecutive extractions of total carotenoid from 50 mg of lyophilized sample. Total carotenoid content of the wild type and mutant strains were calculated by measuring the maximum absorbance value at 470 nm and using the formula: total carotenoid content (μg/g) = [total absorbance × total volume of extract (1 mL) × 10^4]/[absorption coefficient (2500) × sample weight (g)] (Rodriguez-Amaya and Kimura 2004).

Circadian-regulated conidiation

The *N. crassa* strains were inoculated at one end of the race tube containing 1 × Vogel's salts, 0.1% D-glucose, 0.17% L-arginine, 50 ng/mL biotin and 1.5% bacto agar. The cultures were incubated at 25°C in constant light for 24 h and the growth fronts were marked. The cultures were then shifted to constant darkness at 25°C and the growth fronts were marked under a red safe light at regular interval of 24 h for five days. Period lengths were calculated by multiplying distance between conidial bands by the inverse of slope (http://www.fgsc.net/teaching/circad.htm).

Results and discussion

Effect of Δncs-1 Δmid-1 and Δnca-2 mutations in colony morphology, growth rate, aerial hyphae and carotenoid accumulation

We studied morphology and growth rates of the *ncs-1*, *mid-1* and *nca-2* knockout mutants. We found that only the Δ*ncs-1*Δ*nca-2* double mutant showed novel colony morphology with a characteristic swollen sponge-like colony (figure 2a in electronic supplementary material). The average growth rates followed the order wild type > Δ*nca-2* > Δ*ncs-1* > Δ*ncs-1*Δ*nca-2* > Δ*mid-1*Δ*nca-2* ≅ Δ*mid-1* > Δ*ncs-1*Δ*mid-1* (figure 1; table 1 in electronic supplementary material). Growth rates for both Δ*ncs-1*Δ*nca-2* and Δ*ncs-1*Δ*mid-1* double mutants were lower than the parental single mutants. However, the Δ*mid-1*Δ*nca-2* double mutant showed growth rate similar to that of the Δ*mid-1* mutant. In addition, the Δ*ncs-1* and Δ*nca-2* mutants showed shorter aerial hyphae and this phenotype was aggravated in the Δ*ncs-1*Δ*nca-2* double mutant (figure 2b in electronic supplementary material). Interestingly, aerial hyphae growth in the Δ*mid-1* mutant was comparable to the wild type; however, the Δ*ncs-1*Δ*mid-1* and Δ*mid-1*Δ*nca-2* double mutants showed shorter aerial hyphae like the Δ*ncs-1* and Δ*nca-2* mutants, respectively (figure 2b in electronic supplementary material).

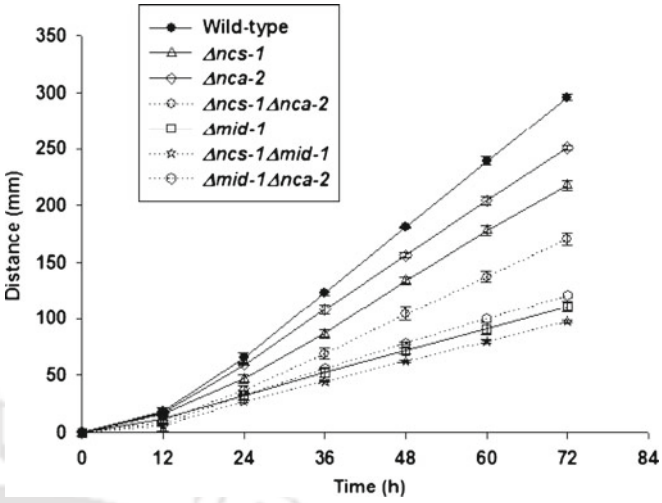

Figure 1. Growth rates. Rates of apical growth of the wild type and mutant strains in race tubes are plotted against the indicated time interval. Error bars show the standard errors calculated from the data for three independent experiments.

We also performed quantitative analysis of carotenoid accumulation in the mutants to test the effect of these mutations in carotenoid synthesis. The carotenoid profile followed the order Δ*mid-1*Δ*nca-2* > Δ*ncs-1*Δ*mid-1* > Δ*mid-1* > Δ*ncs-1* > Δ*nca-2* > wild type ≅ Δ*ncs-1*Δ*nca-2* (figure 2). Thus, except the Δ*ncs-1*Δ*nca-2* double mutant, the other mutants produced more carotenoid than the wild type which suggests that the wild-type gene products negatively affect carotenoid accumulation. Accumulation of the xanthophyll

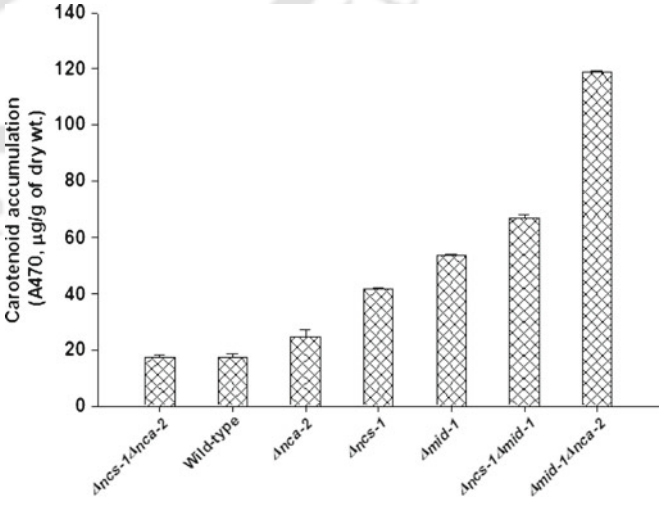

Figure 2. Total carotenoid contents. Carotenoid extracted from the indicated *N. crassa* strains are expressed as μg carotenoid per gram of dry weight. Error bars show the standard errors calculated from the data for three independent experiments.

neurosporaxanthin and variable amounts of carotenoid precursors results in characteristic orange pigmentation of conidia and mycelia in *N. crassa* (Avalos *et al.* 2013). Our studies indicate that Ca^{2+} signalling pathway could be involved in regulating carotenoid accumulation in *N. crassa*.

The Δncs-1Δnca-2 double mutant was hypersensitive to Ca^{2+} and UV stress, and the Δmid-1 and Δnca-2 mutants showed increased sensitivity to UV

The Δ*ncs-1* and Δ*nca-2* mutants were sensitive to Ca^{2+} stress (Bowman *et al.* 2011; Deka *et al.* 2011). In addition, growth of the Δ*mid-1* mutant was inhibited at low extracellular or elevated intracellular Ca^{2+} (Lew *et al.* 2008). To test if Ca^{2+} stress tolerance is influenced by the interactions of *ncs-1*, *mid-1* and *nca-2*, we studied sensitivity of the mutants to various concentrations of $CaCl_2$. The Ca^{2+} stress tolerance followed the order Δ*mid-1* > wild type > Δ*ncs-1*Δ*mid-1* > Δ*nca-2* > Δ*ncs-1* > Δ*mid-1*Δ*nca-2* > Δ*ncs-1*Δ*nca-2* (figure 3a, table 2 in electronic supplementary material).

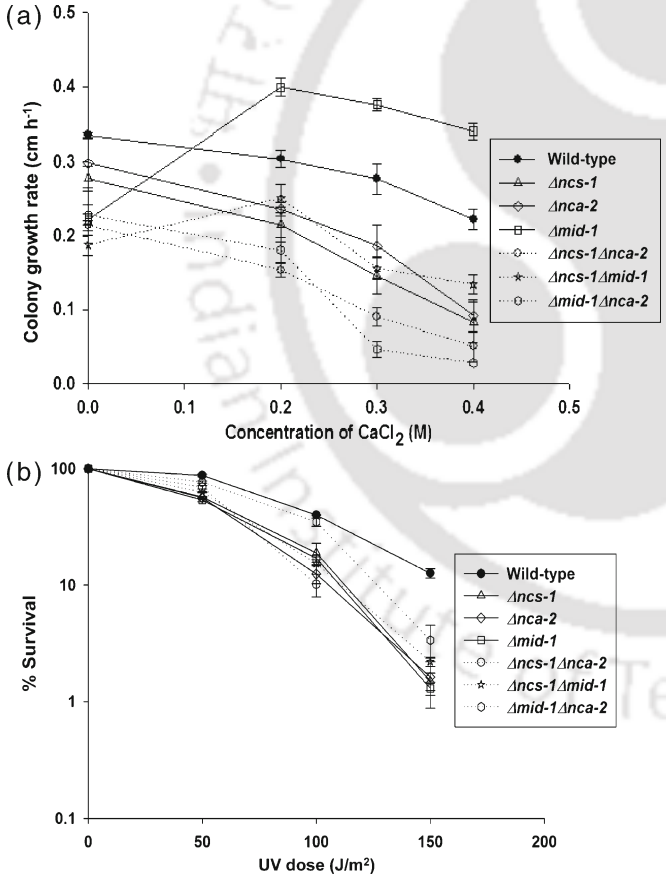

Figure 3. Analysis of Ca^{2+} and UV sensitivity. (a) Ca^{2+} sensitivity assay. Colony diameter (cm h^{-1}) of the *N. crassa* were measured at regular intervals and plotted against various concentrations of $CaCl_2$. Standard errors calculated from the data for three independent experiments are shown using error bars. (b) Dose-response curves of the *N. crassa* wild type and the mutant strains on exposure to UV irradiations. Each data point represents the mean of at least three independent experiments.

Thus, Δ*nca-2* mutation had a synergistic effect on Ca^{2+} sensitivity phenotype of the Δ*mid-1* and Δ*ncs-1* mutants. The growth of Δ*mid-1* mutant was stimulated ~83.8% at 0.2 M $CaCl_2$ concentrations. Interestingly, stimulation of the growth rate of the Δ*mid-1* mutant at 0.2 M $CaCl_2$ was suppressed in the Δ*ncs-1* and Δ*nca-2* backgrounds, growth stimulation was only ~34% in the Δ*ncs-1*Δ*mid-1* double mutant and fully disappeared in the Δ*mid-1*Δ*nca-2* double mutant. The Ca^{2+}-permeable channels regulate passive inflow of Ca^{2+} into the cell, whereas the Ca^{2+}-ATPases reduce the cytosolic free Ca^{2+} ($[Ca^{2+}]_c$) by active pumping of Ca^{2+} into internal stores or efflux of Ca^{2+} from the cell (Møller *et al.* 1996; Zelter *et al.* 2004). This could explain the epistasis of the *nca-2* over *mid-1* for Ca^{2+} sensitivity. It is possible that NCS-1 is also involved in decreasing $[Ca^{2+}]_c$ by stimulating Ca^{2+}-efflux. The Ca^{2+}-sensitivity phenotype was aggravated in the Δ*ncs-1*Δ*nca-2* double mutant, indicating that negative interaction of *ncs-1* and *nca-2* plays a critical role in reducing hazardous amount of $[Ca^{2+}]_c$. However, Ca^{2+} sensitivity phenotype of the Δ*ncs-1* mutant was not fully rescued by the Δ*mid-1* mutant, indicating that the relationship between *ncs-1* and *mid-1* genes are not the same in *N. crassa* as their homologues in *S. pombe* (Hamasaki-Katagiri and Ames 2010; figure 3a).

The null mutant of *N. crassa* homologue of *ncs-1* was sensitive to UV (Deka *et al.* 2011). We tested the sensitivity of the double mutants in exposure to UV irradiation (figure 3b). Both Δ*mid-1* and Δ*nca-2* mutants showed an increased sensitivity to UV; however, to our surprise, the Δ*mid-1*Δ*nca-2* double mutant was more tolerant to UV than either of the single mutants (figure 3b). The Δ*ncs-1*Δ*nca-2* double mutant showed severe sensitivity to UV; however, UV sensitivity of the Δ*ncs-1*Δ*mid-1* double mutant was comparable to the single mutants (figure 3b). These results indicated involvement of MID-1 and NCA-2 in UV induced DNA damage repair. Besides, interactions of *mid-1* with *nca-2* and *ncs-1* with *nca-2* affect the UV survival in a negative and positive manner, respectively.

The Δncs-1Δnca-2, Δncs-1Δmid-1 and Δmid-1Δnca-2 double mutant showed lesser sensitivity to respiratory byproduct CO_2 and produced conidial bands

The analysis of the knockout mutants for the genes *ncs-1*, *mid-1* and *nca-2* indicated their involvement in stress tolerance. Therefore, we also tested if any of the mutants could tolerate the respiratory byproduct CO_2 and produce conidial bands race tube. The conidiation of the wild type in a race tube is suppressed due to accumulation of CO_2. However, conidiation persists despite the CO_2 accumulation in a race tube in the *band* (*bd*) mutant *ras-1*^{bd} that carries a T79I point mutation in *ras-1*; therefore, the *ras-1*^{bd} mutant is used in circadian rhythm studies (Sargent and Kaltenborn 1972; Belden *et al* 2007). We found that both Δ*ncs-1*Δ*mid-1* and Δ*mid-1*Δ*nca-2* double mutants produce

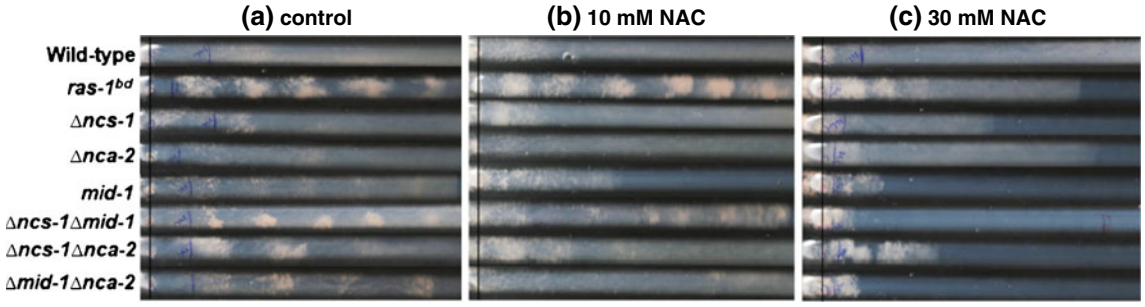

Figure 4. Circadian-regulated conidiation. (a) The Δ*ncs-1*Δ*mid-1* and Δ*mid-1*Δ*nca-2* double mutants produce distinct conidial bands at regular intervals in race tubes. In the Δ*ncs-1*Δ*nca-2* double mutants, bands were distinct till 72 h. (b) Rhythmic conidiation patterns of the Δ*ncs-1*Δ*mid-1* and Δ*mid-1*Δ*nca-2* double mutants were suppressed in the medium supplemented with 10 mM NAC. (c) Growth defects of the *N. crassa* strains in the medium supplemented with 30 mM NAC.

distinct conidial bands with an increased period length of 25.41 ± 0.48 h and 23.96 ± 0.58 h, respectively, and the *ras-1*^{bd} control showed a period length of 22.48 ± 0.72 (figure 4a). The Δ*ncs-1*Δ*nca-2* double mutant showed a less robust effect and produced distinct conidial bands up to 72 h (figure 4a). To test if the conidial band were produced due to the increased level of reactive oxygen species (ROS), we supplemented race tube medium with antioxidant N-acetyl-L-cysteine (NAC) to reduce ROS. Conidial bands were suppressed in the double mutants on addition of 10 mM NAC; however, NAC at 30 mM caused growth arrest, indicating a toxic effect at high concentration (figures 4b, c). In summary, Δ*ncs-1*Δ*nca-2*, Δ*ncs-1*Δ*mid*-1 and Δ*mid-1*Δ*nca-2* double mutants showed lesser sensitivity than the single mutants and the wild-type strains to the respiratory byproduct CO_2 and produced conidial bands, which was possibly due to an increased ROS level in these mutants. Thus, our finding that Δ*ncs-1*Δ*nca-2*, Δ*ncs-1*Δ*mid-1* and Δ*mid-1*Δ*nca-2* double mutants produced distinct conidial bands under the conditions normally unfavourable for conidiation in race tube, indicate that wild-type gene products synthetically act as negative regulators of circadian-regulated conidiation. We also tested if the Δ*ncs-1* mutant could show any synthetic effect in the knockout background of another Ca^{2+}-signalling gene NCU02814 (*prd-4*). The Δ*ncs-1*Δ*prd-4* double mutant did not show any synthetic effect on growth, Ca^{2+} and UV stress tolerance and period length; therefore, ruling out the hypothesis that similar genetic interactions exist between any of the Ca^{2+} signalling gene pair (data not shown). Thus, we showed that genetic interactions of *ncs-1*, *mid-1* and *nca-2* regulate multiple cellular processes in *N. crassa*.

Acknowledgements

The FGSC, University of Missouri, Kansas City, MO 64110, is supported by NSF grant BIR-9222772 and generously waived charges for strains and race tubes. We thank the anonymous reviewer for critical inputs that significantly improved the manuscript. RD was supported by Junior and Senior Research Fellowships from the CSIR-UGC, New Delhi. This work was supported in part by NE-Twinning (DBT) and SERC Fast Track (DST) grants to RT.

References

Avalos J., Luis M. and Corrochano L. M. 2013 Carotenoid biosynthesis in *Neurospora*. In *Neurospora: genomics and molecular biology* (ed. D. P. Kasbekar and K. McCluskey), pp. 227–241. Caister Academic Press, Norfolk, UK.

Belden W. J., Larrondo L. F., Froehlich A. C., Shi M., Chen C. H., Loros J. J. and Dunlap J. C. 2007 The band mutation in *Neurospora crassa* is a dominant allele of *ras-1* implicating RAS signaling in circadian output. *Genes Dev.* **21**, 1494–1505.

Benito B., Garciadeblas B. and Rodriguez-Navarro A. 2000 Molecular cloning of the calcium and sodium ATPases in *Neurospora crassa*. *Mol. Microbiol.* **35**, 1079–1088.

Bowman B. J., Draskovic M., Freitag M. and Bowman E. J. 2009 Structure and distribution of organelles and cellular location of calcium transporters in *Neurospora crassa*. *Eukaryot. Cell* **8**, 1845–1855.

Bowman B. J., Abreu S., Margolles-Clark E., Draskovic M. and Bowman E. J. 2011 Role of four calcium transport proteins, encoded by *nca-1*, *nca-2*, *nca-3*, and *cax*, in maintaining intracellular calcium jevels in *Neurospora crassa*. *Eukaryot. Cell* **10**, 654–661.

Cavinder B., Hamam A., Lew R. R. and Trail F. 2011 Mid1, a mechanosensitive calcium ion channel, affects growth, development, and ascospore discharge in the filamentous fungus *Gibberella zeae*. *Eukaryot. Cell* **10**, 832–841.

Davis R. H. and De Serres F. J. 1970 Genetic and microbiological research techniques for *Neurospora crassa*. *Methods Enzymol.* **17**, 79–143.

Deka R., Kumar R. and Tamuli R. 2011 *Neurospora crassa* homologue of neuronal calcium sensor-1 has a role in growth, calcium stress tolerance, and ultraviolet survival. *Genetica* **139**, 885–894.

Galagan J. E., Calvo S. E., Borkovich K. A., Selker E. U., Read N. D., Jaffe D. *et al.* 2003. The genome sequence of the filamentous fungus *Neurospora crassa*. *Nature* **422**, 859–868.

Hamasaki-Katagiri N. and Ames J. B. 2010 Neuronal calcium sensor-1 (Ncs1p) is up-regulated by calcineurin to promote Ca^{2+} tolerance in fission yeast. *J. Biol. Chem.* **285**, 4405–4414.

Lew R. R., Abbas Z., Anderca M. I. and Free S. J. 2008 Phenotype of a mechanosensitive channel mutant, *mid-1*, in a filamentous fungus, *Neurospora crassa*. *Eukaryot. Cell* **7**, 647–655.

McCluskey K. 2003 The fungal genetics stock center: from molds to molecules. *Adv. Appl. Microbiol.* **52**, 245–262.

Møller J. V., Juul B. and le Maire M. 1996 Structural organization, ion transport, and energy transduction of P-type ATPases. *Biochim. Biophys. Acta* **1286**, 1–51.

Rodriguez-Amaya D. B. and Kimura M. 2004 Harvestplus handbook for carotenoid analysis. *HarvestPlus Technical Monograph 2*, International Food Policy Research Institute (IFPRI) and International Center for Tropical Agriculture (CIAT), Washington, USA.

Sargent M. L. and Kaltenborn S. H. 1972. Effects of medium composition and carbon dioxide on circadian conidiation in *Neurospora Plant Physiol.* **50**, 171–175.

Tamuli R., Kumar R. and Deka R. 2011 Cellular roles of neuronal calcium sensor-1 and calcium/calmodulin-dependent kinases in fungi. *J. Basic Microbiol.* **51**, 120–128.

Tamuli R., Kumar R., Srivastava D. A. and Deka R. 2013 Calcium signaling. In *Neurospora: genomics and molecular biology* (ed. D. P. Kasbekar and K. McCluskey), pp. 35–57. Caister Academic Press, Norfolk, UK.

Zalokar M. 19542 Studies on biosynthesis of carotenoids in *Neurospora crassa*. *Arch. Biochem. Biophys.* **50**, 71–80.

Zelter A., Bencina M., Bowman B. J., Yarden O. and Read N. D. 2004 A comparative genomic analysis of the calcium signaling machinery in *Neurospora crassa*, *Magnaporthe grisea*, and *Saccharomyces cerevisiae*. *Fungal Genet. Biol.* **41**, 827–841.

Received 20 March 2013, in final revised form 12 May 2013; accepted 13 May 2013
Published on the Web: 10 October 2013

TH-1227_09610609

Supplementary data:

Neurospora crassa ncs-1, *mid-1* and *nca-2* double-mutant phenotypes suggest diverse interaction among three Ca^{2+}-regulating gene products

Rekha Deka and Ranjan Tamuli

J. Genet. **92**, xx–xx

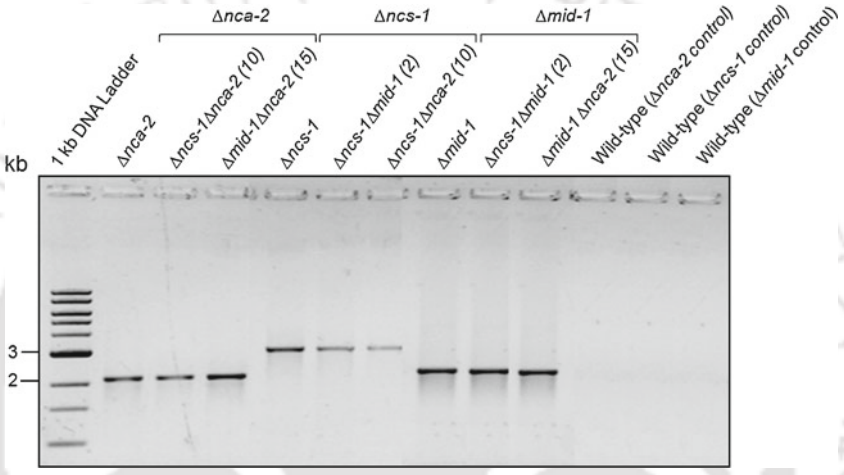

Figure 1. Confirmation of the double mutants by PCR analysis. The Δ*ncs-1*Δ*nca-2*, Δ*ncs-1*Δ*mid-1* and Δ*mid-1*Δ*nca-2* double mutants were verified by using the forward primers HI-NCS-1-F 5′-GTCTCAGCATGAAAGTCGTC-3′, HI-NCU06703-F 5′-CCAAGGCTTATGCCGTCATC-3′, and HI-NCU04736-F 5′-GTCCCATGGATTCCATACCA-3′ specific for upstream of the open reading frame of genes *ncs-1*, *mid-1*, and *nca-2*, respectively, and with the common reverse primer 5HPHR 5′-ATCCACTTAACGTTACTGAAATC-3′ that is specific for the *hph* cassette used to generate the knockout mutants (Colot *et al.* 2006; Deka *et al.* 2011). Amplification of PCR products of size ~2.089, 2.89 and 2.023 kb, respectively, indicate presence of the Δ*nca-2*, Δ*ncs-1* and Δ*mid-1* alleles in the mutants (for each of the three knockout alleles, only a set of three PCR products is shown). For the double mutants, the number in the parenthesis indicates the laboratory strain reference number. The wild-type was used as negative controls for all the three knockout alleles (indicated in the parenthesis) using the allele specific primer pairs. The single knockout mutants were generated by the *N. crassa* genome project (http://www.dartmouth.edu/~neurosporagenome/proj_overview.html) and also verified in independent works (Colot *et al.* 2006; Lew *et al.* 2008; Bowman *et al.* 2011; Deka *et al.* 2011).

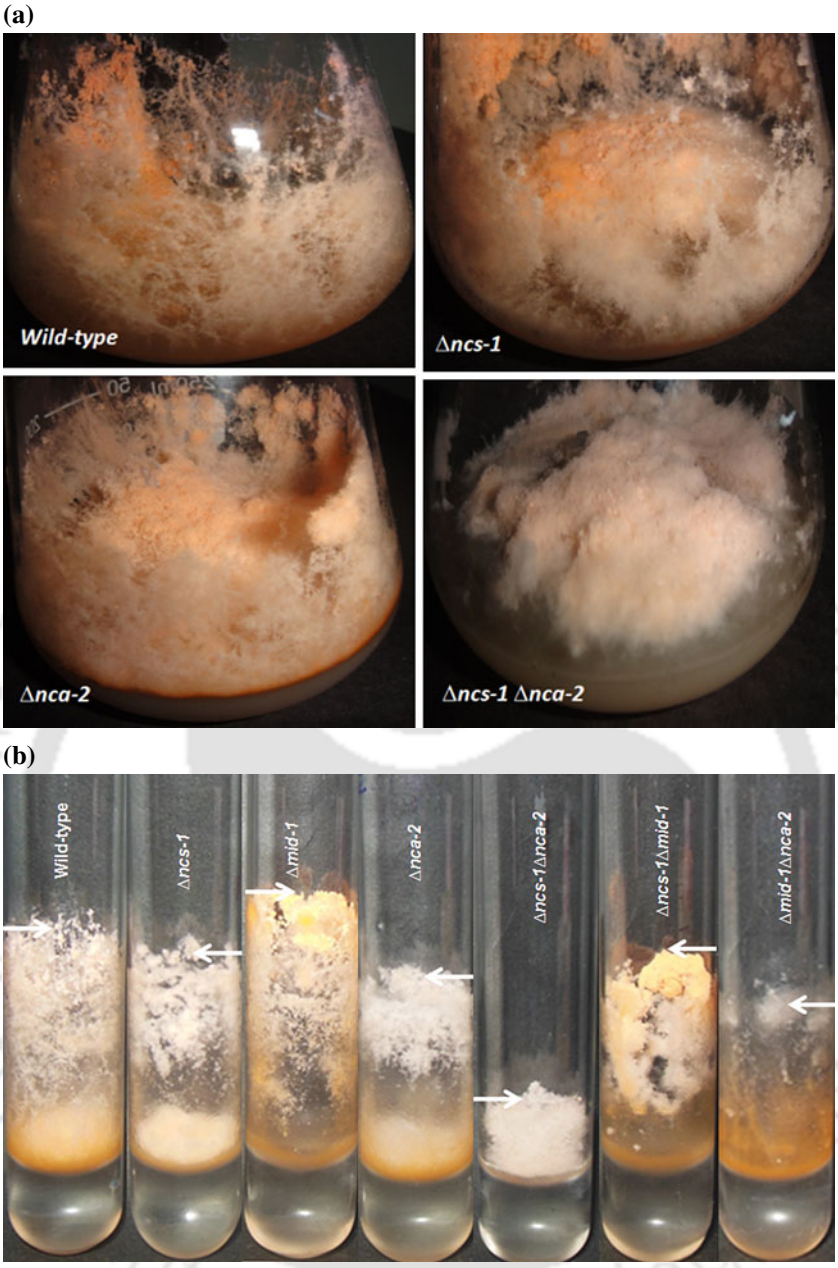

Figure 2. Colony morphology and aerial hyphae. (a) The Δ*ncs-1*Δ*nca-2* double mutant displayed novel colony morphology. The *N. crassa* strains were grown at 30°C for 5 days. (b) Growth of aerial hyphae. The *N. crassa* strains were cultured in standing Vogel's liquid medium at 30°C in darkness for 3 days, tubes were then illuminated for 24 h and photographed. The edges of aerial hyphae are indicated by white arrows.

Table 1. Average growth rates of the *N. crassa* strains in race tubes.

Strains	Average growth rates (cm h^{-1})
Wild-type	0.327 ± 0.099
Δ*ncs-1*	0.239 ± 0.067
Δ*nca-2*	0.276 ± 0.072
Δ*mid-1*	0.137 ± 0.022
Δ*ncs-1*Δ*nca-2*	0.185 ± 0.058
Δ*ncs-1*Δ*mid-1*	0.117 ± 0.022
Δ*mid-1*Δ*nca-2*	0.142 ± 0.039

Table 2. Average growth rates of the *N. crassa* strains in the medium supplemented with various concentrations of $CaCl_2$.

	Growth rates (cm h^{-1}) in various concentrations of $CaCl_2$ (M)			
Strains	0	0.2	0.3	0.4
Wild-type	0.359 ± 0.009	0.327 ± 0.009	0.288 ± 0.018	0.241 ± 0.013
Δ*ncs-1*	0.289 ± 0.018	0.218 ± 0.017	0.122 ± 0.022	0.074 ± 0.029
Δ*nca-2*	0.309 ± 0.028	0.239 ± 0.007	0.187 ± 0.024	0.095 ± 0.013
Δ*mid-1*	0.216 ± 0.011	0.397 ± 0.010	0.385 ± 0.009	0.335 ± 0.016
Δ*ncs-1*Δ*nca-2*	0.213 ± 0.007	0.153 ± 0.009	0.091 ± 0.012	0.05 ± 0.020
Δ*ncs-1*Δ*mid-1*	0.187 ± 0.013	0.251 ± 0.019	0.156 ± 0.015	0.134 ± 0.013
Δ*mid-1*Δ*nca-2*	0.227 ± 0.013	0.180 ± 0.018	0.046 ± 0.010	0.028 ± 0.000

References

Bowman B. J., Abreu S., Margolles-Clark E., Draskovic M. and Bowman E. J. 2011 Role of four calcium transport proteins, encoded by *nca-1*, *nca-2*, *nca-3*, and *cax*, in maintaining intracellular calcium jevels in *Neurospora crassa*. *Eukaryot. Cell.* **10**, 654–661.

Colot H. V., Park G., Turner G. E., Ringelberg C., Crew C. M., Litvinkova L. *et al.* 2006 A high-throughput gene knockout procedure for *Neurospora* reveals functions for multiple transcription factors. *Proc. Natl. Acad. Sci. U.S.A.* **103**, 10352–10357.

Deka R., Kumar R. and Tamuli R. 2011 *Neurospora crassa* homologue of Neuronal Calcium Sensor-1 has a role in growth, calcium stress tolerance, and ultraviolet survival. *Genetica* **139**, 885–894.

Lew R. R., Abbas Z., Anderca M. I. and Free S. J. 2008 Phenotype of a mechanosensitive channel mutant, *mid-1*, in a filamentous fungus, *Neurospora crassa*. *Eukaryot. Cell.* **7**, 647–655.

TH-1227_09610609

PCR BOOKS !!!!
• Real-Time PCR
• qPCR
• PCR Troubleshooting
• Essential Guides
New PCR books !!!

NEW BOOK !!!!
SPORES
New book !!!

NEW BOOK !!!!
REGULATORY NETWORKS
New book !!!

NEW BOOK !!!!
EPIGENETICS
A REFERENCE MANUAL
New book !!!

NEW BOOK !!!!
SYSTEMS MICROBIOLOGY
New book !!!

NEW TITLES
NEW BOOKS FOR 2012
Click here

Home Books New Books Blog Authors & Editors Newsletter Contact Order Search
microbiology bacteriology virology molecular biology pcr genomics bioinformatics environmental medical probiotics mycology parasitology new books

Advanced search
Book search Go

Subscribe to our Newsletter
Your email Go

How to order
Books
Microbiology Books
Bacteriology Books
Virology Books
Molecular Biology Books
PCR Books
Genomics Books
Epigenetics Books
Bioinformatics Books
Environmental Books
Medical Books
Probiotics Books
Mycology Books
Parasitology Books
Regulatory Networks Books
New and Forthcoming 2012 2011 2010
Authors' page
Editors' page

Featured books:

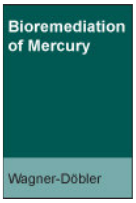

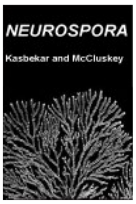

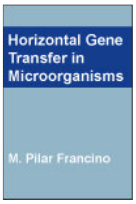

Major new book: PCR Troubleshooting and Optimization Click here

Neurospora: Genomics and Molecular Biology | Book

Buy now!

Publisher: Caister Academic Press
Editor: Durgadas P. Kasbekar and Kevin McCluskey *Centre for Cellular and Molecular Biology, Hyderabad, India and Fungal Genetics Stock Center, University of Missouri-Kansas City, USA (respectively)*
Publication date: January 2013
ISBN: 978-1-908230-12-6
Price: GB £159 or US $319 (hardback)
Pages: c. 280

How to Order . Library recommendation form

Download flyer

Customers who viewed this book also viewed: Microbial Ecological Theory Stress Response in Microbiology Metagenomics

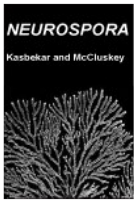

Building on over 70 years of genetics research, *Neurospora* continues to be the leading model for the study of the genomics and molecular biology of filamentous fungi. The ease of culture, amenability to genetic and molecular genetic analysis, and the close correlation between genetic and biochemical traits are some of its advantages. Research with *Neurospora* has provided insights unachievable from work with simpler systems and difficult to extract from more complicated ones, cementing its position as a leading model system. In recent years the application of modern high throughput analyses had led to a deluge of information on the genomics and molecular biology of *Neurospora*. This timely book aims to distil the most important findings to provide a snapshot of the current research landscape.

In this book, internationally recognised *Neurospora* experts critically review the most important research and demonstrate the breadth of applications to industrial biology, biofuels, agriculture, and human health. The opening chapter is an introduction to the organism. Following chapters cover topics such as: carotenoid biosynthesis, polysaccharide deconstruction, genome biology, genome recombination, gene regulation, signal transduction, self-recognition, development, circadian rhythms and mutation. The book closes with a fascinating look at the history and future trends for research on *Neurospora* gene and genome analysis.

This volume is essential for everyone working with *Neurospora* and other filamentous fungi. A recommended book for all biology, agriculture and medical libraries.

Chapter 1 *Neurospora*: The Organism, its Genes and its Genome
A J F Griffiths
The fungus *Neurospora* has been the subject of a large variety of types of research in genetics and other aspects of biology. This chapter provides a short overview of *Neurospora* genetics, both as an introduction for those not familiar with this fungus as a genetic tool, and as a general context for the diverse research described in the ensuing chapters. The overview consists of a description of the organism, how it is used in genetics, and a brief account of how the nature of its genome has been revealed. References have been kept to a minimum in this introduction, so for more details of the approaches described see Davis, 2000.

Chapter 2 The Fungal Sense of Nonself
Myron L. Smith and Denis L. Lafontaine
Fungal incompatibility systems are intricate and complicated, but unifying patterns are emerging that provide a better understanding of the basis for the fungal "sense of nonself". This chapter explores recent advances in understanding fungal vegetative incompatibility (VI) within the broader context of fungal nonself recognition systems. The initial molecular characterization of a limited number of VI factors in *N. crassa* and *P. anserina* has provided a set of search images that can be used to find incompatibility genes in other species. The common features discussed include shared structural aspects and sequence motifs of VI complexes, and the downstream processes triggered by nonself recognition, including VI-associated Programmed Cell Death. Finally, we speculate on the role and origin fungal VI systems.

Chapter 3 Control of Branching in *Neurospora crassa*
Michael K. Watters
The growth and vegetative morphology of filamentous fungi is characterized by two seemingly related activities: Tip growth - the highly polarized extension of hyphal tips, and branching - the process by which new hyphal tips emerge. Tip growth and branching are crucial elements in the colonization and utilization of the organic substrate, keys to the ecological role of this fungus. There appear to be at least two distinct forms of branch formation. One (lateral branching) which results in the new tips which emerge from the side of the tip region of an existing hyphal tube near, but not at, the apex of the tip, and the second (apical branching) in which a growing tip splits to form a pair of tips emerging from what was the apex of the hyphal tip. This review presents a brief description of the tip growth and branching process with a focus on genetic and environmental influences on the control of branching. Evidence that lateral and apical branches are controlled by separate mechanisms will be discussed. An additional focus will be on evidence for a proposed homeostatic system which regulates branch density, including a description of mutants which appear to disrupt the proposed system.

Chapter 4 Glycosyl Hydrolases: Modular Structure, Physiological Roles, Gene Amplification and Evolution
Alan Radford
The ascomycete fungus *Neurospora crassa* has a profusion of glycosyl hydrolase genes encoding a wide range of physiological roles. Domain structure of glycosyl hydrolases is considered in the context of domain shuffling within and between families. Mechanisms of action of glycosyl hydrolases are illustrated. The conservation of sequence and structure of the cellulose-binding domain is examined in detail, as is the sequence and structural basis of endo- and exo-cellulases. The individual *N. crassa* enzymes are classified by predicted function, family, clade (superfamily) and fold. Gene amplification is analysed in *N. crassa* and ascomycete relatives, and the most highly amplified families are examined for evidence of the evolutionary timing of gene amplification events.

Chapter 5 Quantitative genetics in *Neurospora*
Charles Hall
Since the 1940s, researchers have used *Neurospora* species in pioneering genetic analyses providing many discoveries in genetics and molecular biology. Several complex phenotypes continue to be the focus of *Neurospora* research, including spore germination, hyphal growth, aerial hyphae formation and asexual spore production, meiosis and sexual spore development, epigenetics and circadian rhythm. Surprisingly, unlike the many genes that have been discovered to regulate Mendelian trains in *N. crassa*, studies of complex traits in are in their infancy and few researchers have

TH-1227_09610609

taken advantage of natural variation in phenotype. Quantitative trait locus (QTL) mapping and genome-wide association mapping (GWA) have proven to be highly effective methods for studying genetically complex traits. These methods link phenotypic data and genotypic data in an attempt to explain the genetic basis of variation in complex traits. Here I present a review of the principles that underlie these analyses, as well as some common methods for the collection and analysis of QTL and GWA data. We also present a review of quantitative genetics studies in Neurospora. Currently, quantitative studies in Neurospora center around two primary areas of research: circadian clock and the identification of genes involved in the reinforcement of mating barriers between *Neurospora crassa* and *Neurospora intermedia*. Recently the emergence of short-read high-throughput sequencing methods have allowed for the sampling of variation within populations of *N. crassa* at reasonable cost and effort. We further describe the use of these sequencing methods to construct a data set that allows for genome-wide association studies with a Louisiana population of *N. crassa*.

Chapter 6 Genetic Recombination in *Neurospora crassa*
David E. A. Catcheside, Frederick J. Bowring and P. Jane Yeadon
Beadle and Tatum's selection of *Neurospora* to test the hypothesis that genes encode proteins was strongly influenced by the life cycle of this filamentous fungus, which is particularly amenable to genetic experiments. Pertinent features for the student of recombination include two mating types and a mitotic division following meiosis prior to spore formation, yielding an ascus in which the position of each meiotic product mirrors the order of the eight DNA strands as they entered meiosis. This latter feature allows ready detection of rare recombination events. In this chapter we review the contributions *Neurospora* has made to our understanding of recombination. These include the first unequivocal demonstration of gene conversion, fine structure maps of eukaryotic genes, evidence for polarity in gene conversion and identification of recombination hotspots (recombinators) and the genes that regulate them. More recent contributions come from analyses using knockouts of genes involved in recombination, a fluorescent recombination reporter system and whole octad sequencing to reveal genome-wide recombination.

Chapter 7 *Neurospora* Duplications, and Genome Defense by RIP and Meiotic Silencing
Durgadas P. Kasbekar
Repeat-induced point mutation (RIP) and meiotic silencing by unpaired DNA serve to prevent the accumulation of transposable elements and other repetitive DNA in the *Neurospora* genome. RIP occurs in the premeiotic dikaryon that forms following fertilization in a sexual cross, and induces G:C to A:T mutations in duplicated DNA, thus destroying any ORFs present in it. Meiotic silencing uses RNAi to eliminate transcripts of genes that do not pair properly in meiosis with a homologue in the same chromosomal location and thus silences them and even their homologous genes at other chromosomal locations, regardless of whether or not the latter are paired. Chromosome segment duplications (*Dps*) also are substrates for RIP. But RIP is less severe in *Dp*-borne genes than in small gene-sized duplications, and the presence of*Dps* in a cross can lower the efficiency of RIP in small duplications. *Dps* thus behave as dominant suppressors of RIP. Short *Dps* (i.e., < 200 kbp) that individually are unable to suppress RIP can nonetheless do so in multiply heterozygous crosses if the total amount of duplicated DNA exceeds ~300 kbp. This suggests that RIP suppression by *Dps* might occur via titration of the RIP machinery. *Dp*-heterozygous crosses are barren, but their productivity can be increased by suppression of meiotic silencing. Barrenness limits the vertical transmission of *Dps*, therefore meiotic silencing augments genome defense by RIP, but it might also protect the genome independently of RIP. Meiotic silencing is demonstrable using tester strains that silence genes whose silencing can produce striking ascus-development phenotypes. Crosses of the testers with many wild-isolated strains revealed meiotic silencing to be relatively weak and restricted only to the early perithecia of the cross. We hypothesize that genes essential for meiotic silencing might become unpaired with time, possibly aided by sequence polymorphisms between the tester and wild genomes, thus becoming self-silenced, and thereby shorten the duration of silencing. Some wild strains contain genetic factors that when brought together produce a Ä'syntheticÄ" RIP suppressor phenotype. These factors might represent sub-threshold sized and cryptic *Dps*.

Chapter 8 Mutagen Response and Repair
Shin Hatakeyama
George Wells Beadle and Edward Lawrie Tatum chose *Neurospora crassa* as a model organism to uncover the role of the gene in biochemical synthesis pathways. Their studies led them to propose the famous, one gene-one enzyme hypothesis, by generating *Neurospora* mutants by the treatment with the mutagen (X-ray irradiation) to asexual spores (Beadle and Tatum, 1941; Beadle and Tatum, 1945). This artificial mutagenesis was originally reported by Hermann Joseph Muller, who discovered the generation of *Drosophila* mutants by irradiation with X-rays. Artificial mutagenesis has since become a great tool to facilitate progress in the study of gene function.

Although mutagen treatment does damage to DNA, most of the induced lesions are repaired effectively by many modes of DNA repair by which cells maintain the integrity of genome information. But a subset of lesions that escape this repair function can become fixed as mutation. Most mutations cause serious issues, including alteration of cell, tissue, and organ function, disease, tumor, cancer, apoptosis, and so on. However, mutations are also the motive force of evolution.

In this chapter, I summarize mutagen response and repair in *Neurospora* and describe the various DNA damaging agents, mutations and mutagenesis, and DNA repair systems. By the end of the 20th century, many strains, showing mutagen sensitivity, had been isolated as DNA repair defective mutants, i.e. *uvs-* (ultraviolet sensitive-), *mus-* (mutagen sensitive-), *mei-* (meiosis), and *upr-* (ultraviolet photoreactivation) mutants in *Neurospora*. Analyses of the phenotype of these mutants and comparison with repair processes of other organism led to the identification of several DNA repair process. Now, through the contribution of the *Neurospora* genome project, we are able to find additional DNA repair genes in *Neurospora* based on their homology with genes of other organisms. To be sure, many mutagen sensitive strains are caused by abnormalities of the genes included in DNA repair systems. Still, there are some mutants where the responsible genes do not belong to any known DNA repair system. Understanding their phenotypes such as chromosome instability, mitochondrial dysfunction, and senescence is important to advance fundamental knowledge of gene and genome biology.

Chapter 9 Regulation of Gene Transcription by Light in *Neurospora*
Maria Olmedo, Carmen Cuger-Herreros and Luis M. Corrochano
Fungi use light cues to acquire environmental information like day length throughout the year. *Neurospora* adapts its development and behaviour to the changing conditions of the environment using light as a signal for the regulation of gene transcription. *Neurospora* perceives light through the blue light photoreceptor WHITE COLLAR-1 (WC-1). WC-1 dimerizes with WC-2 to form the White Collar Complex (WCC) that activates the transcription of target genes by binding to Light Regulated Elements (LRE) in their promoters. The light-dependent accumulation of certain proteins is responsible for light responses. Light activates genes involved in a variety of processes including development of asexual spores and sexual structures, biosynthesis of photo-protective pigments, and entrainment of the circadian clock. However, the activation of gene transcription by light is transient. After extended illumination, the light-induced transcription ceases and further incubation in the dark is required before transcription in response to light is again activated. This feature, photoadaptation, depends on the blue-light photoreceptor VIVID (VVD). This chapter will present the mechanisms of light perception and regulation of gene expression that lead to light responses in *Neurospora*.

Chapter 10 Regulation and Physiological Function of MAP Kinase and cAMP-PKA Pathways
Masayuki Kamei, Shinpei Banno, Masakazu Takahashi, Akihiko Ichiishi, Fumiyasu Fukumori and Makoto Fujimura
Signal transduction pathways play important roles in growth, differentiation, and pathogenicity of filamentous fungi. *Neurospora crassa* uses two-component histidine kinases and G protein-coupled receptors to sense environmental changes, including osmotic and oxidative stress, chemical challenges, mating pheromone, and nutrient limitation. The environmental signals detected by the receptor/sensor proteins are transmitted to the mitogen-activated protein (MAP) kinase and cAMP-dependent protein kinase (PKA) pathways, both of which play important roles in cellular physiology, including osmoadaptation, mating response, maintenance of cell wall integrity, asexual conidiation, hyphal fusion, circadian response, and accumulation of secondary metabolites. In general, activation of these protein kinases leads to the modification of downstream transcription factors and, consequently, to changes in gene expression. In this chapter, we provide a brief overview of the sensing and signal transduction systems in *N. crassa*, yeasts, and other filamentous fungi, and we focus on the recent progress in our understanding of three different MAP kinase pathways as well as the cAMP-PKA pathway in *N. crassa*.

Chapter 11 Heterotrimeric G Proteins
James D. Kim, Patrick Schacht, Amruta Garud, Gyungsoon Park and Katherine A. Borkovich
One of the major systems used by *Neurospora crassa* to sense and respond to changes in the environment is the heterotrimeric G protein signaling pathway. This system translates signals detected by G protein coupled receptors (GPCRs) or the cytosolic protein RIC8 to an associated intracellular heterotrimeric G protein (α, β and Gγ subunit) to regulate GDP/GTP exchange on the Gα protein. Gα-GTP and the Gβ γdimer have the potential to regulate downstream effectors. In *N. crassa*, all five characterized G protein subunits have some function in sexual and asexual growth and development, nutrient sensing or stress responses. Biochemical evidence indicates that the Gβ and Gγ subunits form a heterodimer, and that loss of either subunit leads to degradation of Gα proteins. GPCRs have been implicated in the pheromone response (PRE-1 and PRE-2), perithecial development (GPR-1) and carbon sensing (GPR-4). GTP binding assays using purified proteins demonstrate that RIC8 activates GDP/GTP exchange on two Gα proteins. cAMP is an important second messenger that regulates aspects of asexual and sexual development. Furthermore, metabolomics experiments using 1H-NMR support a role for one G Gα protein in nutrient sensing.

Chapter 12 Calcium Signaling
Ranjan Tamuli, Ravi Kumar, Dhruv Aditya Srivastava and Rekha Deka
The filamentous fungus *Neurospora crassa* possesses a complex Ca^{2+}- signaling system consisting of 48 Ca^{2+}-signaling proteins. Ca^{2+} is stored in several intracellular stores such as vacuoles, plasma membrane vesicles, microsomes, and mitochondria; however, second messenger systems responsible for Ca^{2+}-release from internal stores have not been identified in *N. crassa* or any other filamentous fungi. The cytosolic free Ca^{2+} ($[Ca^{2+}]_c$) can be measured in living *N. crassa* by using Ca^{2+}-sensitive devices such as microelectrodes, fluorescent probes, or aequorin which is a photoprotein

TH-1227_09610609

isolated from the jellyfish *Aeqorea victoria*. In *N. crassa*, the $[Ca^{2+}]_c$ is ~100 nM that -is effectively regulated by the Ca^{2+} signaling machinery -as high concentrations of Ca^{2+} are toxic, and minute change of $[Ca^{2+}]_c$ may trigger several cell processes. In *N. crassa*, Ca^{2+} signaling is known to be involved in regulating several processes such as Ca^{2+} stress tolerance, circadian clocks, growth, ion transport, sexual development, and UV survival. The Ca^{2+}-signaling genes and proteins in *N. crassa* have several characteristic sequence features. Analysis of Ca^{2+}-signaling in mutants and the availability of the genome sequence has provided deep insight into the functions for some Ca^{2+}-signaling genes in *N. crassa*.

Chapter 13 Carotenoid Biosynthesis in *Neurospora*
Javier Avalos and Luis M. Corrochano
Neurospora produces a mixture of carotenoid and apocarotenoid pigments, with the orange xanthophyll neurosporaxanthin as the major component. The five genes needed to produce this carboxylic apocarotenoid, in sequential order *al-3, al-2, al-1, cao-2* and *ylo-1*, are known and the encoding enzymes have been biochemically investigated. Neurosporaxanthin biosynthesis is induced by light at the level of transcription through the specific action of the White Collar complex, a photoreceptor and transcription factor. Additionally, the pathway is developmentally induced during conidiogenesis and carotenoids are accumulated in the conidia in the dark. The function of the carotenoids has not been well established, but different observations point to protective roles against sun exposure and oxidative stress.

Chapter 14 The *Neurospora* Circadian System: From Genes to Proteins and Back, in Less Than 24 Hours
Alejandro Montenegro-Montero and Luis F. Larrondo
Circadian clocks confer close to 24-hours rhythms to a large number of processes in most organisms across different evolutionary lineages. These endogenous cellular timekeepers regulate rhythms in gene expression, physiology and behavior and enable organisms to anticipate predictable environmental variations. Studies conducted in the ascomycete *Neurospora crassa* have been instrumental in unveiling the molecular and genetic basis of the emergent property of time-telling. The *Neurospora* circadian system integrates a series of cellular processes, including light perception, phosphorylation and dephosphorylation, nuclear trafficking, signal transduction pathways, chromatin remodeling and transcriptional regulation among others, that give rise to a robust pacemaker capable of coordinating rhythmic control of several aspects of *Neurospora* biology, the most obvious one being the daily appearance of asexual spores. This chapter will provide an overview of the major advances in the field, with an emphasis on the later discoveries propelled by the release of the *Neurospora* genome and the adoption of functional genomic strategies. In addition, the state of the art in the studies of the *Neurospora* circadian system will be discussed, along with the main challenges and opportunities ahead.

Chapter 15 *Neurospora* Gene and Genome Analysis: Past Through Future
Aric Wiest, Scott E. Baker and Kevin McCluskey
As modern biological research has developed, so has the analysis of *Neurospora* biology. From beginnings as a simple genetic system to the present where high throughput analysis enables questions in every area of biological inquiry, research on *Neurospora* continues to set a high standard for all filamentous fungal experimental systems. Analysis of materials developed over fifty years at the Fungal Genetics Stock Center (FGSC) using a variety of techniques including genetic mapping, cosmid walking, and gene and whole genome sequencing reveals both new information and reinforces discoveries made over many years. *Neurospora* is and will continue to be the premier organism for studies of the biology of filamentous fungi.

How to buy this book

(EAN: 9781908230126 Subjects: [microbiology] [genomics] [mycology])

Recommended reading: Molecular Biology | PCR | Genomics | Epigenetics | Non-coding RNAs
Home | Microbiology Books | Molecular Biology Books | Virology Books | PCR Books | Medical Microbiology | Microbiology Conferences | Microbiology Blog | Newsletter

TH-1227_09610609

Calcium Signalling

12

Ranjan Tamuli, Ravi Kumar, Dhruv Aditya Srivastava and Rekha Deka

Abstract

The filamentous fungus *Neurospora crassa* possesses a complex Ca^{2+}-signalling system consisting of 48 Ca^{2+}-signalling proteins. Ca^{2+} is stored in several intracellular stores such as vacuoles, plasma membrane vesicles, microsomes, and mitochondria; however, second messenger systems responsible for Ca^{2+}-release from internal stores have not been identified in *N. crassa* or any other filamentous fungi. The cytosolic free Ca^{2+} ($[Ca^{2+}]_c$) can be measured in living *N. crassa* by using Ca^{2+}-sensitive devices such as microelectrodes, fluorescent probes, or aequorin, which is a photoprotein isolated from the jellyfish *Aeqorea victoria*. In *N. crassa*, the $[Ca^{2+}]_c$ is ~ 100 nM and is effectively regulated by the Ca^{2+} signalling machinery as high concentrations of Ca^{2+} are toxic, and a minute change in $[Ca^{2+}]_c$ may trigger several cell processes. In *N. crassa*, Ca^{2+} signalling is known to be involved in regulating several processes such as Ca^{2+} stress tolerance, circadian clocks, growth, ion transport, sexual development, and UV survival. The Ca^{2+}-signalling genes and proteins in *N. crassa* have several characteristic sequence features. Analysis of Ca^{2+}-signalling in mutants and the availability of the genome sequence has provided deep insight into the functions for some Ca^{2+}-signalling genes in *N. crassa*.

Introduction

Calcium ion (Ca^{2+}) is a ubiquitous second messenger molecule that plays a versatile role in intracellular signalling in eukaryotes (Gadd, 1994; Berridge *et al.*, 1998; Shaw and Hoch, 2001; Sanders *et al.*, 2002; Davies and Terhzaz, 2009). Binding of Ca^{2+} changes protein conformation and charge, which are the two universal signalling tools of signal transduction, and thus govern protein functions (Clapham, 2007). The incredible versatility of Ca^{2+}-signalling ranges from processes such as fertilization, development and differentiation, and several other cellular activities including cell death (Berridge *et al.*, 1998). In filamentous fungi, Ca^{2+}-signalling plays an important role in a range of processes such as Ca^{2+} stress tolerance, cell cycle progression, circadian clocks, cytoskeletal organization, growth, hyphal tip branching, infection structure differentiation, secretion, sporulation, sexual development, and ultraviolet (UV) survival (Ohya *et al.*, 1991; Gadd, 1994; Shaw and Hoch, 2001; Deka *et al.*, 2011; Tamuli *et al.*, 2011). However, knowledge about the main components involved in any one Ca^{2+}-mediated signal response pathway is still unclear for filamentous fungi (Galagan *et al.*, 2003; Borkovich *et al.*, 2004). In the filamentous fungus *Neurospora crassa*, hyphal growth has been shown to require a tip-high intracellular $[Ca^{2+}]$ gradient (Silverman-Gavrila and Lew, 2000; Levina *et al.*, 1995). Moreover, cytoplasmic elevation of Ca^{2+} with the divalent cation ionophore A23187 induces hyperbranching in *N. crassa*, suggesting that Ca^{2+} is involved in the branching signal (Reissig and Kinney, 1983; Lew *et al.*, 2008).

Distribution of calcium in *N. crassa* organelles

In *N. crassa*, the vacuolar uptake of Ca^{2+} is responsible for sequestering excess and hazardous amounts of free Ca^{2+} from the cytosol (Cornelius

TH-1227_09610609

and Nakashima, 1987). Ca^{2+} uptake by vacuoles is decreased in absence of $MgSO_4$ in the reaction mixture, indicating that Mg^{2+} has a role in vacuolar uptake of Ca^{2+}. Moreover, vacuolar transport of Ca^{2+} is possibly coupled to an H^+-ATPase (Cornelius and Nakashima, 1987).

It has been demonstrated that most of a cell's Ca^{2+} is sequestered in vacuoles (Bowman *et al.*, 2011). Approximately 10% of the total cellular Ca^{2+} is present in the pellet and the remaining 90% is distributed in three separate cell fractions comprising of dense organelle, heterogeneous microsome, and high-speed supernatant. The dense organelle fraction is composed primarily of mitochondria and vacuoles, however, mitochondria contain only 4% of cellular Ca^{2+}. The microsomal fraction accounts for ~40% of the Ca^{2+} and includes endoplasmic reticulum, Golgi, nuclei, plasma membranes, and various transport vesicles. The source of most of the Ca^{2+} in the high-speed supernatant fraction that contains ~40% Ca^{2+} was likely from the broken vacuoles. Interestingly, all the Ca^{2+} in the vacuolar fraction is soluble, while 90% of the microsomal fraction is insoluble and remained in the pellet. These results supports the hypothesis that >90% of cell Ca^{2+} is sequestered in vacuoles with a significant amount in an insoluble form (Bowman *et al.*, 2011).

Measurement of intracellular calcium concentrations

The cytosolic free Ca^{2+} ($[Ca^{2+}]_c$) can be measured using Ca^{2+}-sensitive fluorescent probes (Caswell, 1979; Schmid and Harold, 1988), microelectrodes (Miller *et al.*, 1990; Silverman-Gavrila and Lew, 2003), and aequorin (Nelson *et al.*, 2004). The Ca^{2+}-selective microelectrode based technique revealed that the mean estimate of $[Ca^{2+}]_C$ in *Neurospora* is 92 ± 15 nM and this value is insensitive to external pH in the range 5.8–8.4 (Miller *et al.*, 1990).

Chlortetracycline (CTC) forms a fluorescent complex with Ca^{2+}, and therefore, it can be used to determine the gradient of intracellular Ca^{2+} (Schmid and Harold, 1988). In this method, *N. crassa* is grown on Fries' agar medium (Davis and de Serres, 1970) supplemented with 100 µm CTC (dissolved in 0.1% dimethyl sulfoxide) and CTC fluorescence is then studied (CTC:400–440 nm excitation filter, 460 nm beam splitter, and 470 nm emission filter). CTC fluorescence is affected by membrane density and Mg^{2+} ions. However, relative CTC fluorescence is much greater for membrane-associated Ca^{2+} than Mg^{2+} (Hallett *et al.*, 1972) and the distribution of intracellular membranes can be assessed with N-phenyl-1-naphthylamine fluorescence (NPN: 380/9 nm excitation filter, 405 nm beam splitter, and 470 nm emission filter; Schmid and Harold, 1988).

Ca^{2+}-selective microelectrodes can be constructed using micropipettes containing a sensor mixture (Tsien and Rink, 1980; Miller *et al.*, 1990). Microelectrodes are then impaled with individual 'cells' (50–100 µm long and 12–15 µm diameter) in a stepwise manner and free Ca^{2+} is derived from the analysis of the pre- and post-impalement calibration data (Miller *et al.*, 1990). This technique has been successfully modified and improved to measure the Ca^{2+} gradient in *N. crassa* (Levina *et al.*, 1995; Silverman-Gavrila and Lew, 2001; 2003). Essentially, the micropipette is filled with Ca^{2+}-sensitive fluorescent dyes such as fluo-3 and Fura Red and subsequently, hyphae are impaled at some distance behind the tip (Silverman-Gavrila and Lew, 2003). The $[Ca^{2+}]_c$ is then imaged and quantified using dual-dye ratio imaging (Silverman-Gavrila and Lew, 2003). In another method, the growing edge of a colony is cultured in dark for 18–20 hours in the presence of two different dyes, Ca^{2+}-sensitive fluo-3 and Ca^{2+}-insensitive SNARF-1 (Levina *et al.*, 1995). Only a few growing hyphae accumulate the dyes, these hyphae are then rinsed with Vogel's medium (pH 4.2) and observed under a confocal microscope (Levina *et al.*, 1995).

It has been recently shown that codon-optimized aequorin can be used for Ca^{2+} measurement in living filamentous fungi including *N. crassa*. Aequorin is a Ca^{2+}-binding photoprotein from the jellyfish, *Aequorea victoria* (Charbonneau *et al.*, 1985; Inouye *et al.*, 1985). It is composed of a ~22 kDa apo-aequorin (the apoprotein), an imidazopyrazine compound called coelenterazine (the luciferin) and bound oxygen (Kendall and Badminton, 1998; Nelson *et al.*, 2004). The protein has three EF-hand Ca^{2+}-binding sites. On Ca^{2+}

TH-1227_09610609

binding to aequorin, a conformational change converts aequorin into an oxygenase (luciferase) that catalyses the oxidation of coelenterazine to form excited phenolate anion of coelenteramide (Kendall and Badminton, 1998). The excited coelenteramide remains non-covalently bound to apo-aequorin, releasing the energy as blue light (λ_{max} = 470 nm) as it relaxes to the ground state (Shimomura and Johnson, 1975; Hirano *et al.*, 1994; Kendall and Badminton, 1998). Thus, the amount of luminescence is dependent upon the concentration of free Ca^{2+}, and therefore, aequorin has been extensively used to investigate intracellular $[Ca^{2+}]_c$ in several systems including living *N. crassa* (Nelson *et al.*, 2004).

Calcium signalling system in *N. crassa*

N. crassa has a complex Ca^{2+}-signalling system consisting of 48 Ca^{2+}-signalling proteins and this system appears to be significantly different from plant and animal cells, especially in relation to second messenger systems responsible for Ca^{2+}-release from internal stores (Galagan *et al.*, 2003; Borkovich *et al.*, 2004; Zelter *et al.*, 2004). *N. crassa* lacks recognizable inositol-1,4,5-trisphosphate ($InsP^3$) receptors, which mediate Ca^{2+} release from intracellular stores in plant and animal cells (Galagan *et al.*, 2003; Borkovich *et al.*, 2004). Moreover, key components of Ca^{2+} release mechanisms in plant and animal cells such as ADP ribosyl cyclase and ryanodine receptor proteins are absent in *N. crassa* (Galagan *et al.*, 2003). *N. crassa* also lacks extracellular Ca^{2+}-sensing receptor protein, as reported in animal cells for sensing changes in the extracellular concentration of Ca^{2+} (Brown *et al.*, 1993; Borkovich *et al.*, 2004). Interestingly, both Ca^{2+}/Na^+ and Ca^{2+}/H^+ exchangers are present in fungi, while animal possess only Ca^{2+}/Na^+ exchangers and plant contain only Ca^{2+}/H^+ exchangers (Borkovich *et al.*, 2004).

The *N. crassa* Ca^{2+}-signalling genes possess several regulatory sequences. The Kozak sequence, consensus sequence for initiation of translation, of the 48 Ca^{2+}-signalling genes is C43(A35/C35)G41C45C52(A68/G20)(C43/A27/T18)C54**A100T100G**100G54C48 (Table 12.1). The consensus is similar to the Kozak sequence described for *N. crassa* (C57NNNC77A81(A44/C43)'T'3**A99T100G99**G51C53; Bruchez *et al.*, 1993), with few differences (Srivastava and Tamuli, unpublished). The methionine start codon (ATG) is 100% conserved within the Kozak sequence of all the 48 Ca^{2+}-signalling genes. The prevalence of stop codons TAA, TAG, and TGA are, respectively, ~47% (23/48), ~29% (14/48), and ~22% (11/48).

In addition, BLASTP search (http://blast.ncbi.nlm.nih.gov/Blast.cgi; Altschul *et al.*, 1997, 2005) with the default parameters for each of the 48 Ca^{2+}-signalling proteins against the non-redundant protein sequence databases at the NCBI shows the respective best overall match in other organisms (Table 12.1; Kumar and Tamuli, unpublished).

Types of calcium signalling proteins in *N. crassa*

The Ca^{2+}-signalling proteins of *N. crassa* can be grouped into seven different types. *N. crassa* has three Ca^{2+} channel proteins, nine Ca^{2+}-and cation-ATPases, six recognizable Ca^{2+}/H^+ exchangers, two novel putative Ca^{2+}/Na^+ exchangers, four novel phospholipase C-δ subtype (PLC-δ) proteins, 23 Ca^{2+} and/or calmodulin (CaM) binding proteins, and one CaM (Galagan *et al.*, 2003; Borkovich *et al.*, 2004; Zelter *et al.*, 2004). These proteins effectively coordinate to maintain Ca^{2+} homeostasis in *N. crassa* and respond to change in $[Ca^{2+}]_c$ through a Ca^{2+} signalling cascade (Fig. 12.1).

Calcium channel proteins

Ca^{2+} channel proteins are present in the cell membranes and regulate passive influx of Ca^{2+} into the cytoplasm (Bootman *et al.*, 2001; Zetler *et al.*, 2004). Ca^{2+} channel proteins are activated through several different activation mechanisms based on which they are classified into different groups (Bootman *et al.*, 2001). In *N. crassa*, two Ca^{2+} channel genes NCU02762 and NCU11680 contain one and two introns, respectively, and these two as well as the another Ca^{2+} channel protein NCU06703 contain conserved domains (Fig. 12.2). The NCU02762, NCU06703, and

TH-1227_09610609

Table 12.1: Ca^{2+}-signaling proteins in *N. crassa*

S. no.	NCU no.	Kozak sequence[a]	Stop codon	Name[b]	Type of protein	Best overall (e-value; organism; protein name; accession number)
1.	02762.5	TCTGTCAAA**ATG**AGC	TAA		Ca^{2+} permeable channel	0; *Verticillium dahliae* (cch1, EGY18507.1)
2.	06703.5	GCGCTTGCG**ATG**CAC	TAG		Ca^{2+} permeable channel	2e-97; *Paracoccidioides brasiliensis* (MID1, EEH23338.1)
3.	11680.5[c]	CAGGGCAGC**ATG**GCA	TGA		Ca^{2+} permeable channel	0; *Ajellomyces dermatitidis* (Yvc1, EGE78766.1)
4.	03305.5	TTTGTGAAT**ATG**GAG	TAG	NCA1	Ca^{2+} -ATPase	0; *Trichophyton tonsurans* (SCA-1, EGD96734.1)
5.	04736.5	CCAGCTATC**ATG**GCG	TAA	NCA2	Ca^{2+} -ATPase	0; *Magnaporthe oryzae* (Plasma membrane calcium-transporting ATPase 3, EHA56671.1)
6.	05154.5	ACAGCGCTC**ATG**GCG	TAG	NCA3	Ca^{2+} -ATPase	0; *Glomerella graminicola* (Calcium-translocating P-type ATPase, EFQ29373.1)
7.	03292.5	TCCGCCATC**ATG**GAC	TAG	PMR1	Ca^{2+} -ATPase	0; *Uncinocarpus reesii* (PMR1, XP_002541437.1)
8.	08147.5	GGATATTGA**ATG**GGG	TAA	PH-7	Ca^{2+} -ATPase	0; *Glomerella graminicola* (Potassium/sodium efflux P-type ATPase, EFQ36596.1)
9.	04898.5	ACCGCTATC**ATG**GCG	TGA		Ca^{2+} -ATPase	0; *Cordyceps militaris* (Cation-transporting ATPase 4, EGX91104.1)
10.	03818.5	CAATGCGGA**ATG**CCT	TAA		Ca^{2+} -ATPase	0; *Verticillium dahliae* (Neo1p, EGY18069.1)
11.	07966.5	CATGCCATA**ATG**GCA	TAA		Cation-ATPase	0; *Trichophyton tonsurans* (Cta3p, EGD97988.1)
12.	10143.5[d]	AGCGCCAAC**ATG**AAC	TAA		Cation-ATPase	0; *Cordyceps militaris* (ATPase type 13A2, EGX92563.1)
13.	07075.5	CGCAAAACC**ATG**GGC	TAA	CAX	Ca^{2+}/H^{+} exchanger	0; *Glomerella graminicola* (Calcium/proton exchanger, EFQ30300.1)
14.	00916.5	TCCATTTCG**ATG**AAG	TAG		Ca^{2+}/H^{+} exchanger	2e-176; *Aspergillus fumigates* (Membrane bound cation transporter, XP_001481534.1)
15.	00795.5	CTTCACGTC**ATG**CCG	TAA		Ca^{2+}/H^{+} exchanger	1e-149; *Aspergillus niger* (Membrane bound cation transporter, XP_001400827.2)
16.	06366.5	AAACACACC**ATG**ACA	TAA		Ca^{2+}/H^{+} exchanger	0; *Sclerotinia sclerotiorum* (Ca^{2+}/H^{+} antiporter, XP_001589752.1)
17.	07711.5	TCTAACGCA**ATG**TCT	TAG		Ca^{2+}/H^{+} exchanger	4e-160; *Trichophyton tonsurans* (Vacuolar calcium ion transporter/H^{+} exchanger, EGD98067.1)
18.	05360.5	CCCCTCACT**ATG**GGT	TGA		Ca^{2+}/H^{+} exchanger	0; *Metarhizium anisopliae* (Calcium permease, EFY95914.1)
19.	02826.5	AGGTCCAGC**ATG**TCG	TAG		Ca^{2+}/Na^{+} exchanger	0; *Verticillium albo-atrum* (Sodium/calcium exchanger protein, XP_003004985.1)
20.	08490.5	TACACATCG**ATG**GCG	TGA		Ca^{2+}/Na^{+} exchanger	1e-83; *Aspergillus niger* (Sodium/calcium transporter, XP_001397155.1)
21.	01266.5	CCCAACATC**ATG**TCT	TGA		Phospholipase C	0; *Sordaria macrospora* (Phosphoinositide-specific phospholipase C, XP_003348116.1)

TH-1227_09610609

S. no.	NCU no.	Kozak sequence[a]	Stop codon	Name[b]	Type of protein	Best overall (e-value; organism; protein name; accession number)
22.	06245.5	GTATTCAAC**ATG**CCA	TAA	PLC-1	Phospholipase C	0; *Glomerella graminicola* (Phosphatidylinositol-specific phospholipase C, EFQ28596.1)
23.	11415.5[e]	GTACGTAAC**ATG**GAT	TGA		Phospholipase C	0; *Glomerella graminicola* (Phosphatidylinositol-specific phospholipase C, EFQ31595.1)
24.	02175.5	TTTCCAACA**ATG**TCG	TGA		Phospholipase C	3e-125; *Botryotinia fuckeliana* (BcPLC2, CCD34776.1)
25.	04120.5	TATATCAAG**ATG**GTA	TAA	CaM	Calmodulin	1e-103; *Gibberella zeae* (CaM, XP_382067.1)
26.	03804.5	ACCAGAGAC**ATG**GAA	TAA	CNA-1	Calcineurin catalytic subunit	0; *Sordaria macrospora* (Serine/threonine-protein phosphatase 2B catalytic subunit protein, XP_003352213.1)
27.	03833.5	GCAGCAACC**ATG**GGC	TAG	CNB-1	Calcineurin regulatory subunit /variant	2e-119; *Trichoderma reesei* (Calcineurin, beta subunit, EGR44907.1)
28.	09265.5	GCCTTCATC**ATG**AGG	TAA		Calnexin	0; *Sordaria macrospora* (cnx1, XP_003347545.1)
29.	05225.5[f]	GAACAAACA**ATG**CTG	TAA		Ca^{2+} and/or CaM binding protein	0; *Magnaporthe oryzae* (Mitochondrial NADH dehydrogenase, EHA47323.1)
30.	02115.5	ATCACCACC**ATG**GAA	TAG		Ca^{2+} and/or CaM binding protein	0; *Magnaporthe oryzae* (EF hand domain-containing protein, EHA48778.1)
31.	01564.5	CAAGCCGGC**ATG**GAC	TAA		Ca^{2+} and/or CaM binding protein	0; *Magnaporthe oryzae* (Calcium dependent mitochondrial carrier protein, EHA48778.1)
32.	06948.5	ACCGCAAAT**ATG**GTG	TAA		Ca^{2+} and/or CaM binding protein	2e-54; *Mycosphaerella graminicola* (Calcium ion binding, calmodulin, EGP88834.1)
33.	04379.5	TATCCGAAA**ATG**GGC	TAA	NCS-1	Ca^{2+} and/or CaM binding protein	4e-126; *Grosmannia clavigera* (Neuronal calcium sensor 1, EFX03580.1)
34.	02738.5	GACACAGCC**ATG**GCC	TGA	PEF-1	Ca^{2+} and/or CaM binding protein	2e-130; *Verticillium dahliae* (Peflin, EGY21808.1)
35.	09871.5	AAACTCGCC**ATG**GCA	TGA		Ca^{2+} and/or CaM binding protein	4e-33; *Verticillium dahliae* (Centrin-3, EGY16271.1)
36.	01241.5	ACAGTCGCC**ATG**TCC	TAA		Ca^{2+} and/or CaM binding protein	0; *Trichoderma reesei* (Mitochondrial carrier protein, EGR44893.1)
37.	06347.5	ACCGCGACA**ATG**CCG	TAA		Ca^{2+} and/or CaM binding protein	0; *Sordaria macrospora* (Actin cytoskeleton-regulatory complex protein, XP_003350109.1)
38.	06617.5	TGAGACACA**ATG**GTA	TAA		Ca^{2+} and/or CaM binding protein	7e-93; *Verticillium albo-atrum* (Myosin regulatory light chain cdc4, XP_003009631.1)
39.	03750.5	GCGCCGCAT**ATG**CGC	TGA		Ca^{2+} and/or CaM binding protein	8e-74; *Botryotinia fuckeliana* (Calmodulin, XP_001560827.1)

TH-1227_09610609

S. no.	NCU no.	Kozak sequence[a]	Stop codon	Name[b]	Type of protein	Best overall (e-value; organism; protein name; accession number)
40.	08980.5	CGACCAACC**ATG**GCG	TAA	NDE-1	Ca^{2+} and/or CaM binding protein	0; *Grosmannia clavigera* (Alternative NADH-dehydrogenase, EFX03867.1)
41.	02283.5	TTAGCGACC**ATG**AGT	TAG		Ca^{2+} and/or CaM binding protein	0; *Sordaria macrospora* (Calcium/ calmodulin-dependent protein kinase type I, XP_003344498.1)
42.	09123.5	ATTGACACC**ATG**AGC	TAG		Ca^{2+} and/or CaM binding protein	0; *Sporothrix schenckii* (Calcium/ calmodulin-dependent kinase, AAV80434.1
43.	02814.5	CCAGCAGCC**ATG**GCT	TAA	PRD-4	Ca^{2+} and/or CaM binding protein	0; *Grosmannia clavigera* (Serine/ threonine-protein kinase chk2, EFX01629.1)
44.	09212.5	TCCGACAAA**ATG**TCG	TAG		Ca^{2+} and/or CaM binding protein	0; *Verticillium dahliae* (Serine/ threonine-protein kinase srk1, EGY15110.1)
45.	06650.5	ACCATCAAG**ATG**AAG	TAG		Ca^{2+} and/or CaM binding protein	3e-61; *Nectria haematococca* (Phospholipase A2, XP_003042542.1)
46.	02411.5	GCCGCCATA**ATG**GTC	TGA		Ca^{2+} and/or CaM binding protein	0; *Glomerella graminicola* (Microtubule associated protein, EFQ31793.1)
47.	06177.5	CAAAGCACA**ATG**GCC	TAG		Ca^{2+} and/or CaM binding protein	0; *Magnaporthe grisea* (CMKK2, ACM41720.1)
48.	04265.5	CTTCCAAAC**ATG**ACA	TAA		Ca^{2+} and/or CaM binding protein	7e-85; *Bacillus megaterium* (Beta-fructosidase FruA, AEN90524.1)

[a]The initiation codon ATG is shown in bold; [b]References are given in the text; [c]Split from NCU07605.1; [d] Split from NCU01437.1; [e] Split from NCU09655.1; [f]NCU05225.5 (was indicated as NCU08980.1 in Borkovich *et al.*, 2004)

NCU11680 (changed from NCU07605) proteins are classified into group I, II, and III Ca^{2+}-permeable channels, respectively, based on BLAST analysis (Zetler *et al.*, 2004).

NCU06703 gene encodes MID-1, a stretch-activated (mechanosensitive) protein, and the *mid-1* knockout mutant exhibits slow growth rate, lower basal turgor, and hypersensitivity to low extracellular [Ca^{2+}] and high intracellular [Ca^{2+}] (Lew *et al.*, 2008). The *Saccharomyces cerevisiae* homologue of MID-1, the *MID1* (*m*ating-*i*nduced *d*eath), is required for Ca^{2+} influx and mating (Iida *et al.*, 1994).

Calcium- and cation-ATPases

TH-1227_09610609

Ca^{2+}- and cation-ATPases are located in plasma membrane and organelle membrane. They hydrolyse ATP to catalyse active Ca^{2+}-efflux across biological membranes, and maintain a steep Ca^{2+} gradient across the plasma membrane (Hao *et al.*, 1994; Moller *et al.*, 1996). In *N. crassa*, nine ATPases have been identified, seven of them are Ca^{2+}-and cation-ATPases and remaining two are cation-ATPases. All the nine ATPases possess introns in their genes as well as conserved cation trasporter/ATPase domain in the proteins (Fig. 12.3).

The NCU03305, NCU04736, NCU05154, NCU03292, and NCU08147 genes encode NCA1, NCA2, NCA3, PMR1, and PH-7 proteins, respectively (Benito *et al.*, 2000). In a phylogentic analysis with type II ATPases (Sorin *et al.*, 1997; BanÄuelos and RodriÂguez-Navarro, 1998), the *N. crassa* ATPases are found distributed in different branches; NCA1 in SERCA (sarcoplasmic reticulum Ca^{2+}), NCA2 and NCA3 in PMCA (plasma membrane Ca^{2+}),

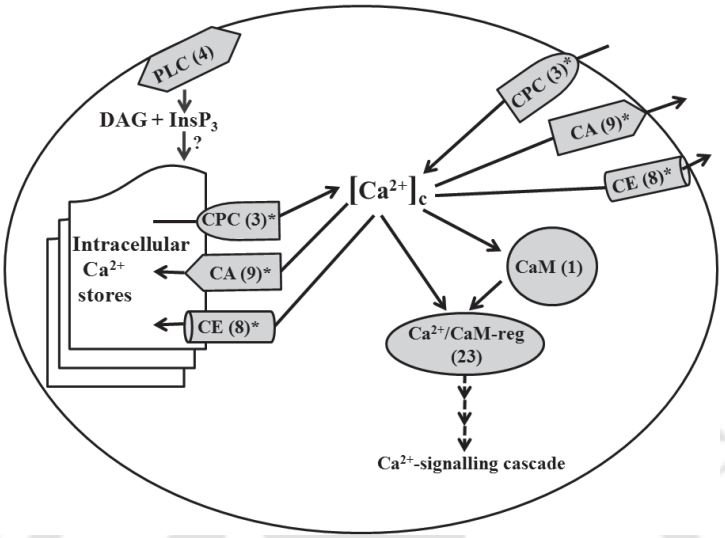

Figure 12.1 Overview of calcium signalling system in *N. crassa*. Numbers in parentheses indicate the number of genes identified in that class and asterisk indicates that the location in the plasma membrane and/or organelle membranes are not determined (Galagan *et al.*, 2003; Borkovich *et al.*, 2004; Zelter *et al.*, 2004). CPC, Ca^{2+}-permeable channel; CA, Ca^{2+}-and cation-ATPases; CE, Ca^{2+}/H^{+} and Ca^{2+}/Na^{+} exchanger; CaM, calmodulin; Ca^{2+}/CaM-reg, calcium- and calmodulin regulated; PLC, phospholipase C; DAG, diacylglycerol; $InsP^3$, inositol-1,4,5-trisphosphate. Minute change in $[Ca^{2+}]_c$ may lead to a Ca^{2+} signalling cascade via Ca^{2+}/CaM-reg proteins.

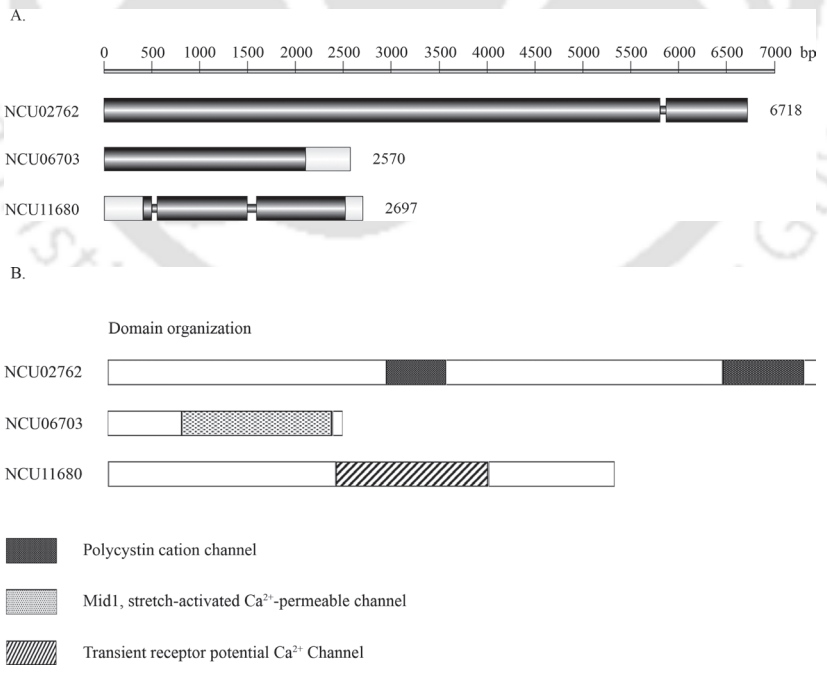

Figure 12.2 Ca^{2+} channel proteins. (A) Gene structure showing the exons (black bar) in the open reading frame (ORF), introns (black line), and untranslated regions (UTRs, light grey bar). (B) Conserved domain organization of the Ca^{2+} channel proteins as predicted using the NCBI conserved domain database (CDD, http://www.ncbi.nlm.nih.gov/Structure/cdd/wrpsb.cgi) search (Marchler-Bauer *et al.*, 2009, 2011).

TH-1225-09610609

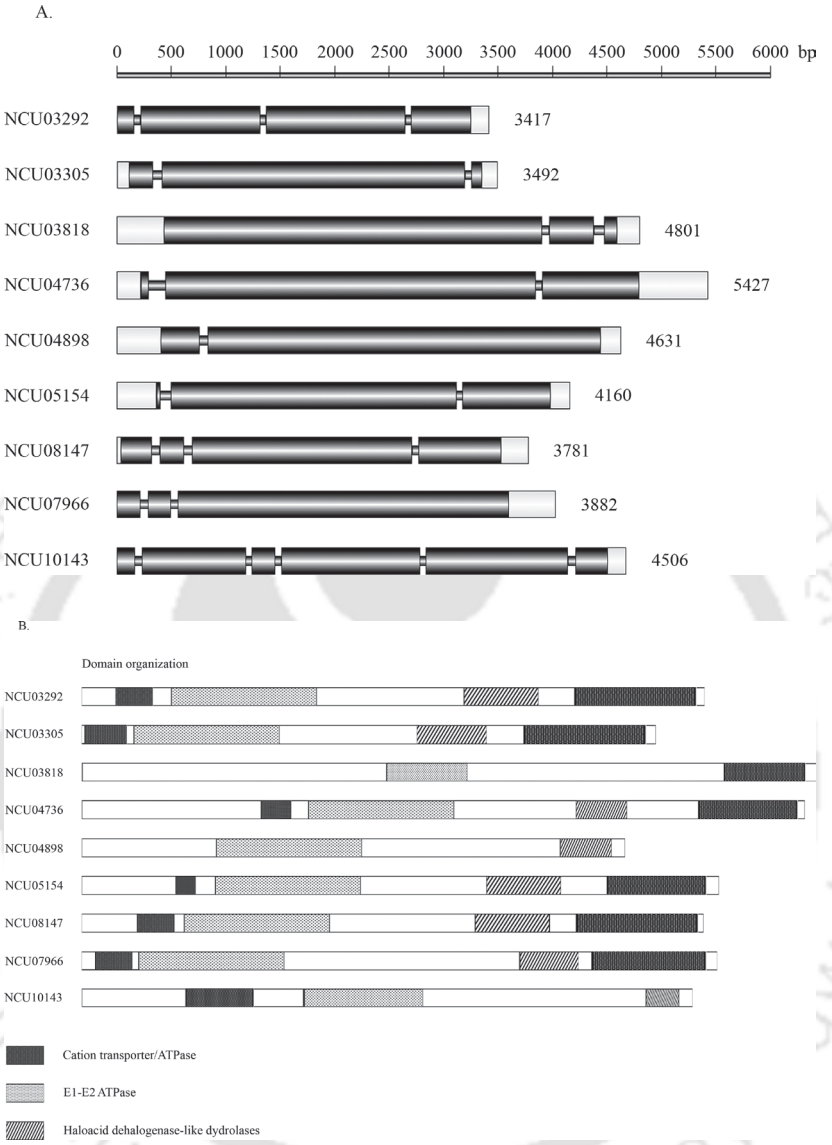

Figure 12.3 Calcium- and cation-ATPases. (A) Gene structure showing the exons (black bar) in the ORF, introns (black line), and UTRs (light grey bar). (B) Conserved domain organization of the Ca^{2+} and cation-ATPases as predicted using the NCBI CDD search.

PMR1 in PMR1, and PH-7 in ENA (*exitus natru*; Latin, 'exit sodium') branch (Haro *et al.*, 1991; Benito *et al.*, 2000).

Analysis of mRNA expression in various external conditions indicates that with the exception of PMR1, the main function of NCA1, NCA2, NCA3, and PH-7 is the adaptation to stress conditions (Benito *et al.*, 2000). Strains lacking NCA-1 and NCA-3 have no obvious defects either in growth or distribution of Ca^{2+} (Bowman *et al.*, 2011). However, lack of NCA-2 results in slow growth, Ca^{2+} sensitivity, and female sterility (Bowman *et al.*, 2011). Besides, a strain lacking NCA-2 accumulates more Ca^{2+} than the wild-type, indicating that it functions in the plasma membrane to pump Ca^{2+} out of the cell. Although, the *N. crassa nca-2* is the homologue of *S. cerevisiae PMC1*, they appear to be functionally different. Unlike Ca^{2+} accumulation in the *N. crassa nca-2* mutant, *S. cerevisiae* cells lacking PMC1 take up

TH-1227_09610609

80% less Ca^{2+} (Cunningham and Fink, 1994; Bowman *et al.*, 2011). Therefore, NCA-2 is more similar to the PMC-type proteins of animal cell than the Pmc1p in *S. cerevisiae* that resides in the vacuole (Bowman *et al.*, 2011). Another cation-ATPase knockout, the ΔNCU04898.2 mutant shows a slow growth phenotype (Sarma and Tamuli, unpublished).

Calcium exchangers

Ca^{2+}-exchangers exchange positive ions across membranes to reduce high $[Ca^{2+}]_c$ to resting level and to transport Ca^{2+} into intracellular Ca^{2+}-stores. In plants, H^+/Ca^{2+} antiport system accounts for Ca^{2+} accumulation in the vacuole with a minimum H^+:Ca^{2+} stoichiometry of at least 3 (Blackford *et al.*, 1990). Evidence in *N. crassa* suggest that the ATP-driven H^+/Ca^{2+} exchange system has a stoichiometric ratio of at least 2 H^+/Ca^{2+} (Miller *et al.*, 1990). *N. crassa* has six Ca^{2+}/H^+ exchangers and two Ca^{2+}/Na^+ exchangers, and all of them contain introns (Fig. 12.4). Among the Ca^{2+}/H^+ exchangers, NCU07075 encodes CAX, and strains lacking *cax* accumulate very little Ca^{2+} in the dense vacuolar fraction (Bowman *et al.*, 2011).

The Na^+/Ca^{2+} exchangers in animal cells exchange Ca^{2+} for the Na^+ with a stoichiometry of 3 Na^+/Ca^{2+} (Reeves and Hale, 1984; Kang and Hilgemann, 2004), however, a transport stoichiometry of 4 Na^+/Ca^{2+} is also reported (Mullins, 1977; Fujioka *et al.*, 2000). The major function of the Na^+/Ca^{2+} exchangers is to remove Ca^{2+} from the cytoplasm; however, exchangers are fully reversible and may allow Ca^{2+} entry under special conditions (Lytton *et al.*, 2007). Two Ca^{2+}/Na^+ exchangers, NCU02826 and NCU08490, have been identified in *N. crassa* genome. All of the *N. crassa* exchanger proteins contain conserved Ca^{2+}-exchanger domains (Fig. 12.4).

Phospholipase C-δ subtype (PLC-δ) proteins

N. crassa possesses four novel phospholipase C-δ subtype (PLC-δ) proteins (Galagan *et al.*, 2003; Borkovich *et al.*, 2004). PLC-δ acts on a plasma membrane phospholipid, phosphotidylinositol 4,5-biphosphate (PIP2) to synthesize second messengers inositol1,4,5-triphosphate ($InsP_3$, also IP_3) and 1,2-diacylglycerol (DAG) (Berridge,1987; 1993). $InsP_3$, induces Ca^{2+} release from vacuoles (Cornelius *et al.*, 1989), and it is present in the lipid extract of *N. crassa* mycelia (Lakin-Thomas, 1993). Besides, two types of IP_3-activated Ca^{2+} channels, one with low conductance (13 picosiemens) and another one with high conductance (77 picosiemens), are demonstrated in *N. crassa* (Silverman-Gavrila and Lew, 2002). Furthermore, the low-conductance channel generates tip-high Ca^{2+} gradient required for hyphal growth (Silverman-Gavrila and Lew, 2002). However, no recognizable $InsP_3$ receptor could be identified in the *N. crassa* genome (Galagan *et al.*, 2003). Therefore, it remains to be determined if $InsP_3$ receptors in *N. crassa* differ from those found in animal cells (Galagan *et al.*, 2003; Borkovich *et al.*, 2004). On the other hand, the second messenger DAG regulates protein kinase C (PKC), however, both the PKCs identified in *N. crassa* lack a C2 domain with Ca^{2+} binding sites (Schmitz and Heinisch, 2003; Borkovich *et al.*, 2004).

N. crassa genome analysis has identified four novel PLC-δ subtypes, NCU01266, NCU02175, NCU06245, and NCU11415, and they contain conserved domains (Table 12.1; Fig. 12.5). The null mutant of NCU06245.1, generated using repeat-induced point mutation (RIP; Selker *et al.*, 1987), grows slowly in a 'spreading colonial' (Garnjobst and Tatum, 1967) manner and displays defects in hyphal size, proportion and branching (Gavric *et al.*, 2007). The mutant contains residual PLC activity, indicating redundancy of this enzyme. NCU06245 gene is highly variable among the natural isolates of *N. crassa*. Divergences are present throughout the gene; however, most of the sequence divergence is in a coding sequence from amino acid positions 200 to 250 unique to *Neurospora* (Gavric *et al.*, 2007).

Calcium and/or calmodulin binding proteins

N. crassa genome analysis has identified 23 genes encoding for Ca^{2+} and/or CaM binding proteins and except NCU02115 and NCU04265, all of them contain introns in the genomic organization

TH-1227_09610609

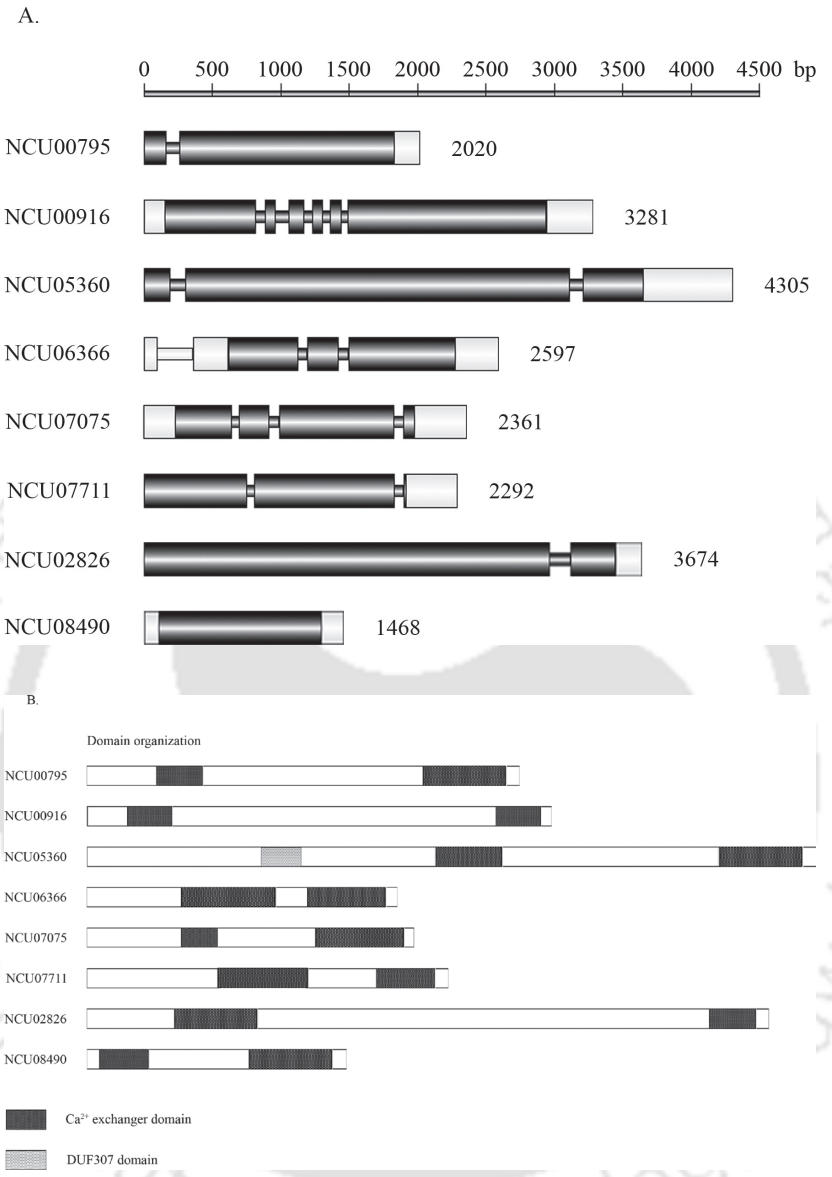

Figure 12.4 Calcium exchangers. (A) Organization of the exons (black bar) in the ORF, introns (black line), and UTRs (light grey bar) of the exchangers. (B) Predicted conserved domains of the exchanger proteins using the NCBI CDD search.

(Fig. 12.6). Occurrence of introns within the coding sequence is frequent and except for the NCU02155 and NCU04265 genes, other 21 genes encoding for Ca^{2+} and/or CaM binding proteins contain introns with a frequency of ~ 2.5 introns per gene. Therefore, the frequency of introns in these 21 genes is higher than the average 1.7 introns per gene in the *N. crassa* genome (Galagan *et al.*, 2003).

TH-1227_09610609

Ca^{2+} and/or CaM binding proteins have several conserved domains like N-terminal catalytic domain, EF-hand Ca^{2+}-binding sites, autoinhibitory and overlapping CaM-binding domain etc. (Fig. 12.6). Little is known about Ca^{2+} and/or CaM binding proteins *N. crassa*.

NCU02283 and NCU09123 encode Ca^{2+}/CaM-dependent protein kinases (Ca^{2+}/CaMKs) Ca^{2+}/CaMKI and CAMK-1, respectively (Deka

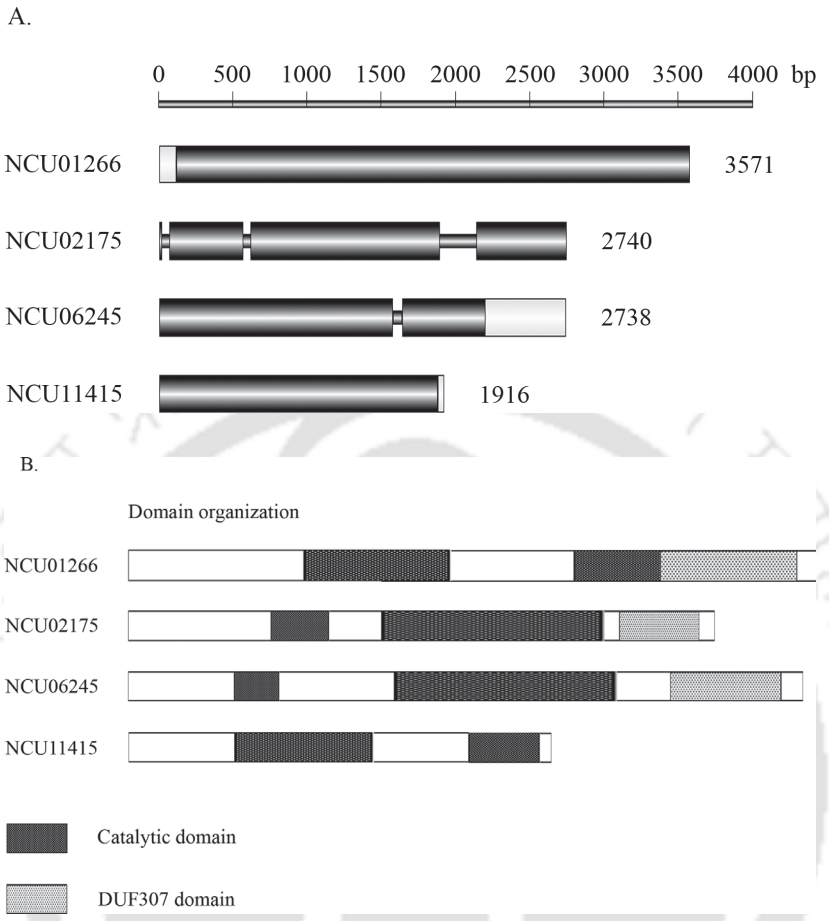

Figure 12.5 Phospholipase C-δ subtypes. (A) Structural organization of the exons (black bar) in the ORF, introns (black line), and UTRs (light grey bar) of the phospholipase C-δ subtypes. (B) Conserved domain organization of the PLC-δ subtypes as revealed by the NCBI CDD search.

et al., 2011; Tamuli *et al.*, 2011). NCU04379 gene encodes a homologue of NCS-1 that possesses a consensus signal for N-terminal myristoylation and four EF hands, which are characteristic features of Neuronal Calcium Sensor-1 (NCS-1) proteins (Deka *et al.*, 2011; Tamuli *et al.*, 2011). The first EF-hand of the NCS-1 proteins is unable to bind Ca^{2+} due to presence of a conserved Cys-Pro substitution in the Ca^{2+}-binding loop (Burgoyne and Weiss, 2001). The Cys-Pro substitution is also present in the EF1 of the *N. crassa* homologue of NCS-1 (Deka *et al.*, 2011). Frq1, the *S. cerevisiae* homologue of NCS-1, binds to a conserved sequence motif in phosphatidylinositol 4-kinase (Pik1) and stimulates its catalytic activity *in vitro* (Hendricks *et al.*, 1999; Huttner *et al.*, 2003; Strahl *et al.*, 2007). However, the target motif of NCS-1 in *N. crassa* remains unknown.

Some of the genes encoding for Ca^{2+} and/or CaM binding protein have been studied using knockout mutants. Knockout mutant for the gene NCU09123 shows modest phase delay, a small period lengthening, light-induced phase shifting of the circadian conidiation rhythm, and a transient slow growth phenotype (Yang *et al.*, 2001). Additionally, crosses homozygous for ΔNCU09123.2 mutant display an intermediate phenotype (produce few hundred ascospores). Besides, crosses homozygous for ΔNCU02283.2 mutant strains display barren phenotype (produce very few ascospores). However, crosses heterozygous for these two mutants are fully fertile. These results

TH-1227_09610609

TH-1227_09610609

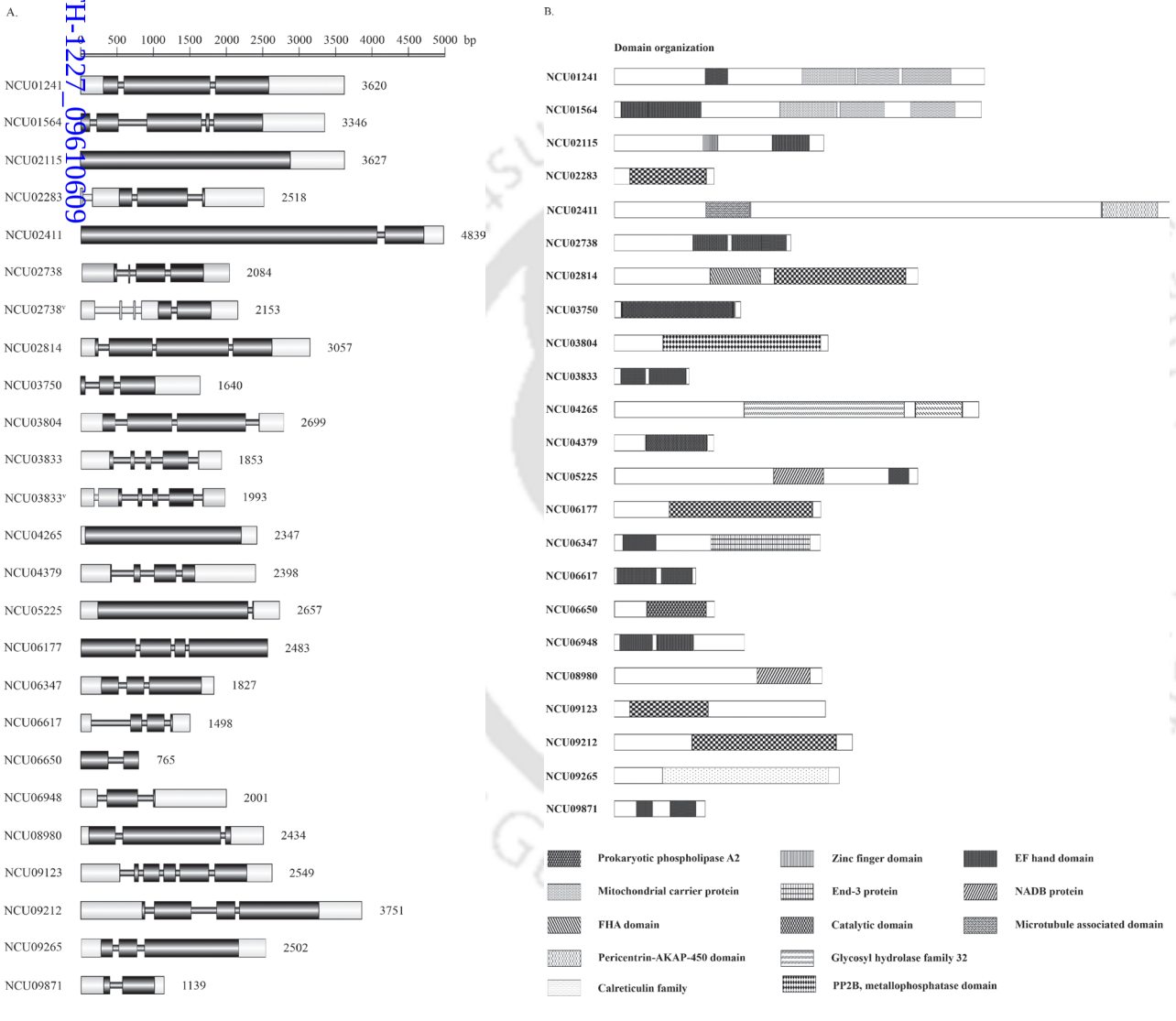

Figure 12.6 Calcium and/or calmodulin binding proteins. (A) Genomic organization of the exons (black bar) in the ORF, introns (black line), and UTRs (light grey bar). NCU02738^{v} and NCU03833^{v} are the predicted variant transcripts of NCU02738 and NCU03833, respectively. (B) Conserved domain organization of the Ca^{2+} and/or CaM binding proteins as revealed by the NCBI CDD search.

indicate that NCU09123 and NCU02283 genes have a role in full fertility in *N. crassa* (Deka *et al.*, 2011; Kumar and Tamuli, unpublished). In addition, preliminary work suggested that NCU02283 gene is not essential for in mating-type-associated *v*egetative *i*ncompatibility (*vic*; Glass *et al.*, 2000; Gedela and Tamuli, unpublished).

Another Ca^{2+}/CaM gene, NCU04379, encodes a homologue of NCS-1 that has a role in growth, Ca^{2+} stress tolerance, and ultraviolet (UV) survival (Deka *et al.*, 2011). The slow growth phenotype of the ΔNCU04379.2 mutant is not due to a defect in sterol biosynthesis since the mutant has the wild-type ergosterol profile (Deka *et al.*, 2011). The ΔNCU04379.2 mutant shows hypersensitivity to $CaCl_2$ stress; however, this is not due to a mere osmotic effect since sucrose and NaCl stress have no effect on the mutant. Moreover, the $CaCl_2$ hypersensitivity phenotype of the mutant can be suppressed on media supplemented with EGTA that has high affinity and selectivity for free Ca^{2+} (Tsien, 1980). Therefore, ΔNCU04379.2 has a higher Ca^{2+} sensitivity phenotype relative to the wild-type (Deka *et al.*, 2011).

Calcineurin is a CaM-dependent protein phosphatase consisting of a catalytic subunit A that binds to CaM (Winkler *et al.*, 1984), and a regulatory subunit B that binds Ca^{2+} (Klee and Crouch, 1979). Conditional expression of the antisense RNA for the *cna-1*, the *N. crassa* catalytic subunit of calcineurin, results in extensive hyphal branching, altered hyphal morphology, loss of the apical tip-high Ca^{2+} gradient, and ultimately, growth arrest (Prokisch *et al.*, 1997). Calcineurin B mutant, *cnb-1*, displays an abnormal morphology indicating that calcineurin regulatory subunit B is required for normal vegetative growth in *N. crassa* (Kothe and Free, 1998). The regulatory subunit of calcineurin was purified from *N. crassa* based on its binding to the CDRE sequence (AGCCTC) of the copper-induced metallothionein (CuMT) gene, indicating that calcineurin has a putative role in the regulation of CuMT gene expression (Kumar *et al.*, 2006).

Another Ca^{2+} and/or CaM binding protein is the NDE-1, also known as the external NADPH dehydrogenase of *N. crassa* mitochondria, contains a Ca^{2+}-binding motif (Melo *et al.*, 1999, 2001; Borkovich *et al.*, 2004; Carneiro *et al.*, 2007). Moreover, the NDE-1 protein contains two dinucleotide binding sites (presumably for FAD and NAD(P)H), consensus GXGXXG, and it has been shown *in vitro* that the NADPH oxidation activity of the NDE-1 protein is Ca^{2+}-dependent (Melo *et al.*, 1999, 2001).

TH-1227_09610609

Calmodulin

In *N. crassa*, CaM was isolated using affinity chromatography and identified based on its characteristic Ca^{2+}-dependent shift in electrophoretic migration, activation of bovine heart CAMP-phosphodiesterase (PDE), and distinct peaks (located at 276, 268, 264, 258 and 252 nm) in an absorption spectrum (Ortega Perez *et al.*, 1981). The complete cDNA encoding *N. crassa* CaM was isolated from a λZAP II cDNA expression library and its sequence analysis identified a protein of 140 amino acid residues (Capelli *et al.*, 1993). Moreover, Southern analysis of *N. crassa* genomic DNA indicated that CaM is encoded by a single-copy gene (Capelli *et al.*, 1993). The genome analysis also confirmed presence of only one CaM in *N. crassa* (Galagan *et al.*, 2003; Borkovich *et al.*, 2004). The *N. crassa* CaM shows 85% sequence identity with the human CaM protein (Melnick *et al.*, 1993).

Coding sequence of the CaM encoding gene NCU04120 contains six exons and five introns, and CaM possesses conserved EF-hand domains (Fig. 12.7). The NCU04120.2 homokaryotic strains could not be isolated from the initial hetrokaryotic knockout strain, suggesting that NCU04120 might be essential for viability (Deka and Tamuli, unpublished). *N. crassa* CaM over-expressed in *Escherichia coli* appears to be identical to the native protein with respect to its molecular weight, electrophoretic properties, and activation of Ca^{2+}-CaM-dependent protein kinase activity (Capelli *et al.*, 1993).

CaM antagonists, such as trifluroperazine, chlorpromazine, and W-7 inhibit the light-induced phase shifting of the circadian conidiation, suggesting a role of CaM in signal transduction process in *N. crassa* circadian clock (Sadakane and Nakashima, 1996). CaM also has a possible role in the activation of *N. crassa* chitin synthase (Suresh and Subramanyan, 1997).

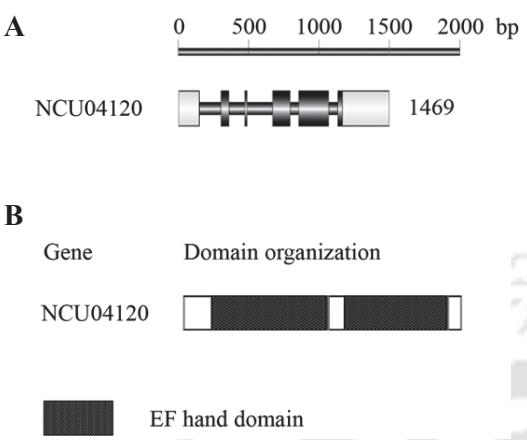

Figure 12.7 Calmodulin. (A) Gene structure showing exons (black bar) in the ORF, introns (black line), and UTRs (light grey bar). (B) Conserved domain organization of the CaM protein as revealed by the NCBI CDD search.

Conclusions

Ca^{2+} is a universal second messenger molecule that plays a versatile role in signal transduction process. Analysis of *N. crassa* genome (Galagan *et al.*, 2003; Borkovich *et al.*, 2004) has revealed several unique features of its Ca^{2+}-signalling system such as (i) *N. crassa* lacks receptor proteins, like those found in plant and animal cells, for Ca^{2+}-release from internal stores; (ii) No external Ca^{2+}-sensing receptor has been identified in the *N. crassa* genome, like those found in animal cells; and (iii) Both Ca^{2+}/Na^{+} and Ca^{2+}/H^{+} exchangers are present in *N. crassa*. The Ca^{2+}-signalling machinery of *N. crassa* has three Ca^{2+} channel proteins, nine Ca^{2+} and cation-ATPases, six Ca^{2+}/H^{+} exchangers, two Ca^{2+}/Na^{+} exchangers, four PLC-δ proteins, 23 Ca^{2+} and/or CaM binding proteins, and one CaM (Galagan *et al.*, 2003; Borkovich *et al.*, 2004; Zelter *et al.*, 2004).

The *Neurospora* genome project (http://www.dartmouth.edu/~neurosporagenome/proj_overview.html) has generated a large number of Ca^{2+}-signalling knockout mutants available for functional analysis, essentially using a high-throughput gene knockout procedure (Colot *et al.*, 2006). Analysis of knockout mutant for a stretch-activated (mechanosensitive) Ca^{2+} channel protein, *mid-1*, has a defect in Ca^{2+} homeostasis suggesting that it plays a role in ion transport (Lew *et al.*, 2008). Ca^{2+}-and cation-ATPases NCA1, NCA2, NCA3, and PH-7 function primarily for adaption to stress conditions (Benito *et al.*, 2000). In addition, NCA-2 has a role in growth, Ca^{2+} efflux, and female fertility (Bowman *et al.*, 2011). Another cation-ATPase NCU04898 has a putative role in growth (Sarma and Tamuli, unpublished). Among the Ca^{2+}/H^{+} exchangers, CAX has a role in accumulation of Ca^{2+} in the vacuole (Bowman *et al.*, 2011). The null mutant of NCU06245, a PLC-δ subtype, displays slow growth and aberrant hyphal branching (Gavric *et al.*, 2007). Moreover, the NCU06245 gene is highly variable, mostly in a coding sequence from amino acid positions 200 to 250 unique to *Neurospora*, among the natural isolates of *N. crassa* (Gavric *et al.*, 2007). The 23 genes coding for Ca^{2+} and/or CaM binding proteins constitute the largest group of *N. crassa* Ca^{2+}-signalling proteins. Interestingly, genes coding for Ca^{2+} and/or CaM binding proteins have a high intron density, introns are of different sizes and present in different positions. This could be a mechanism to escape from RIP-induced gene silencing. RIP has resulted in very few closely related genes in the *N. crassa* genome (Galagan *et al.*, 2003; also see the Chapter 7). Two Ca^{2+}/CaMKs, Ca^{2+}/CaMKI and CAMK-1 have a role in sexual development, and lack of CAMK-1 protein affects circadian conidiation rhythm (Yang *et al.*, 2001; Deka *et al.*, 2011; Tamuli *et al.*, 2011; Kumar and Tamuli, unpublished). Another Ca^{2+} and/or CaM binding protein, NCS-1 has a role in growth, Ca^{2+} and UV stress tolerance (Deka *et al.*, 2011). The UV-sensitivity phenotype of the NCU04379.2 mutant revealed a novel function for the *N. crassa* homologue of NCS-1, suggesting its involvement in UV-induced DNA damage repair process (Deka *et al.*, 2011). UV light absorption may cause formation of cyclobutane pyrimidine dimers (CPD) (Lippke *et al.*, 1981) and pyrimidine (6–4) pyrimidone photoproducts (6–4PP) (Mitchell and Nairn, 1989) that result in DNA damage. UV-induced DNA damage may either lead to induction of DNA repair mechanisms, essential for cell survival, or apoptosis (Lo *et al.*, 2005). The CaM-dependent protein phosphatase calcineurin is consisting of a catalytic subunit and a regulatory subunit (Klee and Crouch, 1979; Winkler *et al.*, 1984). Catalytic

TH-1227_09610609

subunit of calcineurin has a role in maintenance of the apical tip-high Ca^{2+} gradient and is essential for growth of *N. crassa* (Prokisch *et al.*, 1997). Regulatory subunit of calcineurin is required for normal vegetative growth and it has a putative role in the regulation of CuMT gene expression in *N. crassa* (Kothe and Free, 1998; Kumar *et al.*, 2006). The NDE-1 protein contains a Ca^{2+}-binding motif and *in vitro* experiments suggested that the NADPH oxidation activity of the NDE1protein is Ca^{2+}-dependent (Melo *et al.*, 1999, 2001). *N. crassa* possesses only one CaM that appears to be essential for viability and it has possible roles in signal transduction process in circadian clock and activation chitin synthase (Capelli *et al.*, 1993; Sadakane and Nakashima, 1996; Suresh and Subramanyan, 1997; Galagan *et al.*, 2003; Borkovich *et al.*, 2004; Deka and Tamuli, unpublished).

Notwithstanding the importance of Ca^{2+} as a central player of intracellular signalling system, our understanding of Ca^{2+}-signalling in *N. crassa* has remained elusive. However, recent availability of the genome sequence and the knockout mutants has made it possible to gain detailed information about the molecular components of the *N. crassa* Ca^{2+}-signalling system. Therefore, detailed information about the Ca^{2+}-mediated response pathways is expected to emerge in the near future.

Acknowledgements

We thank Fungal Genetics Stock Center (FGSC) for providing strains free of charges. RK and RD were supported by Junior and Senior Research Fellowships from the MHRD and CSIR-UGC, respectively, DAS was supported by an MTech Fellowship from the DBT. This work was supported in part by a NE-Twining grant (DBT), and a SERC FAST Track grant (DST) to RT.

References

Altschul, S.F., Madden, T.L., Schäffer, A.A., Zhang, J., Zhang, Z., Miller, W., and Lipman, D.J. (1997). Gapped BLAST and PSI-BLAST: a new generation of protein database search programs. Nucleic Acids Res. *25*, 3389–3402.

Altschul, S.F., Wootton, J.C., Gertz, E.M., Agarwala, R., Morgulis, A., Schäffer, A.A., and Yu, Y.K. (2005). Protein database searches using compositionally adjusted substitution matrices. FEBS J. *272*, 5101–5109.

BanÄuelos, M.A., and RodriÂguez-Navarro, A. (1998). P-type ATPases mediate sodium and potassium effluxes in *Schwanniomyces occidentalis*. J. Biol. Chem. *273*, 1640–1646.

Benito, B., Garciadeblas, B., and Rodriguez-Navarro, A. (2000). Molecular cloning of the calcium and sodium ATPases in *Neurospora crassa*. Mol. Microbiol. *35*, 1079–1088.

Berridge, M.J. (1987). Inositol trisphosphate and diacylglycerol: two interacting second messengers. Annu. Rev. Biochem. *56*, 159–193.

Berridge, M.J. (1993). Inositol trisphosphate and calcium signalling. Nature *361*, 315–325.

Berridge, M.J., Bootman, M.D., and Lipp, P. (1998). Calcium-a life and death signal. Nature *395*, 645–648.

Blackford, S., Rea, P.A., and Sanders, D. (1990). Voltage sensitivity of H^+/Ca^{2+} antiport in higher plant tonoplast suggests a role in vacuolar calcium accumulation. J. Biol. Chem. *265*, 9617–9620.

Bootman, M.D., Collins, T.J., Peppiatt, C.M., Prothero, L.S., MacKenzie, L., De Smet, P., Travers, M., Tovey, S.C., Seo, J.T., Berridge, M.J., *et al.* (2001). Calcium signalling – an overview. Semin. Cell Dev. Biol. *12*, 3–10.

Borkovich, K.A., Alex, L.A., Yarden, O., Freitag, M., Turner, G.E., Read, N.D., Seiler, S., Bell-Pedersen, D., Paietta, J., Plesofsky, N., *et al.* (2004). Lessons from the genome sequence of *Neurospora crassa*: tracing the path from genomic blueprint to multicellular organism. Microbiol. Mol. Biol. Rev. *68*, 1–108.

Bowman, B.J., Abreu, S., Margolles-Clark, E., Draskovic, M., and Bowman, E.J. (2011). Role of four calcium transport proteins, encoded by *nca-1*, *nca-2*, *nca-3*, and *cax*, in maintaining intracellular calcium levels in *Neurospora crassa*. Eukaryot. Cell *10*, 654–661.

Brown, E.M., Gamba, G., Riccardi, D., Lombardi, M., Butters, R., Kifor, O., Sun, A., Hediger, M.A., Lytton, J., and Hebert, S.C. (1993). Cloning and characterization of an extracellular Ca^{2+}-sensing receptor from bovine parathyroid. Nature *366*, 575–580.

Bruchez, J.J.P., Eberli, J., and Russo, V.E.A. (1993). Regulatory sequences involved in the translation of *Neurospora crassa* mRNA: Kozak sequences and stop codons. Fungal Genet. Newslett. *40*, 85–88.

Burgoyne, R.D., and Weiss, J.L. (2001). The neuronal calcium sensor family of Ca^{2+}-binding proteins. Biochem. J. *353*, 1–12.

Carneiro, P., Duarte, M., and Videira, A. (2007). The external alternative NAD(P)H dehydrogenase NDE3 is localized both in the mitochondria and in the cytoplasm of *Neurospora crassa*. J. Mol. Biol. *368*, 1114–1121.

Capelli, N., van Tuinen, D., Ortega Perez, R., Arrighi, J.F., and Turian, G. (1993). Molecular cloning of a cDNA encoding calmodulin from *Neurospora crassa*. FEBS Lett. *321*, 63–68.

Caswell, A.H. (1979). Methods of measuring intracellular calcium. Int. Rev. Cyto. *56*, 145–181.

TH-1227_09610609

Charbonneau, H., Walsh, K.A., McCann, R.O., Prendergast, F.G., Cormier, M.J., and Vanaman, T.C. (1985). Amino acid sequence of the calcium-dependent photoprotein aequorin. Biochemistry *24*, 6762–6771.

Clapham, D.E. (2007). Calcium Signalling. Cell *131*, 1047–1058.

Colot, H.V., Park, G., Turner, G.E., Ringelberg, C., Crew, C.M., Litvinkova, L., Weiss, R.L., Borkovich, K.A., and Dunlap, J.C. (2006). A high-throughput gene knockout procedure for *Neurospora* reveals functions for multiple transcription factors. Proc. Natl. Acad. Sci. U.S.A. *103*, 10352–10357.

Cornelius, G., and Nakashima, H. (1987). Vacuoles play a decisive role in calcium homeostasis in *Neurospora crassa*. J. Gen. Microbiol. *133*, 2341–2347.

Cornelius, G., Gebauer, G., and Techel, D. (1989). Inositol trisphosphate induces calcium release from *Neurospora crassa* vacuoles. Biochem. Biophys. Res. Commun. *162*, 852–856.

Cunningham, K.W., and Fink, G.R. (1994). Calcineurin-dependent growth control in *Saccharomyces cerevisiae* mutants lacking PMC1, a homolog of plasma membrane Ca^{2+} ATPases. J. Cell. Biol. *124*, 351–363.

Davis, R.H., and De Serres, F.J. (1970). Genetic and microbiological research techniques for *Neurospora crassa.* Methods Enzymol. *17*, 79–143.

Davies, S.A., and Terhzaz, S. (2009). Organellar calcium signalling mechanisms in *Drosophila* epithelial function. J. Exp. Biol. *212*, 387–400.

Deka, R., Kumar, R., and Tamuli, R. (2011). *Neurospora crassa* homologue of Neuronal Calcium Sensor-1 has a role in growth, calcium stress tolerance, and ultraviolet survival. Genetica *139*, 885–894.

Fujioka, Y., Komeda, M., and Matsuoka, S. (2000). Stoichiometry of Na^{+}-Ca^{2+} exchange in inside-out patches excised from guinea-pig ventricular myocytes. J. Physiol. *523 Pt 2*, 339–351.

Gadd, G.M. (1994). Signal transduction in fungi. In The Growing Fungus, Gow, N.A.R., and Gadd, G.M., eds (Chapman & Hall, London), pp. 183–210.

Galagan, J.E., Calvo, S.E., Borkovich, K.A., Selker, E.U., Read, N.D., Jaffe, D., FitzHugh, W., Ma, L.J., Smirnov, S., Purcell, S., *et al.* (2003). The genome sequence of the filamentous fungus *Neurospora crassa*. Nature *422*, 859–868.

Garnjobst, L., and Tatum, E.L. (1967). A survey of new morphological mutants in *Neurospora crassa*. Genetics *57*, 579–604.

Gavric, O., dos Santos, D.B., and Griffiths, A. (2007). Mutation and divergence of the phospholipase C gene in *Neurospora crassa*. Fungal Genet. Biol. *44*, 242–249.

Glass, N.L., Jacobson, D.J., and Shiu, P.K. (2000). The genetics of hyphal fusion and vegetative incompatibility in filamentous ascomycete fungi. Annu. Rev. Genet.*34*, 165–186.

Hallett, M., Schneider, A.S., and Carbone, E. (1972). Tetracycline fluorescence as calcium-probe for nerve membrane with some model studies using erythrocyte ghosts. J. Membr. Biol. *10*, 31–44.

Hao, L., Rigaud, J.L., and Inesi, G. (1994). Ca^{2+}/H^{+} countertransport and electrogenicity in proteoliposomes containing erythrocyte plasma membrane Ca-ATPase and exogenous lipids. J. Biol. Chem. *269*, 14268–14275.

Haro, R., Garciadeblas, B., and Rodríguez-Navarro, A. (1991). A novel P-type ATPase from yeast involved in sodium transport. FEBS Lett. *291*, 189–191.

Hendricks, K.B., Wang, B.Q., Schnieders, E.A., and Thorner, J. (1999). Yeast homologue of neuronal frequenin is a regulator of phosphatidylinositol-4-OH kinase. Nat. Cell Biol. *1*, 234–241.

Hirano T., Mizoguchi, I., Yamaguchi, M., Chen, F.-Q., Ohashi, M., Ohmiya, Y., and Tsuji, F.I. (1994). Revision of the structure of the light-emitter in aequorin bioluminescence. Chem. Commun. *2*, 165–167.

Huttner, I.G., Strahl, T., Osawa, M., King, D.S., Ames, J.B., and Thorner, J. (2003). Molecular interactions of yeast frequenin (Frq1) with the phosphatidylinositol 4-kinase isoform, Pik1. J. Biol. Chem. *278*, 4862–4874.

Iida, H., Nakamura, H., Ono, T., Okumura, M.S., and Anraku. Y. (1994). *MID1*, a novel *Saccharomyces cerevisiae* gene encoding a plasma membrane protein, is required for Ca^{2+} influx and mating. Mol. Cell Biol. *14*, 8259–8271.

Inouye, S., Noguchi, M., Sakaki, Y., Takagi, Y., Miyata, T., Iwanaga, S., and Tsuji, F.I. (1985). Cloning and sequence analysis of cDNA for the luminescent protein aequorin. Proc. Natl. Acad. Sci. U.S.A. *82*, 3154–3158.

Kang, T.M., and Hilgemann, D.W. (2004). Multiple transport modes of the cardiac Na^{+}/Ca^{2+} exchanger. Nature *427*, 544–548.

Kendall, J.M., and Badminton, M.N. (1998). *Aequorea victoria* bioluminescence moves into an exciting new era. Trends Biotech. *16*, 216–224.

Klee, C.B., Crouch, T.H., and Krinks, M.H. (1979). Calcineurin: a calcium- and calmodulin-binding protein of the nervous system. Proc. Natl. Acad. Sci. U.S.A. *76*, 6270–6273.

Kothe, G.O., and Free, S.J. (1998). Calcineurin subunit B is required for normal vegetative growth in *Neurospora crassa*. Fungal Genet. Biol. *23*, 248–258.

Kumar, K.S., Ravi Kumar, B., Siddavattam, D., and Subramanyam, C. (2006). Characterization of calcineurin-dependent response element binding protein and its involvement in copper-metallothionein gene expression in *Neurospora*. Biochem. Biophys. Res. Commun. *345*, 1010–1013.

Lakin-Thomas, P.L. (1993). Effects of inositol starvation on the levels of inositol phosphates and inositol lipids in *Neurospora crassa*. Biochem. J. *292*, 805–811.

Levina, N.N., Lew, R.R., Hyde, G.J., and Heath, I.B. (1995). The roles of Ca^{2+} and plasma membrane ion channels in hyphal tip growth of *Neurospora crassa*. J. Cell Sci. *108*, 3405–3417.

Lew, R.R., Abbas, Z., Anderca, M.I., and Free, S.J. (2008). Phenotype of a mechanosensitive channel mutant, *mid-1*, in a filamentous fungus, *Neurospora crassa*. Eukaryot. Cell *7*, 647–655.

Lippke, J.A., Gordon, L.K., Brash, D.E., and Haseltine, W.A. (1981). Distribution of UV light-induced

TH-1227_09610609

damage in a defined sequence of human DNA: detection of alkaline-sensitive lesions at pyrimidine nucleoside-cytidine sequences. Proc. Natl. Acad. Sci. U.S.A. *78*, 3388–3392.

Lo, H.L., Nakajima, S., Ma, L., Walter, B., Yasui, A., Ethell, D.W., and Owen, L.B. (2005). Differential biologic effects of CPD and 6–4PP UV-induced DNA damage on the induction of apoptosis and cell-cycle arrest. BMC Cancer *5*, 135.

Lytton, J. (2007). Na^+/Ca^{2+} exchangers: three mammalian gene families control Ca^{2+} transport. Biochem. J. *406*, 365–382.

Marchler-Bauer, A., Anderson, J.B., Chitsaz, F., Derbyshire, M.K., DeWeese-Scott, C., Fong, J.H., Geer, L.Y., Geer, R.C., Gonzales, N.R., Gwadz, M., *et al.*, (2009). CDD: specific functional annotation with the Conserved Domain Database. Nucleic Acids Res. *37*, D205–D210.

Marchler-Bauer, A., Lu, S., Anderson, J.B., Chitsaz, F., Derbyshire, M.K., DeWeese-Scott, C., Fong, J.H., Geer, L.Y., Geer, R.C., Gonzales, N.R., *et al.* (2011). CDD: a conserved domain database for the functional annotation of proteins. Nucleic Acids Res. *39*, D225–D229.

Melnick, M.B., Melnick, C., Lee, M., and Woodward, D.O. (1993). Structure and sequence of the calmodulin gene from *Neurospora crassa*. Biochim. Biophys. Acta *1171*, 334–336.

Melo, A.M., Duarte, M., and Videira, A. (1999). Primary structure and characterisation of a 64 kDa NADH dehydrogenase from the inner membrane of *Neurospora crassa* mitochondria. Biochim. Biophys. Acta *1412*, 282–287.

Melo, A.M., Duarte, M., Moller, I.M., Prokisch, H., Dolan, P.L., Pinto, L., Nelson, M.A., and Videira, A. (2001). The external calcium-dependent NADPH dehydrogenase from *Neurospora crassa* mitochondria. J. Biol. Chem. *276*, 3947–3951.

Miller, A.J., Vogg, G., and Sanders, D. (1990). Cytosolic calcium homeostasis in fungi: roles of plasma membrane transport and intracellular sequestration of calcium. Proc. Natl. Acad. Sci. U.S.A. *87*, 9348–9352.

Mitchell, D.L., and Nairn, R.S. (1989). The biology of the (6–4) photoproduct. Photochem Photobiol. *49*, 805–819.

Moller, J.V., Juul, B., and le Maire, M. (1996). Structural organization, ion transport, and energy transduction of P-type ATPases. Biochim. Biophys. Acta *1286*, 1–51.

Mullins, L.J. (1977). A mechanism for Na/Ca transport. J. Gen. Physiol. *70*, 681–695.

Nelson, G., Kozlova-Zwinderman, O., Collis, A.J., Knight, M.R., Fincham, J.R., Stanger, C.P., Renwick, A., Hessing, J.G., Punt, P.J., Van den Hondel, C.A., *et al.* (2004). Calcium measurement in living filamentous fungi expressing codon-optimized aequorin. Mol. Microbiol. *52*, 1437–1450.

Ohya, Y., Kawasaki, H., Suzuki, K., Londesborough, J., and Anraku, Y. (1991). Two yeast genes encoding calmodulin-dependent protein kinases. Isolation, sequencing and bacterial expressions of CMK1 and CMK2. J. Biol. Chem. *266*, 12784–12794.

Ortega Perez, R., Van Tuinen, D., Marmé, D., Cox, J.A.,and Turian, G. (1981).Purification and identification of calmodulin from *Neurospora crassa*. FEBS Lett. *133*, 205–208.

Prokisch, H., Yarden, O., Dieminger, M., Tropschug, M., and Barthelmess, I.B. (1997). Impairment of calcineurin function in *Neurospora crassa* reveals its essential role in hyphal growth, morphology and maintenance of the apical Ca^{2+} gradient. Mol. Gen. Genet. *256*, 104–114.

Reeves, J.P., and Hale, C.C. (1984). The stoichiometry of the cardiac sodium-calcium exchange system. J. Biol. Chem. *259*, 7733–7739.

Reissig, J.L., and Kinney, S.G. (1983). Calcium as a branching signal in *Neurospora crassa*. J. Bacteriol. *154*, 1397–1402.

Sadakane, Y., and Nakashima, H. (1996). Light-induced phase shifting of the circadian conidiation rhythm is inhibited by calmodulin antagonists in *Neurospora crassa*. J. Biol. Rhythms *11*, 234–240.

Sanders, D., Pelloux, J., Brownlee, C., and Harper, J.F. (2002). Calcium at the crossroads of signaling. Plant Cell *14(Suppl.)*, S401–S417.

Schmid, J., and Harold, F.M. (1988). Dual roles for calcium ions in apical growth of *Neurospora crassa*. J. Gen. Microbiol. *134*, 2623–2631.

Schmitz, H.P., and Heinisch, J.J. (2003). Evolution, biochemistry and genetics of protein kinase C in fungi. Curr. Genet. *43*, 245–254.

Selker, E.U., Cambareri, E.B., Jensen, B.C., and Haack, K.R. (1987). Rearrangement of duplicated DNA in specialized cells of *Neurospora*. Cell *51*, 741–752.

Shaw, B.D., and Hoch, H.C. (2001). Biology of the fungal cell. In The Mycota VIII, Howard, R.J., and Gow, N.A.R., eds (Springer-Verlag KG, Berlin), pp. 73–89.

Shimomura, O., and Johnson, F.H. (1975). Regeneration of the photoprotein aequorin. Nature *256*, 236–238.

Silverman-Gavrila, L.B., and Lew, R.R. (2000). Calcium and tip growth in *Neurospora crassa*. Protoplasma *213*, 203–217.

Silverman-Gavrila, L.B., and Lew, R.R. (2001). Regulation of the tip-high $[Ca^{2+}]$ gradient in growing hyphae of the fungus *Neurospora crassa*. Eur. J. Cell Biol. *80*, 379–390.

Silverman-Gavrila, L.B., and Lew, R.R. (2002). An IP3-activated Ca^{2+} channel regulates fungal tip growth. J. Cell Sci. *115*, 5013–5025.

Silverman-Gavrila, L.B., and Lew, R.R. (2003). Calcium gradient dependence of *Neurospora crassa* hyphal growth. Microbiology *149*, 2475–2485.

Sorin, A., Rosas, G., and Rao, R. (1997). PMR1, a Ca2+-ATPase in yeast Golgi, has properties distinct from sarco/endoplasmic reticulum and plasma membrane calcium pumps. J. Biol. Chem. *272*, 9895–9901.

Strahl, T., Huttner, I.G., Lusin, J.D., Osawa, M., King, D., Thorner, J., and Ames, J.B. (2007). Structural insights into activation of phosphatidylinositol 4-kinase (Pik1) by yeast frequenin (Frq1). J. Biol. Chem. *282*, 30949–30959.

TH-1227_09610609

Suresh, K., and Subramanyam, C. (1997). A putative role for calmodulin in the activation of *Neurospora crassa* chitin synthase. FEMS Microbiol. Lett. *150*, 95–100.

Tamuli, R., Kumar, R., and Deka, R. (2011). Cellular roles of neuronal calcium sensor-1 and calcium/calmodulin-dependent kinases in fungi. J. Basic Microbiol. *51*, 120–128.

Tsien, R.Y. (1980). New calcium indicators and buffers with high selectivity against magnesium and protons: design, synthesis, and properties of prototype structures. Biochemistry *19*, 2396–2404.

Tsien, R.Y., and Rink, T.J. (1980). Neutral carrier ion-selective microelectrodes for measurement of intracellular free calcium. Biochim. Biophys. Acta. *599*, 623–638.

Winkler, M.A., Merat, D.L., Tallant, E.A., Hawkins, S., and Cheung, W.Y. (1984). Catalytic site of calmodulin-dependent protein phosphatase from bovine brain resides in subunit A. Proc. Natl. Acad. Sci. U.S.A. *81*, 3054–3058.

Yang, Y., Cheng, P., Zhi, G., and Liu, Y. (2001). Identification of a calcium/calmodulin-dependent protein kinase that phosphorylates the *Neurospora* circadian clock protein FREQUENCY. J. Biol. Chem. *276*, 41064–41072.

Zelter, A., Bencina, M., Bowman, B.J., Yarden, O., and Read, N.D. (2004). A comparative genomic analysis of the calcium signaling machinery in *Neurospora crassa*, *Magnaporthe grisea*, and *Saccharomyces cerevisiae*. Fungal Genet. Biol. *41*, 827–841.

TH-1227_09610609

Genetica (2011) 139:885–894
DOI 10.1007/s10709-011-9592-y

Neurospora crassa homologue of Neuronal Calcium Sensor-1 has a role in growth, calcium stress tolerance, and ultraviolet survival

Rekha Deka · Ravi Kumar · Ranjan Tamuli

Received: 24 September 2010 / Accepted: 22 June 2011 / Published online: 5 July 2011
© Springer Science+Business Media B.V. 2011

Abstract NCU04379 gene encodes a conserved Ca^{2+} and/or calmodulin binding protein that possesses a consensus signal for N-terminal myristoylation and four EF-hands, characteristics of Neuronal Calcium Sensor-1proteins. The NCU04379.2 knockout mutant shows slow growth rate, increased sensitivity to calcium and ultraviolet (UV) irradiation, and a wild-type fragment carrying NCU04379 gene complements the mutant. Therefore, NCU04379 gene has a role in growth, calcium stress tolerance, and UV survival. Crosses homozygous for ΔNCU04379.2 mutant strains were fully fertile; however, we found evidence for involvement of Ca^{2+}/calmodulin-dependent protein kinase encoding genes NCU02283 and NCU09123 in sexual development.

Keywords Calcium signaling genes · Calcium sensitivity · Ca^{2+}/calmodulin-dependent protein kinase · DNA damage · Neuronal Calcium Sensor-1 · Sexual development · UV survival

Introduction

The filamentous fungus *Neurospora crassa* possesses complex calcium (Ca^{2+})-signaling system that appears to be significantly different from plant and animal cells, especially in relation to second messenger systems responsible for Ca^{2+}-release from internal stores (Galagan et al. 2003). The genome analysis of Neurospora has revealed three Ca^{2+} channel proteins, nine Ca^{2+}/cation-ATPases, six recognizable Ca^{2+}/H^{+} exchangers, two novel putative Ca^{2+}/Na^{+} exchangers, four novel phospholipase C-δ subtype (PLC-δ) proteins, 23 Ca^{2+} and/or calmodulin (CaM) binding proteins, and one CaM (Galagan et al. 2003; Borkovich et al. 2004). One of the 23 Ca^{2+} and/or CaM binding proteins, the product of NCU04379 gene, shows significant sequence homology to a protein called Frequenin (Frq) in Drosophila (Pongs et al. 1993), Frq1 in yeast (Hendricks et al. 1999), and Neuronal Calcium Sensor-1 (NCS-1) in mammalian cells (McFerran et al. 1998; Tamuli et al. 2011). These proteins belong to the Neuronal Calcium Sensor (NCS) branch of the CaM superfamily, characterized by a consensus signal for N-terminal myristoylation and four EF-hand Ca^{2+}-binding sites (Johnson et al. 1994; Ames et al. 1996; Strahl et al. 2007; Tamuli et al. 2011). Members of the NCS protein superfamily mediate the effects of the cytosolic Ca^{2+} (Ikura 1996).

Cytosolic Ca^{2+} plays a central role as an intracellular signal, however, high concentrations of Ca^{2+} are toxic to the cell, and therefore, cytosolic free Ca^{2+} ($[Ca^{2+}]_c$) is effectively regulated in Neurospora, Arabidopsis, and human (Cornelius and Nakashima 1987; Sanders et al. 2002; Berridge et al. 1998). The $[Ca^{2+}]_c$ is regulated by specialized proteins, for example, $[Ca^{2+}]_c$ is removed by the ATP-dependent pumps located in the rat plasma membrane (Ambudkar and Baum 1988; Ambudkar et al. 1989; Haghighat and Al-Hashimi 1999). In *N. crassa*, excess and hazardous amounts of $[Ca^{2+}]_c$ are sequestered through vacuolar uptake (Cornelius and Nakashima 1987), although, the mechanism of the vacuolar uptake is still unknown.

One of the versatile Ca^{2+}-signaling proteins, the Ca^{2+}-modulated protein CaM plays an important role in

Electronic supplementary material The online version of this article (doi:10.1007/s10709-011-9592-y) contains supplementary material, which is available to authorized users.

R. Deka · R. Kumar · R. Tamuli (✉)
Department of Biotechnology, Indian Institute of Technology Guwahati, Guwahati 781 039, India
e-mail: ranjantamuli@iitg.ernet.in; ranjan.tam@gmail.com

TH-1227_09610609

mediating the effects of $[Ca^{2+}]_c$ and is believed to be crucial in modulating DNA repair, DNA synthesis, and cell proliferation in both CHO and human cell lines (Chafouleas et al. 1984; Pavelic 1987; Chard 1987; Mirzayans et al. 1995). The process of DNA repair has been extensively studied in *N. crassa*, where three genes, *upr-1* (*ncrev3*), *mus-42* (*ncrev1*), and *mus-26* (*ncrev7*) proved to be induced by DNA damage and function in the mutagenic translesion DNA synthesis (TLS) pathway (Sakai et al. 2002; 2003). However, it is still not known whether and how CaM or any other Ca^{2+}-signaling protein plays a role in DNA damage repair process in *N. crassa*.

Thus far, detailed knowledge about the genes involved in Ca^{2+}-mediated signal response pathway is lacking for *N. crassa* and very few Ca^{2+}-signaling genes have been characterized. To understand the cellular roles of additional Ca^{2+}-signaling genes, we have studied 18 Ca^{2+}-signaling mutants. We report in this paper that a homologue of NCS-1 encoding gene NCU04379 has a role in growth, Ca^{2+} stress tolerance, and UV survival. Moreover, crosses homozygous for ΔNCU04379.2 mutant strains were fully fertile, however, we found evidence for involvement of NCU02283 and NCU09123 genes, encoding a Ca^{2+}/CaM-dependent protein kinase type I and a CAMK-1, respectively, in sexual development.

Materials and methods

Strains, growth, and crosses

The wild-type and Ca^{2+}-signaling mutant strains (Table 1) were obtained from the Fungal Genetics Stock Center (FGSC), University of Missouri, Kansas City, MO 64110 (McCluskey 2003). The Ca^{2+}-signaling mutants were generated using a high-throughput gene knockout procedure, developed by the *Neurospora* genome project (http://www.dartmouth.edu/~neurosporagenome/proj_overview.html; Colot et al. 2006).

Growth, crossing, and maintenance of Neurospora strains were essentially as described by Davis and De Serres (1970). Growth was initially measured by placing either conidia or a plug of agar containing mycelium in the center of a petri dish and colony diameter was measured every 2–3 h to obtain linear rates of diameter increase over a period of 28 h. Strains that show lower growth rate on

Table 1 *N. crassa* strains used in this study

S. no.	FGSC no. (*a*/*A*) blank;or strain no.	NCU no. or strain type	Type of protein	Source
1.	11169/11170	02814.2	Ca^{2+} and/or CaM binding protein	FGSC
2.	11246/11247	06650.2	Ca^{2+} and/or CaM binding protein	FGSC
3.	11403/11404	04379.2	Ca^{2+} and/or CaM binding protein	FGSC
4.	11405/11406	05255.2	Ca^{2+} and/or CaM binding protein	FGSC
5.	11537/11536	06177.2	Ca^{2+} and/or CaM binding protein	FGSC
6.	11541/11542	06948.2	Ca^{2+} and/or CaM binding protein	FGSC
7.	12448/12449	02283.2	Ca^{2+} and/or CaM binding protein	FGSC
8.	12548/12547	09123.2	Ca^{2+} and/or CaM binding protein	FGSC
9.	15898/15899	01564.2	Ca^{2+} and/or CaM binding protein	FGSC
10.	11248/11249	07075.2	Ca^{2+}/H^{+} exchanger	FGSC
11.	11407/11408	06366.2	Ca^{2+}/H^{+} exchanger	FGSC
12.	11685/11686	00916.2	Ca^{2+}/H^{+} exchanger	FGSC
13.	12376/12375	00795.2	Ca^{2+}/H^{+} exchanger	FGSC
14.	11255/11256	08147.2	Ca^{2+}-ATPase	FGSC
15.	11410/11409	07966.2	Cation-ATPase	FGSC
16.	11530/11529	02826.2	Ca^{2+}/Na^{+} exchanger	FGSC
17.	13036/13037	05154.2	Ca^{2+}-ATPase	FGSC
18.	11271/11272	09655.2	Phospholipase C	FGSC
19.	988/987	Wild-type		FGSC
20.	i-94-120a	*erg-3*	Sterol $\Delta^{14,15}$-reductase	Laboratory stock (Prakash et al. 1999)
21.	34-97-3a	*upr-1*	NCREV3	Laboratory stock (Tamuli et al. 2006)

TH-1227_09610609

petri dish were further analyzed by using standard race tube assay (Ryan et al. 1943; Ryan 1950). Growth rates were calculated as cm h^{-1} in both cases.

Assay for calcium and UV sensitivity

Vogel's glucose medium (Davis and De Serres 1970) was supplemented with various concentrations of $CaCl_2$, NaCl and sucrose as indicated. The 0 M $CaCl_2$ control plates were prepared using Vogel's Medium N (Vogel 1964) without $CaCl_2 \cdot 2H_2O$. Growth rate on these plates were determined as described above.

UV sensitivity was essentially as described by Kato and Inoue (2006). Briefly, conidia were grown in flasks containing Vogel's glucose medium at 30°C for 5 days, harvested and assayed for UV sensitivity. For UV dose dependency of the survival of *N. crassa*, conidia were irradiated at various doses of UV and aliquots were sampled and plated after appropriate dilution. The plates were grown at 30°C for 3 days in dark and number of colonies on each plate was counted.

PCR amplification, cloning, and transformation

PCRs were performed using custom oligonucleotide primers (Metabion GmbH, Germany), Phusion High-Fidelity PCR Kit (Finnzymes, Finland) and the manufacturer's protocol. A 3,972 bp of NCU04379 fragment from the wild-type was PCR amplified by using the primers NCU04379-5F 5′ GCTCGAAAGTTTAGTCCTGG 3′and NCU04379-3R 5′ CCCAGTAACGTCTCTTTTGC 3′ (http://www.dartmouth.edu/~neurosporagenome/knockouts_completed.html) and cloned into the *SmaI* site of pBARGEM7-1 (FGSC 19; Pall and Brunelli 1993) that resulted in pRD-1. This construct was transformed into the ΔNCU04379.2 recipient as described by Bhat et al. (2004). Transformants were selected on plate containing basta (200 μg/ml), and initial heterokaryotic transformants were crossed with the opposite mating type of the ΔNCU04379.2 mutant strain to isolate homokaryotic strains.

Sequence analysis

BLAST (Altschul et al. 1990) analysis was performed using software tools available from NCBI (http://www.blast.ncbi.nlm.nih.gov/Blast.cgi), the Conserved Domain Database (CCD; Marchler-Bauer and Bryant 2004; Marchler-Bauer et al. 2009) was used to identify conserved domains in the protein. Protein sequences were aligned with ClustalX 1.83 (Thompson et al. 1997) and transferred to GeneDoc for visualization (Nicholas et al. 1997). Phylogenetic trees were constructed from these alignments using the minimum-evolution method (Rzhetsky and Nei 1992), bootstrap replications as test of phylogeny (Felsenstein 1985) and the software MEGA4 (Tamura et al. 2007).

Results

The ΔNCU04379.2 mutant grows slowly and shows hypersensitivity to $CaCl_2$ stress

We have studied growth rate for 18 Ca^{2+}-signaling mutants (Table 1, entries 1–18), of which the ΔNCU04379.2 mutant (Supplementary Fig. 1) grows consistently slower than the wild-type strain (Fig. 1). The average growth rates were 0.357 and 0.264 cm h^{-1}, for the wild-type and ΔNCU04379.2 mutant strains, respectively ($n = 3$). The slow growth phenotype of the ΔNCU04379.2 mutant prompted us to investigate the ergosterol profile in the mutant, since ergosterol is absent in the *erg-3* mutant that grows slowly (Prakash et al. 1999). Sterol from the ΔNCU04379.2 mutant has UV absorption maxima at 272, 282, and 293 nm thereby indicating presence of ergosterol (Supplementary Fig. 2). To test the effects of Ca^{2+} on growth, we supplemented Vogel's glucose agar media with various amount of $CaCl_2$. We found that the ΔNCU04379.2 mutant is hypersensitive to $CaCl_2$ stress. The ΔNCU04379.2 mutant showed severe growth defect on media supplemented with 0.3 M and 0.4 M $CaCl_2$ (Supplementary Fig. 3), and growth rate of the ΔNCU04379.2 mutant was lower than the wild-type (Fig. 2a). In order to test the effect of Ca^{2+} deprivation, the wild-type and ΔNCU04379.2 mutant strains were grown on Vogel's glucose agar media with various amount of EGTA that has high affinity and selectivity for free Ca^{2+} (Tsien 1980). The decrease of EGTA, and the corresponding increase of Ca^{2+} levels, revealed the higher Ca^{2+}-sensitivity of the ΔNCU04379.2

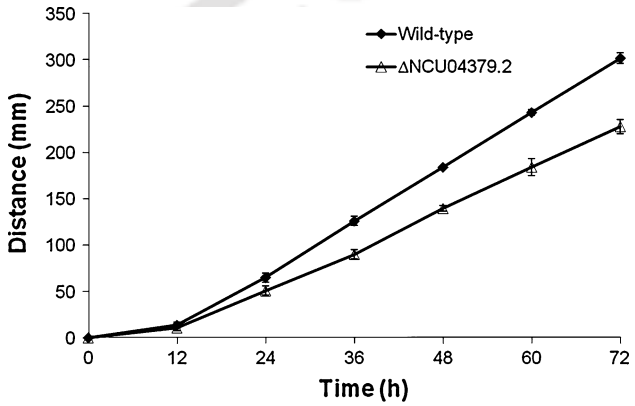

Fig. 1 The ΔNCU04379.2 mutant grows slowly. Rates of apical growth of the wild-type and ΔNCU04379.2 knockout mutant strains were measured using race tubes. *Error bars* indicate the standard errors calculated from the data for three independent experiments

TH-1227_09610609

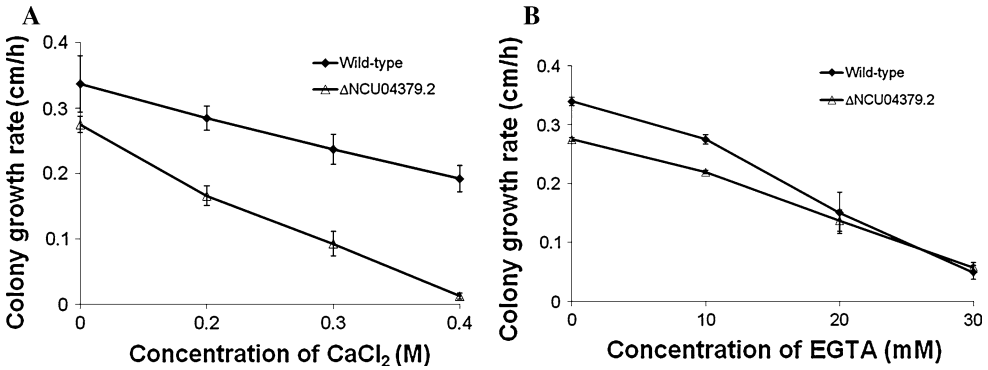

Fig. 2 The ΔNCU04379.2 mutant is sensitive to $CaCl_2$. Growth rate of the wild-type and the ΔNCU04379.2 mutant on Vogel's glucose medium supplemented with different concentrations of $CaCl_2$ (**a**) and EGTA (**b**). *Error bars* indicate the standard errors calculated from the data for three independent experiments

mutant relative to the wild-type (Fig. 2b). To determine whether the Ca^{2+} sensitivity phenotype of the ΔNCU04379.2 mutant is specific to Ca^{2+} stress or due to a mere osmotic effect, we have studied the growth characteristics of the ΔNCU04379.2 mutant on media supplemented with NaCl and sucrose. However, the ΔNCU04379.2 mutant is not sensitive to either NaCl or sucrose stress (data not shown). These results suggest that NCU04379 plays a role in growth and Ca^{2+} stress tolerance.

The ΔNCU04379.2 mutant is sensitive to UV

The sensitivity of the ΔNCU04379.2 mutant to Ca^{2+} stress prompted us to test if ultraviolet (UV) stress has any effect on this strain. Previous work had also indicated that CaM and its binding proteins are crucial in modulating DNA repair (Chard 1987; Mirzayans et al. 1995). We assayed the UV-sensitivity of the ΔNCU04379.2 mutant qualitatively and quantitatively. The ΔNCU04379.2 mutant shows an increased sensitivity to UV irradiation as revealed by the spot test (Supplementary Fig. 4). Dose–response curves constructed following exposure of the wild-type, and the ΔNCU04379.2 mutant to UV irradiations also suggested increased sensitivity of the ΔNCU4379.2 mutant (Fig. 3). However, UV sensitivity of the ΔNCU4379.2 mutant is less than the *upr-1* mutant constructed in the laboratory (Fig. 3; Tamuli et al. 2006). These data indicate that NCU04379 plays a role in UV-survival.

Complementation of the ΔNCU04379.2 mutant

The plasmid vector pRD-1 was transformed into the ΔNCU04379.2 mutant and initial transformants were crossed with the opposite mating type strain of the ΔNCU04379.2 mutant to obtain homokaryotic strains. We have tested three homokaryotic transformants and they complement growth, $CaCl_2$, EGTA, and UV phenotypes of the ΔNCU04379.2 mutant (Supplementary Fig. 5). We have also obtained additional homokaryotic transformants

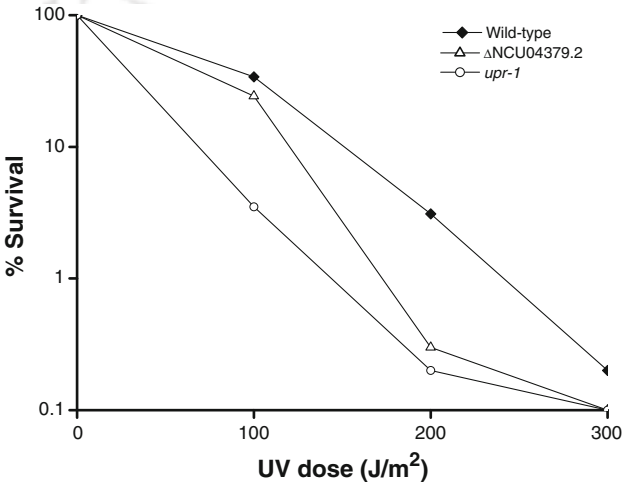

Fig. 3 The ΔNCU04379.2 mutant is sensitive to UV. Dose–response curves of the wild-type, the ΔNCU04379.2 mutant, and the *upr-1* mutant on exposure to UV irradiations. The *upr-1* null mutant was constructed in the laboratory using repeat-induced point mutation (Tamuli et al. 2006), and used to compare the relative UV sensitivity. *Each point* represents the mean of at least three independent experiments

and all of them complement the ΔNCU04379.2 mutant phenotypes (data not shown). Therefore, we conclude that NCU04379 gene has a role in growth, Ca^{2+} stress tolerance, and UV survival.

Sequence analysis of the product of NCU04379 gene

NCU04379 gene is predicted to encode a Ca^{2+} and/or CaM binding protein of 190 amino acid residues (GenBank accession number EAA28220.1) that shows sequence similarity to the *Aspergillus fumigatus*, *Magnaporthe grisea*, *Saccharomyces cerevisiae*, and *Homo sapiens* NCS-1 (also known as Frq) homologues (91, 92, 59, and 66% identity; 95, 97, 79, and 82% similarity; *e*-values 9e-96, 8e-96, 4e-64, and 2e-68, respectively). NCU04379 gene encodes a protein that also possesses a consensus signal for N-terminal myristoylation and four EF-hand Ca^{2+}-binding

TH-1227_09610609

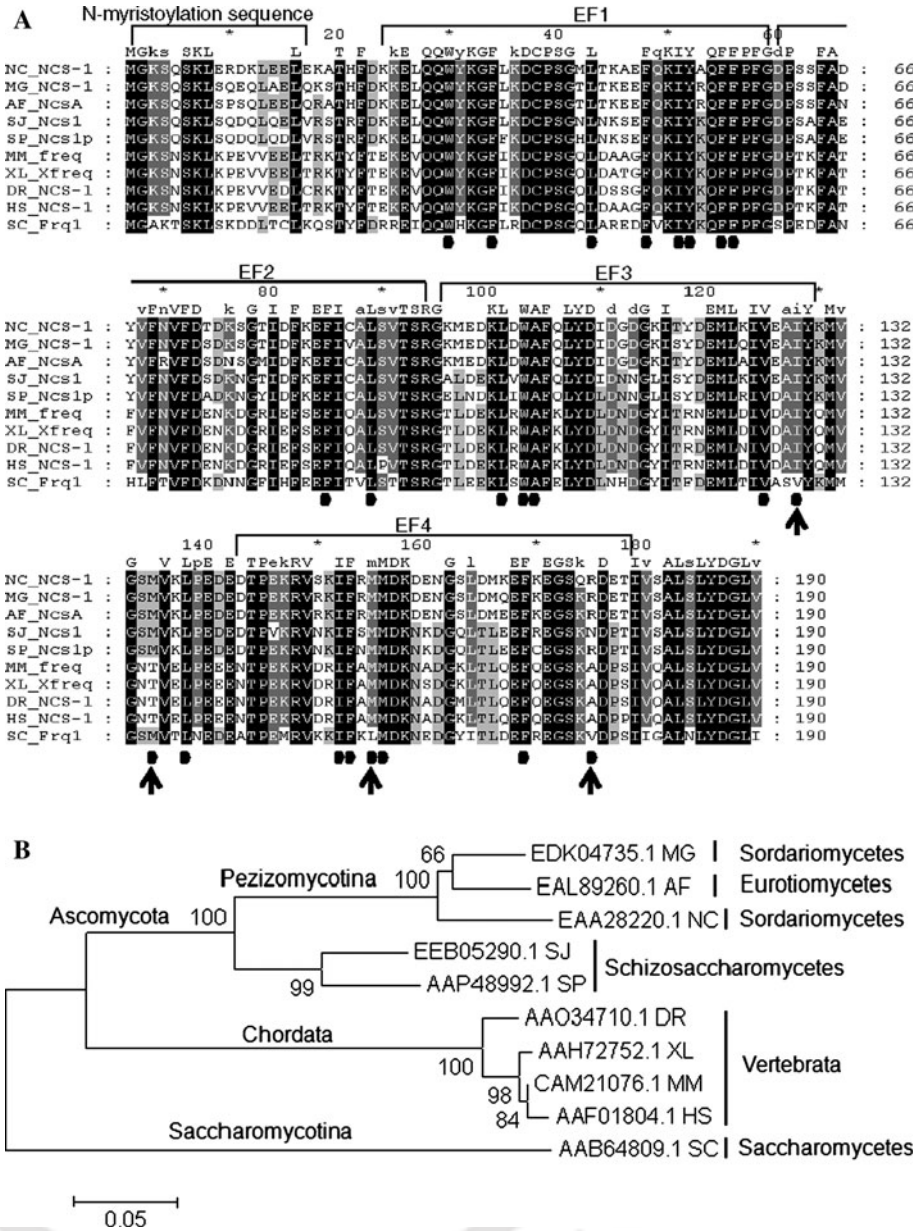

Fig. 4 Alignment and phylogenetic analysis of NCS-1 homologues. **a** Sequence alignment of NCS-1 homologues. The positions of the N-terminal myristoylation sequence and the four EF-hands (EF1, EF2, EF3, and EF4) along with the consensus sequence of the alignment are shown above the sequences. *Solid circles* below the Frq1 sequence indicate the hydrophobic residues that constitute the binding interface with the target peptide of the Frq1 (Strahl et al. 2007), and the *arrow heads* indicate residues that are found altered in other sequences in the alignment. AF, *Aspergillus fumigatus*; DR, *Danio rerio*; HS, *Homo sapiens*; MG, *Magnaporthe grisea*; MM, *Mus musculus*; NC, *Neurospora crassa*; SC, *Saccharomyces cerevisiae*; SJ, *Schizosaccharomyces japonicus*; SP, *Schizosaccharomyces pombe*; XL, *Xenopus laevis*. Conserved amino acids are indicate in *black* (100%), *dark gray* (>80%) and *light gray* (>60%). **b** Phylogenetic analysis of NCS-1 proteins using the minimum-evolution method, 500 Bootstrap replications (bootstrap values are indicated in the point at nodes) as test of phylogeny, and the software MEGA4

sites like the NCS-1 homologues in *A. fumigatus*, *Danio rerio*, *H. sapiens*, *M. grisea*, *Mus musculus*, *S. cerevisiae*, *Schizosaccharomyces japonicus*, *S. pombe*, and *Xenopus laevis* (Fig. 4a). A phylogenetic analysis with a subset of NCS-1 homologues from various organisms revealed that NCU04379 product clustered with the Pezizomycotina clade (Fig. 4b). These results indicate that NCU04379 gene encodes a homologue of NCS-1 in *N. crassa*.

Crosses homozygous for ΔNCU04379.2 mutant strains are fully fertile

To investigate the role of NCU04379 gene in sexual development, we did crosses homozygous for ΔNCU04379.2 mutant strains and all such crosses were fully fertile. We have extended this to another 17 Ca^{2+}-signaling mutants, of which 15 were fully fertile in homozygous crosses (Supplementary Table 1, entries 1–16). However, crosses homozygous for ΔNCU02283.2 mutant strains produce normal looking perithecia, only a few asci were recovered from all perithecia from one petri dish, and display a barren phenotype (produce very few ascospores; Supplementary Table 1, entry 17; Singh et al. 2009). Additionally, crosses homozygous for ΔNCU09123.2 mutant strains display an intermediate phenotype between ΔNCU02283.2 and wild-type (produce a few hundred ascospores; Supplementary Table 1, entry 18). However, both ΔNCU02283.2 and ΔNCU09123.2 mutants mate successfully with wild-type

TH-1227_09610609

and produce thousands of ascospores (data not shown). To exclude the possibility that a direct contact between mutant and wild-type allows complementation of the mutant, we performed crosses using ΔNCU02283.2 and ΔNCU09123.2 mutant strains both as male and female parents, however, crosses were fully fertile. These results indicate that both NCU02283 and NCU09123 play a role in sexual development in a recessive manner.

NCU02283 gene is predicted to encode a Ca^{2+}/CaM-dependent protein kinase type I, Ca^{2+}/CaMKI (accession number XP_959927.2), shares 90% identity and 94% similarity in amino acid sequence with a putative CaM kinase, CgCMK, of *Colletotrichum gloeosporioides* (Kim et al. 1998). Both CgCMK and the *N. crassa* Ca^{2+}/CaMKI possess 11 conserved kinase domains and one putative CaM-binding domain, however, of nine putative phosphorylation sites of CgCMK, only five are conserved in the *N. crassa* Ca^{2+}/CaMKI (Fig. 5a). NCU09123 gene encodes another Ca^{2+}/CaMK, CAMK-1(accession number XP_958895.2), which is highly similar to other eukaryotic Ca^{2+}/CaM-dependent kinases, specifically at the kinase domain (Yang et al. 2001; Valle-Aviles et al. 2007). The Ca^{2+}/CaMKI and CAMK-1 proteins from *N. crassa* form a clade with other Sordariomycetes in a phylogenetic analysis with a subset of homologues from fungi (Fig. 5b, c).

Fig. 5 Alignment and phylogenetic analysis of calcium/calmodulin-dependent protein kinases (Ca^{2+}/CaMKs). **a** Alignment of Ca^{2+}/CaMKI sequences. The sequences in the box represent the putative CaM-binding domain, and *solid circles* below the CG sequence indicate potential autophosporylation sites containing the $^{R}_{K}XX^{T}_{S}$ consensus phosphorylation site for CaMKs (Kim et al. 1998). AC, *Ajellomyces capsulatus*; AD, *Ajellomyces dermatitidis*; AL, *Arthrobotrys dactyloides*; AF, *Aspergillus fumigatus*; AT, *Aspergillus terreus*; CG, *Colletotrichum gloeosporioides*; CI, *Coccidioides immitis*; EN, *Emericella nidulans*; MG, *Magnaporthe grisea*; NC, *Neurospora crassa*; PB, *Paracoccidioides brasiliensis*; PN, *Phaeosphaeria nodorum*; PT, *Pyrenophora tritici-repentis*; ST, *Setosphaeria turcica*; UR, *Uncinocarpus reesii*; VA, *Verticillium albo-atrum*. Conserved amino acids are indicated in *black* (100%), *dark gray* (>80%) and *light gray* (>60%). **b** Phylogenetic analysis of Ca^{2+}/CaMKI proteins using the minimum-evolution method, 500 Bootstrap replications (bootstrap values are indicated in the point at nodes) as test of phylogeny, and the software MEGA4. **c** Phylogenetic analysis of CAMK-1 proteins using the minimum-evolution method, 500 Bootstrap replications (bootstrap values are indicated in the point at nodes), as test of phylogeny and the software MEGA4. The sequences used are AC, *Ajellomyces capsulatus*; AD, *Ajellomyces dermatitidis*; AF, *Aspergillus fumigates*; AG, *Aspergillus niger*; AL, *Aspergillus clavatus*; AN, *Aspergillus nidulans*; AO, *Aspergillus oryzae*; AT, *Aspergillus terreus*; CA, *Candida albicans*; CD, *Candida dubliniensis*; CN, *Cryptococcus neoformans*; CP, *Coccidioides posadasii*; CT, *Candida tropicalis*; NC, *Neurospora crassa*; NF, *Neosartorya fischeri*; PB, *Paracoccidioides brasiliensis*; PN, *Phaeosphaeria nodorum*; PP, *Pichia pastoris*; SC, *Saccharomyces cerevisiae*; SJ, *Schizosaccharomyces japonicus*; SS, *Sporothrix schenckii*; TS, *Talaromyces stipitatus*; UR, *Uncinocarpus reesii*; VA, *Verticillium albo-atrum*

Discussion

Calcium plays an important role in intracellular signaling system in eukaryotes including fungi (Gadd 1994; Shaw and Hoch 2001; Sanders et al. 2002). To understand the cellular roles of the Ca^{2+}-signaling genes in *N. crassa*, we have studied 18 Ca^{2+}-signaling mutants. The ΔNCU04379.2 mutant grows slowly, shows increased sensitivity to Ca^{2+} and UV irradiation. In addition, we found evidence for involvement for NCU02283 and NCU09123 genes in sexual development. Reverse transcription-PCR (RT-PCR) did not show expression of the NCU04379, NCU02283, and NCU09123 gene products in the corresponding mutants (data not shown). We did not notice any phenotype for the remaining 15 Ca^{2+}-signaling mutants in growth, Ca^{2+} stress tolerance, and sexual development. NCU04379, NCU02283, and NCU09123 genes encode, respectively, a homologue of NCS-1, a Ca^{2+}/CaMKI, and a CAMK-1 in *N. crassa*.

In *S. cerevisiae*, Frq1, the NCS-1 ortholog, is essential for cell growth and viability (Hendricks et al. 1999). In *M. grisea*, null-mutants for a neuronal calcium sensor-1/frequenin like gene, *Mg-NCS-1*, showed normal growth, however, high concentrations of Ca^{2+} and acidic conditions suppressed the growth (Saitoh et al. 2003). In *S. pombe*, *ncs1Δ*, deletion mutant of NCS-1 homolog, showed starvation independent sexual development and Ca^{2+}-sensitivity (Hamasaki-Katagiri et al. 2004). In *A. fumigatus*, the *NCS-1* homologue NcsA is involved in sterol distribution in the tip and polar establishment, the *ΔncsA* mutant was more resistant to $CaCl_2$ and sensitive to EGTA (Mota Júnior et al. 2008). We found that knockout mutant of *N. crassa* homologue of NCS-1 displays both slow growth and Ca^{2+}-sensitivity phenotypes (Figs. 1, 2). Additionally, UV-sensitivity of the ΔNCU04379.2 mutant strain uncovers a novel function of NCS-1 homologue in *N. crassa* (Fig. 3). This indicates involvement of NCU04379 gene product in UV-induced DNA damage repair. UV light absorption may cause DNA damage primarily through formation of cyclobutane pyrimidine dimers (CPD; Lippke et al. 1981) and pyrimidine (6–4) pyrimidone photoproducts (6–4PP; Mitchell and Nairn 1989) leading to induction of DNA repair mechanisms or apoptosis (Lo et al. 2005). In human cells, the CaM protein antagonists fully or partially block double-stranded DNA repair and CaM overexpression activates H2AX mediated DNA repair after irradiation (Wang et al. 2000; Herman et al. 2002; Smallwood et al. 2009).

In addition, growth rate of the ΔNCU04379.2 and other Ca^{2+}-signaling mutants (Table 1) were comparable with the wild-type on plates containing hydrogen peroxide

TH-1227_09610609

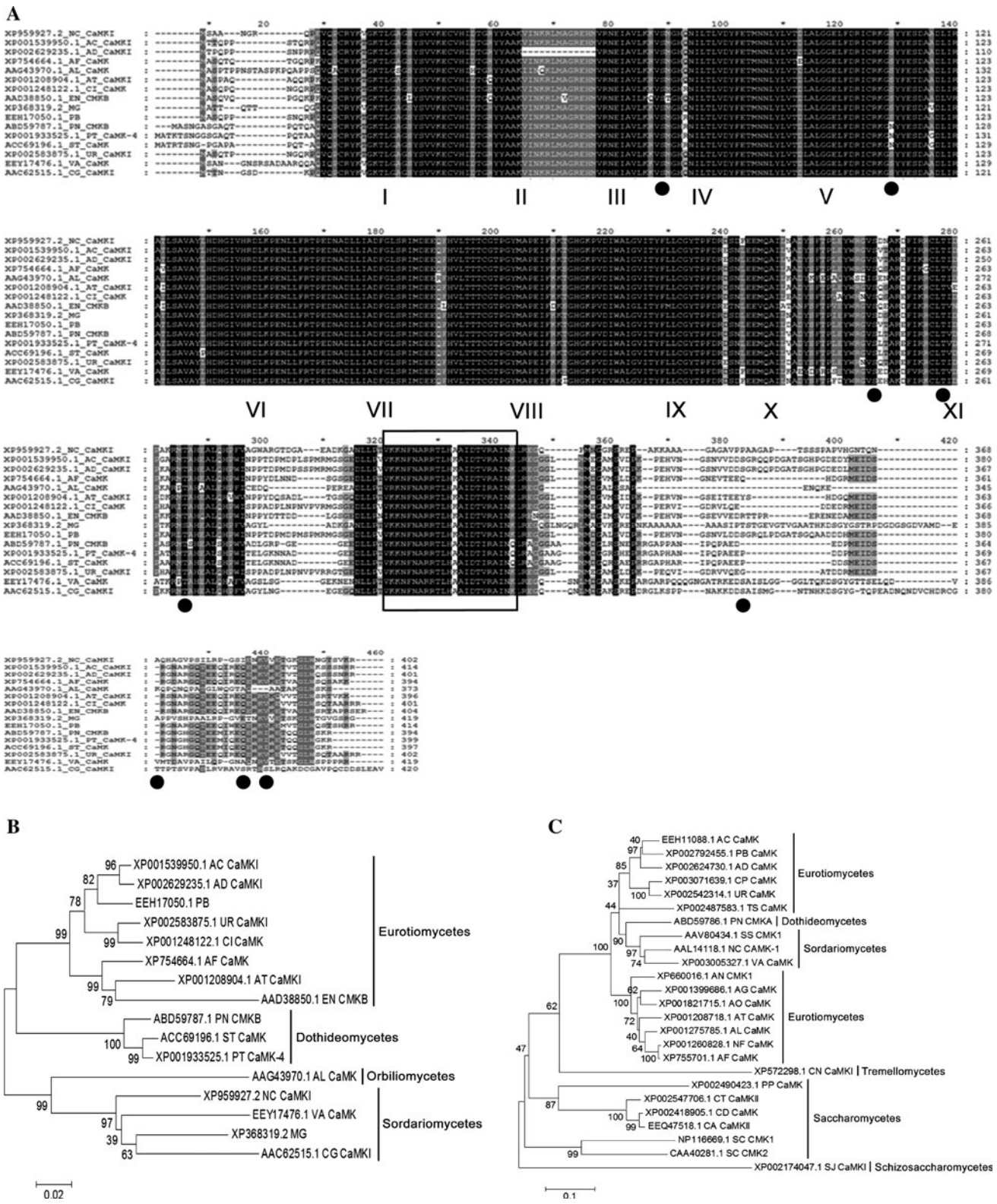

(3 mM) and phytosphingosine (PHS; 5 μg/ml), therefore, we did not find evidence for involvement of these genes in H_2O_2 or PHS mediated cell death in *N. crassa* (Castro et al. 2008; data not shown). The ΔNCU04379.2 mutant phenotypes were complemented upon pRD-1 transformation (Supplementary Fig. 5). Therefore, we conclude that NCU04379 gene has a role in growth, Ca^{2+} stress tolerance, and UV survival in *N. crassa*.

TH-1227_09610609

The predicted protein product of NCU04379 gene consists of 190 amino acid residues, which possesses a consensus signal for N-terminal myristoylation and four EF-hand Ca^{2+}-binding sites, and shows high sequence similarity to NCS-1 proteins (Fig. 4). *N. crassa* homologue of NCS-1 has 58% identity with *S. cerevisiae* Frq1. Recent NMR derived structure of Frq1 had identified hydrophobic residues in the groove that constitute the binding interface with the target peptide (Strahl et al. 2007). These hydrophobic residues are also conserved in *N. crassa* homologue of NCS-1 except for alterations in three residues of which V175R may be the most significant alteration (Fig. 4a). Moreover, both Cys residues in *N. crassa* homologue of NCS-1 appear to be buried in the interior (Fig. 4a). *S. cerevisiae* Frq1 also has two Cys residues, however, one is near its N-terminus and the other buried in the interior (Ames et al. 2000). It will be interesting to investigate the effects of these alterations.

Crosses homozygous for ΔNCU04379.2 mutant strains are fully fertile. In addition, our preliminary work on ΔNCU02283.2 and ΔNCU09123.2 mutants indicate that their normal gene functions are essential for fertility. NCU02283 gene is predicted to encode a Ca^{2+}/CaMKI and its homologue in *C. gloeosporioides*, CgCMK, might be involved in germination and appressorium induction (Kim et al. 1998). NCU09123 gene encodes a CAMK-1 that phosphorylates the *N. crassa* circadian clock protein FREQUENCY (FRQ; Yang et al. 2001). In *Sporothrix schenckii*, *sscmk1*, a CAMK-1 homologue might be regulating dimorphism (Valle-Aviles et al. 2007). Ca^{2+}-signaling proteins also play an important role in development in higher organisms. In the late stages of embryogenesis *X. laevis*, CaMKIx, a Ca^{2+}/CaM-dependent protein kinase I is activated upon phosphorylation that can phosphorylate various proteins including synapsin I, histones, and myelin basic protein (Kinoshita et al. 2004). In human, activation of Ca^{2+} channels leads to Ca^{2+} influx that is the pivotal step in initiation of acrosome reaction during fertilization (Ma and Shi 1999). *N. crassa* undergoes a complex sexual developmental process to form protoperithecia when subjected to nitrogen starvation, light and low temperature (Perkins and Barry 1977; Nelson and Metzenberg 1992; Read 1994; Nelson 1996; Coppin et al. 1997). Specialized receptive hyphae called trichogynes are extended from the protoperithecia and fuses with the fertilizing cell of the opposite mating type. After fertilization, protoperithecia develop into perithecia where multiple asci, each containing eight ordered ascospores, are formed (Raju 1992; Kim and Borkovich 2006). Apart from few *s*exual *dev*elopment (*sdv*) and pheromone related genes, little is known about sexual developmental process in *N. crassa* (Johnson 1978; Nelson and Metzenberg 1992; Kim and Nelson 2005; Kim and Borkovich 2006; Iyer et al. 2009). It is possible that the NCU02283 and NCU09123 encoded Ca^{2+}/CaMKs phosphorylate proteins necessary for the sexual development. Our preliminary data indicate that wild-type fragments carrying NCU02283 and NCU09123 genes complement the respective mutant strains (Kumar and Tamuli, unpublished).

Thus, in this study we have shown that a *N. crassa* homologue of NCS-1 encoding gene NCU04379 has a role in growth, Ca^{2+} stress tolerance, and UV survival. Additionally, we found evidence for involvement of Ca^{2+}/CaMKs encoding genes NCU02283 and NCU09123 in sexual development. Future work will enable us to determine the molecular mechanisms of their actions.

Acknowledgments Charges for strains and race tubes obtained from the Fungal Genetics Stock Center (FGSC) were generously waived. The FGSC is supported by National Science Foundation grant BIR-9222772. We thank Dr. N. B. Raju (Stanford University) for helpful suggestions during the preparation of this manuscript, Dr. D. P. Kasbekar and M. Ramakrishnan (CCMB) for help in Southern analysis. RD and RK were supported by Junior Research Fellowships from the CSIR-UGC and the MHRD, respectively. This work was supported in part by a Start-up grant (IITG), and a SERC FAST Track grant (DST) to RT.

References

Altschul SF, Gish W, Miller W, Myers EW, Lipman DJ (1990) Basic local alignment search tool. J Mol Biol 215:403–410

Ambudkar IS, Baum BJ (1988) ATP-dependent calcium transport in rat parotid basolateral membrane vesicles is modulated by membrane potential. J Mem Biol 102:59–69

Ambudkar IS, Horn VJ, Baum BJ (1989) ATP-dependent Ca^{2+} transport in the rat parotid basolateral membrane is regulated by calmodulin. Archs Biochem Biophys 268:576–584

Ames JB, Tanaka T, Stryer L, Ikura M (1996) Portrait of a myristoyl switch protein. Curr Opin Struct Biol 6:432–438

Ames JB, Hendricks KB, Strahl T, Huttner IG, Hamasaki N, Thorner J (2000) Structure and calcium-binding properties of Frq1, a novel calcium sensor in the yeast *Saccharomyces cerevisiae*. Biochemistry 39:12149–12161

Berridge MJ, Bootman MD, Lipp P (1998) Calcium-a life and death signal. Nature 395:645–648

Bhat A, Tamuli R, Kasbekar DP (2004) Genetic transformation of *Neurospora tetrasperma*, demonstration of repeat-induced point mutation (RIP) in self-crosses and a screen for recessive RIP-defective mutants. Genetics 167:1155–1164

Borkovich KA, Alex LA, Yarden O, Freitag M, Turner GE, Read ND, Seiler S, Bell-Pedersen D, Paietta J, Plesofsky N, Plamann M, Goodrich-Tanrikulu M, Schulte U, Mannhaupt G, Nargang FE, Radford A, Selitrennikoff C, Galagan JE, Dunlap JC, Loros JJ, Catcheside D, Inoue H, Aramayo R, Polymenis M, Selker EU, Sachs MS, Marzluf GA, Paulsen I, Davis R, Ebbole DJ, Zelter A, Kalkman ER, O'Rourke R, Bowring F, Yeadon J, Ishii C, Suzuki K, Sakai W, Pratt R (2004) Lessons from the genome sequence of *Neurospora crassa*: tracing the path from genomic blueprint to multicellular organism. Microbiol Mol Biol Rev 68:1–108

Castro A, Lemos C, Falcao A, Glass NL, Videira A (2008) Increased resistance of complex I mutants to phytosphingosine-induced programmed cell death. J Biol Chem 283:19314–19321

TH-1227_09610609

Chafouleas JG, Bolton WE, Means AR (1984) Potentiation of bleomycin lethality by anti-calmodulin drugs: a role for calmodulin in DNA repair. Science 224:1346–1348

Chard PA (1987) DNA repair in human cells: methods for the determination of calmodulin involvement. Methods Enzymol 139:715–730

Colot HV, Park G, Turner GE, Ringelberg C, Crew CM, Litvinkova L, Weiss RL, Borkovich KA, Dunlap JC (2006) A high-throughput gene knockout procedure for Neurospora reveals functions for multiple transcription factors. Proc Natl Acad Sci U S A 103:10352–10357

Coppin E, Debuchy R, Arnaise S, Picard M (1997) Mating types and sexual development in filamentous ascomycetes. Microbiol Mol Biol Rev 61:411–428

Cornelius G, Nakashima H (1987) Vacuoles play a decisive role in calcium homeostasis in *Neurospora crassa*. J Gen Microbio 133:2341–2347

Davis RH, De Serres FJ (1970) Genetic and microbiological research techniques for *Neurospora crassa*. Methods Enzymol 17:79–143

Felsenstein J (1985) Confidence limits on phylogenies: an approach using the bootstrap. Evolution 39:783–791

Gadd GM (1994) Signal transduction in fungi. In: Gow NAR, Gadd GM (eds) The growing fungus. Chapman & Hall, London, pp 183–210

Galagan JE, Calvo SE, Borkovich KA, Selker EU, Read ND, Jaffe D, FitzHugh W, Ma LJ, Smirnov S, Purcell S, Rehman B, Elkins T, Engels R, Wang S, Nielsen CB, Butler J, Endrizzi M, Qui D, Ianakiev P, Bell-Pedersen D, Nelson MA, Werner-Washburne M, Selitrennikoff CP, Kinsey JA, Braun EL, Zelter A, Schulte U, Kothe GO, Jedd G, Mewes W, Staben C, Marcotte E, Greenberg D, Roy A, Foley K, Naylor J, Stange-Thomann N, Barrett R, Gnerre S, Kamal M, Kamvysselis M, Mauceli E, Bielke C, Rudd S, Frishman D, Krystofova S, Rasmussen C, Metzenberg RL, Perkins DD, Kroken S, Cogoni C, Macino G, Catcheside D, Li W, Pratt RJ, Osmani SA, DeSouza CP, Glass L, Orbach MJ, Berglund JA, Voelker R, Yarden O, Plamann M, Seiler S, Dunlap J, Radford A, Aramayo R, Natvig DO, Alex LA, Mannhaupt G, Ebbole DJ, Freitag M, Paulsen I, Sachs MS, Lander ES, Nusbaum C, Birren B (2003) The genome sequence of the filamentous fungus *Neurospora crassa*. Nature 422:859–868

Haghighat N, Al-Hashimi I (1999) A pilot study on the effect of radiation on calmodulin in rat submandibular salivary glands. Arch Oral Biol 44:383–389

Hamasaki-Katagiri N, Molchanova T, Takeda K, Ames JB (2004) Fission yeast homolog of neuronal calcium sensor-1 (Ncs1p) regulates sporulation and confers calcium tolerance. J Biol Chem 279:12744–12754

Hendricks KB, Wang BQ, Schnieders EA, Thorner J (1999) Yeast homologue of neuronal frequenin is a regulator of phosphatidylinositol-4-OH kinase. Nat Cell Biol 1:234–241

Herman M, Ori Y, Chagnac A, Weinstein T, Korzets A, Zevin D, Malachi T, Gafter U (2002) DNA repair in mononuclear cells: role of serine/threonine phosphatases. J Lab Clin Med 140:255–262

Ikura M (1996) Calcium binding and conformational response in EF-hand proteins. Trends Biochem Sci 21:14–17

Iyer SV, Ramakrishnan M, Kasbekar DP (2009) *Neurospora crassa fmf-1* encodes the homologue of the *Schizosaccharomyces pombe* Ste11p regulator of sexual development. J Genet 88:33–39

Johnson TE (1978) Isolation and characterization of perithecial development mutants in Neurospora. Genetics 88:27–47

Johnson DR, Bhatnagar RS, Knoll LJ, Gordon JI (1994) Genetic and biochemical studies of protein N-myristoylation. Annu Rev Biochem 63:869–914

Kato A, Inoue H (2006) Growth defect and mutator phenotypes of RecQ-deficient Neurospora crassa mutants separately result from homologous recombination and nonhomologous end joining during repair of DNA double-strand breaks. Genetics 172:113–125

Kim H, Borkovich KA (2006) Pheromones are essential for male fertility and sufficient to direct chemotropic polarized growth of trichogynes during mating in *Neurospora crassa*. Eukaryot Cell 5:544–554

Kim H, Nelson MA (2005) Molecular and functional analyses of *poi-2*, a novel gene highly expressed in sexual and perithecial tissues of *Neurospora crassa*. Eukaryotic Cell 4:900–910

Kim YK, Li D, Kolattukudy PE (1998) Induction of Ca^{2+}-calmodulin signaling by hard-surface contact primes *Colletotrichum gloeosporioides* conidia to germinate and form appressoria. J Bacteriol 180:5144–5150

Kinoshita S, Sueyoshi N, Shoju H, Suetake I, Nakamura M, Tajima S, Kameshita I (2004) Cloning and characterization of a novel Ca^{2+}/calmodulin-dependent protein kinase I homologue in *Xenopus laevis*. J Biochem 135:619–630

Lippke JA, Gordon LK, Brash DE, Haseltine WA (1981) Distribution of UV light-induced damage in a defined sequence of human DNA: detection of alkaline-sensitive lesions at pyrimidine nucleoside-cytidine sequences. Proc Natl Acad Sci USA 78:3388–3392

Lo HL, Nakajima S, Ma L, Walter B, Yasui A, Ethell DW, Owen LB (2005) Differential biologic effects of CPD and 6–4PP UV-induced DNA damage on the induction of apoptosis and cell-cycle arrest. BMC Cancer 5:135

Ma X-H, Shi YL (1999) A patch clamp study on reconstitute calcium permeable channels of human sperm plasma membranes. Acta Physiologica Sinica 51:571–579

Marchler-Bauer A, Bryant SH (2004) CD-Search: protein domain annotations on the fly. Nucleic Acids Res 32(Web server issue):W327–W331

Marchler-Bauer A, Anderson JB, Chitsaz F, Derbyshire MK, DeWeese-Scott C, Fong JH, Geer LY, Geer RC, Gonzales NR, Gwadz M, He S, Hurwitz DI, Jackson JD, Ke Z, Lanczycki CJ, Liebert CA, Liu C, Lu F, Lu S, Marchler GH, Mullokandov M, Song JS, Tasneem A, Thanki N, Yamashita RA, Zhang D, Zhang N, Bryant SH (2009) CDD: specific functional annotation with the Conserved Domain Database. Nucleic Acids Res 37(Database issue):D205–D210

McCluskey K (2003) The fungal genetics stock center: from molds to molecules. Adv Appl Microbiol 52:245–262

McFerran BW, Graham ME, Burgoyne RD (1998) Neuronal Ca^{2+} sensor 1, the mammalian homologue of frequenin, is expressed in chromaffin and PC12 cells and regulates neurosecretion from dense-core granules. J Biol Chem 273:22768–22772

Mirzayans R, Famulski KS, Enns L, Fraser M, Paterson MC (1995) Characterization of the signal transduction pathway mediating gamma ray-induced inhibition of DNA synthesis in human cells: indirect evidence for involvement of calmodulin but not protein kinase C nor p53. Oncogene 11:1597–1605

Mitchell DL, Nairn RS (1989) The biology of the (6–4) photoproduct. Photochem Photobiol 49:805–819

Mota Júnior AO, Malavazi I, Soriani FM, Heinekamp T, Jacobsen I, Brakhage AA, Savoldi M, Goldman MH, da Silva Ferreira ME, Goldman GH (2008) Molecular characterization of the *Aspergillus fumigatus* NCS-1 homologue, NcsA. Mol Genet Genomics 280:483–495

Nelson MA (1996) Mating systems in ascomycetes: a romp in the sac. Trends Genet 12:69–74

Nelson MA, Metzenberg RL (1992) Sexual development genes of *Neurospora crassa*. Genetics 132:149–162

Nicholas KB, Nicholas HB, Deerfield DW (1997) GeneDoc: analysis and visualization of genetic variation. EMBnet News 4:1–4

TH-1227_09610609

Pall ML, Brunelli JP (1993) A series of six compact fungal transformation vectors containing polylinkers with multiple unique restriction sites. Fungal Genet Newslett 40:59–62

Pavelic K (1987) Calmodulin antagonist W 13 prevents DNA repair after bleomycin treatment of human urological tumor cells growing on extracellular matrix. Int J Biochem 19:1091–1095

Perkins DD, Barry EG (1977) The cytogenetics of Neurospora. Adv Genet 19:133–285

Pongs O, Lindemeier J, Zhu XR, Theil T, Engelkamp D, Krah-Jentgens I, Lambrecht HG, Koch KW, Schwemer J, Rivosecchi R , Mallart A, Galceran J, Canal I, Barbas JA, Ferrús A (1993) Frequenin-A novel calcium-binding protein that modulates synaptic efficacy in the Drosophila nervous system. Neuron 11:15–28

Prakash A, Sengupta S, Aparna K, Kasbekar DP (1999) The erg-3 (sterol Δ14, 15-reductase) gene of Neurospora crassa: generation of null mutants by repeat-induced point mutation and complementation by proteins chimeric for human lamin B receptor sequences. Microbiology 145:1443–1451

Raju NB (1992) Genetic control of the sexual cycle in Neurospora. Mycol Res 96:241–262

Read ND (1994) Cellular nature and multicellular morphogenesis in higher fungi. In: Ingram DS, Hudson A (eds) Shape and form in plants and fungi. Academic Press, London, pp 251–269

Ryan FJ (1950) Selected methods of Neurospora genetics. Methods Med Res 3:51–75

Ryan FJ, Beadle GW, Tatum EL (1943) The tube method of measuring the growth rate of Neurospora. Am J Bot 30:784–799

Rzhetsky A, Nei M (1992) Statistical properties of the ordinary least-squares, generalized least-squares, and minimum-evolution methods of phylogenetic inference. J Mol Evol 35:367–375

Saitoh K, Arie T, Teraoka T, Yamaguchi I, Kamakura T (2003) Targeted gene disruption of the neuronal calcium sensor 1 homologue in rice blast fungus, *Magnaporthe grisea*. Biosci Biotechnol Biochem 67:651–653

Sakai W, Ishii C, Inoue H (2002) The *upr-1* gene encodes a catalytic subunit of the DNA polymerase zeta which is involved in damage-induced mutagenesis in *Neurospora crassa*. Mol Genet Genomics 267:401–408

Sakai W, Wada Y, Naoi Y, Ishii C, Inoue H (2003) Isolation and genetic characterization of the *Neurospora crassa REV1* and *REV7* homologs: evidence for involvement in damage-induced mutagenesis. DNA Repair (Amst) 2:337–346

Sanders D, Pelloux J, Brownlee C, Harper JF (2002) Calcium at the crossroads of signaling. Plant Cell 14(Suppl):S401–S417

Shaw BD, Hoch HC (2001) Biology of the fungal cell. In: Howard RJ, Gow NAR (eds) The mycota VIII. Springer, Berlin, pp 73–89

Singh PK, Iyer SV, Ramakrishnan M, Kasbekar DP (2009) Chromosome segment duplications in *Neurospora crassa*: barren crosses beget fertile science. BioEssays 31:209–219

Smallwood HS, Lopez-Ferrer D, Eberlein PE, Watson DJ, Squier TC (2009) Calmodulin mediates DNA repair pathways involving H2AX in response to low-dose radiation exposure of RAW 264.7 macrophages. Chem Res Toxicol 22:460–470

Strahl T, Huttner IG, Lusin JD, Osawa M, King D, Thorner J, Ames JB (2007) Structural Insights into activation of phosphatidylinositol 4-kinase (Pik1) by yeast frequenin (Frq1). J Biol Chem 282:30949–30959

Tamuli R, Ravindran C, Kasbekar DP (2006) Translesion DNA polymerases Pol zeta, Pol eta, Pol iota, Pol kappa and Rev1 are not essential for repeat-induced point mutation in *Neurospora crassa*. J Biosci 31:557–564

Tamuli R, Kumar R, Deka R (2011) Cellular roles of neuronal calcium sensor-1 and calcium/calmodulin-dependent kinases in fungi. J Basic Microbio 51:120–128

Tamura K, Dudley J, Nei M, Kumar S (2007) MEGA4: molecular evolutionary genetics analysis (MEGA) software version 4.0. Mol Biol Evol 24:1596–1599

Thompson JD, Gibson TJ, Plewniak F, Jeanmougin F, Higgins DG (1997) The CLUSTAL-X windows interface: flexible strategies for multiple sequence alignment aided by quality analysis tools. Nucleic Acids Res 25:4876–4882

Tsien RY (1980) New calcium indicators and buffers with high selectivity against magnesium and protons: design, synthesis, and properties of prototype structures. Biochem 19:2396–2404

Valle-Aviles L, Valentin-Berrios S, Gonzalez-Mendez RR, Rodriguez-del VN (2007) Functional, genetic and bioinformatic characterization of a calcium/calmodulin kinase gene in *Sporothrix schenckii*. BMC Microbio 7:107

Vogel HJ (1964) Distribution of lysine pathways among fungi: evolutionary implications. Am. Naturalist. 98:435–436

Wang Y, Mallya SM, Sikpi MO (2000) Calmodulin antagonists and cAMP inhibit ionizing-radiation-enhancement of double-strand-break repair in human cells. Mutat Res 460:29–39

Yang Y, Cheng P, Zhi G, Liu Y (2001) Identification of a calcium/calmodulin-dependent protein kinase that phosphorylates the Neurospora circadian clock protein FREQUENCY. J Biol Chem 276:41064–41072

TH-1227_09610609

Review

Cellular roles of neuronal calcium sensor-1 and calcium/calmodulin-dependent kinases in fungi

Ranjan Tamuli, Ravi Kumar* and Rekha Deka*

Department of Biotechnology, Indian Institute of Technology Guwahati, Guwahati, India

The neuronal calcium sensor-1 (NCS-1) possesses a consensus signal for N-terminal myristoylation and four EF-hand Ca^{2+}-binding sites, and mediates the effects of cytosolic Ca^{2+}. Minute changes in free intracellular Ca^{2+} are quickly transformed into changes in the activity of several kinases including calcium/calmodulin-dependent protein kinases (Ca^{2+}/CaMKs) that are involved in regulating many eukaryotic cell functions. However, our current knowledge of NCS-1 and Ca^{2+}/CaMKs comes mostly from studies of the mammalian enzymes. Thus far very few fungal homologues of NCS-1 and Ca^{2+}/CaMKs have been characterized and little is known about their cellular roles. In this minireview, we describe the known sequences, interactions with target proteins and cellular roles of NCS-1 and Ca^{2+}/CaMKs in fungi.

Keywords: Ca^{2+} signaling / Calcium/calmodulin kinase / Neuronal calcium sensor-1 / Phosphorylation / Sexual development

Received: May 13, 2010; accepted: August 03, 2010

DOI 10.1002/jobm.201000184

Neuronal calcium sensor-1 (NCS-1)

Calcium ion (Ca^{2+}) plays a central role as an intracellular signal in fungi and other eukaryotic organisms [1, 2]. In fungi, Ca^{2+} signaling is involved in regulating several processes such as secretion, cytoskeletal organization, hyphal tip growth, hyphal branching, sporulation, infection structure differentiation, cell cycle progression, and circadian clocks [3–5]. The effects of intracellular Ca^{2+} changes are mediated primarily by small Ca^{2+}-binding proteins that include the highly conserved neuronal calcium sensor-1 (NCS-1) protein. NCS-1, also known as Frq1 in yeast, is characterized by a consensus signal for N-terminal myristoylation and four EF-hand Ca^{2+}-binding sites (Fig. 1A) [6–8]. The N-terminal myristoylation is a lipid anchor modification, the attachment of the lipid moiety results in an increase of hydrophobicity that anchors the protein to the membrane [9]. Though NCS-1 possesses four EF hand motifs, only three EF-hands bind to calcium, since most N-terminal EF-hand is non-functional in calcium-binding because of the presence of a cysteine and a proline in the putative calcium-binding loop [10]. Upon Ca^{2+} binding, conformational changes convert the NCS-1 to its active state and thereby mediate effects of cytosolic Ca^{2+} [11]. Thus far, fungal homologues of the NCS-1 have been studied in *Saccharomyces cerevisiae* [7, 8, 12, 13], *Magnaporthe grisea* [14], *Schizosaccharomyces pombe* [15], *Aspergillus fumigatus* [16], and *Neurospora crassa* (R. Deka *et al.*, unpublished) (Fig. 1B).

Regulation of the phosphatidylinositol (PtdIns) 4-kinase activity

S. cerevisiae Frq1 was the first fungal NCS-1 homologue characterized [7]. Frq1 is homologous to the recoverin branch of the EF-hand superfamily of Ca^{2+}-binding proteins that includes neuronal Ca^{2+} sensors such as neurocalcin, hippocalcin, and frequenin [17, 18]. Frq1 binds calcium and is *N*-myristoylated. Ca^{2+}-binding in Frq1 induces structural changes that are evident by many sharp and well-resolved NMR peaks of the Ca^{2+}-bound Frq1 in contrast to highly congested and poorly resolved peaks exhibited by the Ca^{2+}-free protein [12]. Frq1 is essential for cell growth and viability because it regulates the activity and localization of phosphatidylinositol (PtdIns) 4-kinase (Pik1) that has been shown to be essential for secretion in yeast cells [13, 19–22]. Frq1

* These authors contributed equally to this minireview
Correspondence: Dr. Ranjan Tamuli, Department of Biotechnology, Indian Institute of Technology Guwahati, Guwahati 781 039, Assam, India
E-mail: ranjantamuli@iitg.ernet.in
Phone: +91 361 258 2220
Fax: +91 361 258 2249

© 2011 WILEY-VCH Verlag GmbH & Co. KGaA, Weinheim

TH-1227_09610609

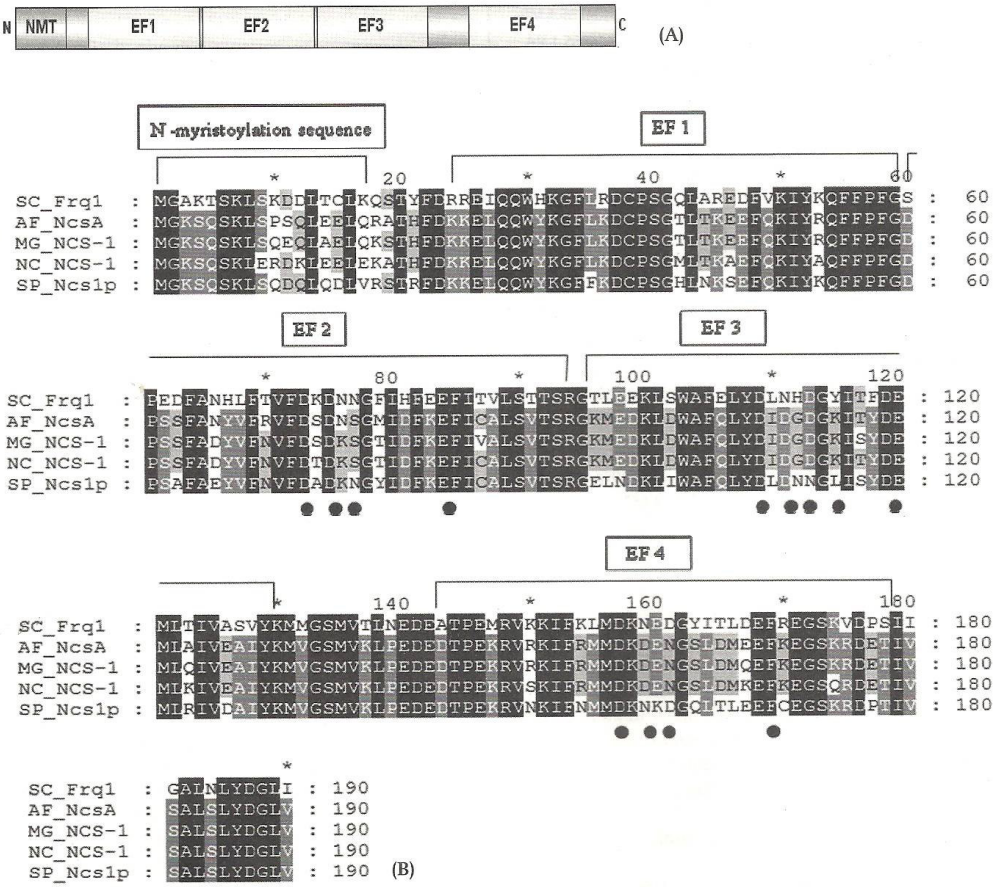

Figure 1. Domain organization, sequence alignment and phylogeny of NCS-1. A) NCS-1 [8] contains a consensus signal for N-terminal myristoylation (NMT) sequence (red) and four EF-hands (blue), of which EF-1 is non-functional. The domain figure was prepared using the software DOG 1.0 [56]. B) Sequence comparison of the frequenin/NCS-1 proteins from *S. cerevisiae*, *A. fumigatus*, *M. grisea*, *N. crassa* and *S. pombe*. Protein sequences were aligned with ClustalX 1.83 [57] and transferred to GeneDoc for visualization [58]. Conserved amino acids are indicated in black (100%), dark gray (>80%) and light gray (>60%). The positions of the N-terminal myristoylation sequence and EF-hand loops are indicated above the sequence. Solid circles below the sequence indicate conserved Ca^{2+}-binding sites. C) Phylogenetic analysis of the frequenin/NCS-1 proteins from fungi to mammals using the Minimum evolution method [59], 500 bootstrap replications (bootstrap values are indicated in the point at nodes) as test of phylogeny [60] and the software MEGA4 [61]. The non-redundant protein sequence databases at the NCBI were searched using the BLASTP (http://blast.ncbi.nlm.nih.gov/Blast.cgi) [62], with the default parameters, using *N. crassa* NCS-1 (EAA28220.1) protein sequence as the query. Proteins were selected based on *E* values, % identities and gaps, and crosschecked by NCBI CDD (http://www.ncbi.nlm.nih.gov/Structure/cdd/wrpsb.cgi) [63] search. GenBank accession numbers of the protein sequences used are those of the nearest neighbours of *Neurospora crassa* (NC) NCS-1 in *Aspergillus fumigatus* (AF), *Botryotina fuckeliana* (BF), *Magnaporthe grisea* (MG), *Microsporum canis* (MC), *Paracoccidioides brasiliensis* (PB), *Pyrenophora tritici-repentis* (PT), *Saccharomyces cerevisiae* (SC), *Schizosaccharomyces japonicas* (SJ), *S. pombe* (SP), *Verticillium albo-atrum* (VA), *Drosophila melanogaster* (DM), *Caenorhabditis elegans* (CE), *Salmo salar* (SS), *Danio rerio* (DR), *Xenopus laevis* (XL), *Gallus gallus* (GG), *Mus musculus* (MM), *Rattus norvegicus* (RN) and *Homo sapiens* (HS). Frequenin/NCS-1 proteins are described by Genbank accession number, organism and class. Phylum is indicated at major clades. Bar indicates scale of genetic distances.

© 2011 WILEY-VCH Verlag GmbH & Co. KGaA, Weinheim

TH-1227_09610609

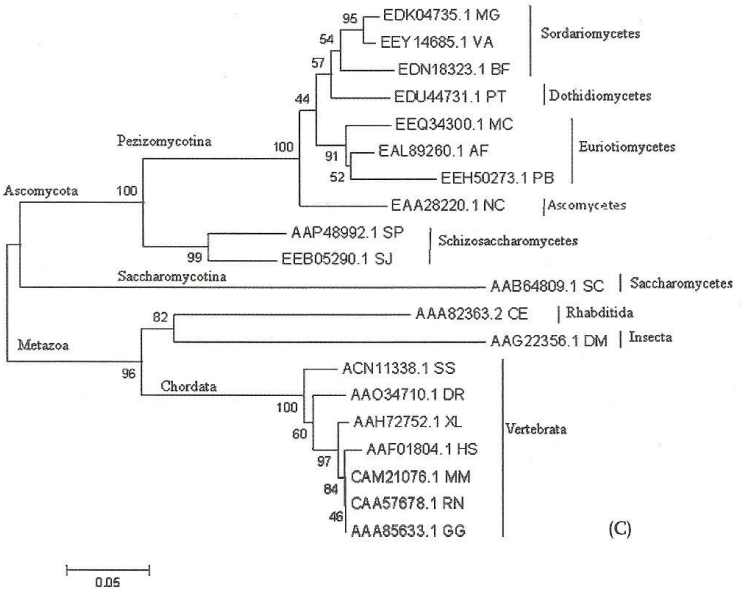

Figure 1. (Continued)

interacts with two antiparallel α-helices of Pik1, producing a U-turn structure that might orient the N-terminal 'lipid-kinase unique' (LKU) motif in close proximity to the C-terminal catalytic domain [8]. Heterologous expression of vertebrate frequenin could rescue the inviability of the *frq1Δ* spores [7].

Calcium tolerance, sexual development and ultraviolet sensitivity

In *M. grisea*, a neuronal calcium sensor-1/frequenin like gene, *Mg-NCS-1* was isolated and the phenotypes of null-mutants were evaluated [14]. The null-mutants had normal growth and pathogenicity similar to the parental strains, but growth was suppressed in high concentrations of calcium and acidic conditions.

Ncs1p, the *S. pombe* ortholog of *NCS-1*, binds calcium and also is *N*-myristoylated [15]. The *ncs1Δ* mutant showed starvation independent sexual development and Ca^{2+}-sensitivity. Starvation independent sexual development of *ncs1Δ* was complemented by retinal recoverin, which controls Ca^{2+}-regulated desensitization of rhodopsin [15]. Moreover, addition of exogenous cAMP, a key regulator for sexual development, suppressed starvation independent conjugation and sporulation of *ncs1Δ*. This suggests that Ncs1p might regulate a G protein cascade upstream of the adenylate cyclase pathway turned on by the glucose-sensing G protein-coupled receptor Git3p [23]. However, the Ca^{2+}-sensitivity of *ncs1Δ* was not rescued by either overexpression of recoverin or by adding exogenous cAMP, suggesting that the starvation independent sexual development and Ca^{2+}-sensitivity phenotypes of *ncs1Δ* mutant are mechanistically independent. Therefore, *S. pombe* Ncs1p may regulate conjugation and sporulation possibly by controlling Ca^{2+}-dependent desensitization Git3p [15].

In *N. crassa*, a knockout mutant of the NCS-1 homologue (NCU04379) grows slowly, shows increased sensitivity to $CaCl_2$ and ultraviolet (UV) irradiation (R. Deka *et al.*, unpublished). The *N. crassa* NCS-1 homologue encodes a 190-residues protein (EAA28220.1) and shows significant homology with the corresponding proteins in *A. fumigatus*, *M. grisea*, *S. cerevisiae* and *S. pombe* (Fig. 1B). A phylogenetic analysis with a subset of frequenin/NCS-1 proteins from fungi to mammals revealed that the *N. crassa* NCS-1 protein clustered with the Pezizomycotina clade (Fig. 1C).

Calcium resistance and expression of ion pumps

In *A. fumigatus*, the *NCS-1* homologue NcsA is not an essential gene, but is involved in sterol distribution in the tip and polar establishment [16]. The *ΔncsA* mutant

© 2011 WILEY-VCH Verlag GmbH & Co. KGaA, Weinheim

TH-1227_09610609

showed sensitivity to SDS, which suggests that NcsA plays a role in the organization of membrane domains and polar growth. Moreover, reduced expression of ion pumps *pmcA* and *pmcB*, a P-type calcium ATPase and a calcium-translocating P-type ATPase, respectively, was observed in the *ΔncsA* mutant [16, 24]. Furthermore, the *ΔncsA* mutant was more resistant to calcium chloride. This result is in contrast to the phenotypic analysis of NCS-1 homologues in *M. grisea* [14], *S. pombe* [15], and *N. crassa* (R. Deka *et al.*, unpublished) which displayed calcium sensitivity instead of calcium-resistance, suggesting a different role for *A. fumigatus* NcsA in calcium regulation.

Calcium/calmodulin-dependent kinases

Calcium/calmodulin-dependent kinases (Ca^{2+}/CaMKs) are Ser/Thr protein kinases and they can modulate diverse cellular responses to increase in intracellular Ca^{2+} [25–27]. The general domain organization of the Ca^{2+}/CaMKs includes an N-terminal catalytic domain, followed by an autoinhibitory and overlapping CaM-binding domain (Fig. 2A). The autoinhibitory domain interacts with the catalytic domain and maintains the kinase in an inactive conformation by preventing binding of the true substrate [28, 29]. Binding of Ca^{2+}/CaM to the CaM-binding domain activates the kinase that allows binding of the substrate to Ca^{2+}/CaMKs [27, 29]. Ca^{2+}/CaMKs are broadly grouped into two major groups according to their substrate specificity. Members of the first group have broad substrate specificity, and include multifunctional kinases such as CaMKI, II and IV [27]. The second group of Ca^{2+}/CaMKs has narrow substrate specificity, and includes dedicated kinases such as phosphorylase kinase, myosin-light chain kinase (MLCK) and CaMKIII [27]. The cellular roles of Ca^{2+}/CaMKs have been intensively investigated using mammlian systems, particulary in regulation of neuronal development and plasticity [30–35], however, little is known about their cellular roles in fungi. Fungal homologues of the Ca^{2+}/CaMKs have been identified in *S. cerevisiae* [3, 36, 37], *A. nidulans* [38–41], *S. pombe* [42], *Colletotrichum gloeosporioides* [43], *Sporothrix schenckii* [44], and *N. crassa* [45] (R. Deka *et al.*, unpublished). In the following part of the review we describe cellular roles of Ca^{2+}/CaMKs in fungi.

Spore germination and thermotolerance

S. cerevisiae genes *CMK1* and *CMK2* encode Ca^{2+}/CaMKII isozymes [3, 36]. The deduced amino-acid sequences of *CMK1* and *CMK2* are 60% identical and 90% similar. CMK2 kinase converts to a constitutively active protein kinase in vitro upon autophosphorylation while CMK1 kinase does not [3]. Deletion of *CMK2*, or both *CMK1* and *CMK2*, was not lethal, although loss of *CMK2* caused a slow rate of spore germination. Moreover, both the *Δcmk1* and the *Δcmk1 Δcmk2* cells lost the induced thermotolerance faster than the wild type and *Δcmk2* cells, indicating that the acquisition of induced thermotolerance depends on CaMKII [36].

Another *S. cerevisiae* Ca^{2+}/CaMKII is encoded by the *CLK1* gene [37]. The Clk1 protein has an N-terminal kinase domain, and a C-terminal basic segment resembling known CaM-binding sites. Clk1 shares 38 and 37% identity in amino acid sequence with rat CaM kinase α and yeast CaM kinase *CMK2*, respectively [37]. The Clk1 protein is located in the cytosol and excluded from the nucleus. The *clk1Δ* mutant is viable; however, elevated expression of Clk1 inhibits growth. Overexpression of the C-terminally truncated Clk1 also inhibits growth, whereas overproduction of catalytically inactive Clk1 had no effect of growth, suggesting that the C terminus is a negative regulatory domain [37].

Hyphal growth and cell cycle progression

Three Ca^{2+}/CaMKs, CMKA, CMKB and CMKC have been reported in *A. nidulans* [38–41]. CMKA shares 29% identity to that of the α-subunit of rat brain Ca^{2+}/CaMKII, 40 and 44% identity with the *S. cerevisiae* Ca^{2+}/CaMKs CMK1 and CMK2, respectively [36, 38]. CMKB and CMKC share high sequence identity with mammalian Ca^{2+}/CaMKs, rat CaMKI/IV and rat CaMKKα/β, respectively [40]. Disruption of either *cmk*A or *cmk*B is lethal but disruption of *cmk*C is non-lethal [39, 40]. CMKA is required for hyphal growth and progression of the nuclear division cycle [39]. Both CMKB and CMKC are required for the proper temporal activation of $NIMX^{cdc2}$ (the mitotic kinase Cdk1 in *A. nidulans*) that is necessary for nuclear divisions [40]. CMKB and CMKA are essential for progression through G_1 and G_2, respectively, while CMKC is important for G_1 progression [39, 40].

A CaMK-I homologue in *S. pombe* is encoded by the *cmk1* gene [42]. The cmk1 protein has significant homology to mammalian CaMK-I. The levels of *cmk1* mRNA are regulated in a cell cycle-dependent manner, peaking at or near the G_1/S boundary. Overexpression of CMK1 caused no obvious effects on growth and division. However, expression of the CMK1-T192D mutant, which mimics phosphorylation of Thr-192, resulted in hyperactivation of CMK1 activity in the presence of CaM and causes cell cycle arrest as well as morphological defects [42]. Thr-192 corresponding residue is conserved in mammalian CaMK-I and its phosphorylation by the CaM-kinase kinase (CaM-KK) produces a hyperactivate CaMK-I [46, 47]. Both CaMK-I and CaM-KK are members of a mammalian CaMK cascade that regulates

© 2011 WILEY-VCH Verlag GmbH & Co. KGaA, Weinheim

TH-1227_09610609

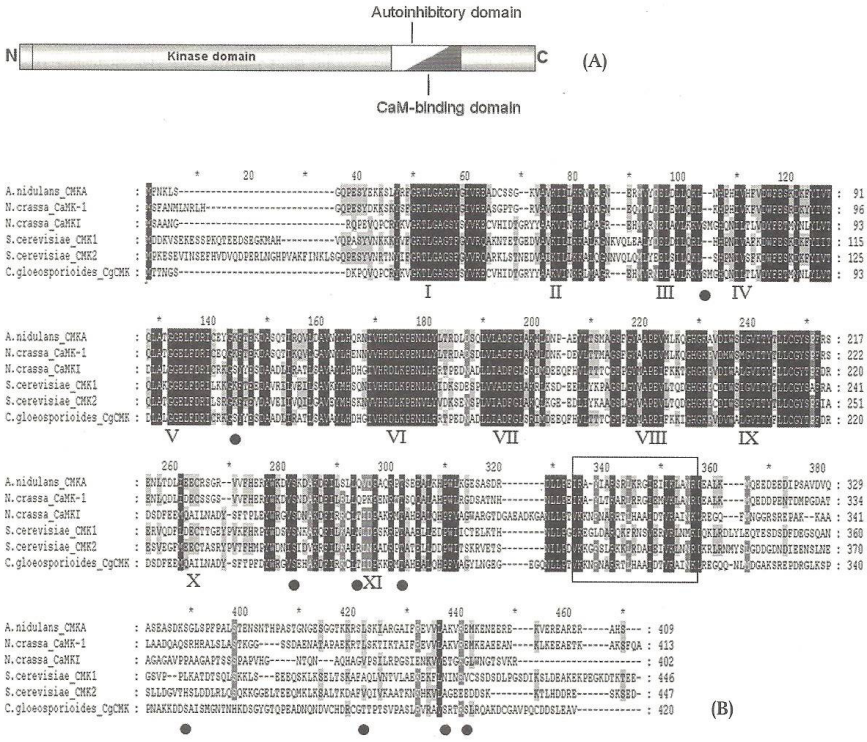

Figure 2. Domain organization, sequence alignment and phylogeny of calcium/calmodulin-dependent kinases (Ca^{2+}/CaMKs). A) Ca^{2+}/CaMKs contain an N-terminal kinase domain (red), followed by an autoinhibitory (yellow) and overlapping CaM-binding domain (blue). B) Sequence comparison of the Ca^{2+}/CaMKs from *A. nidulans*, *C. gloeosporioides*, *N. crassa* and *S. cerevisiae* using the software ClustalX 1.83 [57] and GeneDoc [58]. Conserved amino acids are indicated in black (100%), dark gray (>80%) and light gray (>60%). The sequences in the box represent the putative CaM-binding domain, solid circles below the CgCMK sequence indicate potential autophosporylation sites containing the $^{R}_{x}XX^{T}_{S}$ consensus phosphorylation site for CaMKs and I–XI represents conserved kinase domains [43]. C) Phylogenetic analysis of the Ca^{2+}/CaMKs from fungi to mammals using the Minimum evolution method [59], 500 bootstrap replications (bootstrap values are indicated in the point at nodes) as test of phylogeny [60] and the software MEGA4 [61]. The non-redundant protein sequence databases at the NCBI were searched using the BLASTP (http://blast.ncbi.nlm.nih.gov/Blast.cgi) [62], with the default parameters, using *N. crassa* CAMK-1 (XP_958895.2) and Ca^{2+}/CaMKI (XP_959927.2) protein sequences as queries. Proteins were selected based on *E* values, % identities and gaps, and crosschecked by NCBI CDD (http://www.ncbi.nlm.nih.gov/Structure/cdd/wrpsb.cgi) [63] search. GenBank accession numbers of the protein sequences used are those of the nearest neighbours of *N. crassa* (NC) CAMK-1 and CaMKI in *A. clavatus* (AC), *A. flavus* (AL), *A. fumigatus* (AF), *A. nidulans* (AN), *Ajellomyces capsulatus* (AJ), *A. dermatitidis* (AD), *Candida albicans* (CA), *C. tropicalis* (CT), *Colletotrichum gloeosporioides* (CG), *Cryptococcus neoformans* (CN), *Paracoccidioides brasiliensis* (PB), *Phaeosphaeria nodorum* (PN), *Phytophthora sojae* (PS), *S. cerevisiae* (SC), *S. japonicas* (SJ), *S. pombe* (SP), *Sordaria macrospora* (SM), *Sporothrix schenckii* (SS), *Lodderomyces elongisporus* (LE), *Uncinocarpus reesii* (UR), *Glossina morsitans* (GM), *Aedes aegypti* (AA), *D. rerio* (DR), *Ornithorhynchus anatinus* (OA), *M. musculus* (MM), *R. norvegicus* (RN), *Equus caballus* (EC) and *H. sapiens* (HS). Ca^{2+}/CaMKs are described by Genbank accession number, organism and phylum. Bar indicates scale of genetic distances.

© 2011 WILEY-VCH Verlag GmbH & Co. KGaA, Weinheim

TH-1227_09610609

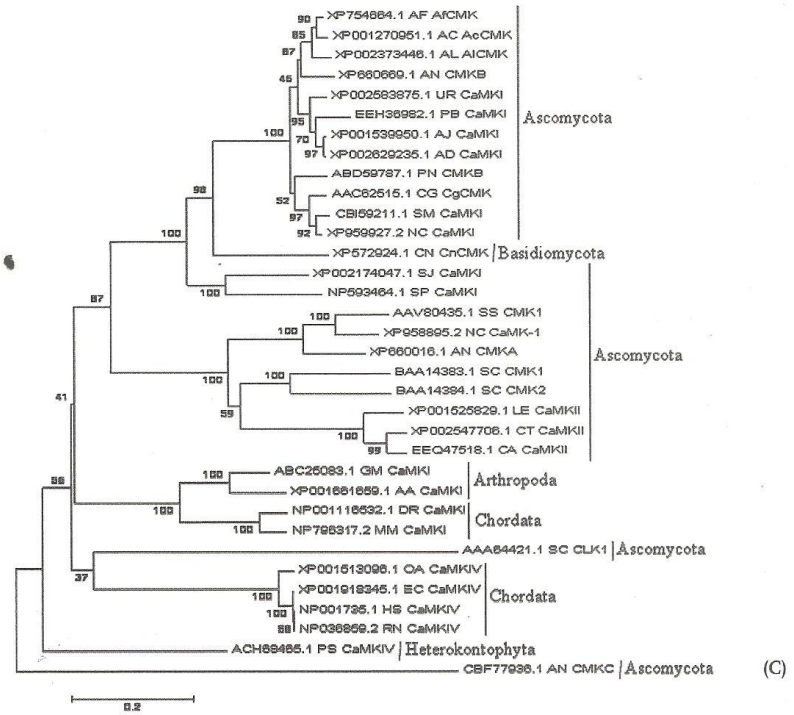

Figure 2. (Continued)

several transcription factors [48, 49]. Therefore, *cmk1* may be important in cell cycle progression, and a CaMK cascade may be present in *S. pombe* [42].

Infection structure differentiation

A putative CaMK cDNA of *Colletotrichum gloeosporioides* (CgCMK) was cloned with transcripts from conidia germinated on glass surface imitating the hard waxy leaf surface [43].

In *C. gloeosporioides* the response to host wax and ethylene, the host ripening hormone, requires the contact of conidia with a hard surface [50, 51]. Hard-surface contact in *C. gloeosporioides* induces Ca^{2+}/CaM signaling that appears to be necessary for the conidia to respond to host signals by germination and differentiation into appressoria required for infection of the host [43].

A selective inhibitor of CaMK, KN93 [52], interferes with germination and appressorium formation effectively in the early phase of hard-surface contact. The application of KN93 also results in formation of the appressoria with unusual morphological features and much less melanization. An intermediate in melanin synthesis, scytalone [53], reversed the inhibition of melanization by KN93 but did not restore appressorium formation. These results suggest that CgCMK affects germination and appressorium formation in the early phase of hard-surface contact and inhibits melanization at some step (s) prior to the formation of scytalone [43].

Ca^{2+}/CaMK signaling pathway also plays an important role during the dimorphic transitions of *S. schenckii*, the etiological agent of sporotrichosis, a subcutaneous lymphatic mycosis [44, 54, 55]. A Ca^{2+}/CaMK gene in *S. schenckii*, *sscmk1*, was predicted to encode SSCMK1that might regulate dimorphism in this fungus [44]. The application of CaM inhibitor W-7 as well as Ca^{2+}/CaMK inhibitors KN-62 and lavendustin C, stimulate the yeast to mycelium transition and inhibit re-entry into the budding cycle by yeast cells. These results suggest a role for Ca^{2+}/CaM dependent signaling pathway in the expression of the yeast morphology in *S. schenckii* [44].

© 2011 WILEY-VCH Verlag GmbH & Co. KGaA, Weinheim

TH-1227_09610609

Circadian clock and fertility

In *N. crassa*, a Ca^{2+}/CaMK (CAMK-1) that can specifically phosphorylate the circadian clock protein FREQUENCY (FRQ) was characterized [45]. Disruption of the *camk-1* gene resulted in a modest phase delay, a small period lengthening, and light-induced phase shifting of the circadian conidiation rhythm [45]. The *camk-1* null strains grow slowly immediately after germination from ascospores, indicating that CAMK-1plays an important role in growth and development of *N. crassa*. The slow growth phenotype is transient, which indicates redundancy of the kinases [45]. The gene that encodes CAMK-1 (XP_958895.2) has been annotated as NCU09123 in the sequenced *N. crassa* genome (http://www.broadinstitute.org/annotation/genome/neurospora/MultiHome.html).

Crosses homozygous for NCU09123 knockout mutants display an intermediate phenotype (produce few hundreds of ascospores). Moreover, the gene NCU02283 in *N. crassa* encodes another Ca^{2+}/CaMKI (XP_959927.2) and crosses homozygous for NCU02283 knockout mutants are barren (produce very few ascospores) (R. Deka *et al.*, unpublished). Both CAMK-1 and Ca^{2+}/CaMKI protein encoded by the gene NCU09123 and NCU02283, respectively, show significant homology with the corresponding proteins in *A. nidulans*, *C. gloeosporioides* and *S. cerevisiae* (Fig. 2B). A phylogenetic analysis with a subset of Ca^{2+}/CaMKs from fungi to mammals revealed that the corresponding proteins in *N. crassa* clustered with the homologues from the Ascomycota phylum (Fig. 2C).

Concluding remarks

NCS-1 is an essential gene in *S. cerevisiae* [7] but not in *M. grisea* [14], *S. pombe* [15], *A. fumigatus* [16] and *N. crassa* (R. Deka *et al.*, unpublished). This suggests that there are other proteins collaborating for calcium sensing in the organisms where NCS-1 is not essential [14–16, R. Deka *et al.*, unpublished]. In *S. cerevisiae*, Frq1 was shown to interact with Pik1 [7, 8, 13]. Changes in free intracellular Ca^{2+} quickly change the activity of several kinases like Ca^{2+}/CaMKs that perform diverse cellular functions including infection structure differentiations in fungi [25, 26, 43]. Recent evidence suggests that the Ca^{2+}/CaMKs of yeasts are evolutionarily distinct from those in filamentous fungi [44]. With the development of post-genomic resources applicable to a diverse variety of fungi, several new insights into the calcium signaling mechanisms in fungi should accumulate over the next few years. Thus, it is possible to address questions such as: (i) What are the proteins in addition to *S. cerevisiae* NCS-1 in *S. pombe*, *M. grisea*, *A. fumigatus* and *N. crassa* that redundantly collaborate for calcium sensing?; (ii) Do NCS-1 proteins in *S. pombe*, *M. grisea*, *A. fumigatus* and *N. crassa* interact with the Pik1 homologue?; (iii) What are the mechanisms of NCS-1 and Ca^{2+}/CaMKs regulation in fungal species where homologues of these proteins have already been identified?; (iv) How are Ca^{2+}/CaMK's involved in infection structure differentiation in pathogenic fungi?; (v) What are the consequences of distinct evolutionary relationship among the fungal Ca^{2+}/CaMKs?; (vi) What are the cellular roles of NCS-1 and Ca^{2+}/CaMKs in other fungal species? The answers to these questions should provide biologists a deeper insight into the calcium signaling mechanisms in fungi that may be useful for the benefit of human welfare.

Acknowledgements

Research in the laboratory of RT is supported by the IITG. The Fungal Genetics Stock Center (FGSC) generously waived charges for strains. The FGSC is supported by National Science Foundation grant BIR-9222772. RK and RD were supported by Junior Research Fellowships from the IITG and the CSIR-UGC, respectively. We thank review editor Dr. M. Raudaskoski for critical comments and Dr. D.P. Kasbekar (CCMB, Hyderabad) for critically reading this manuscript.

References

[1] Sanders D., Pelloux, J., Brownlee, C., Harper, J.F., 2002. Calcium at the crossroads of signaling. Plant Cell, **14**, S401–S417.

[2] Zelter, A., Bencina, M., Bowman, B.J., Yarden, O. *et al.*, 2004. A comparative genomic analysis of the calcium signaling machinery in *Neurospora crassa*, *Magnaporthe grisea*, and *Saccharomyces cerevisiae*. Fungal Genet. Biol., **41**, 827–841.

[3] Ohya, Y., Kawasaki, H., Suzukis, K., Londesborough, J. *et al.*, 1991. Two yeast genes encoding calmodulin-dependent protein kinases. Isolation, sequencing and bacterial expressions of CMK1 and CMK2. J. Biol. Chem., **266**, 12784–12794.

[4] Gadd, G.M., 1994. Signal transduction in fungi. In: The Growing Fungus (N.A.R. Gow, G.M. Gadd, eds.). Chapman and Hall, London, UK. 183–210 p.

[5] Shaw, B.D., Hoch, H.C., 2001. Biology of the fungal cell. In: The Mycota VIII (R.J. Howard, N.A.R. Gow, eds.). Springer-Verlag KG, Berlin, Germany, pp. 73–89.

[6] Johnson, D.R., Bhatnagar, R.S., Knoll, L.J., Gordon, J.I., 1994. Genetic and biochemical studies of protein N-myristoylation. Annu. Rev. Genet., **63**, 869–914.

© 2011 WILEY-VCH Verlag GmbH & Co. KGaA, Weinheim

TH-1227_09610609

[7] Hendricks, K.B., Wang, B.Q., Schnieders, E.A., Thorner, J., 1999. Yeast homologue of neuronal frequenin is a regulator of phosphatidylinositol-4-OH kinase. Nat. Cell Biol., **1**, 234–241.

[8] Strahl, T., Huttner, I.G., Lusin, J.D., Osawa, M. *et al.*, 2007. Structural insights into activation of phosphatidylinositol 4-kinase (Pik1) by yeast frequenin (Frq1). J. Biol. Chem., **282**, 30949–30959.

[9] Peitzsch, R.M., Stuart McLaughlin, S., 1993. Binding of acylated peptides and fatty acids to phospholipid vesicles: Pertinence to myristoylated proteins. Biochemistry, **32**, 10436–10443.

[10] Burgoyne, R.D., 2004. The neuronal calcium-sensor proteins. Biochim. Biophys. Acta, **1742**, 59–68.

[11] Ikura, M., 1996. Calcium binding and conformational response in EF-hand proteins. Trends Biochem. Sci., **21**, 14–17.

[12] Ames, J.B., Hendricks, K.B., Strahl, T., Huttner, I.G. *et al.*, 2000. Structure and calcium-binding properties of Frq1, a novel calcium sensor in the yeast *Saccharomyces cerevisiae*. Biochemistry, **39**, 12149–12161.

[13] Huttner, I.G., Strahl, T., Osawa, M., King, D.S. *et al.*, 2003. Molecular interactions of yeast frequenin (frq1) with the phosphatidylinositol 4-kinase isoform, Pik1. J. Biol. Chem., **278**, 4862–4874.

[14] Saitoh, K., Arie, T., Teraoka, T., Yamaguchi, I. *et al.*, 2003. Targeted gene disruption of the neuronal calcium sensor 1 homologue in rice blast fungus, *Magnaporthe grisea*. Biosci. Biotechnol. Biochem., **67**, 651–653.

[15] Hamasaki-Katagiri, N., Molchanova, T., Takeda, K., Ames, J.B., 2004. Fission yeast homolog of neuronal calcium sensor-1 (Ncs1p) regulates sporulation and confers calcium tolerance. J. Biol. Chem., **279**, 12744–12754.

[16] Mota Júnior, A.O., Malavazi, I., Soriani, F.M., Heinekamp, T. *et al.*, 2008. Molecular characterization of the *Aspergillus fumigatus NCS-1* homologue, NcsA. Mol. Genet. Genomics, **280**, 483–495.

[17] Kawasaki, H., Nakayama, S., Kretsinger, R. H., 1998. Classification and evolution of EF-hand proteins. Biometals, **11**, 277–295.

[18] Yap, K.L., Ames, J.B., Swindells, M.B., Ikura, M., 1999. Diversity of conformational states and changes within the EF-hand protein superfamily. Proteins, **37**, 499–507.

[19] Garcia-Bustos, J.F., Marini, F., Stevenson, I., Frei, C. *et al.*, 1994. PIK1, an essential phosphatidylinositol 4-kinase associated with the yeast nucleus. EMBO J., **13**, 2352–2361.

[20] Hama, H., Schnieders, E.A., Thorner, J., Takemoto, J.Y. *et al.*, 1999. Direct involvement of phosphatidylinositol 4-phosphate in secretion in the yeast *Saccharomyces cerevisiae*. J. Biol. Chem., **274**, 34294–34300.

[21] Walch-Solimena, C., Novick, P., 1999. The yeast phosphatidylinositol-4-OH kinase Pik1 regulates secretion at the Golgi. Nat. Cell. Biol., **1**, 523–525.

[22] Strahl, T., Hama, H., DeWald, D.B., Thorner, J., 2005. Yeast phosphatidylinositol 4-kinase, Pik1, has essential roles at the Golgi and in the nucleus. J. Cell. Biol., **171**, 967–979.

[23] Welton, R.M., Hoffman, C.S., 2000. Glucose monitoring in fission yeast via the gpa2 Gα, the git5 Gβ and the git3 putative glucose receptor. Genetics, **156**, 513–521.

[24] Soriani, F.M., Malavazi, I., Silva, M.E., Savoldi, M. *et al.*, 2008. Functional characterization of the *Aspergillus fumigatus* CRZ1 homologue, CrzA. Mol. Microbiol., **67**, 1274–1291.

[25] Wilmann, M., Gautel, M., Mayans, O., 2000. Activation of calcium/calmodulin regulated kinases. Cell. Mol. Biol. (Noisy-le-grand), **46**, 883–894.

[26] Mellström, M., Naranjo, J.R., 2001. Mechanisms of Ca^{2+}-dependent transcription. Curr. Opin. in Neurobiology., **11**, 312–319.

[27] Hook, S.S., Means, A.R., 2001. Ca^{2+}/CaM-dependent kinases: from activation to function. Annu. Rev. Pharmacol. Toxicol., **41**, 471–505.

[28] Okuno, S., Kitani, T., Fujisawa, H., 1994. Purification and characterization of Ca^{2+}/calmodulin-dependent protein kinase IV kinase from rat brain. J. Biochem., **116**, 923–930.

[29] Braun, A.P., Schulman, H., 1995. The multifunctional calcium/calmodulin-dependent protein kinase: from form to function. Annu. Rev. Physiol., **57**, 417–445.

[30] Soderling, T.R., 2000. CaM-kinases: modulators of synaptic plasticity. Curr. Opin. Neurobiol., **10**, 375–380.

[31] Colbran, R.J., 2004. Protein phosphatases and calcium/calmodulin-dependent protein kinase II-dependent synaptic plasticity. J. Neurosci., **24**, 8404–8409.

[32] Elgersma, Y., Sweatt, J.D., Giese, K.P., 2004. Mouse genetic approaches to investigating calcium/calmodulin-dependent protein kinase II function in plasticity and cognition. J. Neurosci., **24**, 8410–8415.

[33] Griffith, L.C., 2004. Calcium/calmodulin-dependent protein kinase II: an unforgettable kinase. J. Neurosci., **24**, 8391–8393.

[34] Griffith, L.C., 2004. Regulation of calcium/calmodulin-dependent protein kinase II activation by intramolecular and intermolecular interactions. J. Neurosci. **24**, 8394–8398.

[35] Schulman, H., 2004. Activity-dependent regulation of calcium/calmodulin-dependent protein kinase II localization. J. Neurosci., **24**, 8399–8403.

[36] Pausch, M.H., Kaim, D., Kunisawa, R., Admon, A. *et al.*, 1991. Multiple Ca^{2+}/calmodulin-dependent protein kinase genes in a unicellular eukaryote. EMBO J., **10**, 1511–1522.

[37] Melcher, L., Thorner, J., 1996. Identification and characterization of the *CLK1* gene product, a novel CaM kinase-like protein kinase from the yeast *Saccharomyces cerevisiae*. J. Biol. Chem., **271**, 29958–29968.

[38] Kornstein, L.B., Gaiso, M.L., Hammell, R.L., Bartelt, D.C., 1992. Cloning and sequence determination of a cDNA encoding *Aspergillus nidulans* calmodulin-dependent multifunctional protein kinase. Gene, **113**, 75–82.

[39] Dayton, S., Means, A.R., 1996. Ca^{2+}/calmodulin-dependent kinase is essential for both growth and nuclear division in *Aspergillus nidulans*. Mol. Biol. Cell., **7**, 1511–1519.

© 2011 WILEY-VCH Verlag GmbH & Co. KGaA, Weinheim

TH-1227_09610609

[40] Joseph, J.D., Means, A.R., 2000. Identification and characterization of two Ca^{2+}/CaM-dependent protein kinases required for normal nuclear division in *Aspergillus nidulans*. J. Biol. Chem., **275**, 38230–38238.

[41] Joseph, J.D., Means, A.R., 2002. Calcium binding is required for calmodulin function in *Aspergillus nidulans*. Eukaryot. Cell, **1**, 119–125.

[42] Rasmussen, C.D., 2000. Cloning of a calmodulin kinase I homologue from *Schizosaccharomyces pombe*. J. Biol. Chem., **275**, 685–690.

[43] Kim, Y., Li, D., Kolattukudy, P.E., 1998. Induction of Ca^{2+}-calmodulin signaling by hard-surface contact primes *Colletotrichum gloeosporioides* conidia to germinate and form appressoria. J. Bacteriology., **180**, 5144–5150.

[44] Valle-Aviles, L., Valentin-Berrios, S., Gonzalez-Mendez, R.R., Rodriguez-del, V.N., 2007. Functional, genetic and bioinformatic characterization of a calcium/calmodulin kinase gene in *Sporothrix schenckii*. BMC Microbiology, **7**, 107.

[45] Yang, Y., Cheng, P., Zhi, G., Liu, Y., 2001. Identification of a calcium/calmodulin-dependent protein kinasethat phosphorylates the *Neurospora* circadian clock protein FREQUENCY. J. Biol. Chem., **276**, 41064–41072.

[46] Haribabu, B., Hook, S.S., Selbert, M.A., Goldstein, E.G. *et al.*, 1995. Human calcium-calmodulin dependent protein kinase 1: cDNA cloning, domain structure and activation by phosphorylation at threonine-177 by calcium-calmodulin dependent protein kinase I kinase. EMBO J., **14**, 3679–3686.

[47] Tokumitsu, H., Enslen, H., Soderling, T.R., 1995. Characterization of a Ca^{2+}/calmodulin-dependent protein kinase cascade. Molecular cloning and expression of calcium/calmodulin-dependent protein kinase kinase. J. Biol. Chem., **270**, 19320–19324.

[48] Soderling, T.R. 1999. The Ca^{2+}-calmodulin-dependent protein kinase cascade. Trends Biochem Sci., **24**, 232–236.

[49] Means, A.R., 2000. Regulatory cascades involving calmodulin-dependent protein kinases. Mol. Endocrinol., **14**, 4–13.

[50] Flaishman, M.A., Kolattukudy, P.E., 1994. Timing of fungal invasion using host's ripening hormone as a signal. Proc. Natl. Acad. Sci., USA **91**, 6579–6583.

[51] Flaishman, M.A., Hwang, C.H., Kolattukudy, P.E., 1995. Involvement of protein phosphorylation in the induction of appressorium formation in *Colletotrichum gloeosporioides* by its host surface wax and ethylene. Physiol. Mol. Plant Pathol., **47**, 103–117.

[52] Mamiya, N., Goldenring, J.R., Tsunoda, Y., Modlin, I.M. *et al.*, 1993. Inhibition of acid secretion in gastric parietal cells by the Ca^{2+}/calmodulin-dependent kinase II inhibitor KN93. Biochem. Biophys. Res. Commun., **195**, 608–615.

[53] Kubo, Y., Suzuki, K., Furusawa, I., Yamamoto, M., 1983. Scytalone as a natural intermediate of melanin biosynthesis in appressoria of *Colletotrichum lagenarium*. Exp. Mycol., **7**, 208–215.

[54] Travassos, L.R., Lloyd, K.O., 1980. *Sporothrix schenckii* and related species of Ceratocystis. Microbiol Rev., **44**, 683–721.

[55] Serrano, S., Rodriguez-del Valle, N., 1990. Calcium uptake and efflux during the yeast to mycelium transition in *Sporothrix schenckii*. Mycopathologia, **112**, 1–9.

[56] Ren, J., Wen, L., Gao, X., Jin, C. *et al.*, 2009. DOG 1.0: illustrator of protein domain structures. Cell Research., **19**, 271–273.

[57] Thompson, J.D., Gibson, T.J., Plewniak, F., Jeanmougin, F. *et al.*, 1997. The CLUSTAL-X windows interface: flexible strategies for multiple sequence alignment aided by quality analysis tools. Nucleic Acids Res., **25**, 4876–4882.

[58] Nicholas, K.B., Nicholas, H.B., 1997. GeneDoc: a tool for editing and annotating multiple sequence alignments. Distributed by the author. http://www.psc.edu/biomed/genedoc.

[59] Rzhetsky, A., Nei, M., 1992. Statistical properties of the ordinary leastsquares, generalized least-squares, and minimum-evolution methods of phylogenetic inference. J. Mol. Evol., **35**, 367–375.

[60] Felsenstein, J., 1985. Confidence limits on phylogenies: An approach using the bootstrap. Evolution, **39**, 783–791.

[61] Tamura, K., Dudley, J., Nei, M., Kumar, S., 2007. MEGA4: Molecular Evolutionary Genetics Analysis (MEGA) software version 4.0. Mole. Biol. Evol., **24**, 1596–1599.

[62] Altschul, S.F., Madden, T.L., Schaffer, A.A., Zhang, J. *et al.*, 1997. Gapped BLAST and PSI-BLAST: a new generation of protein database search programs. Nucleic Acids Res., **25**, 3389–3402.

[63] Marchler-Bauer, A., Anderson, J.B., Chitsaz, F., Derbyshire, M.K. *et al.*, 2009. CDD: specific functional annotation with the Conserved Domain Database. Nucleic Acids Res., **37**, D205–D210.

© 2011 WILEY-VCH Verlag GmbH & Co. KGaA, Weinheim

TH-1227_09610609